CHARACTERISATION AND REACTION STUDIES OF SUPPORTED METAL CATALYSTS

By

LINDA ELIZABETH FARRELL

A THESIS SUBMITTED FOR THE DEGREE OF

DOCTOR OF PHILOSOPHY

OF THE UNIVERSITY OF GLASGOW

DEPARTMENT OF CHEMISTRY, SEPTEMBER 1988

ProQuest LLC.
789 East Eisenhower Parkway
P.O. Box 1346
Ann Arbor, MI 48106 – 1346

To Simon

Acknowledgements

I should like to express my sincere gratitude to my supervisor, Professor G. Webb, for his advice and encouragement throughout this project. I should also like to express my thanks to the technical staff, in particular Mr. T. Boyle and Mr. K. Shepherd for their advice, help and patience; to Mr. D. Thom for carrying out the electron microscopy and to many others in the Chemistry Department for their technical support.

I would like to say thank you to Dr. K.C. Waugh for his encouragement, enthusiasm and advice; to I.C.I. Chemicals and Polymers Group for allowing me to perform experimental measurements in their department at Runcorn, and to Dr. S.D. Jackson for his interest and many helpful suggestions.

I acknowledge the award of an S.E.R.C. maintainance grant.

I should like to thank my friends and colleagues, both past and present, for their kindness and encouragement - it was much appreciated.

Finally, thanks to my parents, and to Simon, for giving me their support when I needed it most.

Summary

A series of silica-, molybdenum trioxide- and tungsten trioxide-supported platinum catalysts (1.1% w/w metal) have been prepared by impregnation of the appropriate oxide support with an aqueous solution of chloroplatinic acid. Series of silica-, molybdenum trioxide-, and tungsten trioxide-supported rhodium catalysts (1.5% w/w metal) have been prepared by impregnation using either aqueous rhodium(III) nitrate or aqueous rhodium(III) chloride solutions.

Each of the catalysts has been characterised by

a) temperature programmed reduction,

b) chemisorption and temperature programmed desorption of carbon monoxide, to determine variations in the nature of the chemisorbed state of carbon monoxide and the metal areas of the different catalysts,

c) thermo-gravimetric analysis and differential scanning calorimetry, to obtain information relevant to the chemical nature of the supported salt and its mode of reduction,

and

d) physical adsorption of nitrogen to determine total surface areas,

to obtain information regarding the influence of (i) the support and (ii) the metal salt precursor on the physical and chemical characteristics of the catalyst.

Evidence for an effect of both of these variables has been found. Thus, differences have been observed in the temperature

programmed reduction profiles and hence in the reduction/activation temperatures of the catalysts, and in the metal areas, and hence dispersions, as determined by carbon monoxide chemisorption and transmission electron microscopy.

Thermo-gravimetric analysis and temperature programmed reduction have shown that in both the molybdenum trioxide- and tungsten trioxide-supported metals hydrogen bronze formation occurs. The composition of these hydrogen bronzes have been determined as:

$Pt/MoO_3(a) \longrightarrow H_{0.9}MoO_3$ by T.G.A., $H_{0.3}MoO_3$ by T.P.R.

$Pt/WO_3(a) \longrightarrow H_{0.3}WO_3$ by T.P.R.

$Rh/MoO_3(b) \longrightarrow H_{0.3}MoO_3$ by T.P.R.

$Rh/WO_3(b) \longrightarrow H_{0.7}WO_3$ by T.P.R.

$Rh/MoO_3(c) \longrightarrow H_{0.7}MoO_3$ by T.G.A. and by T.P.R.

$Rh/WO_3(c) \longrightarrow H_{0.36}WO_3$ by T.P.R.

where (a), (b) and (c) denote catalysts prepared using chlroplatinic acid, rhodium(III) nitrate and rhodium(III) chloride, respectively.

Temperature programmed reaction studies of the hydrogenation of carbon monoxide over the supported platinum catalysts and molybdenum trioxide-supported rhodium have shown that the molybdenum trioxide-supported catalysts are particularly good for the methanation reaction and have provided strong evidence for the existence of metal-support inter-

actions with this particular support.

Buta-1,3-diene hydrogenation studies over the various catalysts have shown that whilst the selectivity is dependent upon the support, the metal and the metal salt precursor, the distribution of the three isomeric n-butenes formed as initial products is, particularly with rhodium, almost independent of the nature of the support and the metal salt precursor used in the preparation. Analysis of the pressure fall against time curves and of variations in the activity of the catalyst as a function of catalyst usage provide indirect evidence for the formation of surface carbonaceous residues and their involvement in the reaction. Deactivation of each of the catalysts during usage has a greater effect on the rate of butene hydrogenation than on the rate of buta-1,3-diene hydrogenation, as witnessed by the disappearance of the acceleration point in the pressure/time curves.

The product distributions and their variations with conversion and temperature, activation energies and kinetic orders are interpreted in terms of a mechanism in which (i) but-2-ene formation occurs by both 1,4-addition of hydrogen to adsorbed buta-1,3-diene and by the subsequent isomerisation of but-1-ene formed by 1,2-addition and (ii) the formation of n-butane by a direct route not involving the intermediate formation of butenes.

Examination of the turnover frequencies for buta-1,3-diene hydrogenation shows that the activities decrease in the order:

(i) $Pt/WO_3(a) > Pt/MoO_3(a) > Pt/SiO_2(a)$

(ii) $Rh/WO_3(b) > Rh/SiO_2(b)$

and (iii) $Rh/MoO_3(c) > Rh/SiO_2(c) > Rh/WO_3(c)$

although the metal particle sizes as determined by carbon monoxide chemisorption are in the order:

(i) $Pt/WO_3(a) > Pt/SiO_2(a) > Pt/MoO_3(a)$

(ii) $Rh/SiO_2(b) > Rh/WO_3(b)$

and (iii) $Rh/WO_3(c) > Rh/SiO_2(c) > Rh/MoO_3(c)$

suggesting that whilst the reaction is structure-insensitive in terms of metal dispersion, the support plays a significant rôle in determining the overall activity.

TABLE OF CONTENTS

Page

CHAPTER FIVE: RESULTS

CHAPTER ONE

CHAPTER 1

INTRODUCTION

1.1 Platinum Metals

The earliest known use of the platinum metals was over twenty-seven centuries ago in the "Thebes Casket", where platinum was used for decorative purposes. However, it was not until the 18th century that the Spaniards discovered platinum among gold deposits in the Chocó region of New Granada (now Colombia). Unknown to the Spanish, the natives of that area had been aware of the separate identity of platinum many centuries before, and had learned to use it in jewellery and other decorative forms. Examples of such artefacts include platinum-surfaced gold pendants and platinum nose rings, estimated to be over a thousand years old, which were found in Ecuador at the beginning of the twentieth century and which are now housed in the Museum of the American Indian in New York. (1)

Platinum was called 'platina' by the Spanish - this was a rather derogatory term derived from 'plata', the Spanish for silver. The reason for this was that the platinum was found associated with gold, and as such it was regarded as a nuisance because it was costly to separate.

Platinum got its name in 1777 from Torbern Bergman, a professor of chemistry at Uppsala, Sweden. Rhodium, on the other hand, was formally identified by William Hyde Wollaston and his partner, Smithson Tennant in 1804. This partnership was responsible for the discovery of three other platinum group metals: palladium in 1892 and iridium and

osmium in 1804. The last of the platinum group metals, ruthenium, was discovered by Klaus in Russia some forty years later.

In the 19th century, platinum began to be used in laboratories in the form of platinum dishes and crucibles. Another use of platinum was in sulphuric acid boilers - such boilers continued to be used until 1926 when they were superceded by the "contact" process which employed a platinum catalyst. (1)

From 1828 to 1846 platinum was used in the form of coins in Russia. However, in 1846, these coins had to be withdrawn because the market value of platinum had fallen below the face value of the coins.

1.2 Early Catalysis

The first purely chemical description of a catalytic process was given by Charles Bernard Désormes and Nicolas Clément in 1806. (2) They suggested a theory of the formation of sulphuric acid in the lead chamber process. (3) In 1822, Döbereiner discovered that oxygen and hydrogen combined in the presence of finely divided platinum. (4)

Although various observations on the subject of catalysis are scattered throughout the literature, it was left to a Swedish chemist by the name of Jöns Jacob Berzelius in 1836, to propose a unifying theory. In a review of all such examples with which he was familiar, Berzelius proposed that a new "force" was acting in all these examples. He was unsure of the nature of this force, although he believed it could be related to electron affinities. He suggested that this force was a catalytic force, and that the operation of such a force should be called catalysis, a word derived from the Greek for decomposition. (2)

In 1894, Ostwald gave us the modern view of a catalyst as a substance that increases reaction rates without altering the general energy relations. (5) Ostwald linked catalysis with the field of kinetics. Both platinum and rhodium have been used in a variety of catalytic processes. Amongst the more important processes are the manufacture of nitric acid in which a Rh-Pt gauze catalyses the oxidation of ammonia at high temperature. In petroleum reforming, platinum catalysts help to convert low octane petroleum naphthas to high quality products. Rhodium is used in a low pressure oxo process for making butyraldehyde, an essential intermediate in the manufacture of plasticisers, detergents and solvents. Catalytic convertors, containing a mixture of platinum group metals on a ceramic honeycomb support, are fitted between the manifold and silencer in vehicle exhausts to catalyse the conversion of carbon monoxide and hydrocarbons to carbon dioxide and water, and to reduce NO_x to the less harmful N_2.

The general definition of a catalyst is "a substance which increases the rate of attainment of equilibrium of a reacting system without causing any great alteration in the free energy changes involved". (6) The equilibrium so obtained is the same as that observed in the corresponding homogeneous system. Therefore, the catalyst must increase the rate of both forward and reverse reactions. A catalyst can only increase the rates of a reaction which is thermodynamically feasible.

Catalysis involves the adsorption of the reactant (or at least one of the reactants if there are more than one) on to the surface of the catalyst. Metals are good catalysts for reactions involving the addition or subtraction of hydrogen, for example, hydrogenation, dehydrogenation

and hydrogenolysis. Adsorption is an exothermic process which involves saturation of the surface "free valencies" of the metal. A reactant must be neither too strongly adsorbed, in which case it would be difficult to remove and, therefore, act as a poison, nor too weakly adsorbed, in which case it would have little chance of remaining on the surface long enough to react.

Metals are used as catalysts in a variety of physical forms: wires, gauzes, finely divided metal powders or most commonly when supported on a carrier.

A supported-metal catalyst usually contains more than 80% w/w carrier. The purpose of the carrier is to act as a means of increasing the dispersion of the supported metal, giving the resulting catalyst physical and mechanical properties superior to those of the unsupported metal. (7)

The majority of catalysts used in industry are in the form of supported metal. The carrier provides a structural framework for the catalytic component, and increases the surface area per unit weight of metal above that of the unsupported metal. The use of a carrier, or support, also gives added stability by allowing small metal crystallites to be sufficiently separated to prevent sintering, and gives greater resistance to poisoning.

In 1962, Bond (7) stated that "Although it has been generally felt that there is no chemical interaction between the metal and the carrier, there is a growing body of evidence to show that this view may be naive". Evidence has been growing steadily to suggest that in many cases the support does interact with the metal, and supposedly inert

supports such as silica may have a role to play in catalysis. It is now believed that many of the differences between supported and unsupported catalysts may be attributable to the presence of the support. (8)

1.3 Metal-Support Interactions

Research carried out by Tauster et al. (9) in the 1970s served to bring together many separate ideas on the influence of the support on catalytic properties. Tauster defined what he called "strong metal-support interactions" (SMSI) as an interaction "consisting of a covalent bond between the metal atoms of the supported phase and the cations of the support". (8)

Tauster et al. (9) carried out their initial work on noble metals supported on titanium dioxide. They reported that following low temperature reduction (200°C) in hydrogen, the titania-supported catalysts exhibited what they considered to be a normal chemisorption capacity for both hydrogen and carbon monoxide, indicating a moderate to high dispersion. However, following reduction at temperatures $\geqslant$ 500°C, adsorption of hydrogen and carbon monoxide was found to be near zero. (9). These authors (9) examined catalyst samples which had been reduced at both low and high temperatures using electron microscopy and x-ray diffraction. The results showed that the loss of adsorption capacity was not due to sintering. They proposed an explanation for the observed manifestations of SMSI in terms of either metal-metal bonding between the noble metal and the titanium cations, or the formation of intermetallic compounds such as $TiPt_3$. Tauster et al. also ruled out encapsulation

of the metal by the support on the grounds that the BET area was not significantly changed by the high temperature reduction treatment.

Tauster and Fung (10) extended their study of SMSI by examining iridium supported on MgO, Sc_2O_3, Y_2O_3, ZrO_2, HfO_2, TiO_2, V_2O_3 and Nb_2O_5. They discovered that hydrogen chemisorption was reduced to near zero following high temperature reduction only when the support was TiO_2, V_2O_3 or NbO_5. From this they concluded that the occurrence of Strong Metal-Support Interactions required the use of a reducible transition metal oxide support.

The manifestations of Strong Metal-Support Interactions include a reduction in the ability to adsorb hydrogen or carbon monoxide after high temperature reduction; a slight decrease in activity for structure-insensitive reactions such as hydrogenation, dehydrogenation, hydrogen exchange or isomerisation; a much lower activity for hydrogenolysis reactions which are structure-sensitive; and an increase in activity and change in selectivity for the CO/H_2 reaction which is also structure-sensitive. (8)

Many explanations have been proposed to account for the observed manifestations of SMSI. These explanations tend to be of two main types: electronic or geometric.

The decrease in carbon monoxide and hydrogen chemisorption capacity was thought to be due to electronic perturbation of metal atoms (11) but Tauster (12) discredits this concept, since even large metal particles suffer this suppression.

Schwab (13) proposed that the interaction between a catalyst and its support, and the subsequent effect on catalytic activity, were determined by the electronic properties of the metal and the support. This took into account the electronic effects in the boundary layer. In 1967, Solymosi (14) stated that the electronic properties of the support played a definite role in determining the catalytic activity of the supported metal for reactions such as formic acid decomposition, ethylene hydrogenation and selective hydrogenation of cyclohexene.

Fung (15) carried out XPS studies on Pt/TiO_2 and concluded that electrons were transferred from the reduced titanium centres to the platinum particles. In 1984, Herrmann (16) found evidence of electron migration from the support to the metal following both low (473K) and high (773K) temperature reduction. He believed that partial or total suppression of hydrogen chemisorption was due to an electronic effect. This electronic effect occurred when the extra electrons saturated unfilled d-orbitals of the surface metals or induced long distance electronic interactions, which counteract M-H bond formation.

When a metal and an oxide are placed in contact, if the work function of the metal is greater than the work function of the oxide, their Fermi levels will spontaneously align enabling electron transfer to take place. The work function of the oxide depends on the reduction state of the oxide: the more reduced the oxide, the smaller its work function and hence the stronger the electron migration to the metal. (16)

Herrmann proposed that when platinum in the SMSI state became strongly enriched in electrons, it tended to resemble its neighbour in the periodic table. Gold, with its d^{10} configuration, is notoriously poor for

hydrogen adsorption and as a hydrogenation catalyst, and Herrmann believes that this explains why platinum in the SMSI state loses its capacity for hydrogen chemisorption.

However, if this was true for platinum, it should also be true for other supported metals entering the SMSI state. In this way, osmium should become more like iridium, and iridium should become more like platinum, and in neither case should this result in suppression of chemisorption. (8)

Chen and White (17) studied platinum on a variety of oxides of titanium using a variety of physical techniques and concluded that the SMSI behaviour depended on the ability of the support to donate electrons to the platinum particles. The XPS results suggested that electron transfer from reduced oxide regions to platinum crystallites occurred through a thin barrier of TiO_2.

Using a variety of electron spectroscopic techniques, Henrich and Sadeghi (18) found that electronic charge was transferred from reduced titanium cations to rhodium particles. This resulted in a partially ionic Rh-Ti bond. Although in this study carbon monoxide chemisorption was not suppressed, the authors believed that the formation of a Rh-Ti bond may be the driving force for encapsulation of rhodium. Thus, the authors have found evidence for modification of the electronic properties of the metal due to its interaction with the support.

Other explanations proposed to account for metal-support interactions are predominantly geometric in nature. The support used may influence the shape of the metal particles through the interfacial energy at the point where the metal and the support are in contact.

If the interfacial energy at the point of contact is high, the metal will tend to spread and maximise the area of contact between the metal and the support resulting in the formation of hemi-spherical particles or even two-dimensional rafts. (8) A low interfacial energy value results in minimal metal-support interaction and three-dimensional particles are usually formed. The support may also influence the crystal habit of the metal particle. For very small particles, icosahedra are more stable than cubes or octahedra of the face-centre cubic structure. (19). However, this preference can be overturned if the interfacial energy where the metal and support are in contact is high. (8)

Electron microscopy studies by Baker et al.(20, 21) produced evidence that, in the SMSI state, platinum had adopted the form of thin, hexagonal, pill-box structures, grown over a reduced oxide of titania, Ti_4O_7.

Although early explanations of SMSI included electron transfer from a partially reduced transition metal oxide support to Group VIII metal crystallites, more recently it has been proposed that the inhibition of chemisorption of carbon monoxide and hydrogen, and the changes in catalytic activity may be due to a combination of local geometric and electronic effects caused by partially reduced oxide species on the surface of the metal crystallites. (22)

The surface layer of oxide species can be formed in two ways. First, following the proposals of Tauster et al. (9), during reduction a Pt/Ti solid solution or intermetallic compound may be formed. According to Cairns et al. (23) partial oxidation of the Ti atoms at the Pt surface could give adsorbed TiO_x with titanium bonded to both platinum and

oxygen. Second, TiO_x produced by partial reduction of the titania support by spillover hydrogen during catalyst reduction may migrate across the platinum surface giving the same result as above. (22)

There is much evidence in the literature for encapsulation of the supported metal by reduced support species. Powell and Whittington (24) studied silica-supported platinum and found evidence of encapsulation of the platinum which converted exposed platinum surface area into platinum-support interfacial area. The driving force for this process was the reduction in free energy of the Pt/SiO_2 system. The encapsulation involved hemi-spherical platinum particles becoming lens-shaped, during which time the platinum particles became partially encapsulated by the SiO_2 support.

The study of metal-support interactions on model catalysts has often provided experimental evidence for encapsulation. Belton et al. (25) studied Rh/TiO_2 and Pt/TiO_2 model catalysts. Their results suggested that encapsulation and electronic interactions occur simultaneously, altering the behaviour of the model catalysts.

Tatarchuk and Dumesic (26), in their study of Fe/TiO_2 model catalysts, produced evidence which suggested that during hydrogen treatment at high temperatures, the support undergoes reduction and the iron diffuses in to the support. This is in contrast to reports (27, 28) of encapsulation for titania-supported Group VIII noble metals, which suggest that it is the reduced suboxide species which migrates on to the supported metal particles.

Belton et al. (29) believed that heating a thin-film model rhodium-titania catalyst at 775K caused Ti and O to migrate through and

segregate at the surface of the thin rhodium overlayer. These authors reported that this blocked sites for hydrogen chemisorption by a combination of site-blocking and electronic effects.

In a further study involving the chemisorption of CO, NO and H_2 on rhodium-titania and platinum-titania thin film model catalysts, Belton et al. (30) reported that TiO_x ($1.0 \leqslant x \leqslant 2.0$) blocked adsorption sites and induced new desorption states. The authors believe that site-blocking cannot fully explain metal-support interactions (SMSI). For example, on Rh/TiO_2, in addition to site-blocking, the TiO_x is believed to change the bonding of CO and NO on Rh. On Pt encapsulated with TiO_x it was observed that hydrogen desorption from nearest neighbour Pt atoms was affected.

In a study of Ni/TiO_2, Baker et al. (31) concluded that although electronic interactions may take place for highly dispersed metal clusters, the origin of SMSI for larger metal particles was due to the presence of reduced support species on the surfaces of the metal particles.

Sanchez and Gazquez (32) published their oxygen vacancy model in 1987 to explain strong metal-support interactions. Vacancies appear when hydroxylated surfaces are dehydrated or when cations of an oxide are reduced by chemical means or by thermal dissociation. In the vacancy model, the metal migrates into the support and becomes covered and buried. The metal atoms occupy anion vacancies. This supports the molecular orbital study of SMSI carried out by Horsley (32) which favoured a model in which platinum atoms were inserted into oxygen anion vacancies in the support, with bonding between titanium cations and platinum atoms.

Haller et al. (33) produced EXAFS evidence for metal-metal bonding in reduced Rh/TiO_2 catalysts. These authors believed that they had found physical evidence for migration of a reduced titania species on to metal particles during heating and reduction by H_2. This migration implied a chemical interaction on bonding of Rh to Ti, which provided the thermodynamic driving force for the movement of the reduced oxide species to the surface of the metal particle. The authors concluded that the migration must result in an electronic and a geometric perturbation of the surface.

Huizinga et al. (34), while working with Pt and Rh on TiO_2 catalysts, observed a phase change in the TiO_2 structure from anatase to rutile, accompanied by a strong decrease in specific surface area of the support from ca. 50 $m^2 g^{-1}$ to 1 $m^2 g^{-1}$, as well as a decrease in carbon monoxide and hydrogen chemisorption capacities, but with no apparent loss in specific metal surface area as observed by electron microscopy. The reduction in total surface area from 50 $m^2 g^{-1}$ to 1 $m^2 g^{-1}$ after reduction of the catalysts at elevated temperature contradicts the work of Tauster et al. (9), who observed no loss in surface area following high temperature reduction; an observation which led them to rule out encapsulation as a possible explanation for the manifestations of SMSI, because there was apparently no change in support structure.

The reaction of carbon monoxide with hydrogen is a structure-sensitive reaction and as such it is to be expected that the activity and selectivity would change if a catalyst in which metal-support interactions were observed was used. Using a catalyst in the SMSI state, for which carbon monoxide and hydrogen chemisorption are observed to be suppressed,

the CO/H_2 reaction shows increased activity and increased selectivity to higher hydrocarbons compared to a catalyst in the non-SMSI state. This suggests that site-blocking (or encapsulation) cannot fully explain SMSI. Belton et al. (29) observed for TiO_2 that although carbon monoxide chemisorption was suppressed, carbon monoxide hydrogenation activity was high. They proposed that new carbon monoxide chemisorption sites created by the presence of TiO_x may be responsible for the enhancement in carbon monoxide hydrogenation rates by facilitating carbon monoxide dissociation on the TiO_x sites. Vannice and Garten (35) stated that for the CO/H_2 reaction on supported nickel catalysts, the catalyst which favoured the more weakly bound CO adsorbed species possessed the higher specific activity: this was found to be the TiO_2-supported catalyst. Studying the CO/H_2 reaction over supported palladium catalysts, Vannice et al. (36) found that the turnover numbers increased in the order:

$$Pd/SiO_2 \ll Pd/SiO_2\text{-}Al_2O_3,\ Pd/Al_2O_3 \simeq Pd/TiO_2\ (448K) < Pd/TiO_2\ (SMSI)$$

They also concluded that the methanation reaction appeared to be structure-insensitive over supported palladium catalysts. Vannice (37) found that for the CO/H_2 reaction, using TiO_2 as a support enhances the activity for Ni, Pd, Pt, Rh and Ir.

Burch and Flambard (38) found very high activity for the CO/H_2 reaction over Ni/TiO_2 under conditions where SMSI were absent. They proposed that the role of titania was to create new active sites at the interface between the metal particles and the support. Under similar

circumstances, the specific activities of Ni/TiO_2 and Ni/SiO_2 were in good agreement for the hydrogenolysis of n-hexane and ethane.

In their study of reactions on model Rh/TiO_2 catalysts, Resasco and Haller (39) found that the activity of the Group VIII metal was affected very little for the structure-insensitive reaction of dehydrogenation, whereas for the structure-sensitive hydrogenolysis reaction, activity was depressed by orders of magnitude. The authors concluded that, following high-temperature reduction, the rhodium reacted with the reduced titania at the edges of the particles. The energy of interaction was sufficient to cause migration of reduced support species on to the rhodium particles. The smallest particles are therefore affected most by this action since the migratory species have to move a shorter distance to reach the centre of small particles. Following high-temperature reduction, there is a greater extent of interaction for the smaller particles for hydrogenolysis. Therefore, migration of reduced support on to small rhodium particles results in an interaction which is strongly deactivating for hydrogenolysis.

Boumarafi (40) studied rhodium and platinum supported on titania, alumina and silica. Chemisorption studies provided evidence of a metal-support interaction for the titania-, and to a lesser extent, the alumina-supported metals. The metal-support interaction, which can be induced by high-temperature reduction, led to a reduction in the amount of carbon monoxide chemisorption. However, there was apparently no effect on the activity, selectivity and butene distribution in the hydrogenation of buta-1,3-diene.

1.4 Hydrogen Spillover

Described as "an apparent metal-support interaction" by Sermon and Bond (8), the phenomenon of hydrogen spillover involves the dissociative adsorption of molecular hydrogen on metal sites. The atomic hydrogen so-formed then migrates to another phase of the catalyst which contains hydrogen acceptor sites but which could not adsorb hydrogen directly under identical conditions. A schematic diagram of hydrogen spillover is shown in fig. 1.1

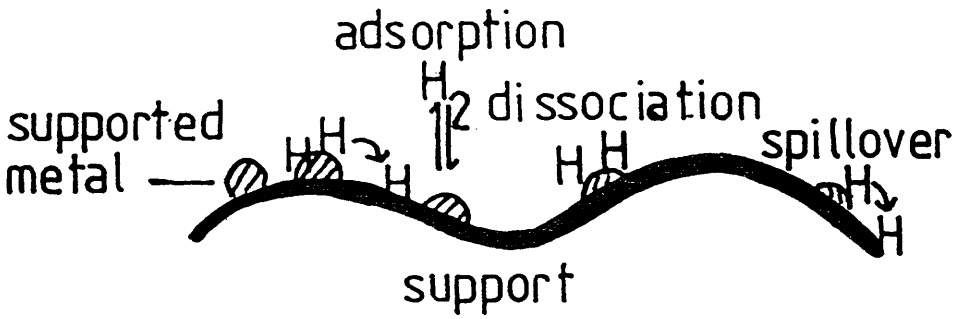

Fig. 1·1 Schematic Diagram of Hydrogen Spillover

Spillover hydrogen may reside on the surface of the support, diffuse into the support and even lead to its partial reduction (41).

Sermon and Bond (42) defined two types of spillover: Primary spillover occurs in systems where the initiating and accepting phases are in contact; secondary spillover occurs where the phases are not in direct contact. Primary spillover is faster and more extensive than secondary spillover.

The first observation of spillover was made by Kuriacose (43) while he was working on the decomposition of germane, GeH_4, on germanium films. He observed that the rate of decomposition of GeH_4 was increased by contact with platinum wire which was present to measure conductivity during the experiments. Although this work was not published until 1967, the observation was discussed by E.H. Taylor (44) at the Second International Congress on Catalysis in 1961. The effect observed by Kuriacose is what is now known as reverse spillover, in which hydrogen atoms migrate back from the support or accepting phase to the metal (in this case platinum) where they can either desorb as molecular hydrogen or react with some other hydrogen acceptor such as oxygen or ethylene.

Khoobiar (45) published the first direct experimental evidence for hydrogen spillover. He was examining the formation of hydrogen tungsten bronze, H_xWO_3, at room temperature from a mechanical mixture of Pt/Al_2O_3 and WO_3. Under the same experimental conditions, neither WO_3 nor Al_2O_3/WO_3 could be reduced at room temperature. On the basis of this work, Khoobiar concluded that the mechanism of hydrogen spillover was dissociative adsorption at the platinum centres followed by migration of H^+ or $H^\cdot$ across the alumina surface and diffusion to WO_3. The rate of hydrogen spillover was found to depend more on the nature of the initiating phase (46). An example of this is the spillover of hydrogen to carbon which only takes place at temperatures above 350°C (47, 48) compared to room temperature spillover for Pt to WO_3 or MoO_3. Hydrogen spillover will only occur when the metal content is above 0.0008% w/w. Furthermore, increasing the metal content above 0.8% has

no further influence on the spillover process. (49)

The addition of small quantities of metal catalysts such as Pt or Pd has been shown to substantially lower the temperature of reduction of oxides such as MoO_3, WO_3 and V_2O_5. (50) For example, for Pd/MoO_3, the reduction temperature of the MoO_3 is lowered by 400°C by formation of atomic hydrogen on the palladium which then spills over on to the MoO_3 resulting in its reduction. The presence of small amounts of metallic platinum or palladium in an alumina-supported NiO catalyst enhances the activation of the catalyst by hydrogen. Atomic hydrogen formed on palladium or platinum spills over to the NiO enabling reduction of the NiO to take place at a lower temperature and, therefore, lessens the possibility of sintering. (51)

Boudart et al. (46) demonstrated the requirement for the presence of water or some other proton acceptor during the spillover process. Levy and Boudart (52) studied a variety of co-catalysts with varying proton affinities and concluded that a solvated proton was formed on the surface of the metal. More recently, Ambs and Mitchell (53) studied the effect of water on the spillover of hydrogen on platinum-alumina. They concluded that when water was present in the catalyst, it reacted with the alumina to form surface hydroxyls which act as bridges, enabling H-atoms to migrate further than if no water had been present.

The phenomenon of hydrogen spillover is believed to take place via surface rather than gas phase transport of hydrogen species. (54) The passage of H-atoms from the metal to the support may be the rate-determining step in the spillover process. Stepping-stone molecules such as water, alcohols or even grease, may be adsorbed on the support close

to the edge of the metal particles to facilitate transport of H-atoms across the phase boundary. Carbon present on the surface of a catalyst can act as a bridge between the metal and the support, facilitating hydrogen spillover. (49)

Hydrogen can spill over on to irreducible oxides such as Al_2O_3 and SiO_2. Such oxides show no evidence of being reduced, even at temperatures of 500°C. Although it is unlikely that spillover occurs to any appreciable extent to irreducible oxides, evidence for its occurrence comes from the exchange of the surface -OH groups with deuterium. (55) This exchange reaction is a sensitive indicator of the occurrence of spillover since exchange is extremely slow when no metal is present. (56)

When hydrogen spills over on to reducible oxides such as MoO_3 and WO_3, hydrogen metal bronzes can be formed at or just above ambient temperature. (57) A fuller description of the formation, structure and reactivity of hydrogen metal bronzes will be given in section 1.5.

Spillover of hydrogen onto partially reducible oxides such as TiO_2 can lead to the formation of Ti^{3+} and OH^- ions for Rh/TiO_2 or Pt/TiO_2. (58) Partial reduction of the support followed by its migration to the metal particles can give rise to metal-support interactions which alter the chemisorption and catalytic properties of the catalyst. NMR and TPD studies of Rh/TiO_2 have shown two types of adsorbed hydrogen, namely metal-bound H and surface hydroxyls. (59)

Bond and Tripathi (60) found that a requirement for the catalysed reduction of a metal oxide was the availability of an oxidation state one below that in the oxide being reduced. They found that Pd/SiO_2 catalysed the reduction of V_2O_5, Cr_2O_3, MoO_3, WO_3, UO_3, Re_2O_7

and Co_3O_4. Each of these oxides was reduced at markedly lower temperatures than in the absence of the supported metal. On the other hand, with CuO, Cu_2O, NiO, ZnO, CdO and SnO_2, the presence of Pd/SiO_2 had little effect on the reduction rates.

Spillover hydrogen can undergo a reverse migration process whereby the atomic hydrogen migrates back to the metal particles where it can either combine to form molecular hydrogen, which can then desorb, or it can react with a hydrogen acceptor such as oxygen or ethylene.

In the majority of cases if spillover hydrogen is to react, it must first undergo reverse spillover from the support to the metal. Sermon and Bond (61) titrated hydrogen adsorbed on silica-supported platinum using pent-1-ene. They found that the pent-1-ene first reacted with the hydrogen chemisorbed on the platinum to form n-pentane. Only after all the platinum-bound hydrogen had reacted did the hydrogen on the silica migrate back to the platinum where it reacted with 1-pentene to form n-pentane and the pent-2-enes. Sermon and Bond (41) believed that spillover may enhance the activity of supported metals as heterogeneous catalysts.

Teichner et al. (62) found that hydrogen was adsorbed on alumina in the presence of a Ni/Al_2O_3 catalyst. After the catalyst was removed, ethylene in a hydrogen-ethylene mixture was converted into ethane. The amount of ethane formed was found to be much higher than the amount of hydrogen initially adsorbed on the alumina. The authors concluded, therefore, that the reaction was catalytic and that the reaction used hydrogen from the gas phase instead of a simple addition of the hydrogen pre-adsorbed on the alumina to the ethylene.

The authors also found that the spillover hydrogen could be removed by evacuation at room temperature, implying that spillover H or D was only weakly bound to the surface.

Lenz and Conner (63) found that silica could be activated using hydrogen spillover without direct contact between the silica and the supported metal. Hydrogenation and exchange activity was induced, which was found to be independent of the metal. The induced catalytic activity was an activated process, which required high temperatures and long contact times. The hydrogenation mechanism was found to be similar to that on metal oxides and, as such, the molecular identity of the reacting hydrogen was retained.

Teichner et al (64) found that silica gel could be activated for the hydrogenation of ethylene at temperatures as low as 170°C. The spillover hydrogen adsorbed on the surface of the silica inhibited the hydrogenation of the first sample of ethylene, resulting in an induction period at the start of the catalytic reaction of ethylene and hydrogen. Ethylene and hydrogen are strongly chemisorbed on distinct sites. However, competitive adsorption of these reactants takes place when hydrogen is present in large excess and the ethylene is displaced.

Henderson and Worley (65) studied the methanation reaction over supported rhodium catalysts. They used D_2 as a reducing gas and observed isotopic exchange for both CO_2/D_2 and CH_4/D_2 mixtures. The mechanism of the isotopic exchange involved migration of hydrogen from the support to the rhodium sites by reverse spillover. The reverse spillover was believed to enhance the dissociation of CO_2 on supported Rh catalysts in the absence of H_2 gas.

Altham and Webb (66) investigated the behaviour of ^{14}C-ethylene, ^{14}C-propylene and tritium on platinum supported on alumina and silica. They found evidence which showed that hydrogen migration between the metal and the support was of significance. The rate of hydrogen exchange between the gas phase and the tritiated catalyst was found to be fast relative to the rate of reaction of the adsorbed hydrocarbon with hydrogen. It was concluded that the support may play an important role in determining catalytic activity in reactions involving hydrogen and hydrocarbons.

Baumgarten et al. (67), however, questioned the importance of spillover hydrogen in direct reactions during conversion of hydrocarbons with alumina as a support. They found that although $OH\text{-}D_2$ exchange took place, the spillover hydrogen leading to this exchange was unable to hydrogenate unsaturated carboyxlic acids to a detectable degree.

1.5 Hydrogen Metal Bronzes

Hydrogen metal bronzes, H_xMO_3, can be formed from metal oxides with an incomplete d shell, and for which the nd electron energy is higher than the (n+1)p electron energy. (68) Examples of oxides which form hydrogen metal bronzes are molybdenum(VI) oxide, MoO_3, and tungsten(VI) oxide, WO_3.

The term "bronze" was originally used by Wohler (69) in 1825 to describe Na_xWO_3, but it is now used to describe a variety of crystalline phases of transition metal oxides.

Hydrogen metal bronzes are formed from atomic hydrogen. Catalytically, this is achieved by hydrogen spillover. Finely divided platinum or palladium particles are dispersed on the oxides by impregnation of an aqueous salt or by mechanically mixing the oxide with the supported platinum or palladium catalyst or with platinum or palladium blacks. When compounds formed in this way are brought into contact with molecular hydrogen, hydrogen atoms are produced on the metal particles by dissociative adsorption, and the hydrogen atoms then diffuse inside the host lattice with or without the help of a co-catalyst. The hydrogen metal bronzes formed in this way are insertion compounds. In hydrogen tungsten bronzes, H_xWO_3, x lies in the range $0 < x < 0.6$ (70), whereas for the analogous hydrogen molybdenum bronzes H_xMoO_3, $0 < x < 2$. (71) The bronzes formed by hydrogen spillover are $H_{0.4}WO_3$ and $H_{1.6}MoO_3$. (57)

Hydrogen metal bronzes may be potentially useful for the purposes of storing hydrogen, as hydrogenation catalysts or as gas sensors. (71)

Both molybdenum trioxide and tungsten trioxide are based on the distorted rhenium trioxide structure although they are not isostructural.

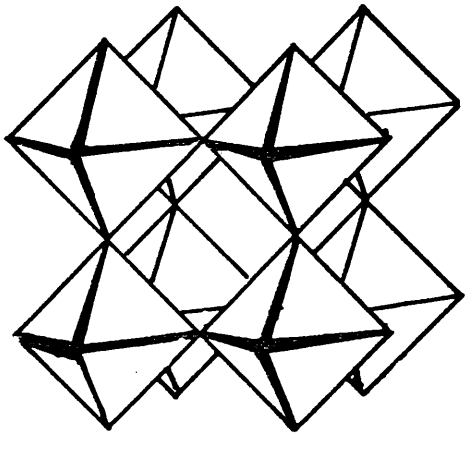

Fig. 1·2 Crystal Structure of ReO_3

Both MoO_3 and WO_3 are built of octahedral MO_6 groups. MoO_3 has a unique layer structure in which each octahedral MoO_6 group shares two adjacent edges with similar groups and in a direction perpendicular to the plane the octahedra are linked through vertices. (72) Fig. 1.2 shows the crystal structure of ReO_3. Fig. 1.3 shows the layer structure of MoO_3.

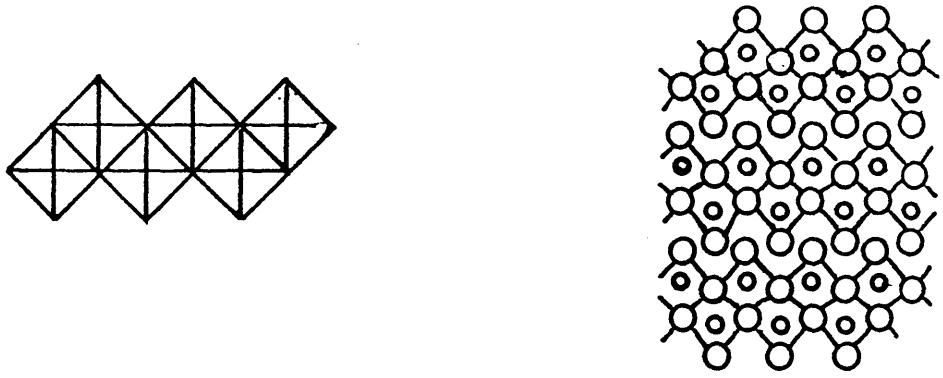

Fig. 1.3 Layer Structure of MoO_3

Tungsten trioxide has a monoclinic structure at ordinary temperatures.

The bronzes H_xMoO_3 and H_xWO_3 are formed topotactically, characterised by the fact that they are formed without any major structural change to the layer lattice. Dickens et al. (73) found that the x-ray powder patterns of the H_xMoO_3 bronze closely resembled that of MoO_3 from which they concluded that hydrogen had been readily inserted into the parent oxide with little crystallographic rearrangement.

By carrying out elastic and inelastic neutron studies of hydrogen metal bronzes, Dickens et al. (73) were able to conclude that hydrogen was present as -OH groups in $H_{0.4}WO_3$ and $H_{0.34}MoO_3$. However, for bronzes with a higher hydrogen content, they found evidence that hydrogen was present in the form of $-OH_2$ groups. This was confirmed by solid state NMR studies carried out on $H_{0.36}MoO_3$ and $H_{1.71}MoO_3$. (74) On the basis of these results, Slade et al. (74) suggested that $H_{0.36}MoO_3$ and $H_{0.4}WO_3$ should be formulated as oxide hydroxides $MO_{3-x}(OH)_x$. The molybdenum and tungsten oxide bronzes are believed to have analogous structures at these similar hydrogen contents. (74)

Figure 1.4 shows the positions of hydrogen atoms in $H_{0.36}MoO_3$ and $H_{1.68}MoO_3$. For comparison, the structure of MoO_3 alone is shown. This indicates that little structural rearrangement takes place on bronze formation.

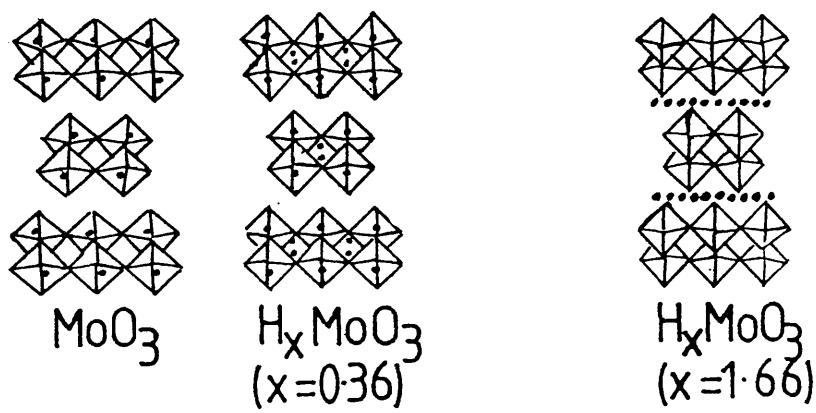

Fig. 1·4 Structures of MoO_3 and H_xMoO_3

Ritter et al. (75) carried out NMR studies on hydrogen molybdenum bronzes prepared electrochemically. They found that for $x < 0.85$ in H_xMoO_3 almost all hydrogen was intralayer, lying along a zig-zag line connecting vertex-sharing oxygen atoms of the MoO_6 octahedra, as shown in Figure 1.5.

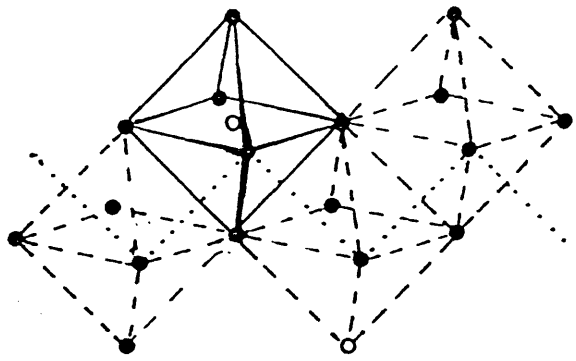

Fig. 1.5 Intralayer Positions of Hydrogen Within H_xMoO_3

For higher values of x, the hydrogen starts to occupy interlayer positions coordinated with terminal oxygen atoms at the van der Waals' gap. Figure 1.6 shows the intra- and inter-layer hydrogen positions for $H_{1.66}MoO_3$ and $H_{2.0}MoO_3$

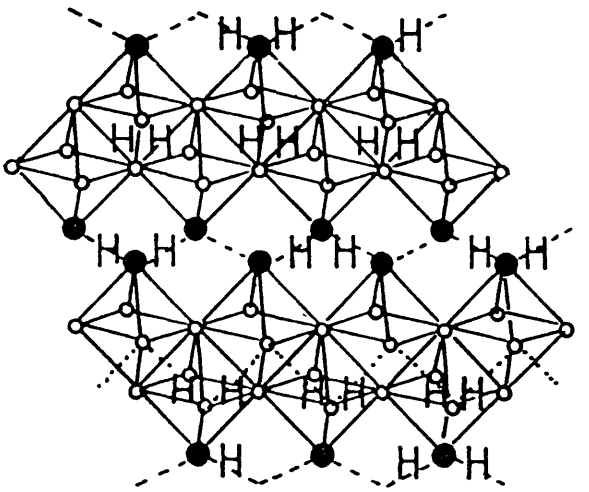

Fig. 1·6 Intralayer and Interlayer Proton Positions in H_xMoO_3

For $H_{1.66}MoO_3$ about half the protons reside in the interlayer positions associated with terminal oxygens in the van der Waals' gap. (75) Fripiat et al. (76) carried out proton NMR studies on hydrogen molybdenum bronzes, and concluded that there was predominantly only one type of proton present. Evidence indicated that this was not a hydroxyl proton.

Sienko and Oesterreicher (77) studied hydrogen tungsten bronze using infrared and electron spin resonance techniques. They found no evidence for the existence of -OH in H_xWO_3. However, Dickens et al. (70), concluded that hydrogen tungsten bronzes H_xWO_3 ($0 < x < 0.6$) could be classified as oxide hydroxides $WO_{3-x}(OH)_x$ and by carrying out NMR studies they found that the H atoms participated in a hydroxyl bond. The $WO_{6-2x}(OH)_{2x}$ octahedra link together forming a distorted ReO_3 structure, with an H atom directed towards an O atom of a neighbouring octahedron. This work of Dickens et al. (70) was confirmed by Wright (78), who carried out inelastic neutron scattering experiments on $H_{0.4}WO_3$ and found that the spectra produced

showed only vibrations which would be expected of a metal hydroxide.

Structural modifications to MoO_3 can take place during the formation of $H_{1.6}MoO_3$ from spillover hydrogen. When the hydrogen atoms enter the MoO_3 lattice, there is a tendency for the oxide to cleave in planes parallel to its c crystallographic axis. (79) This results in an increase in surface area, but is also decreases the contact between the metal particles, for example, platinum, and the oxide layers. There is also a tendency for rather large clusters of metal particles to form. The surface area can increase from around 1 m^2 g^{-1} for MoO_3, by a factor of two or three. (68)

H_xWO_3 can be decomposed under vacuum or by thermal treatment. Crystalline hydrogen tungsten bronzes are stable in vacuo to temperatures greater than 400K. (79) However, they are unstable in air with respect to oxidation. Over the temperature range 470-670K, decomposition of H_xWO_3 takes place with the formation of both H_2 and H_2O as gaseous products, indicating that decomposition and disproportionation occur simultaneously at elevated temperatures. (80)

Hydrogen molybdenum bronzes undergo dehydrogenation and dehydration under vacuum at temperatures higher than 120°C, and in flowing H_2 at temperatures higher than 100°C. (80) Water molecules are formed from inserted hydrogen atoms and lattice oxygen atoms. The removal of lattice oxygen atoms in the form of water is accompanied by structural modifications. As a result, the external layers of the oxide become partially amorphous. Depletion of hydrogen affects the outer layers first.

Decomposition of hydrogen metal bronzes due to thermal and/or vacuum treatment leads to reduction of the molybdenum or tungsten trioxides to lower oxides. (79) Beyond a certain value, elimination of hydrogen as water becomes irreversible and the bronze can no longer be restored to its initial state.

Within $H_{1.7}MoO_3$, Mo can exist in the +4, +5 and +6 oxidation states. (81) Lower oxides such as Mo_2O_5 and MoO_2 are formed on reduction of MoO_3. Structurally these lower oxides are quite different to MoO_3. Figure 1.7 shows the structure of MoO_2 which is based on a distorted rutile structure.

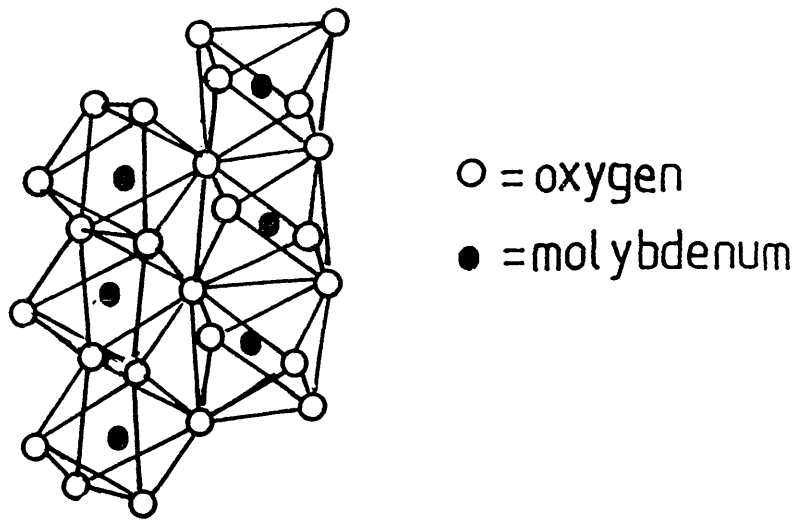

Fig. 1·7 Rutile Structure of MoO_2

Dehydration of MoO_3 at around 200°C leads to the formation of Mo_2O_5. The behaviour of Mo_2O_5 formed in this way is different to the normal oxide of this composition. (55)

The hydrogen metal bronzes H_xMO_3 (M = Mo or W) formed by hydrogen spillover may become catalytically active. Sermon and Bond (57) found that the chemical stability and reactivity of hydrogen molybdenum bronze, $H_{1.6}MoO_3$, and hydrogen tungsten bronze, $H_{0.5}WO_3$, was different. They found that it was more difficult to remove hydrogen from $Pt/H_{1.6}MoO_3$ than from $Pt/H_{0.5}WO_3$ by reverse spillover using oxygen or other hydrogen acceptors.

It is believed that for spillover hydrogen to react, it must first undergo the process of reverse spillover from the support back to the metal. Removal of hydrogen from the hydrogen metal bronzes must occur via reverse spillover since H_xWO_3 alone in air is stable at ambient temperature (41), whereas the introduction of air into a mixture of Pt/Al_2O_3 and WO_3 at ambient temperature leads to re-oxidation of the bronze. (82) It is generally believed that spillover hydrogen on supports is rather unreactive. (64)

The rate of hydrogenation of hydrogen acceptors such as ethylene or oxygen gives a measure of the rate of reverse spillover. This rate depends on the concentration of spillover hydrogen, its stability on the support and the degree of contact between the metal and the hydrogen acceptor phase. (55) The rate of reverse spillover is lower than the rate of spillover. (79)

$H_{1.6}MoO_3$ containing Pt reacts with ethylene at 160°C to form ethane. The reaction rate depends on the platinum content, and can be increased by the presence of gaseous hydrogen. The platinum particles are regarded as "gates" by which the H-atoms leave the host oxide by a reverse spillover process. The platinum particles are also

believed to be the catalytic sites (79, 80) which are in contact with the bronze, which thereby acts as a hydrogen reservoir. (80) For the hydrogenation of ethylene to ethane, about 30% of the initial hydrogen content can be removed, whereas about 90% of the initial hydrogen content can be removed by treatment with oxygen. (80)

Benali et al. (83) found that hydrogenation of ethylene on $H_{1.6}MoO_3$ took place in the absence of the Pt/Al_2O_3 required to produce the bronze. Reaction commenced at ca. 80°C and resulted in the transformation of $H_{1.6}MoO_3$. From this, the authors concluded that palladium or platinum particles did not need to be present to act as gates through which the H atoms could leave the host lattice to hydrogenate ethylene. If gaseous hydrogen is present, $H_{1.6}\ MoO_3$ can catalyse the hydrogenation of ethylene without structural modifications. (83) Fripiat et al. (79) found that for the hydrogenation of ethylene over H_xMoO_3, the reaction rate increased with increasing hydrogen pressure, indicating that the gaseous hydrogen was consumed before the spillover hydrogen.

Jackson et al. (84) investigated the hydrogenation of carbon monoxide over Group VIII metals supported on molybdenum trioxide and tungsten trioxide. By using these supports rather than silica, a rate enhancement of up to two orders of magnitude was observed for Ni, Ru, Rh and Pd. Iron showed no such enhancement in activity. The authors suggested that fast spillover and reverse spillover took place under reaction conditions, resulting in a higher effective hydrogen concentration and hence an increase in reaction rate. No such enhancement was observed with iron and this was attributed to its inability to facilitate the fast spillover/reverse spillover necessary to enhance rates.

Sachtler (85) proposed that the rate determining step in the hydrogenation of carbon monoxide to hydrocarbons was the addition of hydrogen to CH_x species. Therefore, an increase in hydrogen concentration at the surface should enhance the reaction rate. In the case of M/MoO_3 or M/WO_3, the increase in hydrogen concentration could be provided by reverse spillover of hydrogen from the support to the metal. (84)

1.6 Reactions Over Supported Metal Catalysts

Group VIII metals such as platinum and rhodium are frequently used to catalyse hydrogenation reactions. Hydrogenation is generally considered to be a structure-insensitive reaction. It would, therefore, be expected that such a reaction would be relatively unaffected by metal-support interactions. Any observable differences could simply be due to differences in methods of catalyst preparation. (8)

In the present study, the hydrogenation of buta-1,3-diene over supported platinum and rhodium catalysts has been of particular interest. The selective hydrogenation of buta-1,3-diene is a reaction of practical importance for the purification of C_4-olefins containing residual buta-1,3-diene (86) whilst hydrogenation of diolefins is an important reaction in oil refining, especially in reforming. (87)

The study of conjugated diolefins in particular is appropriate because studies may show a preference for a catalyst to produce mono-olefins rather than alkanes, or vice-versa. In addition, hydrogenation of such alkadienes may lead to preferential production of one isomer of the olefin rather than another. (88)

In 1965, Wells et al. (89) published the first of a series of papers on the hydrogenation of alkadienes catalysed by Group VIII metals. During the course of this work, the authors examined the selectivity of various catalysts in the production of butenes, selectivity (S) being defined as

$$S = \frac{\text{(yield of butenes)}}{[\text{(yield of butenes)} + \text{(yield of butane)}]}$$

It was discovered that, in the majority of cases, the initial products of the hydrogenation of buta-1,3-diene were 1-butene, trans-but-2-ene, cis-but-2-ene and n-butane. The exception to this was palladium, which was found to be totally selective for butene formation. (88)

Negative or zero orders of reaction in butadiene and positive orders in hydrogen indicated that the alkadiene was the more strongly held reactant. (88) Butene re-adsorption was found to be slow before around 80% removal of the alkadiene. (88) This led the authors to conclude that the relative order of the strengths of adsorption of reactants and products in the hydrogenation of butadiene was:

buta-1,3-diene > butenes > hydrogen > n-butane (88)

Since buta-1,3-diene is observed to be more strongly adsorbed than butene, this may imply that the buta-1,3-diene is adsorbed by the interaction of both olefinic linkages to the surface. (88)

In the adsorbed state, buta-1,3-diene must be bonded via either four carbon-metal σ-bonds, one bond per carbon atom:

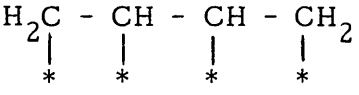

(* represents a surface site)

in which case the carbon exhibits sp^3 hybridisation; or as a di-π-adsorbed species, in which case two π-bonds are formed between the surface and the olefinic linkages, and the carbons retain their sp^2 hybridisation:

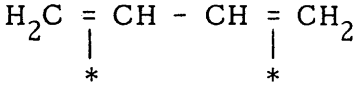

(89)

Bond and Wells (85) believed that there was more internal strain on the σ-bonded species in view of its sp^3 hybridisation and as such, concluded that the di-π adsorbed species was more likely.

Di-adsorbed buta-1,3-diene can adopt one of two possible conformations:

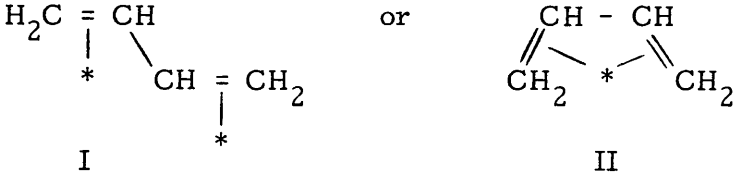

I or II

In species II, the bonds may retain their olefinic character, or the electrons may delocalise over all four carbons, giving species III:

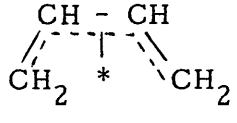

III

A recent publication by Oudar et al. (87) on the hydrogenation of buta-1,3-diene on Pt (110) proposed that buta-1,3-diene was initially adsorbed

in the valleys of the (110) plane, as shown in Figure 1.8

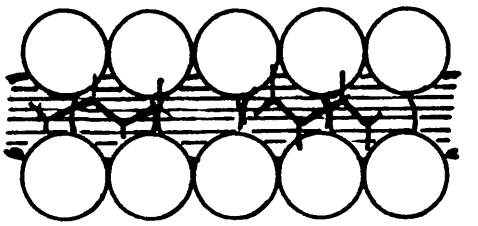

Fig. 1·8 Model of Buta-1,3-diene Adsorption on Pt (110)

The first level saturation corresponds to one molecule of buta-1,3-diene for two Pt atoms. In the second stage of adsorption, the species are adsorbed on the top-most layer of Pt atoms. In the first stage, buta-1,3-diene molecules are believed to be adsorbed flat whereas for the second stage, the species are believed to be adsorbed in the form of butadienyl or butylidine species, corresponding to one buta-1,3-diene species per Pt atom.

Hydrogenation reactions proceed by the following steps:

i) adsorption of one, or both, reactants

ii) formation of one, or more, half-hydrogenated states

iii) reaction of half-hydrogenated state with hydrogen to give product.

This can be shown schematically for the hydrogenation of buta-1,3-diene:

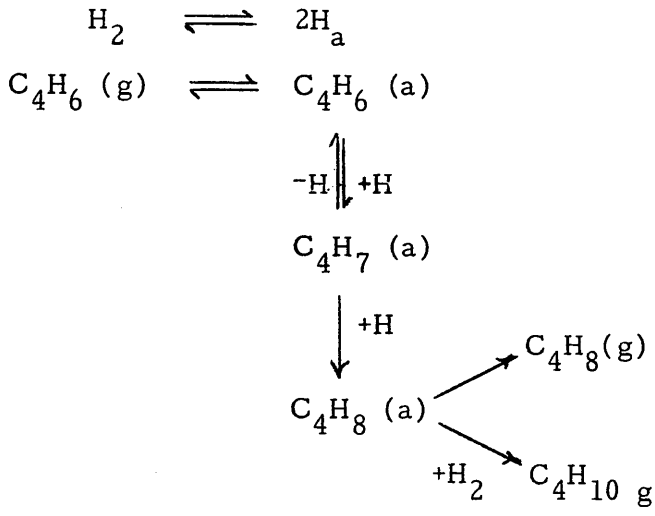

C_4H_7 (a) is the half-hydrogenated state. Using deuterium as a tracer, Bond and various co-workers (90-93) showed that the formation of the half-hydrogenated state was a readily reversible step.

But-1-ene is formed from buta-1,3-diene by 1,2-addition of two hydrogen atoms (88):

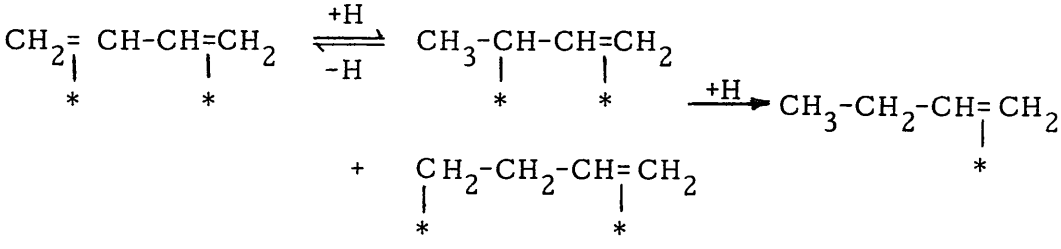

But-2-ene may be formed by the 1,4-addition of two hydrogen atoms to adsorbed buta-1,3-diene:

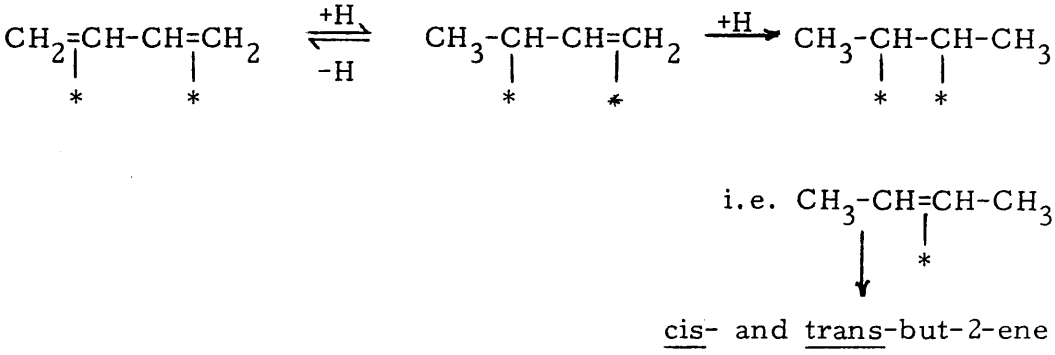

However, but-2-ene may also be formed by isomerisation of but-1-ene formed by 1,2-addition. If but-2-ene is formed by 1,4-addition of hydrogen to buta-1,3-diene, the conformation of the adsorbed C_4H_7 determines the configuration of but-2-ene produced.

In the gas phase, the proportions of syn- and anti-buta-1,3-diene lie in the range 93-97% and 3-7%, respectively. (94)

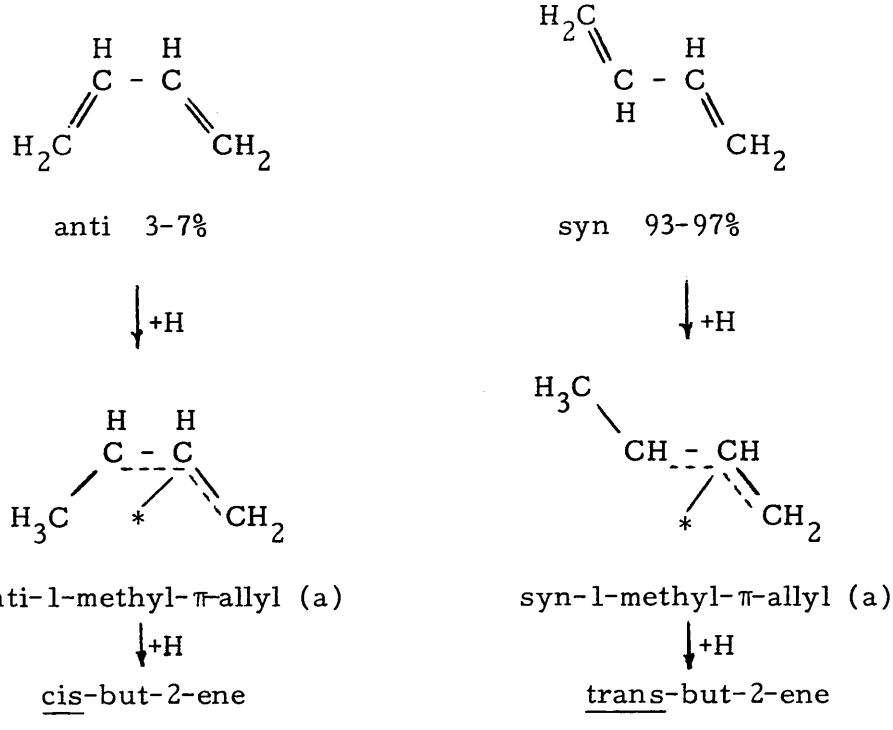

Wells et al. (88) suggest that the relative proportions of adsorbed anti- and syn-buta-1,3-diene reflect the proportions found in the gas phase, and that in addition, neither the conformations of adsorbed buta-1,3-diene nor the conformations of adsorbed C_4H_7 readily interconvert.

The results shown would seem to indicate that a high ratio of adsorbed I:adsorbed III, i.e.

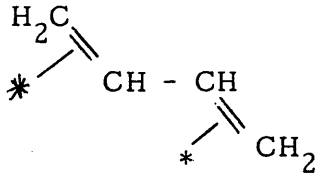

I

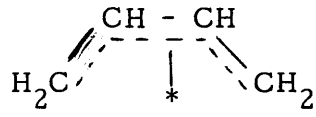

III

results in a high trans:cis ratio. This has been found to be the case for palladium. (88) Lower trans:cis ratios are obtained over metals which are better isomerisation catalysts. In fact, the trans:cis ratios obtained from studies of 1-butene isomerisation over the same metals correlate very well with the ratios found for buta-1,3-diene hydrogenation (88) indicating that but-2-ene is almost certainly formed by isomerisation of 1-butene. Only a small proportion of but-2-ene yield is formed by the 1,4-addition process. The low amount of but-2-ene formed over palladium apparently occurs because, once formed, the butenes cannot readily readsorb on the surface. Therefore butene isomerisation cannot take place easily under these circumstances, despite the fact that Pd is a good isomerisation catalyst.

In 1969, Wells et al. (95) proposed a mechanism for the gas phase hydrogenation of buta-1,3-diene. In the selective hydrogenation over alumina-supported iron, cobalt, nickel and copper, and cobalt and nickel powders, two types of behaviour could be observed. In type A, the yield of but-1-ene was high and the trans:cis ratio in but-2-ene was low. In this case, mechanism A was followed. In type B behaviour the but-1-ene yield was relatively low, a high trans:cis ratio was observed and mechanism B was followed. Type A behaviour was

Mechanism A

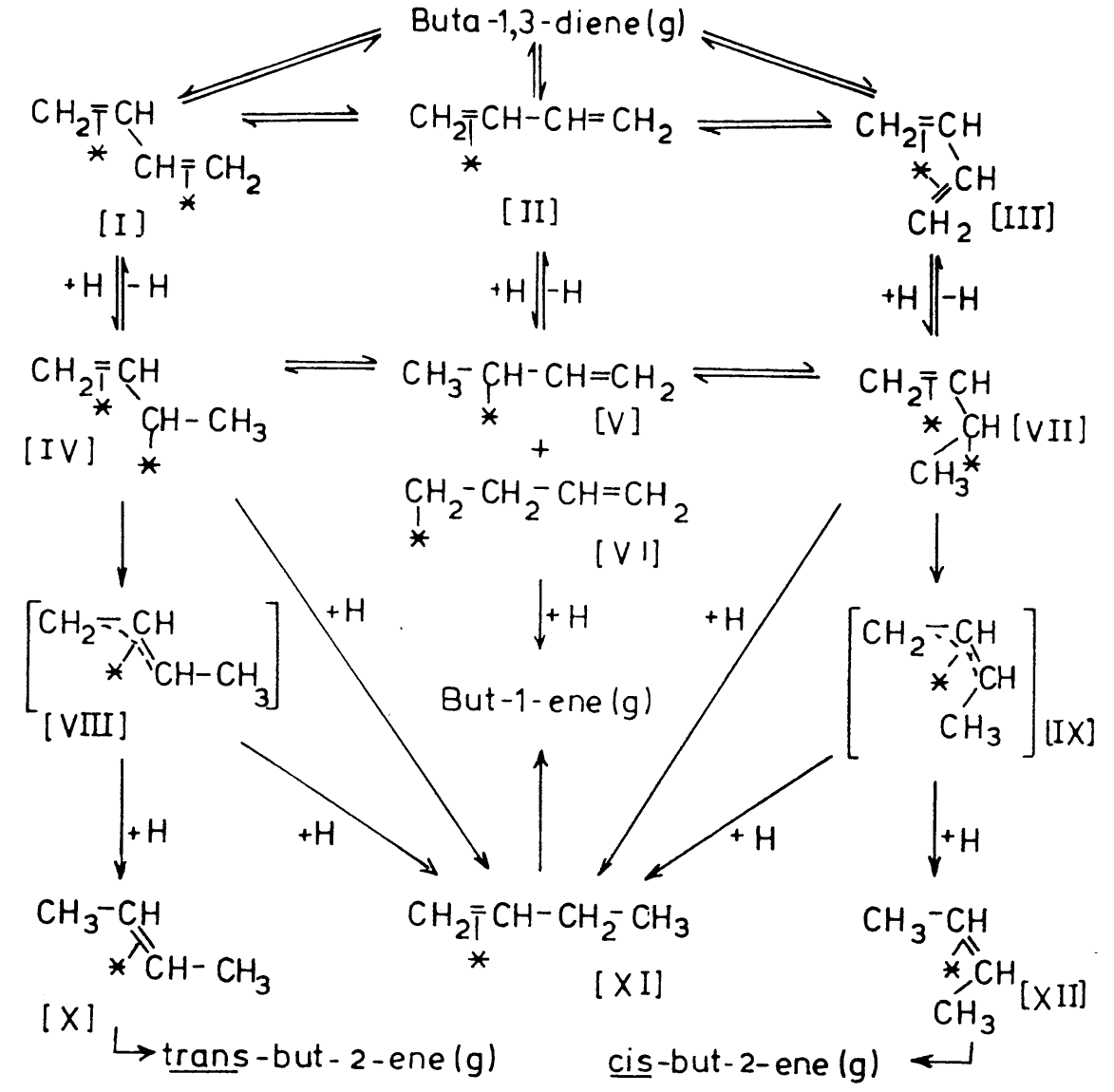

Mechanism B

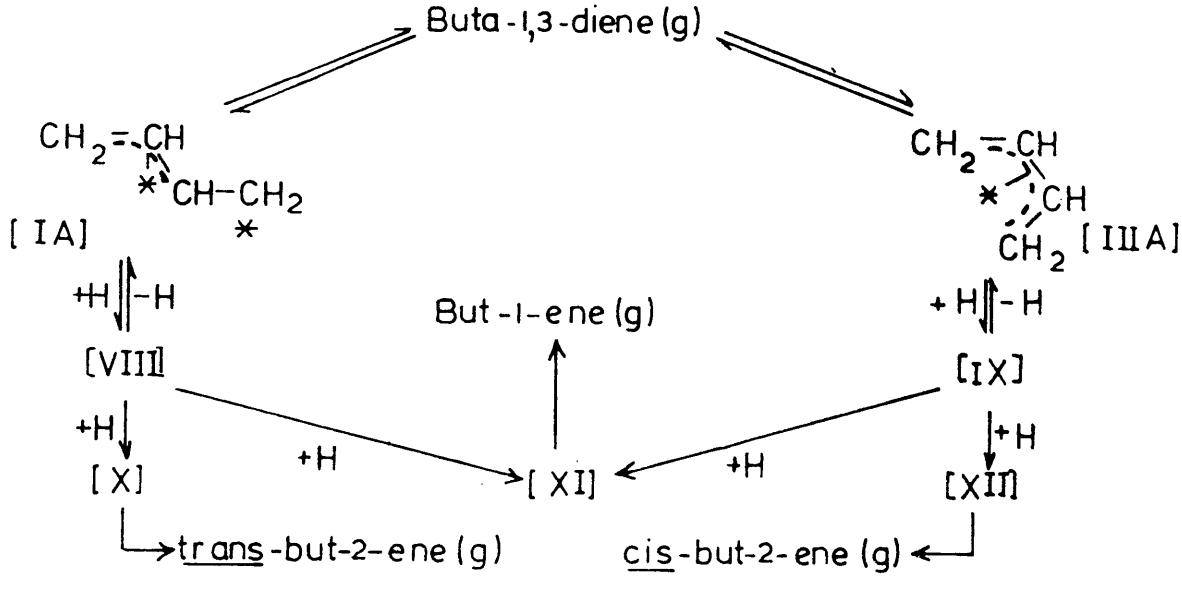

observed for iron, cobalt and nickel reduced below 350°C. Cobalt and nickel reduced above 400°C showed type B behaviour. In this way it can be seen that the hydrogenation of buta-1,3-diene can lead to the formation of 1-butene, trans-but-2-ene, cis-but-2-ene and n-butane.

In 1970, Wells et al. (96) published their work on the reaction of buta-1,3-diene with deuterium catalysed by rhodium, palladium and platinum. This study provided evidence that over these metals, but-1-ene occurred by 1,2-addition of hydrogen atoms to buta-1,3-diene and that but-2-ene formation occurred by 1,4-addition of hydrogen atoms to buta-1,3-diene rather than by the initial formation and subsequent isomerisation of but-1-ene.

More recently, buta-1,3-diene hydrogenation studies have been carried out on Pt single crystals. Oudar et al. (97) compared buta-1,3-diene hydrogenation on Pt (100) and Pt (110) and found that, under steady state conditions, the surface is covered with a reproducible hydrocarbon deposit. They believe that on Pt (110) the deposit is $C_4H_6(a)$, whereas on Pt (100) the deposit is $C_4H_7(a)$. In both cases the activation energies are nearly the same at around 33 kJ mol^{-1}. Heat treatment above 250°C on Pt (110) and 200°C on Pt (100) leads to irreversible poisoning.

Boitiaux et al. (98, 99) carried out studies on liquid phase hydrogenation of unsaturated hydrocarbons over platinum, rhodium and palladium. Their reason for carrying out the reactions in the liquid phase was to mimic conditions used industrially (liquid phase, low temperature, super-atmospheric pressure) where such conditions are

chosen to avoid the excessive energy consumption involved in vaporisation and condensation, and also to continuously wash the catalyst free from oligomers either present in the feed-stock or formed during the reaction. These authors found that buta-1,3-diene hydrogenation was sensitive to palladium dispersion. At high dispersion, very strong complexes were formed between the hydrocarbons and the small particles. The hydrogenation reaction mainly followed the 1,2-addition pathway, together with a small amount of 1,4-addition of hydrogen atoms. Hydrogenation of 1-butene only occurs after high buta-1,3-diene conversion, a consequence of the greater strength of adsorption of buta-1,3-diene than the butenes. It was also observed that the rate of 1-butene hydrogenation was faster than the rate of buta-1,3-diene hydrogenation. However, if 1-butene was present in a feed-stock, it was hydrogenated more rapidly than 1-butene formed from buta-1,3-diene. The difference is believed to be due to the presence of but-2-enes, in the latter case, which cover a non-negligible part of the surface.

In the case of palladium, the turnover number for buta-1,3-diene decreases with increasing dispersion. However, the turnover number for buta-1,3-diene on platinum is constant for dispersion in the range 3 to 99%. (98) Boitiaux et al. (99) report that rhodium shows a sensitivity to dispersion for the hydrogenation of buta-1,3-diene and but-1-yne, whereas platinum only shows the sensitivity to dispersion for but-1-yne hydrogenation.

Hydrogenation reactions are generally believed to be structure insensitive. However, Boitiaux et al. (98, 99) have shown variations in

turnover numbers with changes in metal dispersion. These authors proposed that the rate constant k was constant, irrespective of dispersion, but that the rate equation contained a "multicomplexation constant", K', which was sensitive to metal dispersion. K' increases with increasing dispersion, and is a linear combination of the influences of metallic sites of various coordination numbers. (98)

The hydrogenation of carbon monoxide is a structure-sensitive reaction and, as such, it is to be expected that reaction rate and selectivity may be affected by metal particle size and morphology, as well as by electronic effects.

Where the ratio of hydrogen to carbon monoxide is greater than or equal to three, the most likely reaction is the so-called methanation reaction:

$$CO + 3H_2 \rightleftharpoons CH_4 + H_2O$$

The methanation reaction is particularly important in industry, where it is used routinely to eliminate carbon monoxide, which may be present in small amounts in hydrogen-rich gases such as those used for ammonia synthesis, by converting it to methane and thereby preventing catalyst poisoning. The reaction is also carried out to produce a methane-rich fuel with a low carbon monoxide content. (100)

The earliest work on methanation was carried out by Sabatier and Senderens (101), who found that nickel was an extremely efficient catalyst for this reaction. The same authors then extended their study from nickel to include other metals. (102) They found that copper, iron,

platinum and palladium did not form active catalysts. In 1925, Fischer et al. (103) published a paper on the methanation activities of various metals. They found that the order of activity was:

$$Ru > Ir > Rh > Ni > Cr > Os > Pt > Fe > Pd$$

However, research by Vannice (104) showed that when the specific activities were calculated, taking into account the metal surface area, the order of specific activity was:

$$Ru > Fe > Ni > Co > Rh > Pd > Pt > Ir$$

Vannice (104) concluded that particle size effects and metal-support interactions should also be taken into consideration. He found that Ru, Fe, Ni and Co had large average particle sizes ($> 100\text{Å}$ diameter) and suggested that, because of this, their behaviour is more like that of unsupported metals. Rh, Pt, Ir and Pd were more highly dispersed and had average particle sizes $\lesssim 40\text{Å}$.

In his study of the kinetics of the methanation reaction over supported metals, Vannice (105) found a correlation between the strength of the metal-CO bond and the specific activities of the metals in the synthesis reaction. The highest activity is observed for the lowest M-CO bond strength. Further evidence of this effect was found when Vannice (106) investigated the formation of methane over supported and unsupported platinum and palladium. The reaction was observed to proceed much more rapidly over the supported metal catalysts. Since

the catalysts had been characterised by carrying out carbon monoxide and hydrogen chemisorption experiments, the specific activities for the reaction could be calculated for each catalyst. It was observed that the increase in specific activity was related to an increase in the surface concentration of the more weakly bound CO species. For platinum, this was found to be a particle size effect. An increase in platinum dispersion by a factor of greater than 200 led to an increase in specific activity of two orders of magnitude whereas varying the support led to variations in specific activity of less than a factor of two.

Freel (107) investigated the adsorption of carbon monoxide on platinum and observed that there was a tendency towards formation of bridged CO on large platinum particles, whereas on smaller platinum particles, the less strongly held linear form predominated. This decrease in adsorption strength was proposed by Vannice (106) as an explanation of the increase in specific activity with decreasing platinum particle size.

Palladium, however, showed no such dependence on particle size. Although supported palladium has a higher specific activity than unsupported palladium, an increase in dispersion of two orders of magnitude did not lead to a large increase in turnover number for methane. For particles $\lesssim$ 100Å in diameter, a metal-support interaction existed which was independent of particle size. It was the nature of the support itself which had the influence on specific activity by increasing the relative amount of the more weakly bonded CO which in turn enhanced the rate of methanation. The metal-support interaction may result in electron transfer between the metal particles and the

support or in the stabilization of surface structures not normally present on such large metal particles.

From this it appears that any effect which enhances the formation of the more weakly bound, linearly adsorbed CO will enhance methanation activity. It has been found (8) that the activity of a TiO_2-supported metal for the CO/H_2 reaction is higher than the activity of the corresponding SiO_2- or Al_2O_3-supported metal catalysts as a result of metal-support interactions. Solymosi et al. found that the product distribution of the CO/H_2 reaction over supported Rh sensitively depended on the support. (108) Vannice (109) also looked at the methanation reaction over supported and unsupported nickel. Although he found that the smaller, supported nickel particles had a higher specific activity than the larger unsupported particles, the variation in specific activity with dispersion, and with various supports was found to be much less than an order of magnitude. It was believed that the changes in specific activity reflected changes in the heat of adsorption of CO on the different Group VIII metals. It was to be expected that the changes in specific activity would be low for Ni since the heat of adsorption of CO on Ni was low relative to that on other Group VIII metals.

The methanation reaction can be accompanied by various complicating reactions. (110) These include

The Water Gas Shift : $CO + H_2O \longrightarrow CO_2 + H_2$

The Boudouard Reaction : $2CO \longrightarrow C + CO_2$

Coke Deposition : $H_2 + CO \longrightarrow C + H_2O$

Carbide Formation : $xM + C \longrightarrow M_xC$

Since water is a primary product of the methanation reaction, the water gas shift reaction often accompanies methanation. The water formed during methanation reacts with carbon monoxide, changing the oxygen containing product from water to carbon dioxide and altering the feed gas ratio.

The deposition of carbon or coke on the catalyst surface can alter the catalytic activity of the metal, as can carbide formation. However, the lay-down of carbon in the form of a hydrocarbonaceous residue is believed to play an important role in carbon monoxide hydrogenation reactions.

Jackson et al. (111) found that hydrocarbonaceous material was deposited during carbon monoxide hydrogenation over rhodium catalysts. The hydrocarbonaceous material acts as a hydrogen transfer medium to supply hydrogen to surface intermediates. In a further study using isotopic tracers, Jackson et al. (112) found evidence which confirmed that, far from having a detrimental effect on the catalyst, the hydrocarbonaceous residue plays a central role in the reaction. Carbon monoxide is not hydrogenated directly to methane, but goes through the hydrocarbonaceous residue present on the surface.

It is believed that the mechanism of the methanation reaction involves the direct dissociative adsorption of carbon monoxide to adsorbed carbon and adsorbed oxygen.

Araki and Ponec (113) used isotopic labelling experiments to show that the hydrogen from a CO/H_2 mixture reacts preferentially with carbon already present on the surface. The authors carried out the experiments on nickel, and found that the carbon monoxide could be

adsorbed in valleys among several nickel atoms or on top of nickel atoms. It appears that the carbon monoxide adsorbed in the valleys is able to undergo fast dissociation and subsequent reaction. (114)

Tanaka et al. (115) investigated the hydrogenation of carbon monoxide and carbon dioxide over rhodium supported on various metal oxides. They found that the order of activity was:

$$Rh/ZrO > Rh/Al_2O_3 > Rh/SiO_2 >> Rh/MgO$$

The authors concluded that the dissociation of carbon monoxide was a key to obtaining high catalytic activity, supporting the work of Araki and Ponec. (113)

The work of Vandervell and Bowker (116) on the methanation reaction on a nickel catalyst also supports the dissociative mechanism for methanation. Sachtler (85) proposed that the initial steps of methanation, and of Fischer-Tropsch synthesis, involved the dissociative adsorption of carbon monoxide and hydrogen followed by the formation of CH_x groups. The CH_x groups are precursors for CH_3 and CH_4 and are also building blocks for alkyl chain growth in Fischer-Tropsch synthesis.

Both the support and the metal precursor can influence the properties of supported rhodium catalysts for the carbon monoxide hydrogenation reaction. (117) Interactions can occur between the support and the metal salt precursor which can lead to the formation of rhodium species which are difficult to reduce. This may lead to the rhodium retaining a positive charge after reduction, which may or may

not affect its catalytic properties. When rhodium trichloride is supported on Al_2O_3, MgO or SiO_2, the support hydrolyses the rhodium trichloride resulting in the formation of a difficult-to-reduce oxychloride and a chlorinated support. (117)

If the rhodium species produced on reduction have a positive charge, $Rh^{\delta+}$, when carbon monoxide chemisorption is carried out, the metal-CO bond is observed to be weaker than if the metal is present as $Rh^{\bar{o}}$. The carbon monoxide desorbs from the positively charged rhodium at a lower temperature. (117)

When choosing a metal salt precursor, it is important to remember that the products of reduction of such salts may be retained on the support. Catalysts derived from $RhCl_3.3H_2O$ on Al_2O_3 retain appreciable amounts of chlorine even following reduction at 673K. (118) Furthermore, there is evidence to suggest that residual counter-ions such as acetate and sulphate poison the metal surface, leading to minimal carbon monoxide adsorption. (119) Worley et al. (119) found that $Rh(NO_3)_3.2H_2O$ is reduced more efficiently on Al_2O_3 than is $RhCl_3.3H_2O$. $Rh_6(CO)_{16}$ is also reduced more efficiently than $RhCl_3.3H_2O$.

Hyde et al. (120) investigated rhodium(III)nitrate, chloropentammine rhodium(III)chloride and rhodium(III)sulphite. They found that rhodium(III)nitrate gave more sites for adsorption of carbon monoxide on hydrogen, had smaller particles and was better dispersed than the catalysts derived from other precursors.

Jackson et al. (121) investigated the effect of the rhodium precursor on carbon monoxide hydrogenation over silica-supported catalysts. Of the nine metal salt precursors investigated, turnover

numbers were found to vary by up to two orders of magnitude and differences were observed in specific activities. Five possible reasons were proposed for the variations in activity and selectivity. These were variations in oxidation state of the metal, variations in dispersion, the presence of residual counter-ions such as chloride, the presence of hydrocarbonaceous residues on the surface of the catalyst and differences in particle size and geometry.

It was found that the oxidation state of the metal had little effect on product selectivity for oxygenates. The authors (121) found that there was a link between the specific activity of the catalyst and the amount of surface hydrocarbonaceous deposit retained by each site with the highest hydrocarbonaceous deposit to site ratio giving the highest activity. The hydrocarbonaceous deposit acts as a hydrogen transfer agent. The variation in selectivity, by up to a factor of five, was attributed to variations in site geometry rather than particle geometry. The presence of residual counter-ions and differences in metal dispersion apparently had little effect on either activity or selectivity.

CHAPTER 2

OBJECTIVES OF THE PRESENT STUDY

The main objective of the work described in this thesis was to examine the effects of changes in the support and in the metal salt precursor, used to prepare the catalysts on the physical characteristics and chemical behaviour of a series of supported rhodium and platinum catalysts.

To achieve these objectives, a series of platinum catalysts supported on silica, molybdenum trioxide and tungsten trioxide have been prepared by impregnation using chloroplatinic acid (H_2PtCl_6), and a series of rhodium catalysts supported on silica, molybdenum trioxide and tungsten trioxide have been prepared by impregnation techniques using both rhodium chloride and rhodium nitrate as precursor salts.

Catalysts have been subjected to characterisation by:

a) temperature programmed reduction,

b) chemisorption and temperature programmed desorption of carbon monoxide, to determine the variations in the nature of the chemisorbed state of carbon monoxide and the metal areas of the different catalysts,

c) thermo-gravimetric analysis and differential scanning calorimetry, to obtain information relevant to the chemical nature of the supported salt and its mode of reduction,

CHAPTER TWO

and

d) by physical adsorption of nitrogen to determine total surface areas.

The influence of the catalyst variables specified above on their behaviour in catalytic hydrogenation has been examined. Buta-1,3-diene hydrogenation studies have been carried out over all catalysts to determine variations in

i) selectivity and butene distribution with extent of reaction and reaction temperature

and

ii) the kinetics of the reaction .

Temperature programmed reaction studies of carbon monoxide hydrogenation have been carried out on selected catalysts.

CHAPTER THREE

CHAPTER 3

EXPERIMENTAL

3.1 Introduction

Characterisation studies have been carried out on a series of platinum and rhodium catalysts. Characterisation techniques have included temperature programmed reduction (hereafter referred to as T.P.R.), carbon monoxide chemisorption, temperature programmed desorption (hereafter referred to as T.P.D.) and temperature programmed reaction studies. The reaction investigated in the temperature programmed reaction studies was the hydrogenation of carbon monoxide.

The hydrogenation of buta-1,3-diene was investigated over each of the catalysts. Reactions were carried out to study the activity and selectivity of each catalyst. Kinetic studies were carried out to investigate the order of reaction with respect to both hydrogen and buta-1,3-diene. The results were examined for evidence of effects arising from differences in support and in metal salt precursor.

3.1.1 Materials

Chloroplatinic acid, H_2PtCl_6 (Johnson Matthey Chemicals Ltd.), rhodium nitrate, $Rh(NO_3)_3.nH_2O$ (Johnson Matthey Chemicals Ltd., containing 7.95% w/w Rh) and rhodium(III)chloride, $RhCl_3$ (Aldrich Chemical Company Inc.) were used to prepare the catalysts used in this study. The supports used were molybdenum(VI)oxide, 99.5% A.C.S. reagent (Aldrich Chemical Company Inc.), tungsten(VI)oxide,

99.5% (Koch-Light Ltd.) and silica (Davison, Grade 952). The molybdenum oxide and tungsten oxide were both used as supplied. The silica was pre-treated, as described below, before use.

3.1.2 Pre-Treatment of Silica

Before being used as a support, the silica was subjected to an oxalic acid wash pre-treatment to remove iron impurities.

A mixture of silica (250 cm^3), oxalic acid (127.6g) (May & Baker Ltd., 99.5 %), glycerol (191.4g) (Koch-Light Laboratories Ltd.) and de-ionised water (319g) was placed in a round-bottomed flask. The mixture was stirred for 6 hours at 90°C before being filtered through a sintered funnel (No. 2) and washed with hot, de-ionised water. The silica was dried initially at 100°C to remove water; the temperature was then raised to 450°C and the silica calcined at this temperature overnight.

3.1.3 Catalyst Preparation

Each of the catalysts used in this study was prepared by impregnation. De-ionised water was added to the oxide support to make a slurry and to this was added an aqueous solution containing the required amount of the appropriate metal salt. The resultant mixture was heated gently with frequent stirring, until it had been evaporated to near dryness. The supported salt was then dried overnight at 80°C before being stored for future use. Nine catalysts were prepared:

H_2PtCl_6/SiO_2	$RhCl_3/SiO_2$	$Rh(NO_3)_3/SiO_2$
H_2PtCl_6/MoO_3	$RhCl_3/MoO_3$	$Rh(NO_3)_3/MoO_3$
H_2PtCl_6/WO_3	$RhCl_3/WO_3$	$Rh(NO_3)_3/WO_3$

Assuming no losses during the impregnation procedure, the supported platinum catalysts contained 1.1% platinum by weight and the supported rhodium catalysts contained 1.5% rhodium by weight.

3.1.4 Gases

The following gases were used in all experiments carried out using Flow System I or the Static Vacuum System.

Helium (Grade A, British Oxygen Company, hereafter referred to as B.O.C.) was purified by passing it through a series of traps consisting of, in order, cuprous oxide (CuO), powdered metallic copper, manganous oxide (MnO) and molecular sieve (Hopkin and Williams - 4A) to remove traces of water, oxygen and hydrogen.

6% Hydrogen/nitrogen (B.O.C.), carbon monoxide (C.P. Grade, 99.5%, B.O.C.) and hydrogen (B.O.C.) were all used without further purification. Buta-1,3-diene (99%, B.D.H.) was degassed before use. Iso-butane was detectable as an impurity in the buta-1,3-diene.

3.2 Buta-1,3-diene Hydrogenation

3.2.1 The Vacuum System

A conventional high vacuum system, shown schematically in Fig. 3.1, was used to carry out buta-1,3-diene hydrogenation studies. This was maintained at pressures of $\leqslant 10^{-4}$ Torr by means of a mercury diffusion pump, backed by a rotary oil pump. The vacuum was measured using a Pirani gauge (Speedivac Pirani Type Vacuum Gauge, Edwards High Vacuum Ltd.). Bulbs V1 to V3 were used to store the gases used in the hydrogenation experiments namely hydrogen, a 3:1:: hydrogen:buta-1,3-diene mixture and buta-1,3-diene respectively. An additional storage bulb V4 was used as required.

The cylindrical Pyrex reaction vessel was attached to the system via a B10 cone and socket. The required weight of catalyst was placed on the bottom of the reaction vessel. Pressure changes, which occurred during reaction, were monitored using a pressure transducer (SE Labs., EMI Ltd., Type SE 21/V) linked to a potentiometric chart recorder. One arm of the pressure transducer was attached just above the reaction vessel, with the other maintained under vacuum. Changes in pressure could be measured to an accuracy of ± 0.01 Torr.

Gases could be admitted to the evacuated reaction vessel by closing off the taps to the vacuum and opening the required two-way tap (either T1 or T2). The pressure of gas being admitted was continuously monitored by the pressure transducer and the associated potentiometric chart recorder.

Reaction products could be analysed by expanding the gas into expansion vessel, EV, and freed of unreacted hydrogen by pumping

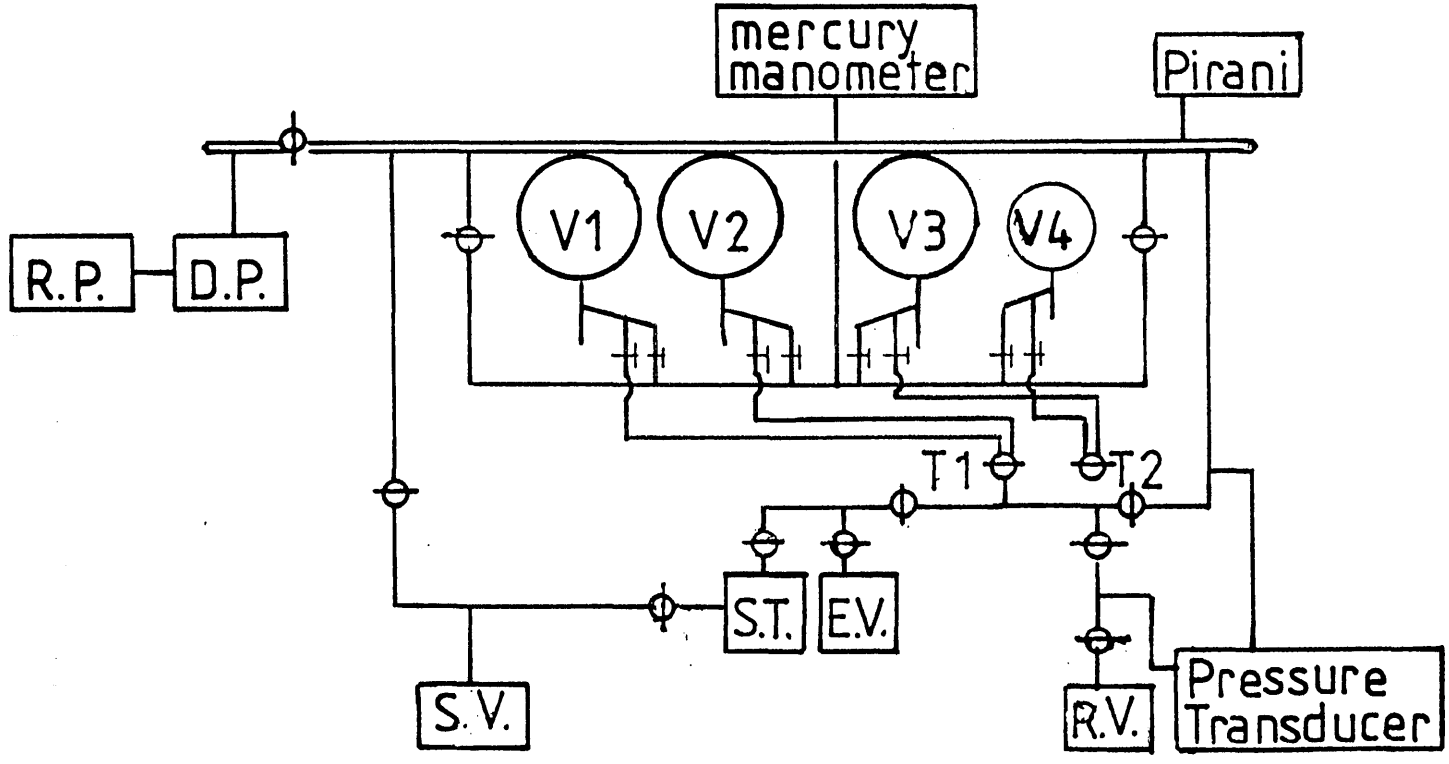

Fig. 3·1 The Static Vacuum System

through the liquid nitrogen cooled spiral trap, ST. The products were then distilled from the spiral trap into a liquid nitrogen cooled sample vessel, SV, attached to the line *via* a B10 cone and socket. The sample vessel could then be transferred to the gas chromatographic system, where the products were analysed.

3.2.2 Catalyst Activation

A catalyst sample, typically 30 to 50 mg, was placed in the reaction vessel, which was then attached to the line and evacuated. An electric furnace was placed around the reaction vessel and the temperature was raised to the required value for catalyst activation (200°C unless stated otherwise). The power supply to the furnace, and hence the temperature, was controlled by means of a Variac variable transformer. Temperatures were measured using a 'Comark' electronic thermometer and a Cr/Al thermocouple, which was placed in contact with the reaction vessel. The temperature was raised to 200°C while the reaction vessel was under vacuum. On reaching the required temperature, 150-200 Torr of hydrogen was admitted to the reaction vessel. The temperature was maintained at 200°C for a minimum of two hours (maximum reduction time: overnight (12 hours)). To ensure complete reduction of the catalyst, the hydrogen was removed from the reaction vessel, by pumping, after a minimum of 30 minutes. Fresh hydrogen (150-200 Torr) was then admitted. This procedure was repeated a minimum of twice during the course of the reduction. Following reduction, the catalyst was cooled to ambient temperature *in vacuo*.

3.2.3 Experimental Procedure

Following the reduction of each catalyst, the hydrogenation of buta-1,3-diene over the catalyst was studied using the static vacuum system described in section 3.2.1. Two alternative reaction procedures were used. In the first procedure, the reactions studied involved the use of a standard 3:1::hydrogen:buta-1,3-diene gas mixture. The total pressure in the reaction vessel was followed using a pressure transducer. The output from the pressure transducer was plotted against time on a potentiometric chart recorder. In this way, pressure versus time curves were obtained. At a variety of pressure falls, the reaction products, together with any unreacted gases, were expanded into an expansion vessel, pumped at -196°C to remove any unreacted hydrogen and condensed into a removable sample vessel. In this way the products could be removed from the vacuum system for analysis by gas chromatography.

In the second hydrogenation reaction procedure, the buta-1,3-diene and hydrogen were admitted separately to the reaction vessel. Buta-1,3-diene was admitted to the reaction vessel first, to a pressure measured by the pressure transducer and potentiometric chart recorder. To this, hydrogen was added until the required total pressure was reached. The total pressure in the reaction vessel was measured by the pressure transducer, and the signal plotted against time on the potentiometric chart recorder. By following this reaction procedure, either the partial pressure of buta-1,3-diene was held constant while the partial pressure of hydrogen was varied, or *vice-versa*.

3.2.4 Gas Chromatographic System

The gas chromatographic system used to analyse the products of the hydrogenation reactions is shown schematically in Fig. 3.2. A 40 foot long column consisting of 6 mm i.d. glass tubing packed with 30% w/w dimethyl sulpholane (DMS) (Phase Separations Ltd.) on 60-80 mesh NAW Chromasorb P (Phase Separations Ltd.) was used with helium as carrier gas. The column packing was prepared using 10 ml DMS to 20g NAW Chromasorb P. The DMS was dissolved in methanol, added to the column packing and stirred to ensure an even coating. The excess solvent was then removed under vacuum.

The sample vessel containing the reaction products was attached to the inlet of the chromatographic system via a B10 cone and socket. Taps T1 and T2 were arranged in such a way that the helium carrier gas could be directed towards the column, while the glass sample loop and mercury manometer were evacuated using a rotary oil pump. The sample to be analysed was then expanded into the sample loop to the required pressure, which was measured using the mercury manometer. Taps T1 and T2 were then manipulated to divert the carrier gas through the sample loop, flushing the contents onto the column.

The flow rate of the helium carrier gas was maintained at the desired level of 60 ml min^{-1} by a Negretti-Zambra Precision Air Pressure Regulator.

As each product was eluted from the column, the signal change detected on the thermal conductivity detector was amplified. The amplified signal was then detected by a Pye Unicam PU4810 computing printer/integrator which plotted the change in signal for each product

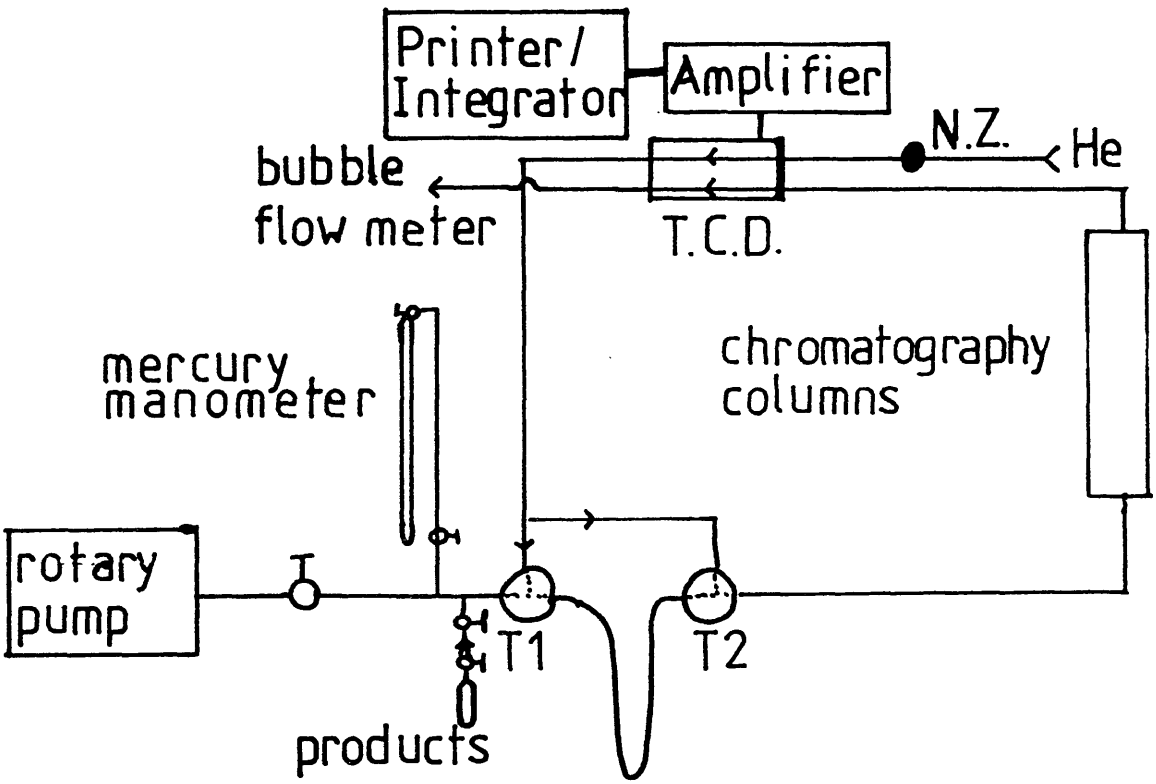

Fig. 3·2 Gas Chromatographic System

(as a peak) against time. The signal was integrated, and the corresponding numerical value was tabulated against its corresponding retention time. By calibrating the system using a known pressure of a gas mixture containing known percentages of the components in the product mixture, the values for the peak areas could be coverted to partial pressures.

3.3 Temperature Programmed Reduction

3.3.1 Flow System I

Figure 3.3 shows a schematic diagram of the flow system used for temperature programmed reduction, carbon monoxide chemisorption and temperature programmed desorption experiments (Flow System I).

During T.P.R. experiments, taps T1, T2 and T3 were arranged in such a way that 6% H_2/N_2 flowed firstly over one side of the thermal conductivity detector then through the catalyst reaction tube before finally passing over the other side of the thermal conductivity detector. The thermal conductivity detector signal was amplified and recorded as a peak on a potentiometric chart recorder. During the temperature programmed reduction process, the 6% H_2/N_2 flow rate was 20 ml min^{-1}. It could be adjusted using a Nupro fine metering valve and monitored using a Rotameter flowmeter (GEC-Elliot 1100). The temperature of the catalyst reaction tube was increased linearly from ambient temperature to 500°C at a heating rate, β, of 5°C min^{-1}, in the course of the reduction process. The heating was carried out using a furnace (Stanton Redcroft) surrounding the reaction tube. The furnace

Key to Figure 3.3

TR1	:	CuO Trap
TR2	:	Cu Trap
TR3:	:	MnO Trap
TR4,TR5	:	Molecular Sieve Traps
V1, V2	:	4-Way Valves
V3	:	Gas Sampling Valve
N.V.	:	Nupro Fine Metering Valves
N.Z.	:	Negretti-Zambra Pressure Regulator
r	:	Rotameter Flowmeter
R	:	Restrictor
Q.M.S.	:	Quadrupole Mass Spectrometer
T.P.	:	Turbomolecular Pump
R.P.	:	Rotary Pump
T.C.D.	:	Thermal Conductivity Detector
T1 to T5	:	3-Way Valves

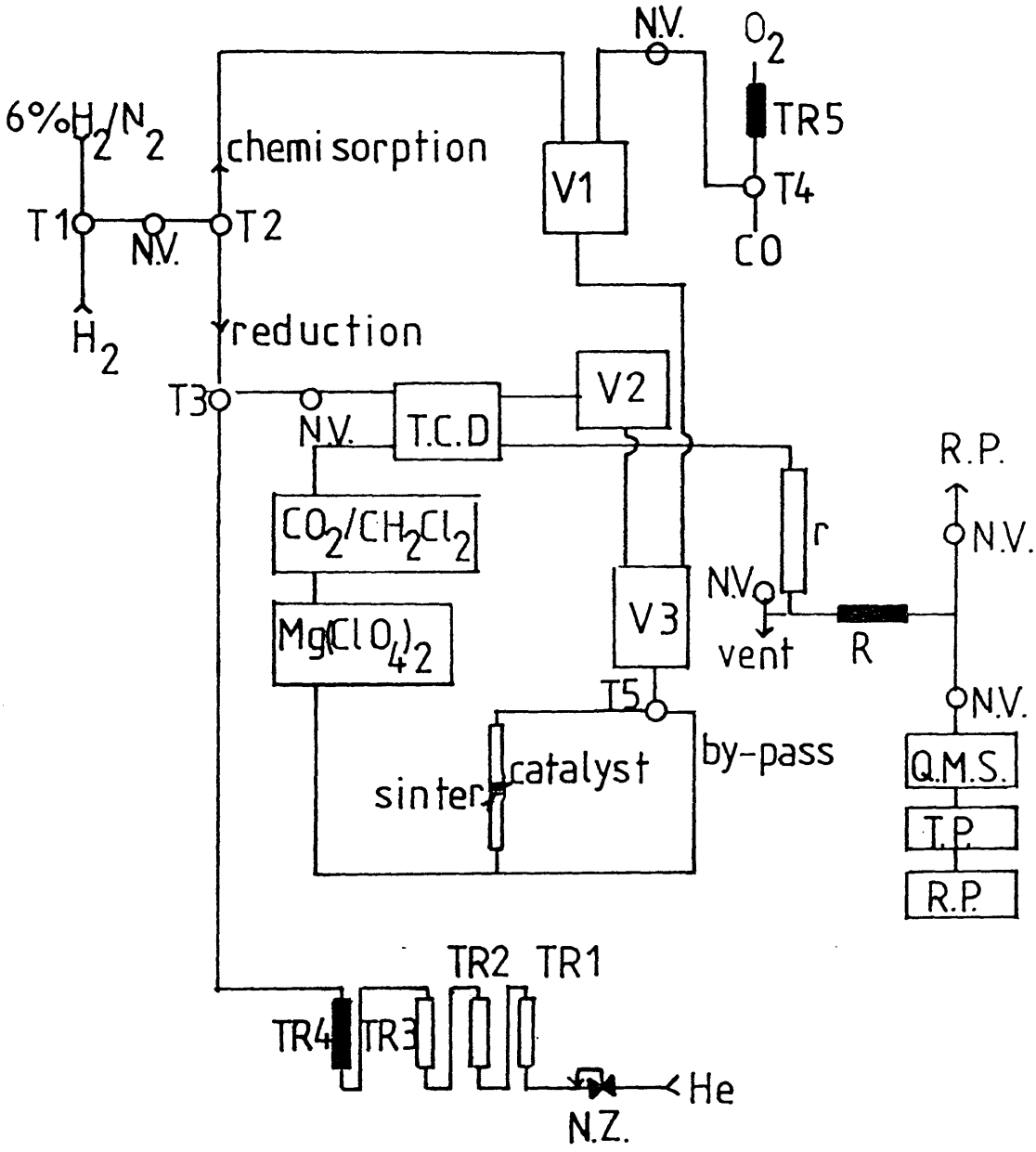

Fig. 3-3 Schematic Diagram of Flow System I

current, and hence the temperature of the furnace, was programmed using a Stanton Redcroft temperature programmer (Cambridge Process Controls 702). The temperature was monitored using a Cr/Al thermocouple placed in contact with the wall of the reaction tube, the output from which was plotted on a chart recorder simultaneously with peaks due to changes in concentration of hydrogen occurring during T.P.R.

A magnesium perchlorate drying tube (to remove excess moisture associated with the catalyst or formed during the reduction process) and a dry ice/methylene chloride cold trap (to remove any products of the reduction process which may be harmful to the tungsten filaments of the thermal conductivity detector) were placed between the catalyst reactor tube and the thermal conductivity detector.

3.3.2 Experimental Procedure

A catalyst sample, typically in the range 0.1g to 0.2g, was placed in the catalyst reaction tube. 6% H_2/N_2 was flowed through the by-pass at 20 ml min^{-1} until a steady baseline was observed on the chart recorder. The 6% H_2/N_2 gas was then diverted to pass through the catalyst reaction tube and any adjustments made to re-establish the flow-rate at 20 ml min^{-1}. At this point the temperature program was started. This procedure incorporated a 15 minute "delay" period during which time the 6% H_2/N_2 flowed over the catalyst at ambient temperature. The heating rate was 5°C min^{-1} and the maximum temperature reached was 500°C.

3.4 Carbon Monoxide Chemisorption and Temperature Programmed Desorption

3.4.1 Carbon Monoxide Chemisorption

Flow System I (shown schematically in Fig. 3.3) was used to carry out pulsed-flow carbon monoxide chemisorption experiments. Helium was used as the carrier gas. The helium was flowed through tap T3, through the reference side of the thermal conductivity detector, through valve V2 and into valve V3. The carbon monoxide was flowed through tap T4 and valve V1 before reaching valve V3.

A comprehensive diagram of valve V3 (Fig. 3.4) shows that this 10-port valve (Valco CIOU Gas Sampling Valve) incorporates two identical 50 µl sample loops. These sample loops were alternately filled with carbon monoxide or flushed out with helium, depending on the position of the valve. The valve was switched between position 1 and position 2 as required, and as shown in the diagram. Thus the path of the helium carrier gas could be diverted and the carbon monoxide pulse flushed on to the catalyst sample.

Before a carbon monoxide chemisorption experiment could be carried out, the catalyst sample (0.1g to 0.2g) was first reduced overnight (12 hours) in 6% H_2/N_2 flowing at 20 ml min^{-1}. The temperature chosen to ensure complete reduction of the catalyst was 10°C higher than the temperature corresponding to the peak maximum of the major reduction peak (the T_{max} value) for that catalyst.

Following reduction, the catalyst sample was cooled to ambient temperature in flowing 6% H_2/N_2 and flushed with helium flowing at

Fig. 3·4 Gas Sampling Valve

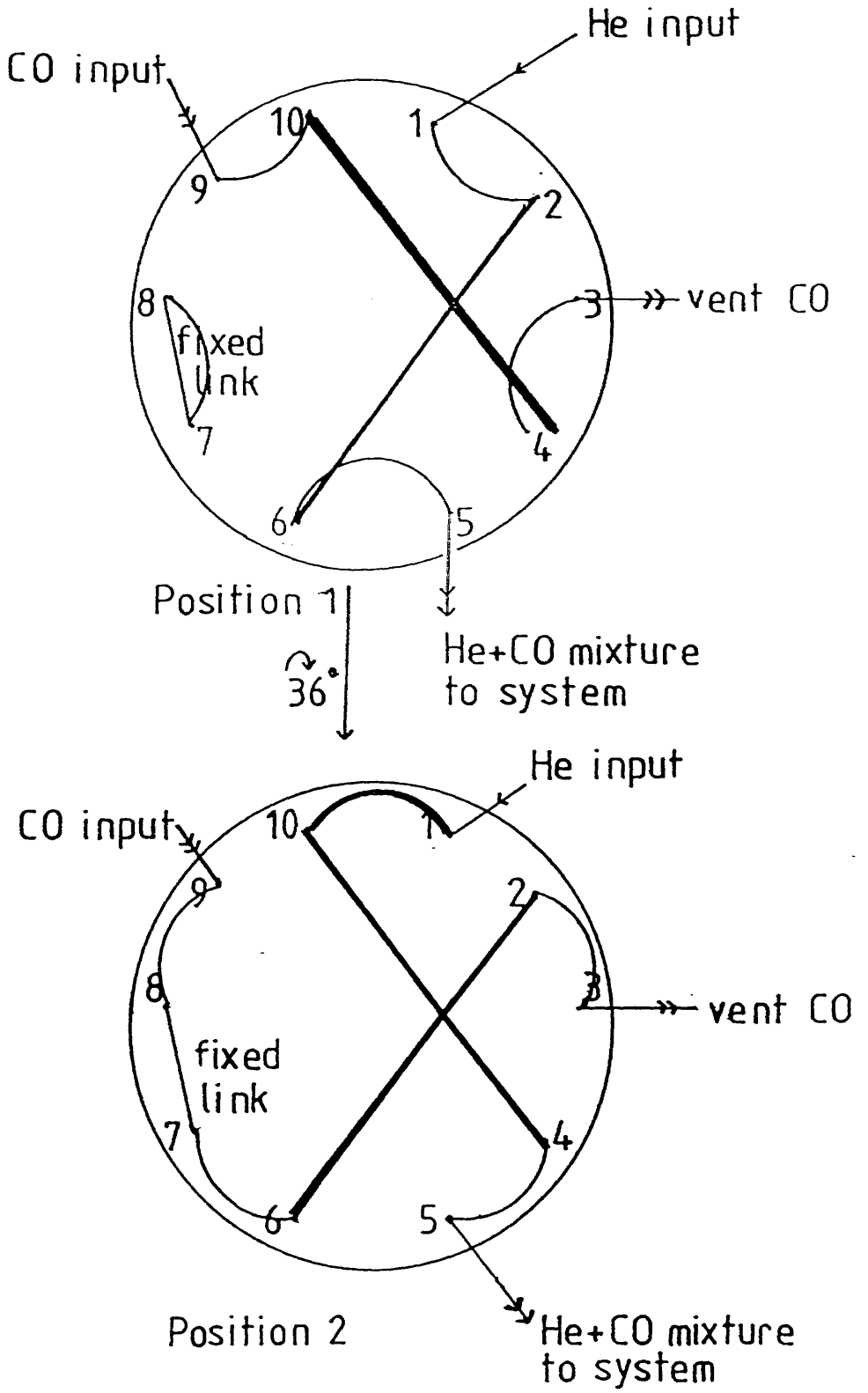

Port 4 to Port 10: 50µl sample loop

Port 2 to Port 6 : 50µl sample loop

20 ml min^{-1} for 30 minutes. With the helium flowing through the by-pass, the system was calibrated by injecting pulses of carbon monoxide. The pulses of carbon monoxide were recorded as peaks on the chart recorder, the area under the peak being proportional to the volume of carbon monoxide injected into the system. The carrier gas was re-directed to pass through the catalyst reactor tube and pulses of carbon monoxide in helium were passed over the catalyst. Any carbon monoxide not adsorbed by the catalyst was detected as a peak on the chart recorder.

The difference in area between a calibration peak and a peak corresponding to non-adsorbed carbon monoxide gave a measure of the quantity of carbon monoxide adsorbed by the catalyst. Further pulses of carbon monoxide continued to be admitted until saturation of the catalyst surface had been reached, at which point the peaks detected were the same size as the calibration peaks.

3.4.2 Temperature Programmed Desorption

Immediately after carrying out a chemisorption experiment, a temperature programmed desorption experiment was carried out. This involved flowing helium over the catalyst at 20 ml min^{-1} while the temperature was increased at 5°C min^{-1} to 500°C. The change in concentration of the desorbing species in the eluant gas was monitored using a thermal conductivity detector. After passing through the thermal conductivity detector a portion of the eluant gas was vented and the remainder passed into a quadrupole mass spectrometer (Spectramass

DAQ 3.1) in order to identify the desorbing species. The mass spectrometer was evacuated to 10^{-8} - 10^{-11} Torr by a combination of a turbomolecular pump (Edwards ETP 4/80) and a rotary oil pump. Since only changes in the relative concentrations of the desorbing species were being studied, precise calibration of the mass spectrometer was not carried out. Hence the results obtained are only qualitative in nature.

3.5.1 Flow System II

Flow System II, shown schematically in Fig. 3.5, was used to carry out temperature programmed reduction, temperature programmed desorption, carbon monoxide chemisorption and temperature programmed reaction experiments at I.C.I. plc, Chemicals and Polymers Group, Research and Technology Centre, Runcorn. In situ nitrogen BET surface area measurements could also be carried out.

Catalysts from the same stock as those described in section 3.1.2 were used. Typically, 0.5g of catalyst was mixed with acid washed glass beads (Phase Separations Ltd., 85-100 mesh) which were used to prevent the catalyst sample compacting and to lengthen the catalyst bed for use in chromatographic detection techniques. The catalyst/glass beads mixture was placed in a 1/4" diameter stainless steel reactor tube. The catalyst was held in place by a plug of quartz wool at either end of the tube. A thermocouple inserted into the catalyst monitored the temperature during experiments.

Fig. 3·5 Schematic Diagram of Flow System II

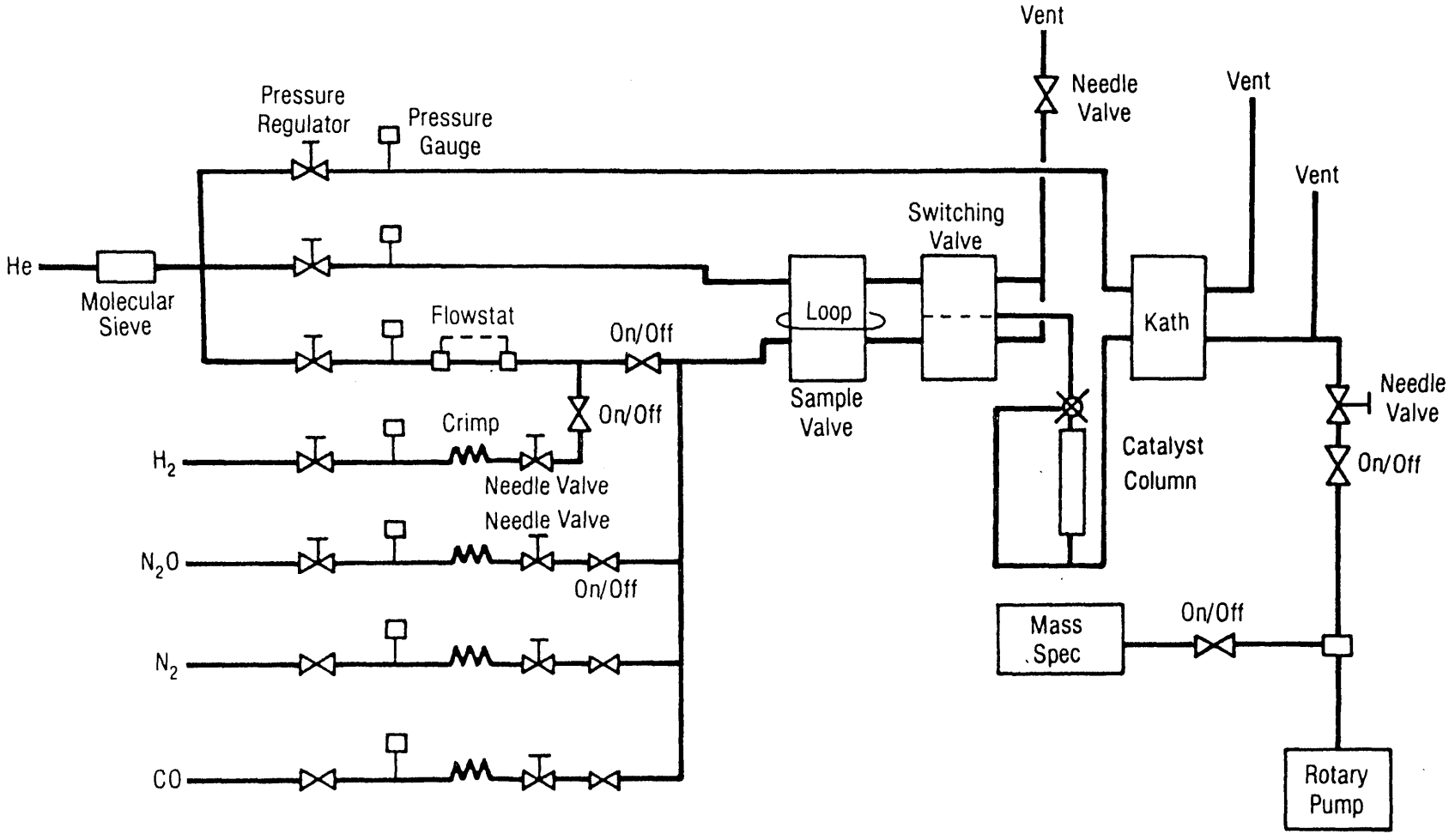

3.5.2 The Gas Feed System

The helium (B.O.C., 99.995% purity) was scrubbed by passing it through a B.O.C. Mark III rare gas purifier which removed, to p.p.m. level, all traces of N_2, H_2, H_2O, CO_2 and hydrocarbons. The helium was then passed over a molecular sieve (Linde-4A) before being divided into three independently controlled streams. Each stream was controlled by a combination of a pressure regulator and a flowstat. One stream acted as the katharometer refererence stream. A second stream acted as a carrier gas during desorption. The third stream acted as a carrier gas to which various gases, for example hydrogen (B.O.C. 99.995%), nitrogen (B.O.C.), carbon monoxide (Air Products, 99%), or nitrous oxide, could be added. By using the flow switching valve, either helium, or helium plus reactant gas, was passed through the catalyst reaction tube. The helium to reactant ratio was controlled using the pressure regulator and crimp placed in the inlet line for each reactant gas.

3.5.3 The Gas Analytical System

The analytical system in this apparatus consisted of a katharometer (Taylor Servomex Microcatharometer) and an on-line Vacuum Generators "Supavac" mass spectrometer. The gas flow (flow-rate, 25 ml min^{-1}) passed through the katharometer after leaving the catalyst reactor. Thereafter, by combination of a needle valve and a rotary pump, a constant (20%) portion of the total gas flow was fed to the mass spectrometer.

The katharometer and 1/8" stainless steel pipe between the catalyst reactor and the mass spectrometer inlet were maintained at 110°C to prevent condensation of gaseous material before it could be detected by the katharometer and mass spectrometer.

3.6.1 Temperature Programmed Reduction

A catalyst sample (typically 0.5g) was mixed with glass beads and admitted to the catalyst reactor tube. A gas flow containing hydrogen in nitrogen was established through the by-pass. (The percentage of hydrogen lay in the range 5 to 10% and was constant for each T.P.R. experiment). The gas mixture was then switched to pass through the catalyst. Any changes in katharometer signal were amplified and recorded on a chart recorder. At the same time, the eluant gas was monitored for changes in hydrogen and water concentration using the mass spectrometer. The heating rate used during the T.P.R. was 8°C min^{-1}. Both the heating rate and the maximum required temperature (400°C) were controlled by a temperature programmer incorporated into the chromatographic oven which housed the catalyst reactor.

3.6.2 Temperature Programmed Desorption Following Temperature Programmed Reduction

Following T.P.R., the catalyst reactor tube was allowed to cool to ambient in flowing hydrogen/nitrogen. The reaction tube was then immersed in liquid nitrogen (-196°C). Hydrogen/nitrogen gas continued to be passed over the catalyst until the temperature had

reached -196°C. At this point, the gas flow was switched from hydrogen/nitrogen to helium. The liquid nitrogen was removed and the reactor was allowed to warm to ambient temperature. During this time the desorption was followed on the mass spectrometer and katharometer. When the reaction temperature reached ambient, the temperature program was started and the catalyst was heated linearly to 300°C to desorb hydrogen from the catalyst before further experiments, for example either chemisorption or temperature programmed reaction studies, were carried out.

3.7 In Situ Total Surface Area Measurements

The total surface area of a catalyst could be calculated by carrying out a nitrogen adsorption measurement at -196°C followed by a subsequent nitrogen desorption experiment. This enabled calculation of the area using the modified BET point B method. (122)

A gas flow comprising not more than 10% nitrogen was established *via* the reactor by-pass. Helium was then flowed over the catalyst at 25 ml min^{-1}. The catalyst reactor was cooled to -196°C using liquid nitrogen. The nitrogen/helium gas mixture was then flowed over the catalyst. The eluant gas was monitored using the katharometer and the mass spectrometer. No deflection was observed until saturation of the catalyst surface by nitrogen had occurred. Using the technique of frontal chromatography pioneered by K.C. Waugh *et al.* (123), the quantity of nitrogen adsorbed at -196°C can be calculated from the time taken for the nitrogen deflection to be detected and the percentage of nitrogen in the gas mixture flowing at a known flow rate. (The details of this are given in Chapter 4, section 4.4). At saturation, the nitrogen

deflection detected by the katharometer is constant. At this point, the gas stream is switched to helium only and the nitrogen is desorbed off the catalyst surface. By carrying out a strip-wise integration of the desorption tail-shape produced in this way, and using the integrals together with a knowledge of the total amount of nitrogen originally adsorbed on the sample, a linearised BET plot was made which allowed a second calculation of the quantity of nitrogen adsorbed, and hence the total surface area, to be calculated. The surface area was determined both before and after the catalyst had been reduced.

3.8.1 Carbon Monoxide Chemisorption

Carbon monoxide chemisorption experiments were carried out at various sub-ambient temperatures, ranging from -196°C to -70°C, in a manner similar to that employed for nitrogen adsorption at -196°C. The catalyst was first taken through a T.P.R./T.P.D. cycle. A gas stream (flow-rate, 25 ml min^{-1}) containing a fixed percentage of carbon monoxide (in the range 8 to 10%, constant for each experiment) was passed over the catalyst which had been cooled to the required sub-ambient temperature. The eluant gas was monitored using the katharometer and mass spectrometer. When saturation of the catalyst had been achieved, a deflection corresponding to the amount of carbon monoxide in the gas stream was observed on the chart recorder. The quantity of carbon monoxide adsorbed was calculated in a similar way to that employed to calculate nitrogen adsorption.

3.8.2 Temperature Programmed Desorption Following Carbon Monoxide Chemisorption

Following carbon monoxide chemisorption experiments, as described above, the carbon monoxide/helium gas stream was replaced by a helium gas stream, which was flowed over the catalyst at sub-ambient temperature. When the immediate desorption of carbon monoxide was complete, the low temperature bath surrounding the catalyst reactor was removed and the catalyst allowed to warm to ambient temperature in flowing helium and the eluant gas monitored by the katharometer and mass spectrometer. Having reached ambient temperature, the catalyst was heated linearly (β = 6°C min^{-1} or 8°C min^{-1}) to a maximum temperature of 400°C and the eluant gas monitored for further desorption.

3.9 Temperature Programmed Reaction Studies

Temperature programmed reaction studies were carried out on catalysts prepared and reduced as previously described.

A gas stream comprising not more than 10% carbon monoxide (range 8 to 10%, fixed for each experiment) in hydrogen was passed through the catalyst reactor as the temperature was increased linearly (β = 8°C min^{-1}) to a maximum temperature of 400°C. The mass spectrometer was used to detect changes in concentration of hydrogen, carbon monoxide, water, methane and carbon dioxide, which were plotted as a function of temperature and time.

CHAPTER FOUR

CHAPTER 4

TREATMENT OF RESULTS

4.1 Introduction

In order to obtain the results presented in Chapter 5, calculations were performed on the raw data obtained by carrying out experiments according to the procedures outlined in Chapter 3. In this chapter, details are presented to show how these calculations were carried out.

4.2 Temperature Programmed Reduction

Flow System I was calibrated for temperature programmed reduction by injecting pulses of hydrogen into a nitrogen carrier gas, which then flowed through a sample of silica (0.1605g) in the reaction tube. The volume of hydrogen injected was 50 μl. In this way, the area corresponding to 50 μl of hydrogen, under known chart recorder sensitivity settings, was obtained. The volume of hydrogen consumed during a temperature programmed reduction experiment could, therefore, be obtained by integrating the peak area of the T.P.R. profile and comparing it with the area of the calibration peak. The volume of hydrogen calculated in this way was converted to an equivalent number of hydrogen molecules, and expressed as hydrogen molecules consumed per gram of catalyst.

4.3 Carbon Monoxide Chemisorption

Carbon monixide chemisorption experiments were carried out in a pulsed flow system, as described in Chapter 3, section 3.4.1. The system was calibrated by injecting 50 μl pulses of carbon monoxide into a helium carrier gas. The pulses were detected by a thermal conductivity detector linked to a potentiometric chart recorder. The volume of carbon monoxide adsorbed by the catalyst from a pulse of carbon monoxide corresponds to the difference in area between the calibration peak and a chemisorption peak. In this way, the total volume of carbon monoxide adsorbed by the catalyst was calculated. This volume was then converted to the number of carbon monoxide molecules per gram of catalyst. The metal area of the catalyst was calculated from the number of carbon monoxide molecules adsorbed. The calculation is based on the assumption that the carbon monoxide was adsorbed linearly on the supported metal, with a metal to carbon monoxide ratio of one to one. Thus, the metal area was obtained by multiplying the number of carbon monoxide molecules adsorbed by the area occupied by one carbon monoxide molecule when it is adsorbed linearly (16.8×10^{-20} m^2). The answer was expressed in m^2 per gram of catalyst. The number of carbon monoxide molecules adsorbed was also used to calculate its dispersion. Dispersion, D, is defined as

$$D = \frac{\text{number of surface metal atoms}}{\text{total number of metal atoms}} \times \frac{100}{1}$$

Assuming that the metal to carbon monoxide ratio is one to one, the number of surface metal atoms is equal to the number of carbon

monoxide molecules adsorbed by the catalyst. The total number of metal atoms in a one gram sample is calculated from its metal loading.

4.4 In Situ Total Surface Area Calculations

Experiments were carried out, using Flow System II, to determine the total surface area of catalyst samples by N_2 adsorption at -196°C. The experiments were carried out according to the procedure outlined in Chapter 3, section 3.7.

The technique of frontal chromatography (123) was used to follow the adsorption of N_2 at -196°C. Figure 4.1 shows a typical frontal chromatogram obtained by adsorbing nitrogen on a catalyst sample at -196°C. At point a, the gas passing over the catalyst was switched from helium only to a mixture of x% N_2/He, where $x \leqslant 10\%$. The dead-time of the system is the time required for the nitrogen to reach the detector when no adsorption takes place. The dead-time of the system corresponds to point t_o on Figure 4.1 (point b). If no adsorption takes place, a deflection would be expected here. However, when adsorption did take place, no nitrogen was detected until point c, when a sharp deflection was observed, rising to point d. The height of the deflection at point d is proportional to the concentration of nitrogen in the gas phase. The volume of nitrogen adsorbed by the catalyst sample at -196°C was calculated as follows:

$$\text{Volume of } N_2 = \begin{array}{c}\text{time of } N_2 \text{ flow} \\ \text{(time between point b and point c)}\end{array} \times \text{flow rate } (25 \text{ ml min}^{-1}) \times x\% \ N_2$$

This corresponds to the area 'bcde' in Figure 4.1. This volume was converted to the number of N_2 molecules adsorbed per gram of catalyst. The total surface area of the catalyst was obtained by multiplying the number of N_2 molecules adsorbed by the area occupied by one N_2 molecule (16.2×10^{-20} m^2)

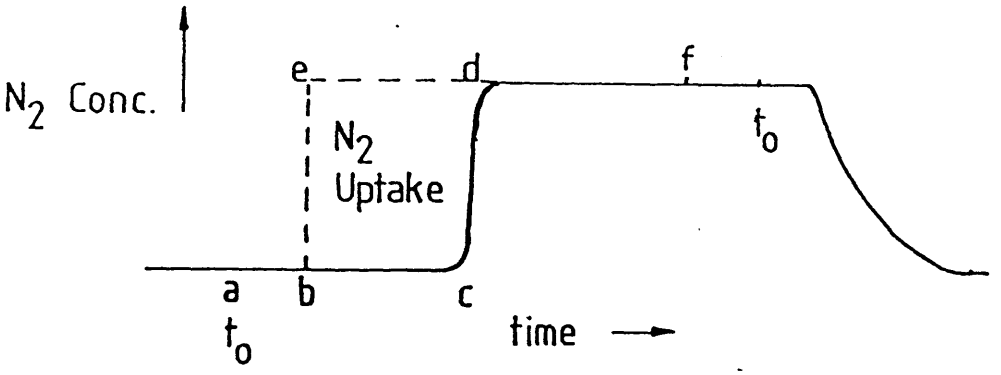

Fig 4.1 Frontal Chromatogram of N_2 Adsorption at -196°C

The value thus obtained was confirmed by following the desorption of nitrogen from the surface at -196°C. At point f in Fig. 4.1, the N_2/He gas mixture was switched to helium only, causing the nitrogen to desorb from the catalyst surface. After the gas switching point (point f) there was a sweep out time corresponding to the dead-time of the system. After this time, nitrogen desorption was observed.

Strip-wise integration of the desorption tail-shape, together with a knowledge of the total quantity of nitrogen originally adsorbed by the catalyst, allowed calculation of the volume of nitrogen still on the surface at particular pressures. Thus an isotherm of the adsorption of nitrogen at -196°C, as shown in Figure 4.2, was obtained.

According to Brunauer, Emmett and Teller, (122) adsorption of N_2 at -196°C on substrates generates an S-shaped isotherm. A point, defined by Brunauer et al. (122) as point B, at the start of the linear region of the isotherm corresponds to monolayer coverage of the sample by adsorbed nitrogen. The isotherm can be linearised with respect to the B.E.T. equation, which is of the form:

$$\frac{p}{V(p_o - p)} = \frac{1}{V_m c} + \frac{c-1}{V_m c} \cdot \frac{p}{p_o}$$

where p = pressure of gas

p_o = saturation vapour pressure

V_m = volume corresponding to monolayer coverage

c = constant

A plot of $\frac{p}{V(p_o-p)}$ versus $\frac{p}{p_o}$ gives a straight line of gradient $\frac{c-1}{V_m c}$ and intercept $\frac{1}{V_m c}$. Thus, V_m, the volume of nitrogen corresponding to monolayer coverage of the catalyst sample, can be obtained. This value can then be converted to the total surface area by multiplying by the area occupied by one molecule of nitrogen.

Sub-ambient carbon monoxide chemisorption experiments were carried out according to the procedure described in Chapter 3, section

Fig. 4·2 N_2 Isotherm at -196°C on $Pt/MoO_3(a)$

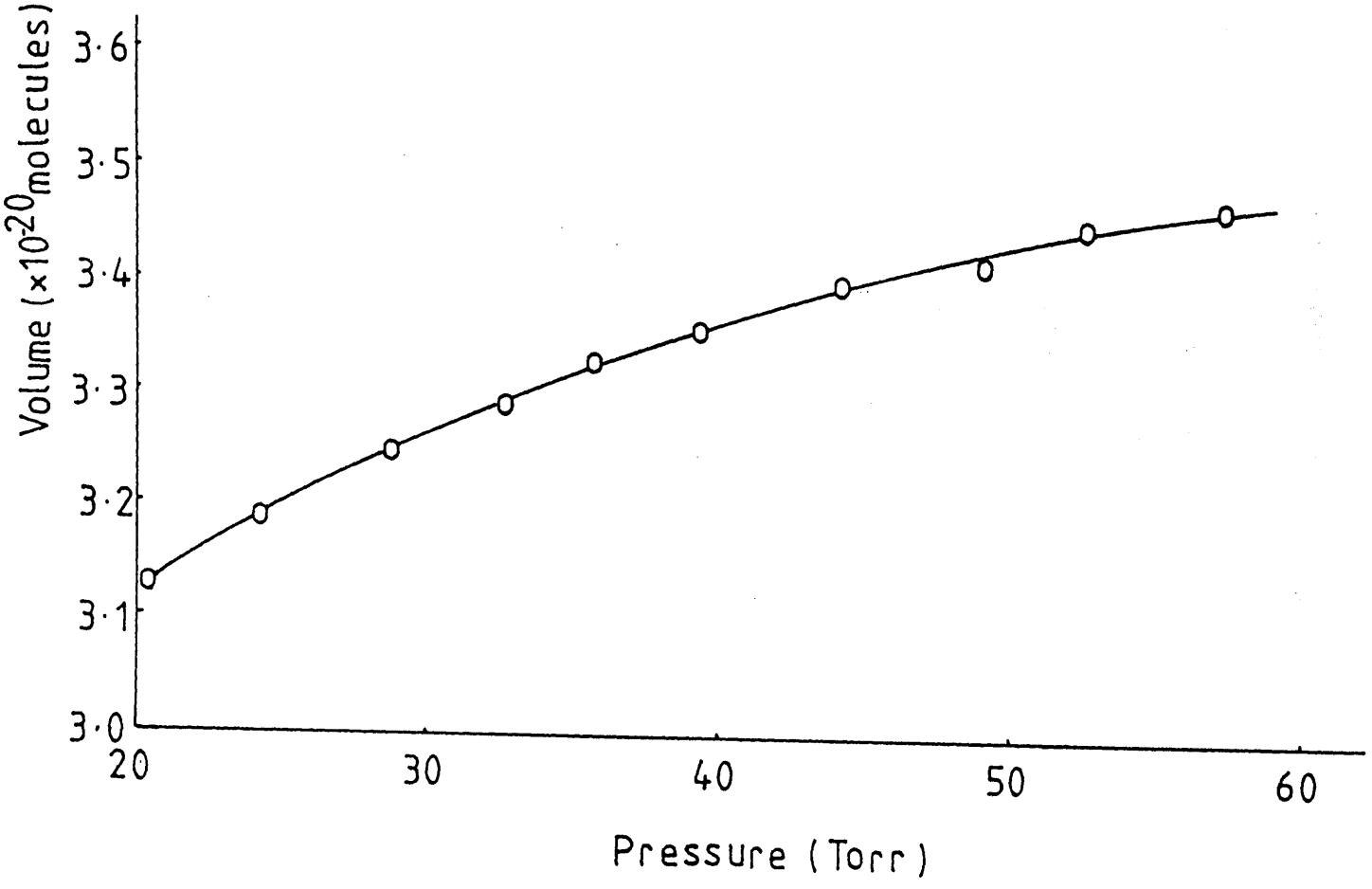

3.8.1. The uptake of carbon monoxide by the catalyst sample was calculated from the frontal chromatograms obtained, in a manner analogous to that used to calculate nitrogen uptake.

4.5 Gas Chromatographic Analysis of Buta-1,3-diene Hydrogenation Products

The gas chromatographic system shown in Chapter 3, section 3.2.4, was calibrated using a standard gas mixture containing known percentages of the reactant and product hydrocarbons. The gases were eluted from the column in the order:

butane < 1-butene < trans-but-2-ene < cis-but-2-ene < buta-1,3-diene

Separate peaks were observed for each product. Since both the total pressure of the sample being analysed and the percentage of each component in the mixture were known, by integrating the peak area for each product, a response factor in units of area/Torr could be calculated. These response factors were used to calculate the partial pressures of products present in gas mixtures of unknown composition.

During buta-1,3-diene hydrogenation reactions, the butene distribution was calculated for reactions in which either the temperature or the reaction extent was varied. The calculation of the butene distribution involved expressing the partial pressure of each butene as a percentage of the total butene pressure.

The reaction extent is defined as

$$\text{reaction extent} = \{2p_{(\text{butane})} + P_{(\text{butenes})}\}/\Sigma P_{(\text{hydrocarbons})}$$

where $P_{(\text{butenes})}$ is the sum of the partial pressures of 1-butene, trans-but-2-ene and cis-but-2-ene.

The selectivity, S, of a catalyst at a particular temperature or reaction extent is defined as:

$$S = P_{(\text{butenes})} / \{P_{(\text{butenes})} + P_{(\text{butane})}\}$$

The rate values used to calculate the order of reaction with respect to the reactants, or the activation energy for each catalyst, were obtained from the pressure fall versus time plots produced during the course of the reaction. The rates quoted correspond to the initial rates, since the rate of reaction can change during the course of the reaction. The rate was obtained by finding the gradient of a tangent to the curve at the start of the pressure/time plot.

By varying the temperature at which buta-1,3-diene hydrogenation was carried out, with all other variables held constant, a variation in the initial rate of reaction was observed.

The Arrhenius equation, rate = $Ae^{-E_a/RT}$, where the rate is the initial rate, and E_a is the activation energy, shows the relationship between the initial rate and the activation energy. By plotting the natural log of the initial rate against the inverse of the temperature in Kelvin, a straight line with a gradient of $\frac{-E_a}{R}$ is obtained. Hence,

the activation energy for each catalyst can be calculated.

Kinetics experiments were carried out to determine the order of reaction with respect to the partial pressure of each of the reactants. The rate of reaction depends on the partial pressure of both reactants, and on the rate constant, k. They can be linked by an equation of the form:

$$\text{rate} = k p_{H_2}^{x} \, p_{C_4H_6}^{y}$$

where x and y are the orders of reaction with respect to p_{H_2} and $p_{C_4H_6}$, respectively.

By holding the partial pressure of one reactant constant while the other is varied, any variation in rate which occurred as a result of varying the partial pressure of one reactant, could be observed. A linear plot of either the initial rate against the partial pressure of one reactant, or of log (initial rate) against log (partial pressure of reactant) yields the order of reaction with respect to that reactant.

CHAPTER FIVE

CHAPTER 5

RESULTS

In view of the fact that nine catalysts were prepared and used in this study, it was necessary to find a method of distinguishing the catalysts. In the results presented in this chapter, catalysts prepared using chloroplatinic acid will be denoted (a), those prepared from rhodium nitrate will be denoted (b), and those prepared from rhodium chloride will be denoted (c).

For example:

$Pt/SiO_2(a)$: silica supported platinum, prepared from chloroplatinic acid

$Rh/MoO_3(b)$: molybdenum trioxide supported rhodium, prepared from rhodium nitrate

$Rh/WO_3(c)$: tungsten trioxide supported rhodium, prepared from rhodium chloride

5.1 Temperature Programmed Reduction

5.1.1 T.P.R. Using Flow System I

A series of temperature programmed reduction experiments was carried out, using Flow System I, following the procedure described in Chapter 3, section 3.3.

Table 5.1 shows the T_{max} values (the temperature at each peak maximum) obtained for each catalyst, together with the total quantity of hydrogen involved in the reduction of the catalyst.

Figures 5.1 to 5.9 show the temperature profiles obtained for each catalyst. Throughout, the heating rate was 5°C min^{-1}.

The theoretical quantity of hydrogen required for reduction of 1g of catalyst which gives 1.1% w/w Pt/support on reduction or 1.5% w/w Rh/support on reduction was calculated. 1g of the platinum containing catalyst requires 6.8×10^{19} molecules of H_2 for complete reduction of the supported platinum salt to supported platinum metal. Complete reduction of either of the supported rhodium salts to supported rhodium metal requires 1.32×10^{20} molecules of H_2.

To ensure complete reduction of each catalyst during its preparation for carbon monoxide chemisorption, the reduction temperatures used were 10°C greater than the T_{max} of the major reduction peak for each catalyst. Table 5.2 shows the temperatures used to reduce each catalyst prior to carrying out chemisorption experiments.

5.1.2 T.P.R. Using Flow System II

Temperature programmed reduction experiments were also carried out on a selection of catalysts using Flow System II. The catalysts studied were Pt/SiO_2(a), Pt/MoO_3(a), Pt/WO_3(a) and Rh/MoO_3(c).

Figure 5.10 shows the temperature programmed reduction profile for Pt/MoO_3(a). Following the first reduction peak at around 80°C, the partial pressure of hydrogen in the system dropped drama-

Table 5.1. Temperature Programmed Reduction Results

Supported Salt	T_{max} (°C)	Total Hydrogen Uptake (No. of molecules (g catalyst)$^{-1}$)
H_2PtCl_6/SiO_2	162	2.12×10^{19}
H_2PtCl_6/MoO_3	29	6.57×10^{20}
	106	
	257	
	500	
H_2PtCl_6/WO_3	118	4.59×10^{20}
	385	
$Rh(NO_3)_3/SiO_2$	167	6.91×10^{20}
	250	
$Rh(NO_3)_3/MoO_3$	24	6.71×10^{20}
	164	
	269	
	584	
$Rh(NO_3)_3/WO_3$	158	1.09×10^{21}
	406	
$RhCl_3/SiO_2$	120	1.77×10^{20}
$RhCl_3/MoO_3$	106	1.49×10^{21}
	140	
	262	
	500	
$RhCl_3/WO_3$	111	5.89×10^{20}
	385	
	500	

Table 5.1 (contd.)

Supported Salt	T_{max} (°C)	Total Hydrogen Uptake (No. of molecules (g catalyst)$^{-1}$)
SiO_2	642	2.8×10^{19}
MoO_3	756	4.16×10^{21}
	891	
WO_3	693	7.83×10^{21}
	835	

Fig. 5.1 T.P.R. Profile of Pt/SiO_2

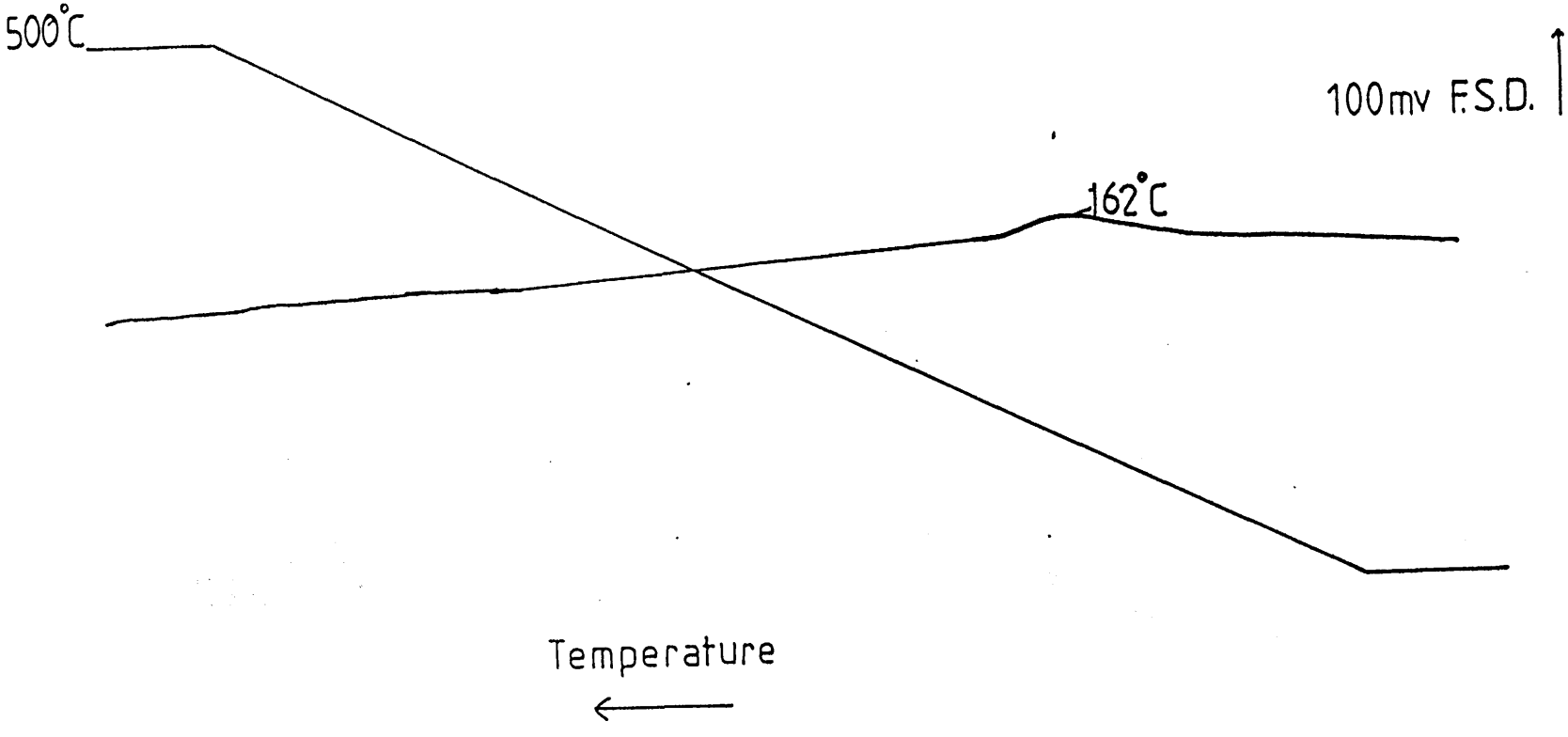

Fig. 5.2 T.P.R. Profile of Pt/MoO_3

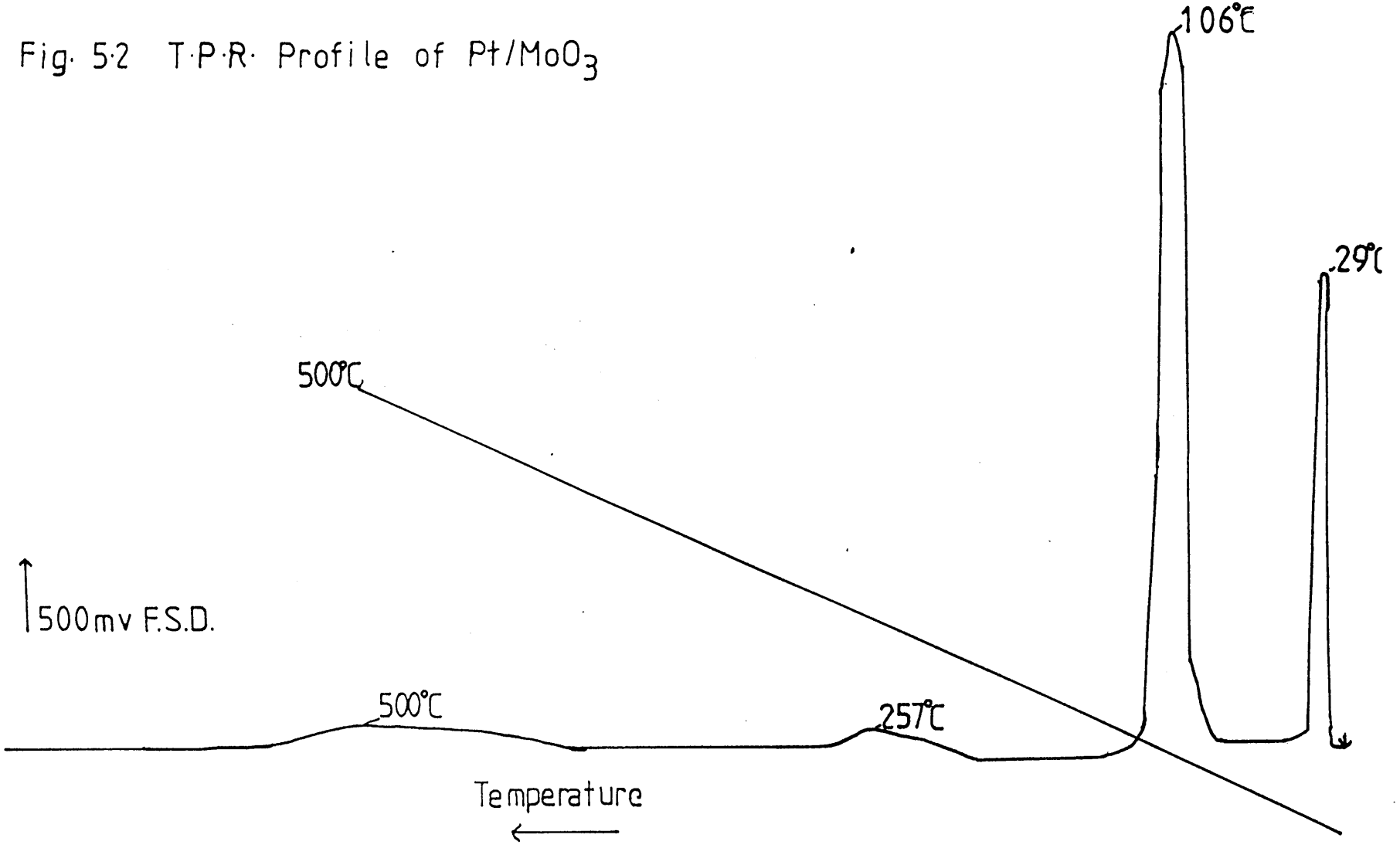

Fig. 5·3 T.P.R. Profile of Pt/WO_3

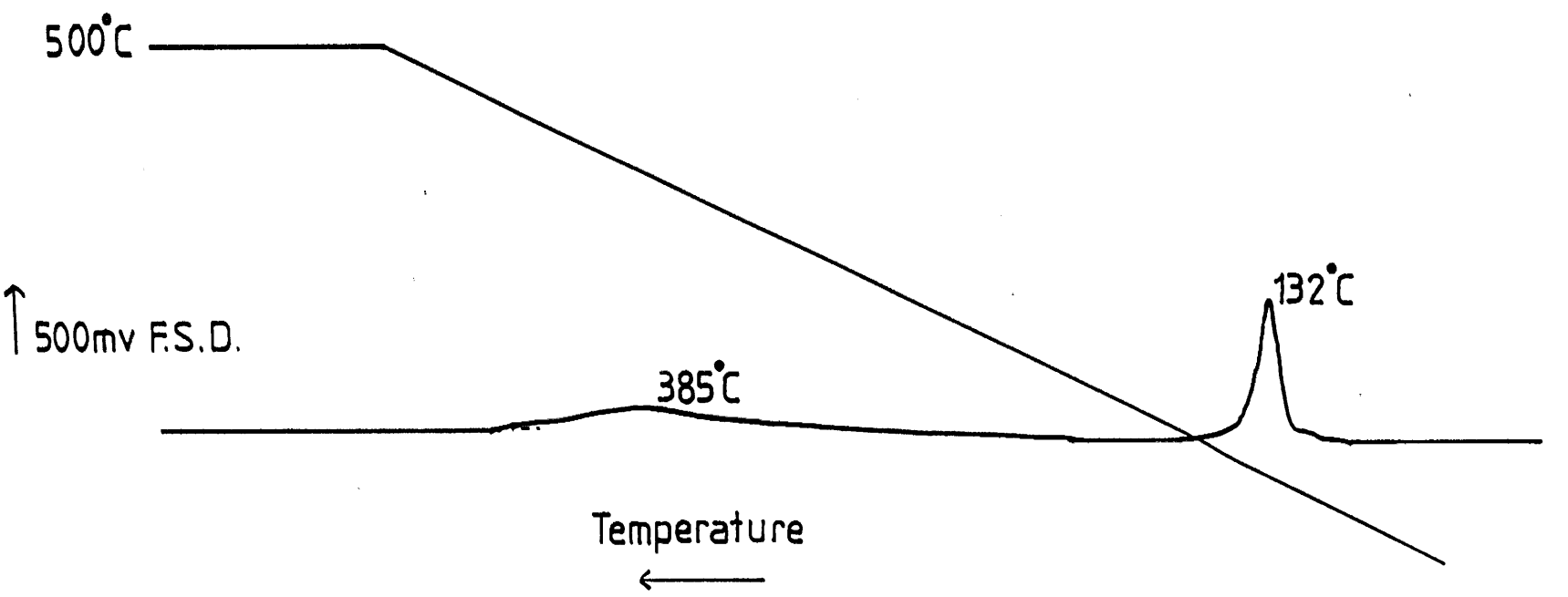

Fig. 5·4 T.P.R. Profile of Rh/SiO_2(b)

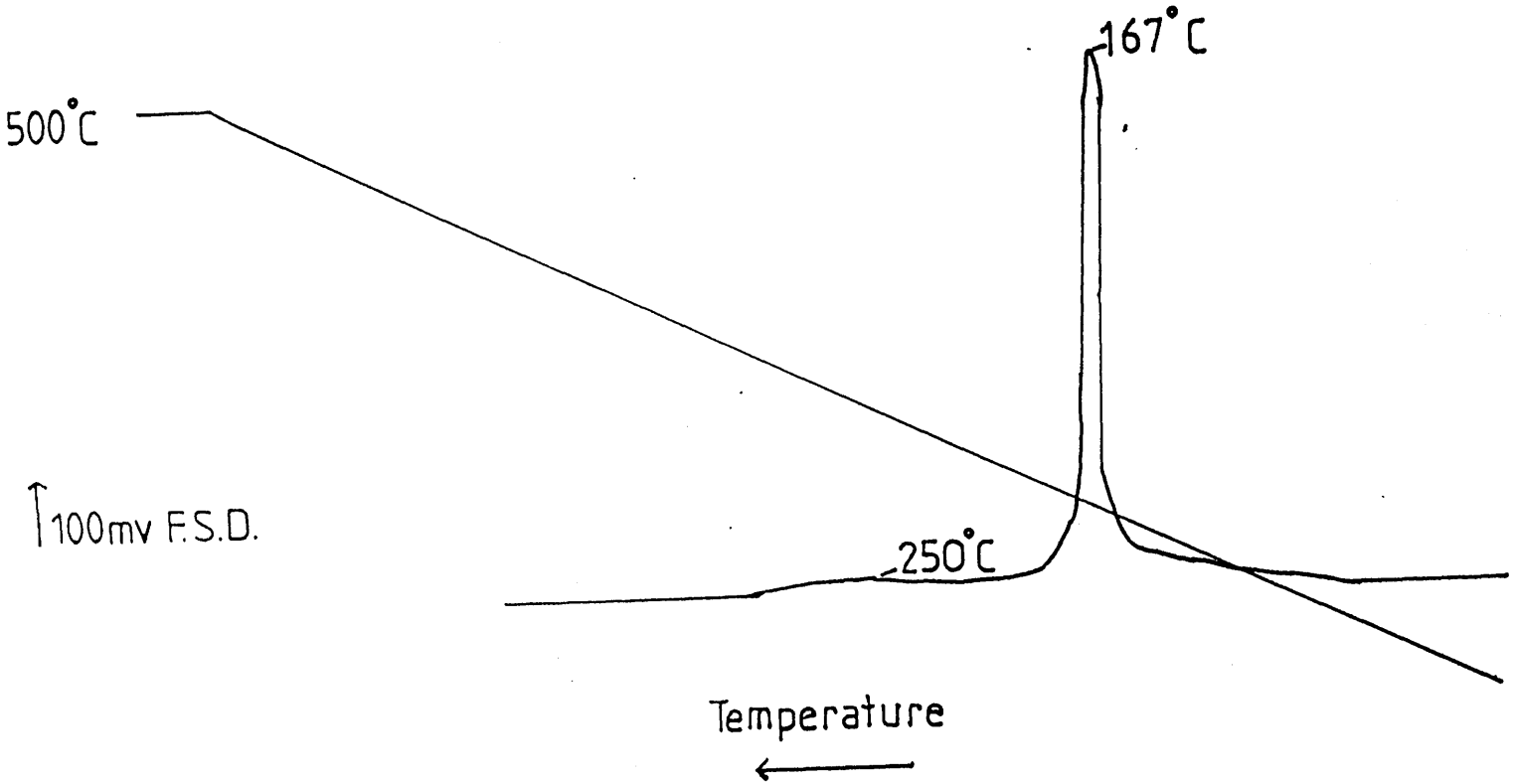

Fig. 5·5 T.P.R. Profile of Rh/MoO_3(b)

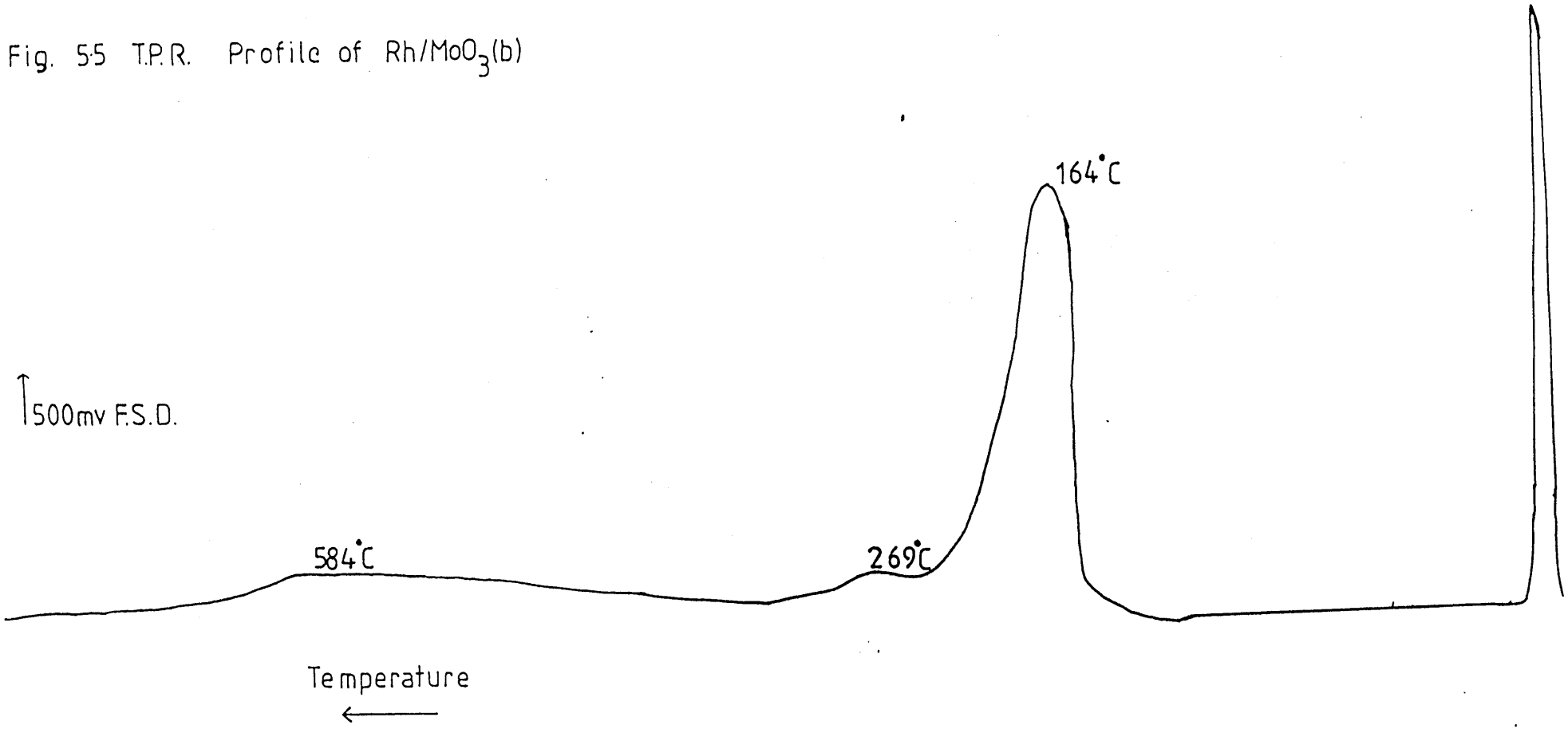

Fig. 5·6 T.P.R. Profile of $Rh/WO_3(b)$

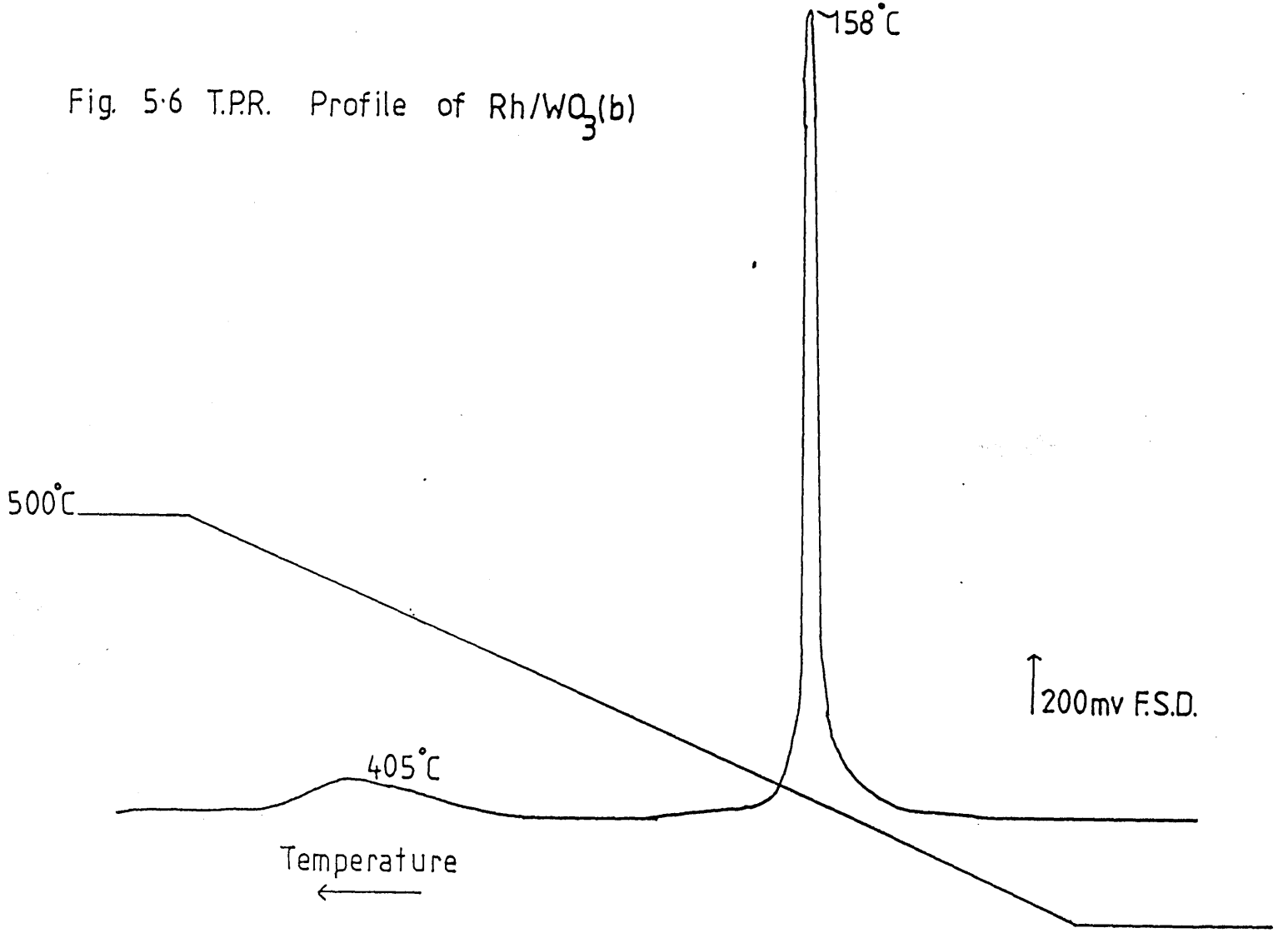

Fig. 5·7 T.P.R. Profile of $Rh/SiO_2(c)$

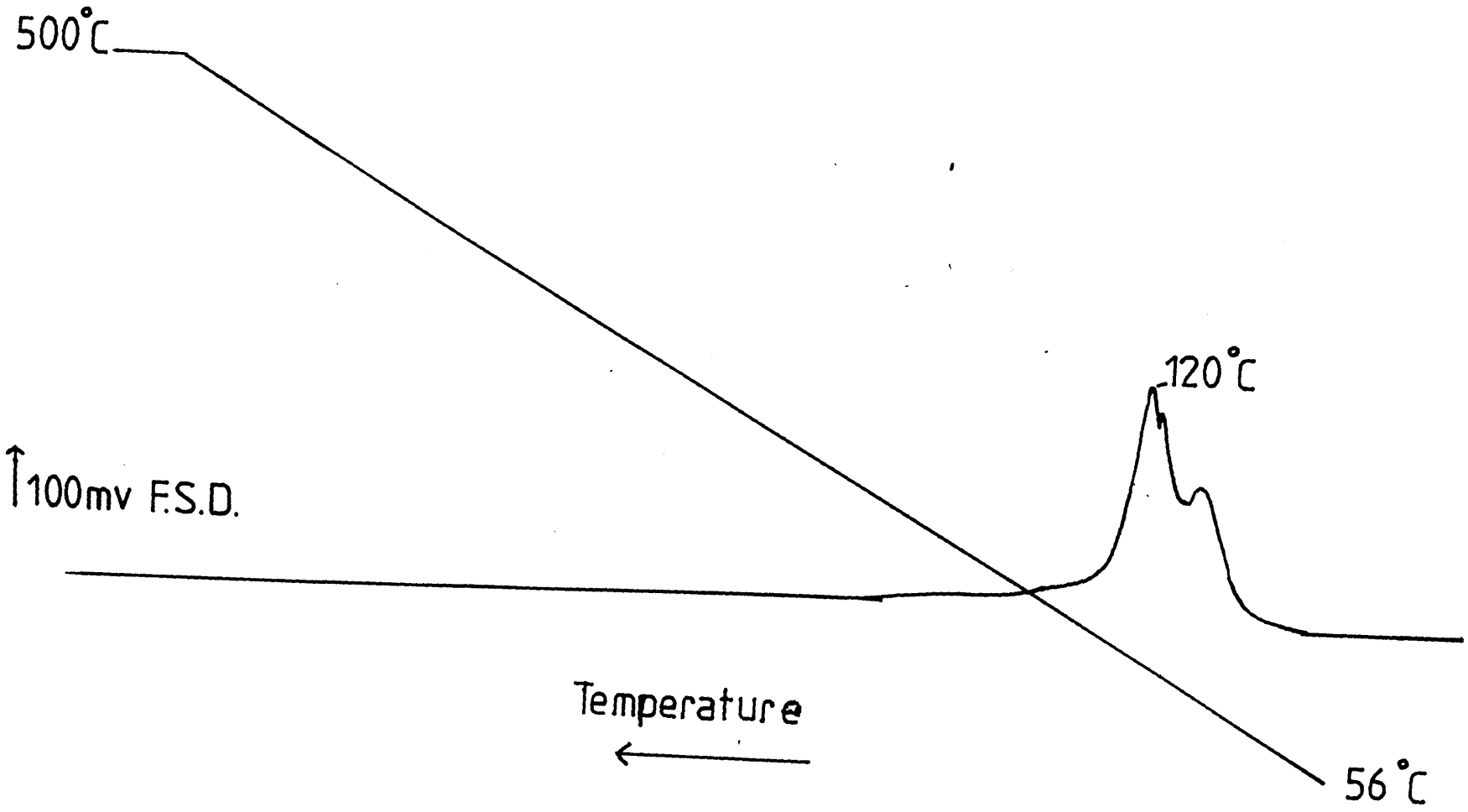

Fig. 5·8 T.P.R. Profile of $Rh/MoO_3(c)$

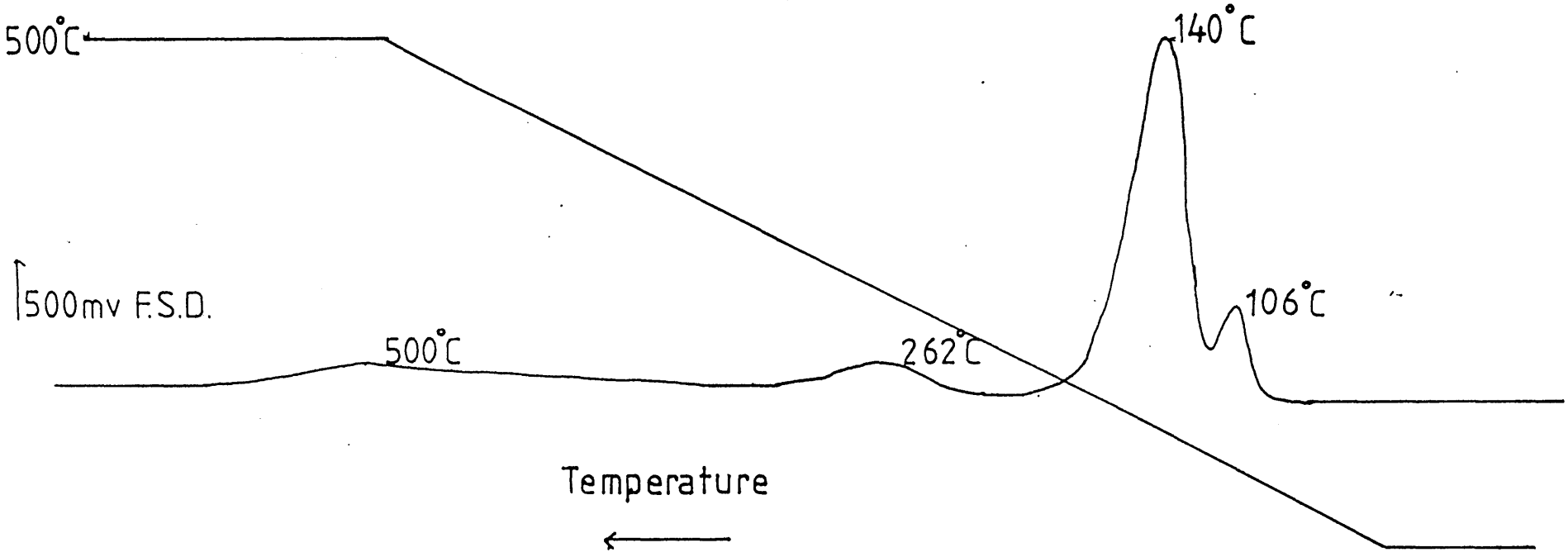

Fig. 5·9 T.P.R. Profile of $Rh/WO_3(c)$

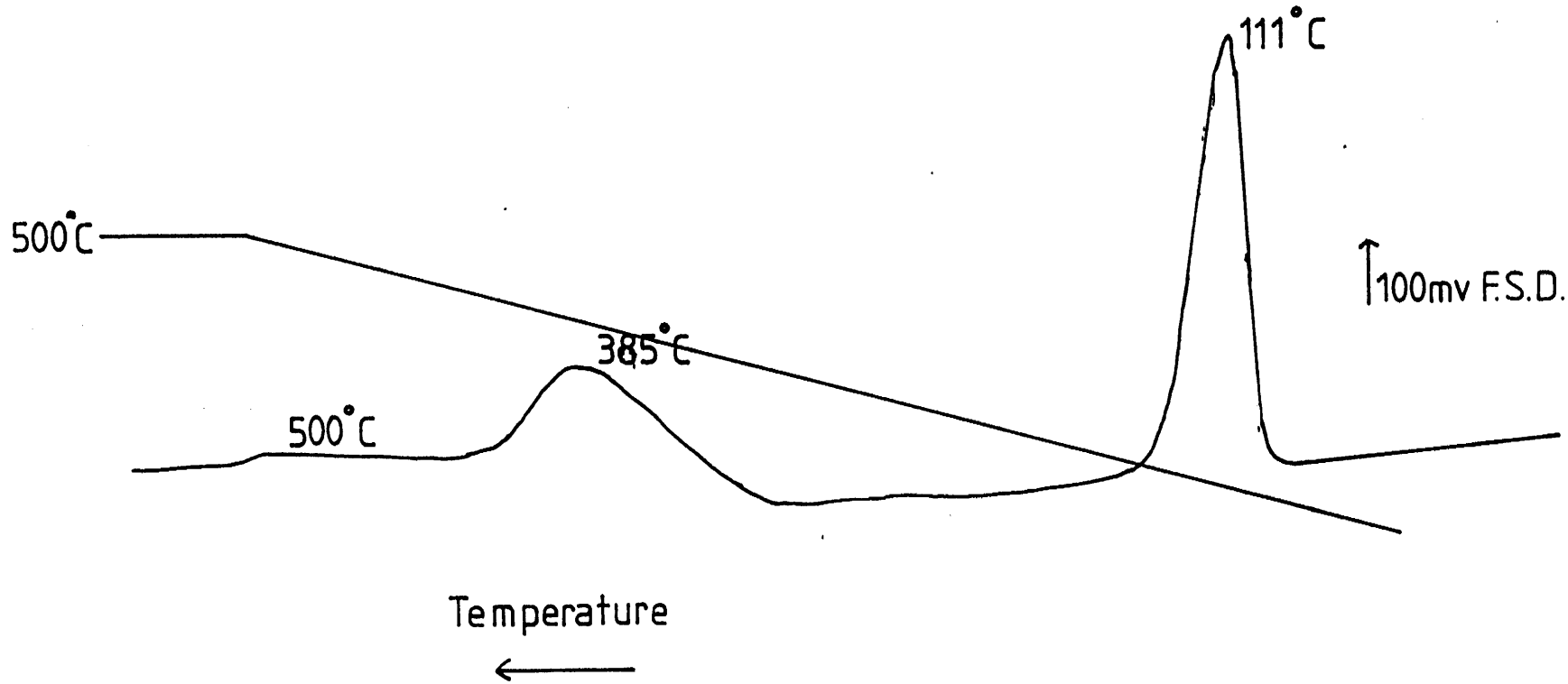

Table 5.2. Reduction Temperatures

Supported Salt	Reduction Temperature (°C)
$Rh(NO_3)_3/SiO_2$	176
$RhCl_3/SiO_2$	135
H_2PtCl_6/SiO_2	180
$Rh(NO_3)_3/MoO_3$	175
$RhCl_3/MoO_3$	155
H_2PtCl_6/MoO_3	120
$Rh(NO_3)_3/WO_3$	170
$RhCl_3/WO_3$	125
H_2PtCl_6/WO_3	140

tically to very low levels, and remained at low levels for the duration of the temperature range studied. Further water peaks were observed at approximately 100°C, 176°C and 250°C. Above 250°C, the partial pressure of water being detected rose dramatically, and remained at very high levels over the remainder of the temperature range studied.

The temperature programmed reduction profile obtained for $Pt/WO_3(a)$ (Figure 5.11) again shows the partial pressure of hydrogen decreasing sharply as reduction of the platinum salt proceeds, as shown by the formation of water. In this case, the partial pressure of hydrogen returned to high levels as reduction neared completion, as shown by the decreasing partial pressure of water. The reduction profile for the catalyst (shown in terms of water formation) is a complex series of unresolved peaks with peak maxima over the range 100°C to 150°C. Since the maximum temperature reached was 190°C, there was no major evidence of support reduction of the kind observed for reduction of $Pt/WO_3(a)$ in Flow System I (Figure 5.3), where the maximum temperature reached was 500°C.

A much simpler reduction profile was obtained for $Pt/SiO_2(a)$ (Figure 5.12). T_{max} is around 100°C, with a slight shoulder at 170°C.

A very complex reduction profile was obtained for the reduction of $Rh/MoO_3(c)$, as shown in Fig. 5.13. Reduction, signified by the production of water, starts around 50°C, with the T_{max} of the first reduction peak occurring at 85°C. The second major reduction peak, T_{max} = 301°C, appears as an unresolved shoulder on the third reduction peak, which has a $T_{max} \simeq 380°C$. (The T_{max} of the third reduction peak is estimated to occur at 380°C - the peak maximum is off-scale).

Fig. 5·10 T.P.R. Profile of Pt/MoO_3

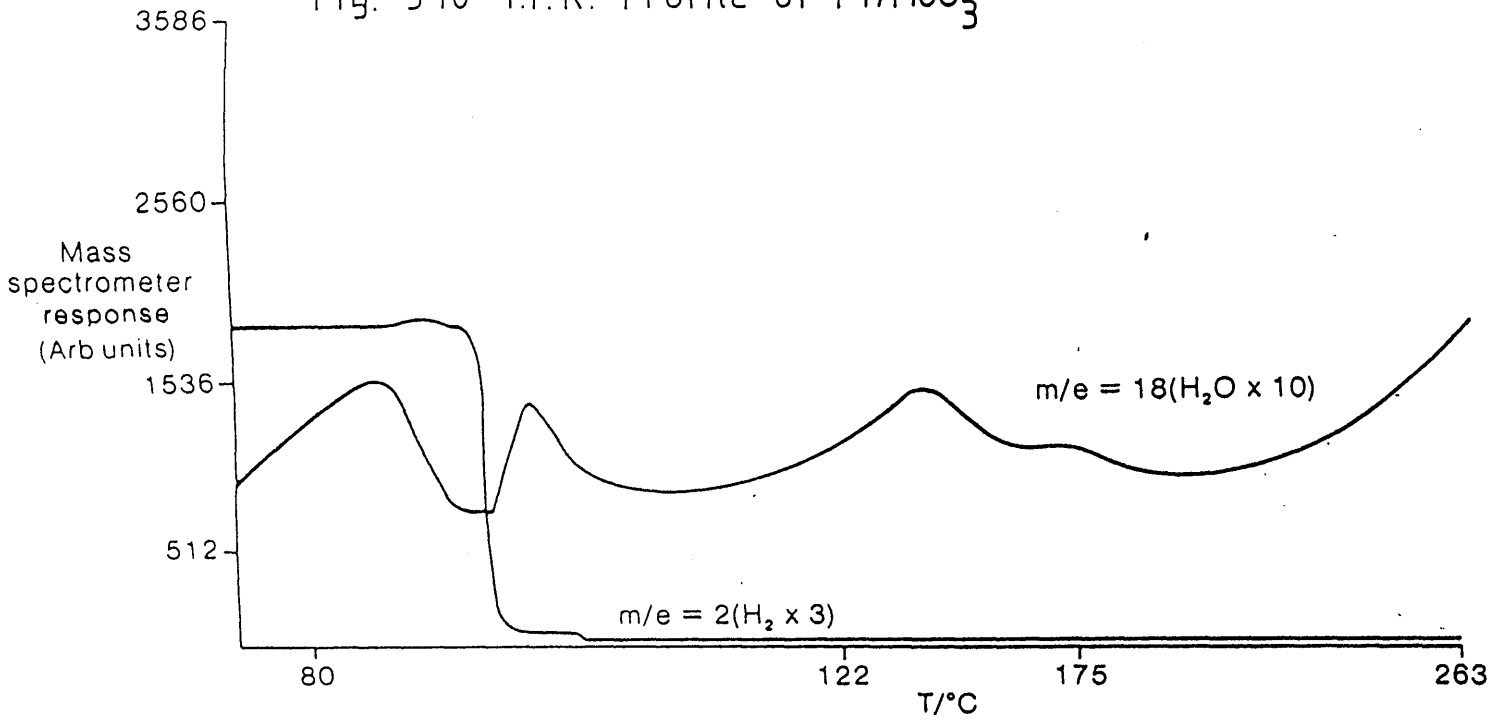

Fig. 5·11 T.P.R. Profile of Pt/WO_3

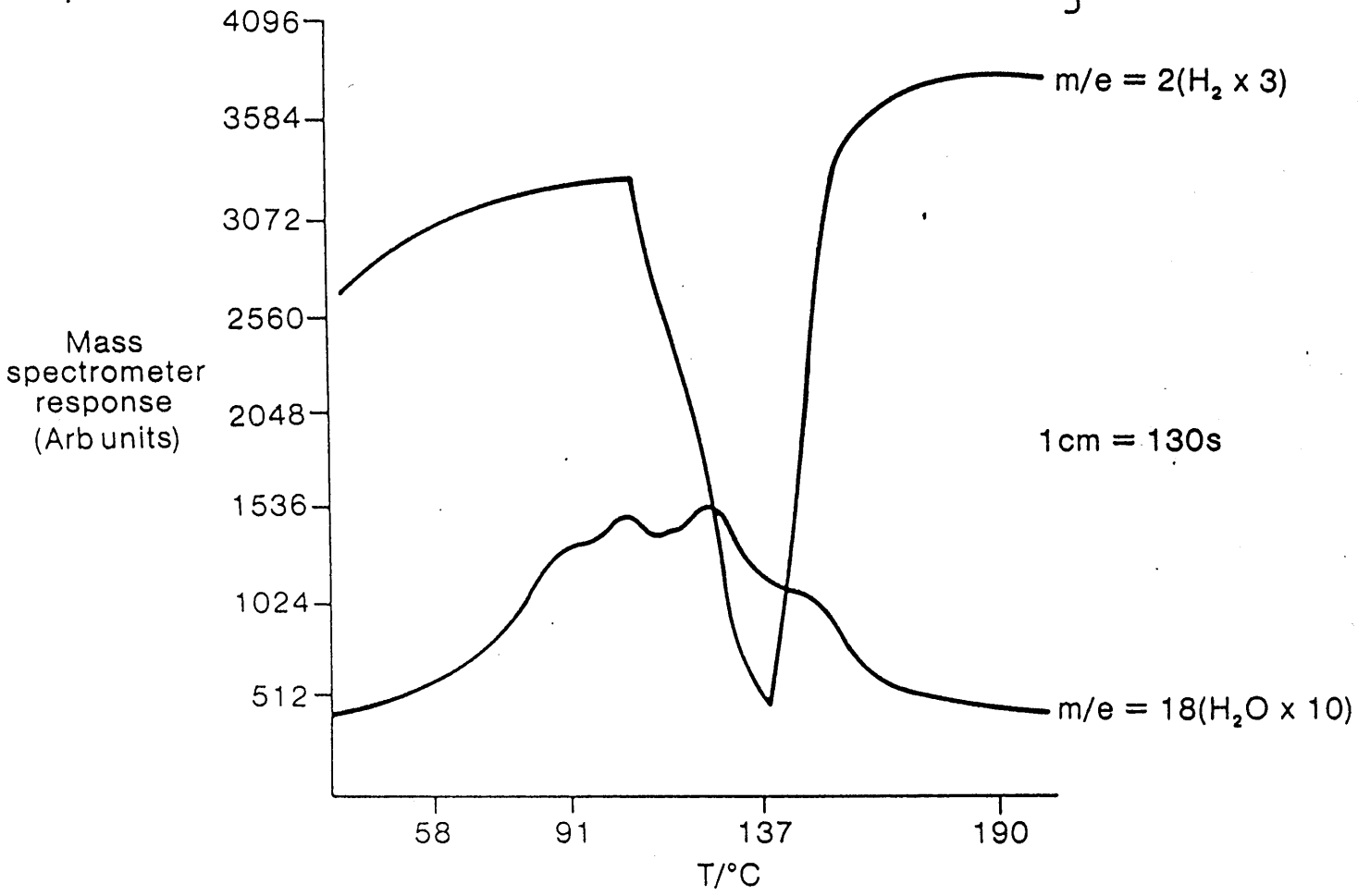

Fig. 5·12 T.P.R. Profile of Pt/SiO_2

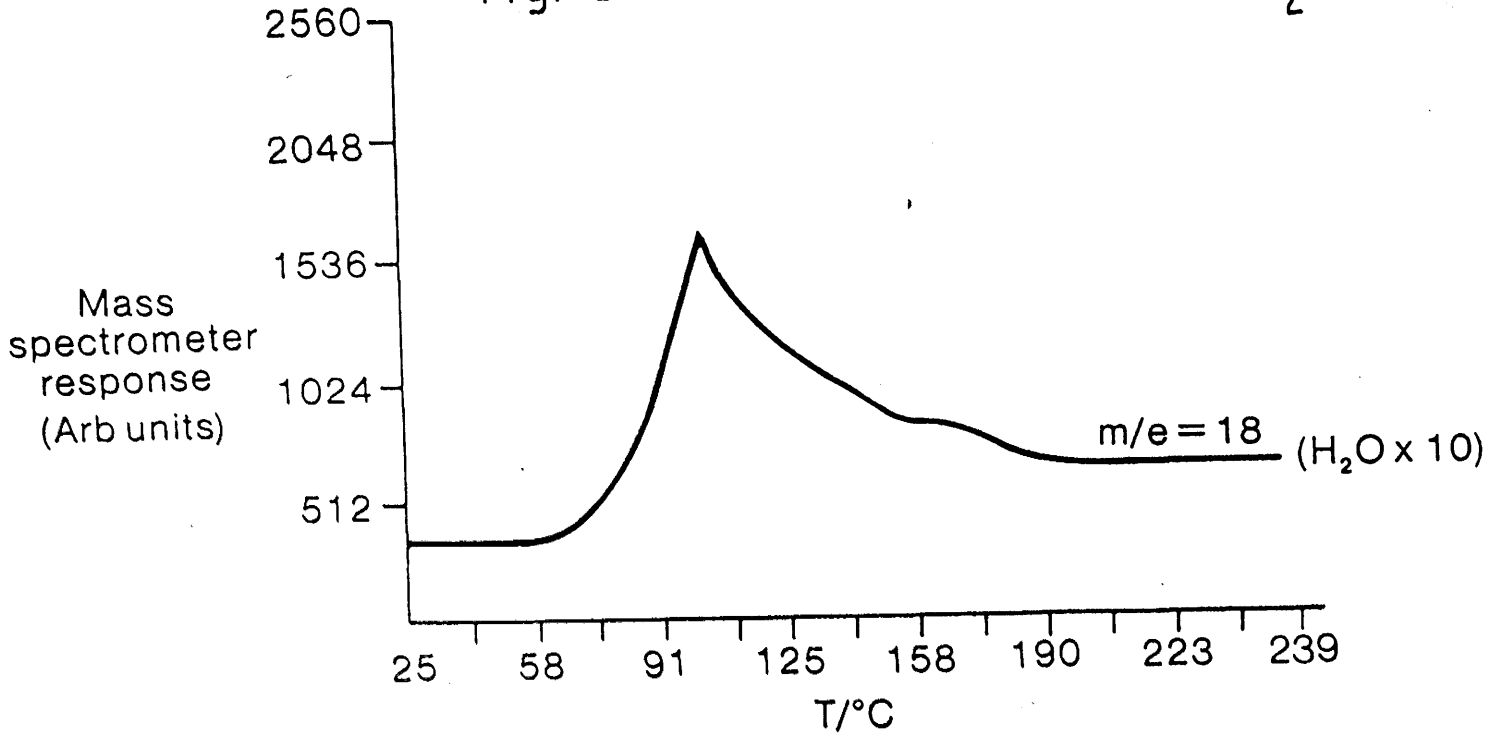

Fig. 5·13 T.P.R. Profile of Rh/MoO_3(c)

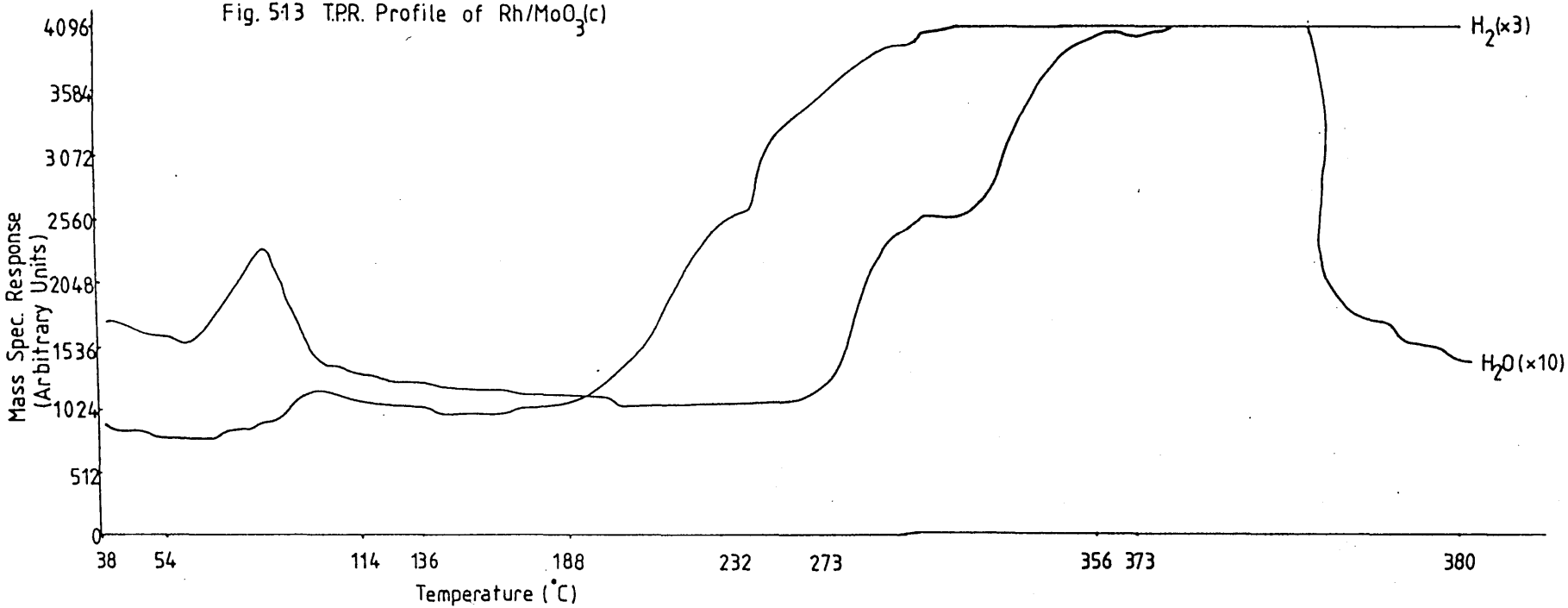

5.1.3 Temperature Programmed Desorption Following Temperature Programmed Reduction

Following each temperature programmed reduction experiment carried out using Flow System II, a temperature programmed desorption experiment was carried out to remove adsorbed hydrogen from the catalysts. The experiments were carried out according to the procedure outlined in Chapter 3, section 3.6.2.

The temperature programmed desorption profile obtained immediately after a T.P.R. experiment for $Pt/MoO_3(a)$ is shown in Figure 5.14. Hydrogen is observed to desorb at temperatures $\gtrsim$ 30°C. Above 190°C, water is observed to desorb. The peak maxima are observed at 40°C, 160°C, 240°C and 247°C. The total number of hydrogen molecules desorbed was calculated as 2.25×10^{20} (by prior calibration of the mass spectrometer). Even assuming a 1:1 H:Pt ratio, this gives a total far in excess of the number of platinum atoms in the sample, indicating that hydrogen has spilled over on to the support.

Figure 5.15 shows the temperature programmed desorption profile for $Pt/WO_3(a)$. Over the temperature range studied (-196°C to 240°C) only one desorption peak is observable. Calibration of the mass spectrometer enabled a calculation of the total number of hydrogen molecules desorbed to be made. For $Pt/WO_3(a)$, the value obtained was 4.46×10^{19} molecules $(g.catalyst)^{-1}$. For $Rh/MoO_3(c)$, a large desorption peak was observed, with T_{max} = 390°C. 3.47×10^{20} molecules H_2 $(g.catalyst)^{-1}$ were desorbed. The desorption profile for $Rh/MoO_3(c)$ is shown in Figure 5.16. Desorption of hydrogen begins at temperatures above 180°C.

Fig. 5.14 T.P.D. Profile Following T.P.R. of Pt/MoO_3(a)

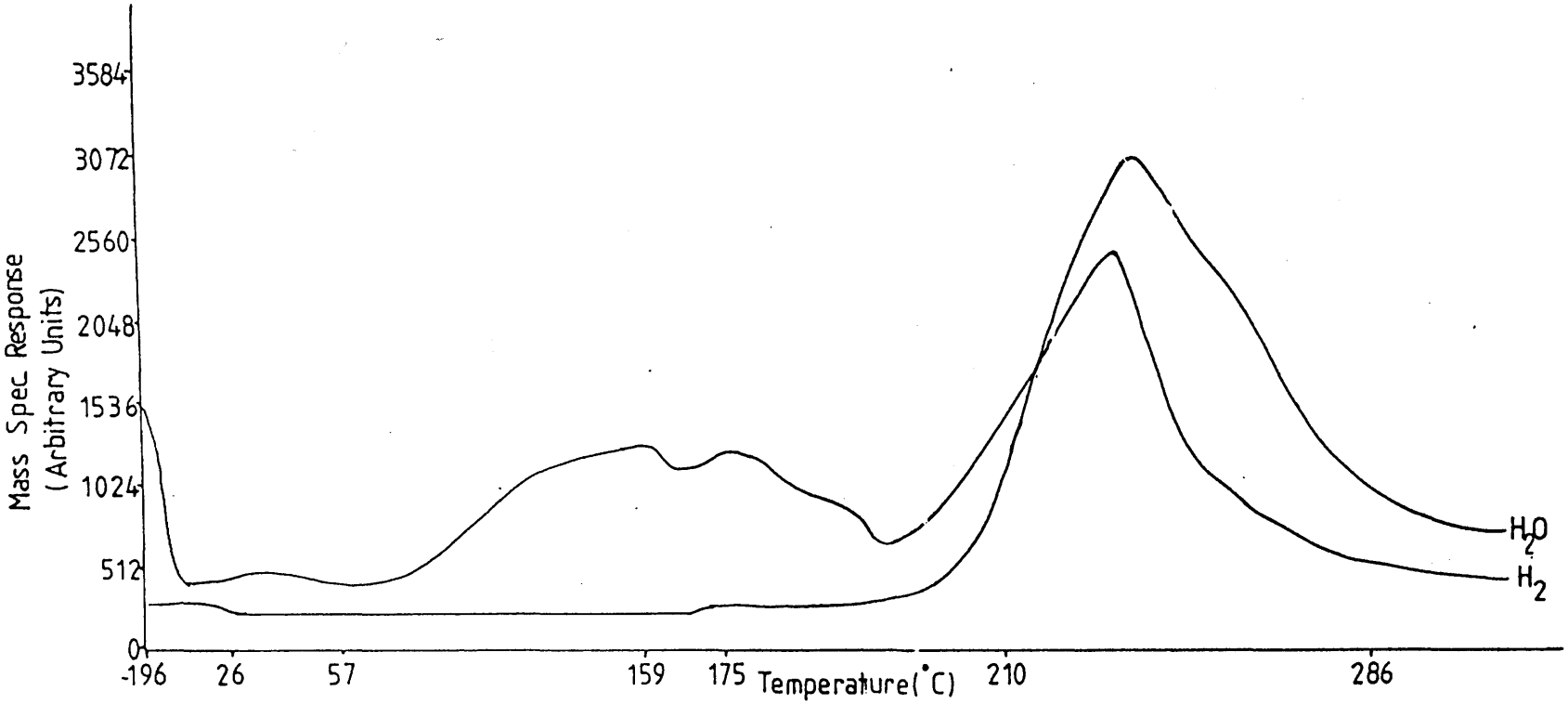

Fig. 5·15 T.P.D. Profile Following T.P.R of Pt/WO_3

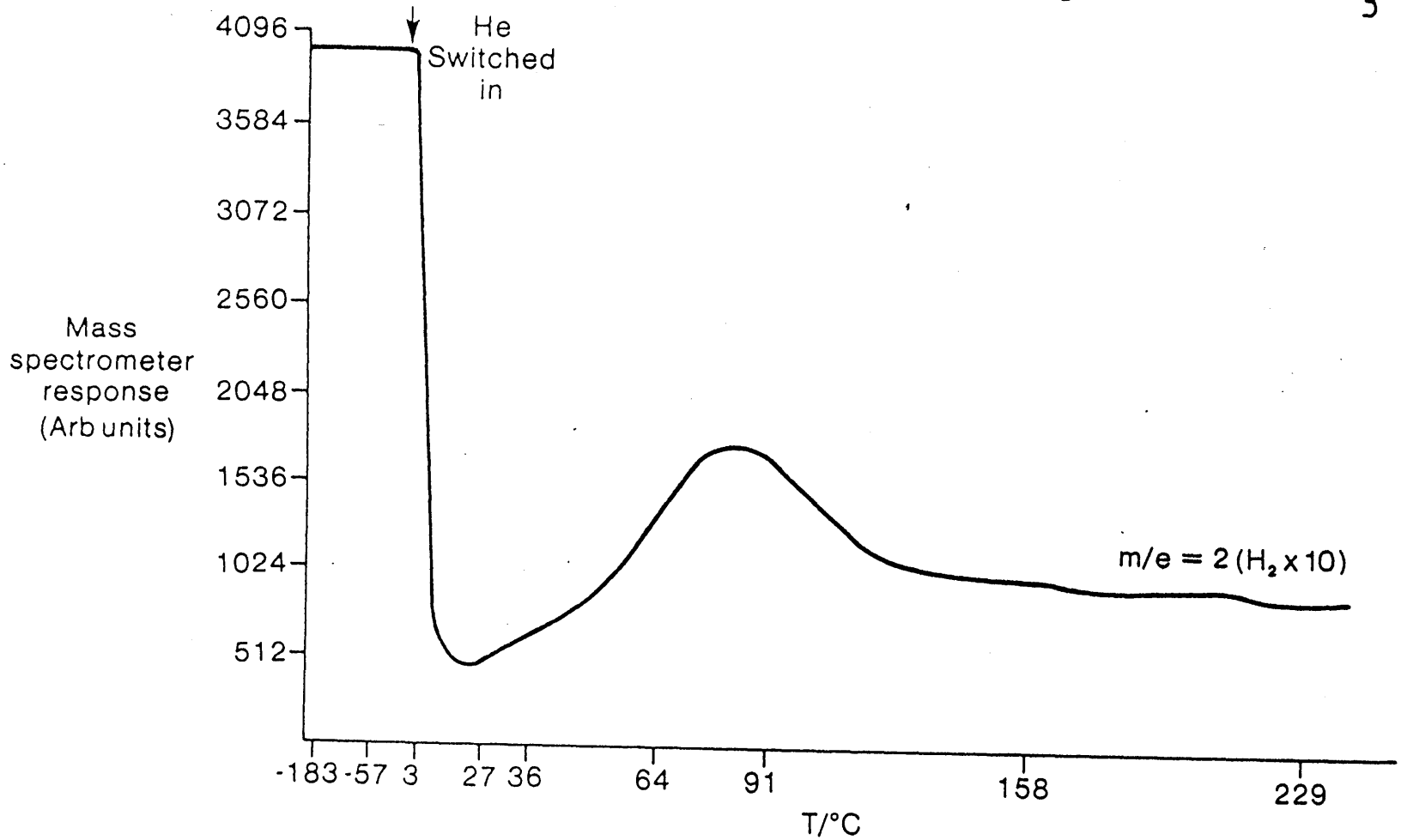

Fig. 5·16 T.P.D. Profile Following T.P.R. of Rh/MoO_3(c)

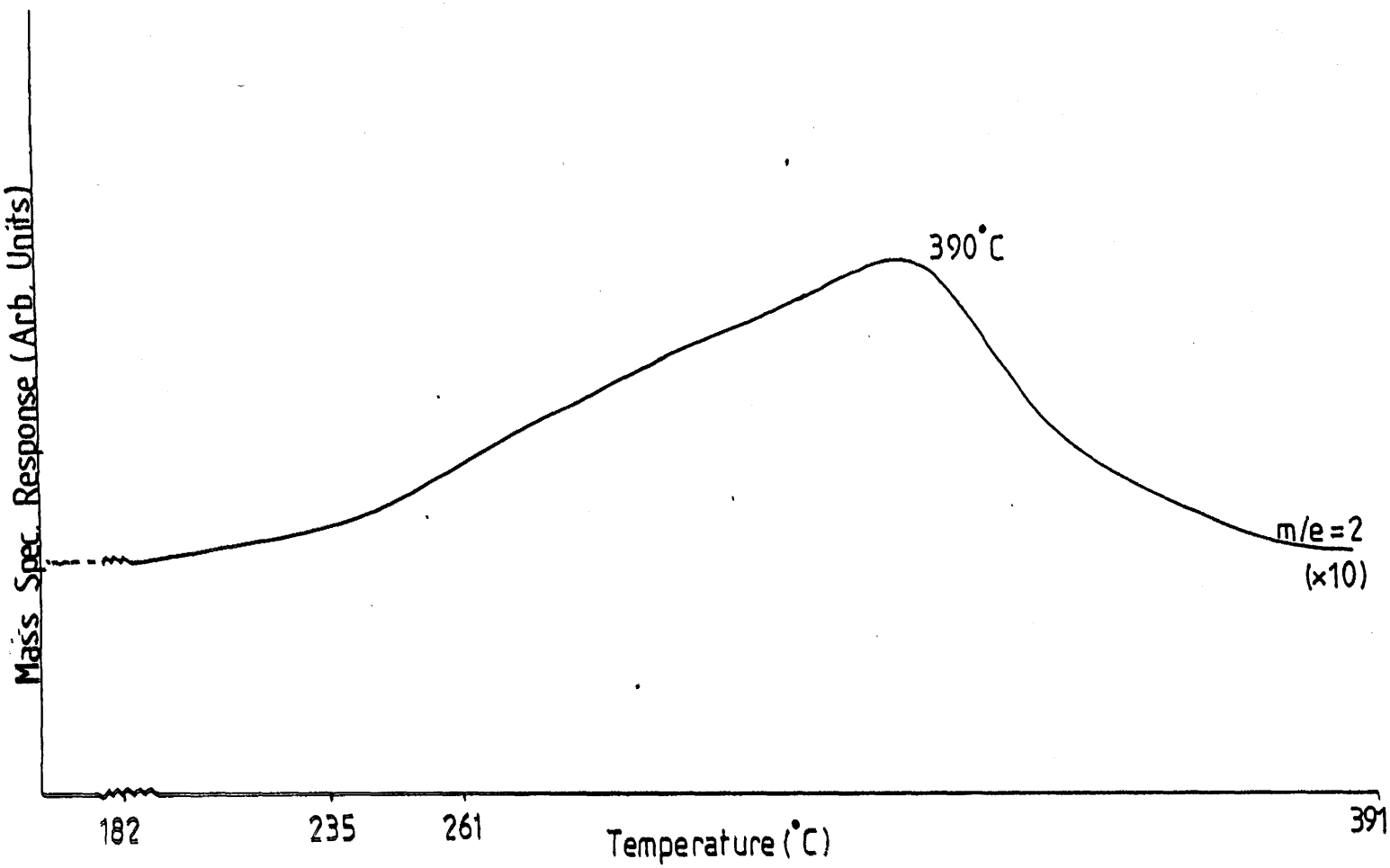

5.2 Carbon Monoxide Chemisorption and Temperature Programmed Desorption

5.2.1 Ambient Temperature Carbon Monoxide Chemisorption

Carbon monoxide chemisorption experiments were carried out in a pulsed flow reactor system, Flow System I, at ambient temperature, following the procedure described in Chapter 3, section 3.4.1. From the number of molecules of carbon monoxide calculated to be present on the surface, the metal area and the dispersion can be calculated. The calculation of these values involves making two assumptions: i) each carbon monoxide molecule is bonded to one metal atom in a linear manner, and ii) the area occupied by one carbon monoxide molecule corresponds to the van der Waals' radii of the carbon monoxide molecule, calculated to be 16.8×10^{-20} m^2. The results obtained are presented in Table 5.3. The metal area and dispersion calculations are described in Chapter 4, section 4.3.

Metal particle sizes can be calculated from the metal area of a catalyst sample using the following method:

$$\frac{S.A.}{g \text{ metal}} = \frac{4\pi r^2}{\frac{4}{3}\pi r^3 \rho} = \frac{3}{r\rho}$$

where S.A. is the metal surface area, r is the radius of the metal particle and ρ is the density of the metal. The metal particle sizes calculated in this manner are presented in Table 5.4a. Table 5.4b shows the average particle sizes for each catalyst obtained by transmission electron microscopy.

Table 5.3. Carbon Monoxide Chemisorption

Catalyst	No. of CO Molecules	Metal Area $m^2(g\ catalyst)^{-1}$	Dispersion %
Pt/SiO_2(a)	8.69×10^{18}	1.46	26
Pt/MoO_3(a)	2.50×10^{17}	0.042	0.7
Pt/WO_3(a)	9.23×10^{18}	1.55	27
Rh/SiO_2(b)	1.40×10^{19}	2.35	16
Rh/MoO_3(b)	-	Negligible	-
Rh/WO_3(b)	6.61×10^{18}	1.11	8
Rh/SiO_2(c)	4.17×10^{18}	0.70	5
Rh/MoO_3(c)	2.14×10^{18}	0.36	2
Rh/WO_3(c)	2.76×10^{19}	4.64	31

(a): prepared from chloroplatinic acid

(b): prepared from rhodium nitrate

(c): prepared from rhodium chloride

Table 5.4a. Calculated Metal Particle Sizes

Catalyst	Diameter of Metal Particles (Calculated)
Pt/SiO_2(a)	2.10×10^{-8} m
Pt/MoO_3(a)	7.36×10^{-7} m
Pt/WO_3(a)	1.99×10^{-8} m
Rh/SiO_2(b)	3.08×10^{-8} m
Rh/MoO_3(b)	-
Rh/WO_3(b)	6.54×10^{-8} m
Rh/SiO_2(c)	1.04×10^{-7} m
Rh/MoO_3(c)	2.02×10^{-7} m
Rh/WO_3(c)	1.56×10^{-8} m

(a): prepared from chloroplatinic acid

(b): prepared from rhodium nitrate

(c): prepared from rhodium chloride

Table 5.4b. Particle Sizes Obtained by T.E.M.

Catalyst	Average Particle Size (nm)	Range (nm)
Pt/SiO_2(a)	1.4	0.3 to 2.96
Pt/MoO_3(a)	2.7	0.69 to 5.75
Pt/WO_3(a)	2.7	0.59 to 4.7
Rh/SiO_2(b)	1.7	0.59 to 2.96
Rh/MoO_3(b)	1.3	0.59 to 3.6
Rh/WO_3(b)	2.2	0.89 to 3.6
Rh/SiO_2(c)	1.6	0.6 to 5.4
Rh/MoO_3(c)	2.4	0.9 to 4.2
Rh/WO_3(c)	2.9	1.2 to 7.5

5.2.2 Temperature Programmed Desorption Following Ambient Temperature Carbon Monoxide Chemisorption

Immediately following each carbon monoxide chemisorption experiment at ambient temperature, a temperature programmed desorption experiment was carried out. Temperature programmed desorption profiles such as those shown in Figures 5.17 and 5.18 were obtained. Figure 5.17 shows the desorption of carbon monoxide and carbon dioxide from $Pt/WO_3(a)$. Figure 5.18 shows hydrogen (H_2) and water desorbing from $Rh/MoO_3(c)$ following a carbon monoxide chemisorption; no carbon monoxide or carbon dioxide was detected during this T.P.D.

Table 5.5 summarises the data obtained from T.P.D. following carbon monoxide chemisorption. The results were obtained using a mass spectrometer. Since the mass spectrometer was not calibrated, the results are only qualitative in nature.

5.2.3 Temperature Programmed Desorption Following Temperature Programmed Reduction

The formation of both hydrogen and water was observed during T.P.D. following carbon monoxide chemisorption. It was, therefore, decided that the molybdenum trioxide- and tungsten trioxide-supported catalysts should be investigated by carrying out temperature programmed desorption experiments immediately after carrying out temperature programmed reduction (using Flow System I). This was to enable a comparison to be made between desorption profiles obtained immediately after reduction of the catalyst with those obtained following carbon monoxide chemisorption.

Fig. 5·17 T.P.D. Profile Following CO Chemisorption on Pt/WO_3

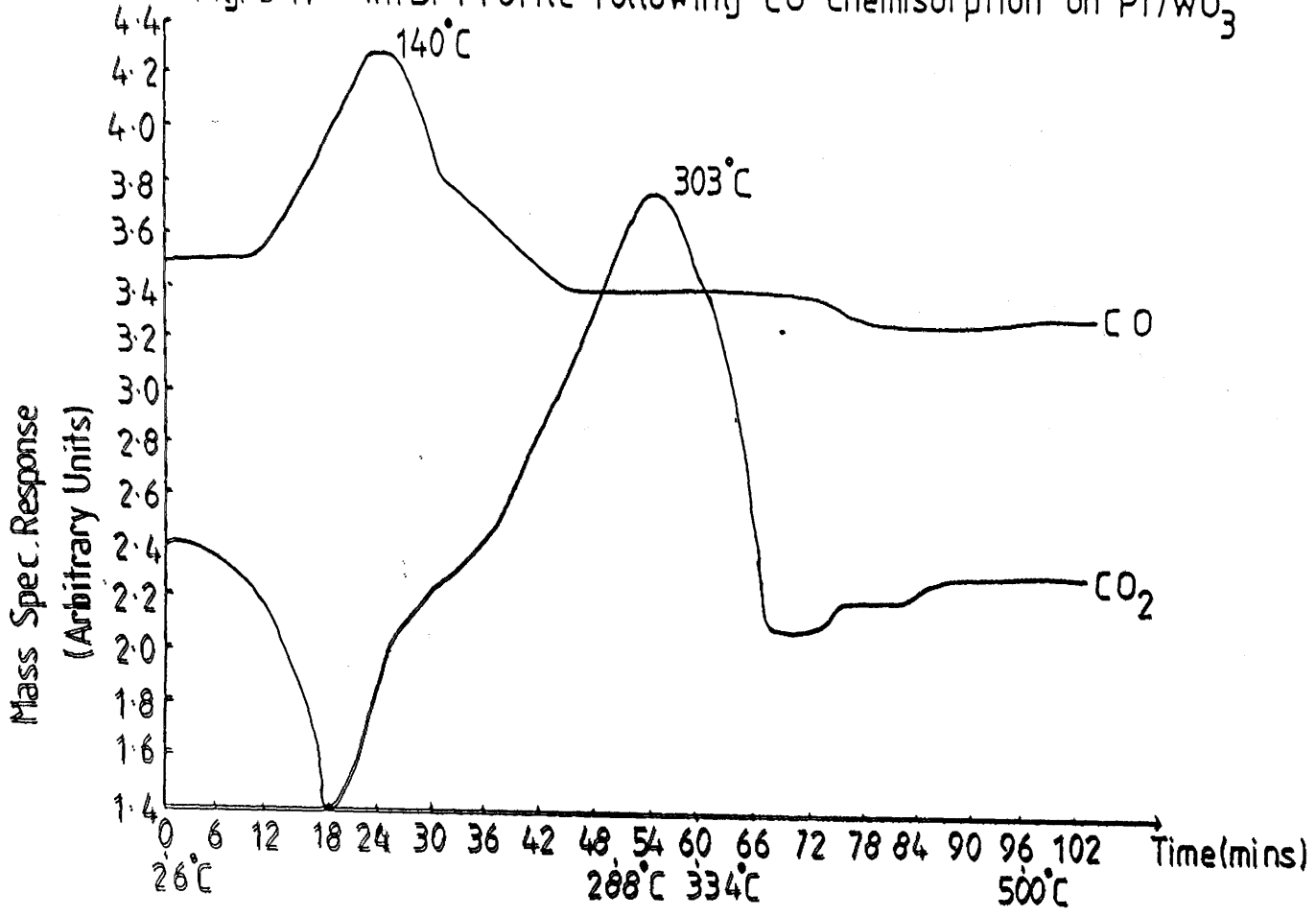

Fig. 5·18 T.P.D. Profile Following CO Chemisorption on $Rh/MoO_3(c)$

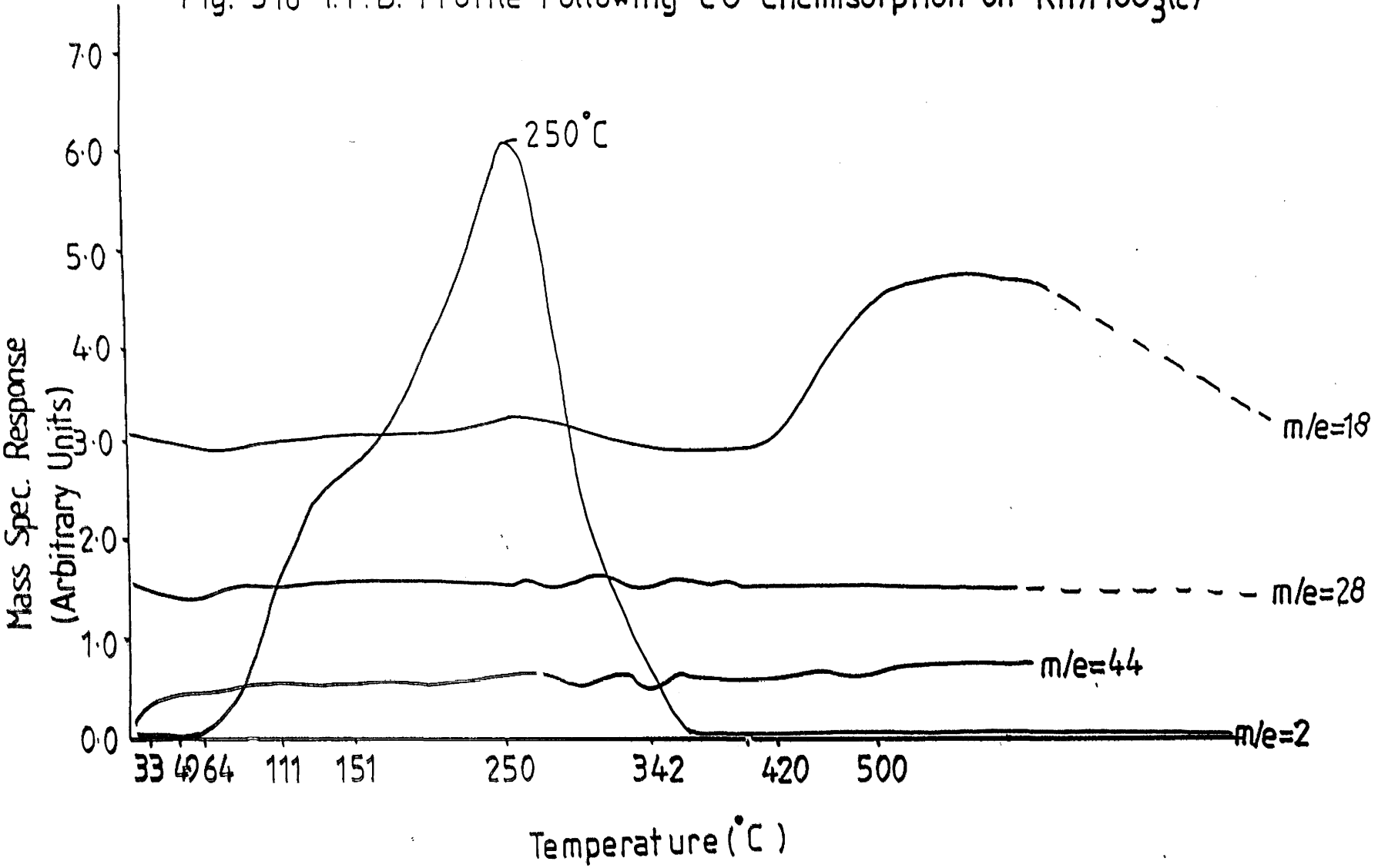

Table 5.5. Temperature Programmed Desorption

Catalyst	Desorbing Species	$T_{max\ (des)}$* °C
Pt/SiO_2(a)	H_2	358
Pt/MoO_3(a)	CO	251
	CO_2	426
Pt/WO_3(a)	CO	140
	CO_2	303
Rh/SiO_2(b)	CO	90
	CO_2	350
Rh/MoO_3(b)	H_2	471
Rh/WO_3(b)	none	-
Rh/SiO_2(c)	CO_2	114
	CO_2	361
Rh/MoO_3(c)	H_2	250
	H_2O	500
Rh/WO_3(c)	CO	130
	CO_2	295

* $T_{max\ (des)}$ = temperature at the desorption peak maximum.

For each of the catalysts studied, namely $Rh/MoO_3(b)$, $Rh/MoO_3(c)$ and $Rh/WO_3(c)$, the temperature programmed reduction procedure was identical to that used to prepare the catalyst for carbon monoxide chemisorption.

Figure 5.19 shows the T.P.D. profile obtained for $Rh/MoO_3(c)$ following temperature programmed reduction. H_2 is observed to desorb. The T_{max} appears at 305°C. A comparative study, where the catalyst was taken through an identical heating cycle, but this time in flowing helium, rather than 6% H_2/N_2, before being taken through the T.P.D. procedure, was carried out. The desorption profile obtained showed no evidence of changes in relative concentrations of hydrogen or water.

Figure 5.20 shows the desorption profile obtained immediately after carrying out a carbon monoxide chemisorption experiment on $Rh/MoO_3(b)$. This shows hydrogen desorbing with a T_{max} of 239°C and water desorbing with T_{max} = 463°C. This can be compared with the desorption profile obtained following temperature programmed reduction (Figure 5.21) of a fresh catalyst sample. The T_{max} for hydrogen desorption occurs around 237°C, with the T_{max} for water formation at 500°C (m/e = 17).

Figure 5.22 shows the desorption profile obtained following carbon monoxide chemisorption on $Rh/WO_3(c)$. Carbon monoxide is observed to desorb at T_{max} = 106°C, and hydrogen desorbed with T_{max} = 290°C. However, a T.P.D. experiment carried out immediately after temperature programmed reduction of $Rh/WO_3(c)$, failed to show any evidence of hydrogen or water desorption over the temperature range studied.

Fig. 519 T.P.D. Profile Following T.P.R. of $Rh/MoO_3(c)$

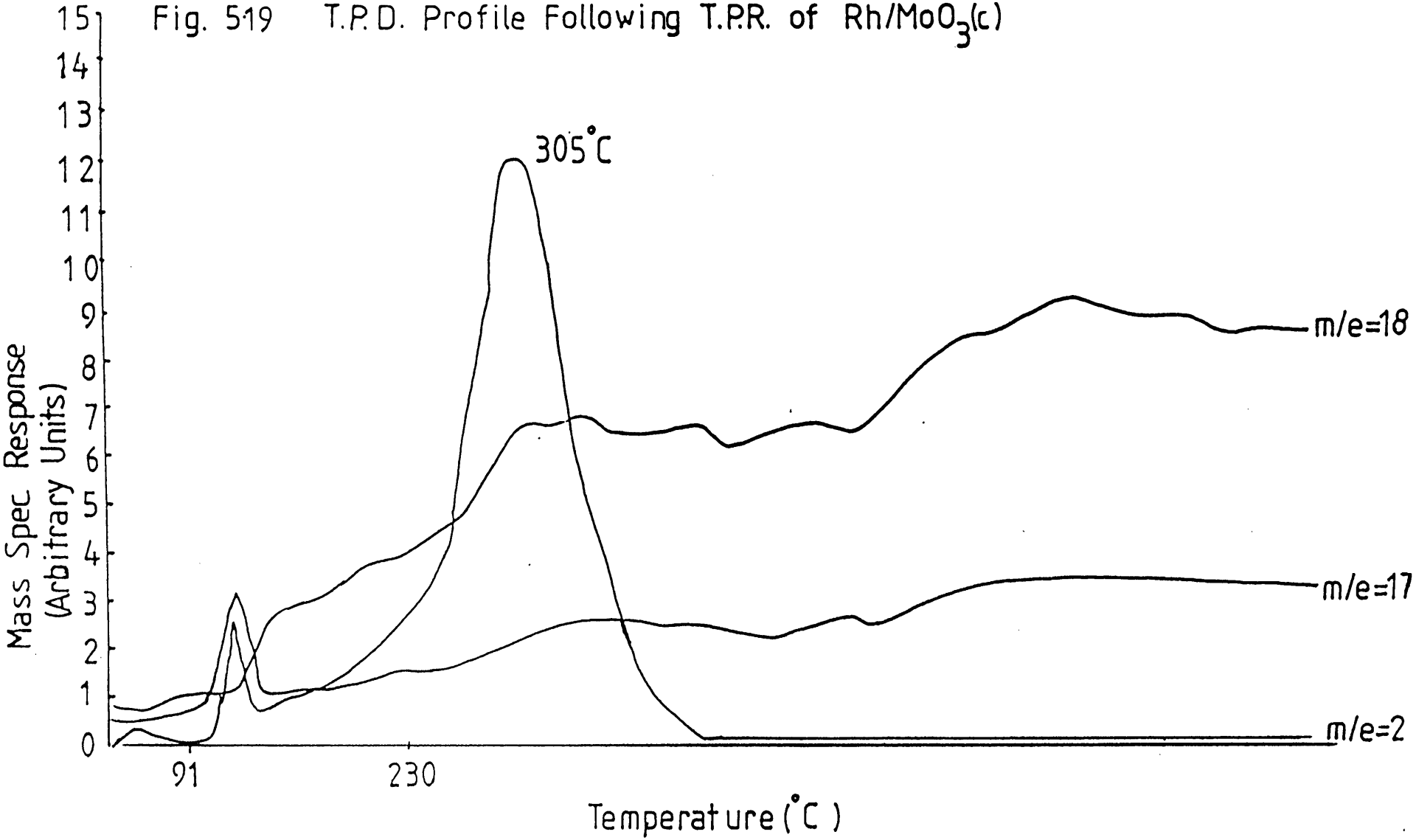

Fig. 5·20 T.P.D. Profile Following CO Chemisorption on Rh/MoO_3(b)

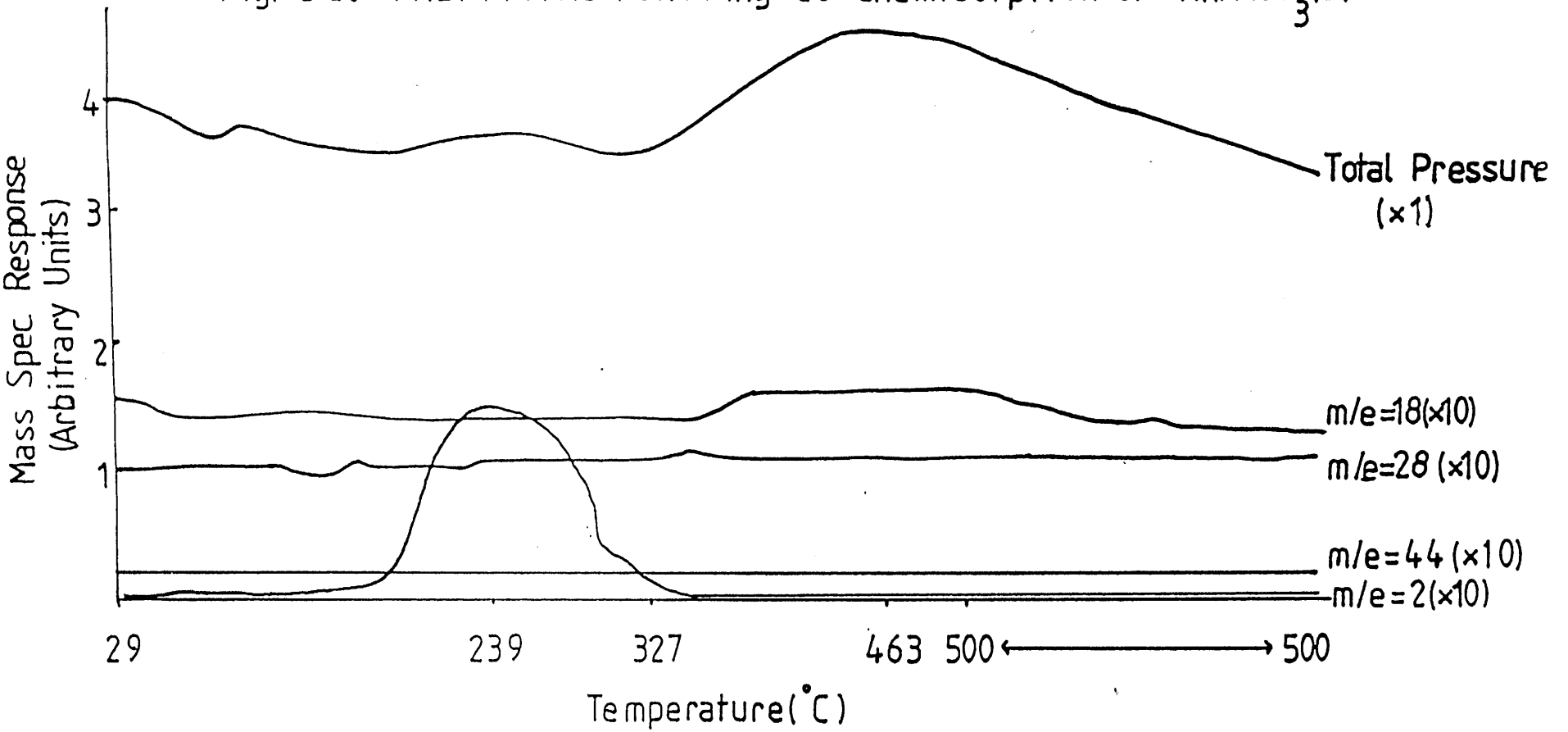

Fig. 5·21 T.P.D. Profile Following T.P.R. of Rh/MoO_3(b)

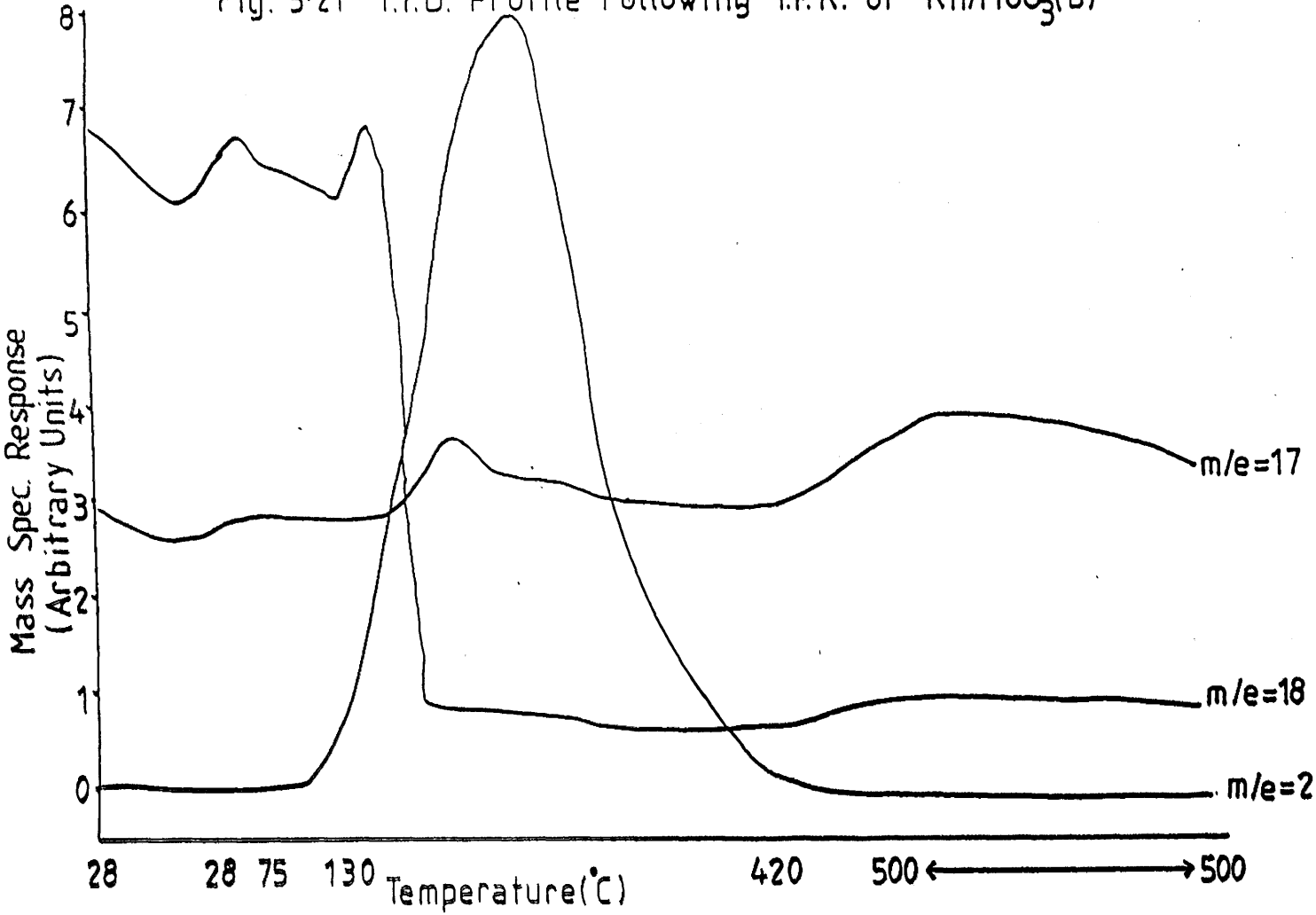

Fig. 5·22 T.P.D. Profile Following CO Chemisorption on $Rh/WO_3(c)$

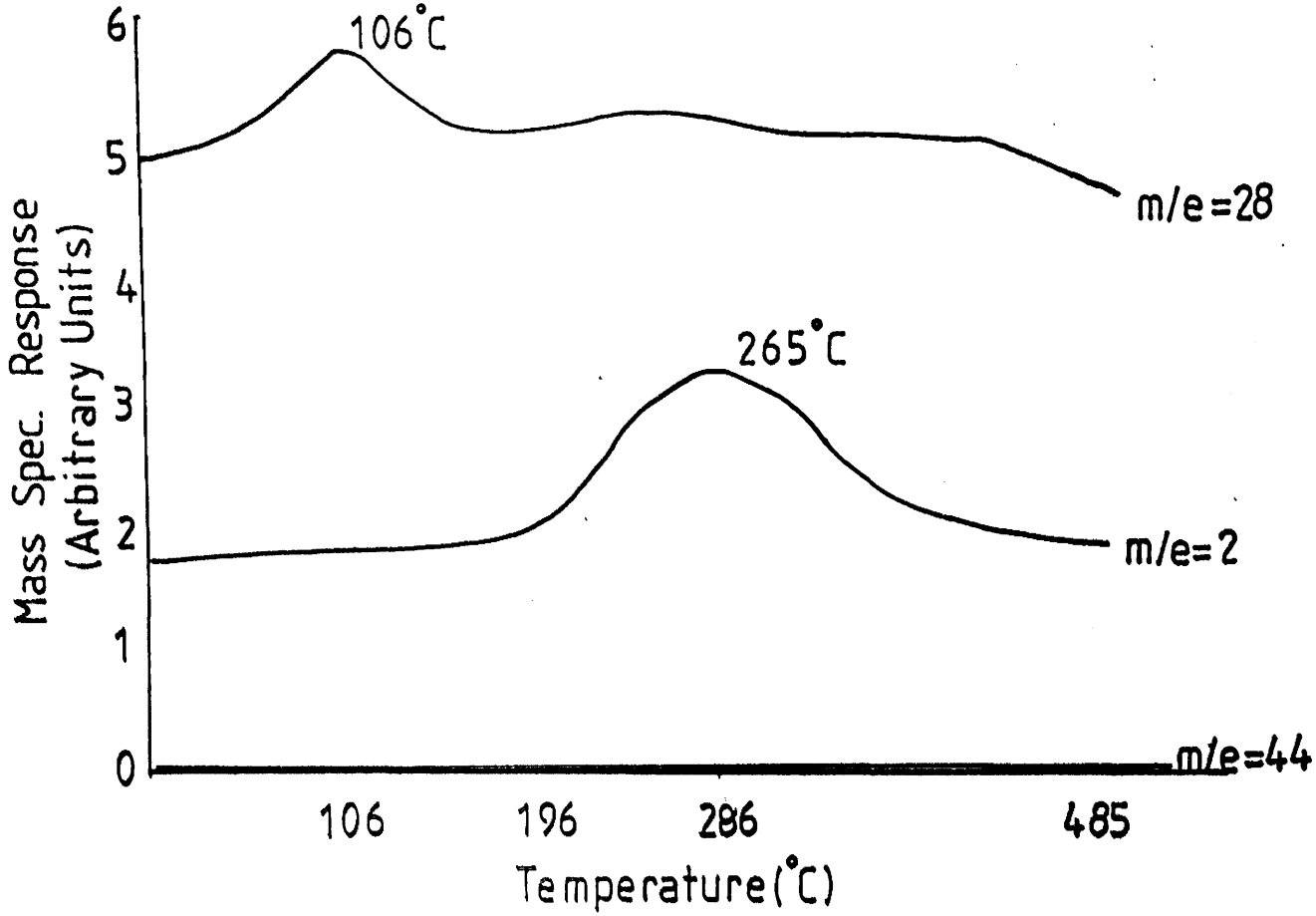

5.2.4 Sub-Ambient Carbon Monoxide Chemisorption

Sub-ambient carbon monoxide chemisorption experiments were carried out on $Pt/SiO_2(a)$, $Pt/MoO_3(a)$, $Pt/WO_3(a)$ and $Rh/MoO_3(c)$ using Flow System II, as described in Chapter 3, section 3.8.1.

The results are presented in terms of the number of carbon monoxide molecules calculated to be on the surface at saturation of the catalyst. This number is then converted to a metal area, assuming a 1:1 ratio of metal:CO, and an area of 16.8×10^{-20} m^2 for each CO molecule.

The sub-ambient carbon monoxide chemisorption experiments were carried out using the technique of frontal chromatography developed by Waugh et al. (123). Figure 5.23 shows a typical trace obtained during carbon monoxide chemisorption. The quantity of carbon monoxide adsorbed by the catalyst was calculated from such results using the method described in Chapter 4, section 4.4.

For each catalyst, the results are presented in Table 5.6 in the order in which the experiments were performed.

5.3 Thermal Analysis

5.3.1 Differential Scanning Calorimetry

Differential scanning calorimetry (or D.S.C.) experiments were carried out on four supported salts, namely $Rh/SiO_2(c)$, $Rh/WO_3(c)$, $Pt/MoO_3(a)$ and $Pt/WO_3(a)$. The experiments were performed at I.C.I. plc, Chemicals and Polymers Group, Billingham. The D.S.C. profiles

Fig. 5·23 CO Adsorption on Pt/MoO_3

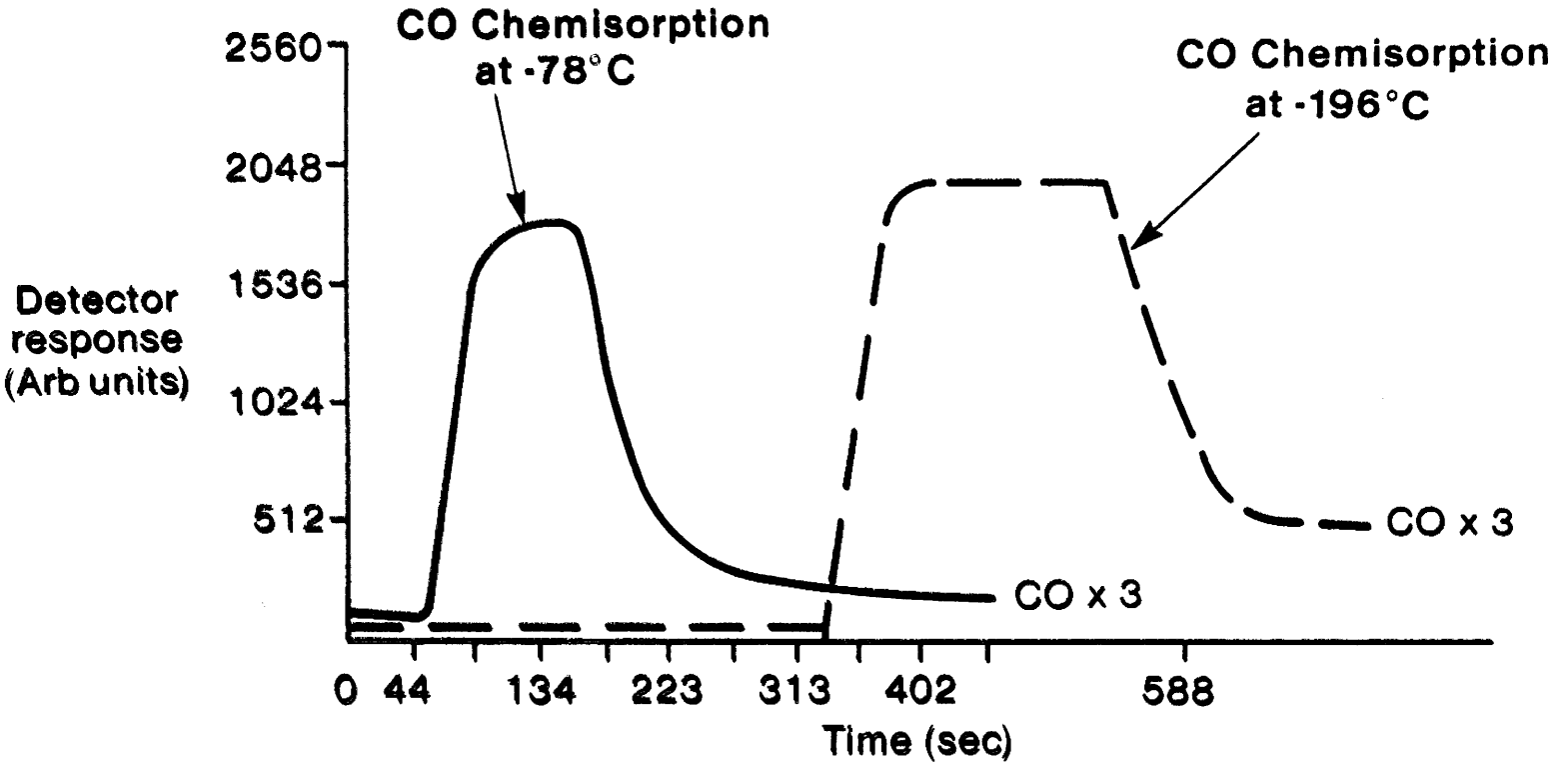

Table 5.6. Sub-Ambient Carbon Monoxide Chemisorption

Catalyst	Temperature	No. of CO molecules $(g\ catalyst)^{-1}$	Area $m^2(g\ catalyst)^{-1}$
$Pt/SiO_2(a)$	- 78	1.32×10^{19}	2.22
$Pt/SiO_2(a)$	-196	1.14×10^{21}	191.52
$Pt/MoO_3(a)$	- 78	4.83×10^{19}	8.11
$Pt/MoO_3(a)$	-196	3.54×10^{20}	59.47
$Pt/MoO_3(a)$	- 97	1.29×10^{20}	21.67
$Pt/MoO_3(a)$	-137	8.79×10^{19}	14.77
$Pt/WO_3(a)$	-196	3.32×10^{19}	5.57
$Pt/WO_3(a)$	- 78	3.28×10^{18}	0.55
$Rh/MoO_3(c)$	-196	8.14×10^{19}	13.67
$Rh/MoO_3(c)$	- 70	9.95×10^{19}	16.72

obtained for samples of $Rh/SiO_2(c)$, $Rh/WO_3(c)$, $Pt/MoO_3(a)$ and $Pt/WO_3(a)$ are shown in Figures 5.24 to 5.27, respectively.

The profile obtained for $Rh/SiO_2(c)$ shows only one major decomposition peak, with the peak maximum (T_{max}) at 35°C. $Rh/WO_3(c)$ shows a much more complicated profile. The sharp, major decomposition peak has T_{max} = 65°C, with a shoulder at 135°C. A smaller, broader peak with T_{max} = 370°C can also be observed.

The supported platinum catalysts show very complex decomposition profiles. $Pt/MoO_3(a)$ shows seven peak maxima, at 30°C, 55°C, 75°C, 315°C, 450°C and 565°C. The major peaks have maxima at 75°C, 155°C, 315°C, 450°C and 565°C; the maxima at the other temperatures are for unresolved 'shoulders'. For $Pt/WO_3(a)$, the peak maxima are observed at 40°C, 80°C, 130°C, 410°C, 465°C and 540°C.

5.3.2 Thermo-Gravimetric Analysis

Thermo-gravimetric analysis (T.G.A.) was carried out on $Pt/SiO_2(a)$, $Pt/MoO_3(a)$, $Pt/WO_3(a)$, $Rh/SiO_2(c)$, $Rh/MoO_3(c)$, $Rh/WO_3(c)$, SiO_2, MoO_3, WO_3, $RhCl_3.3H_2O$ and Pt foil.

The platinum foil reference indicates a negligible weight loss up to 1150°C. T.G.A. of fresh silica gel showed weight losses corresponding to the presence of between 0.8 and 1.5% by weight of water up to 65°C. An additional 0.2% (by weight) maximum could be removed by heating to 300°C due to further dehydration, but no further weight loss was observed up to 1000°C.

The molybdenum trioxide was heated in both nitrogen and in 5.5% hydrogen/nitrogen. In nitrogen, no weight loss was observed

Fig. 5.24 D.S.C Profile of Rh/SiO_2(c)

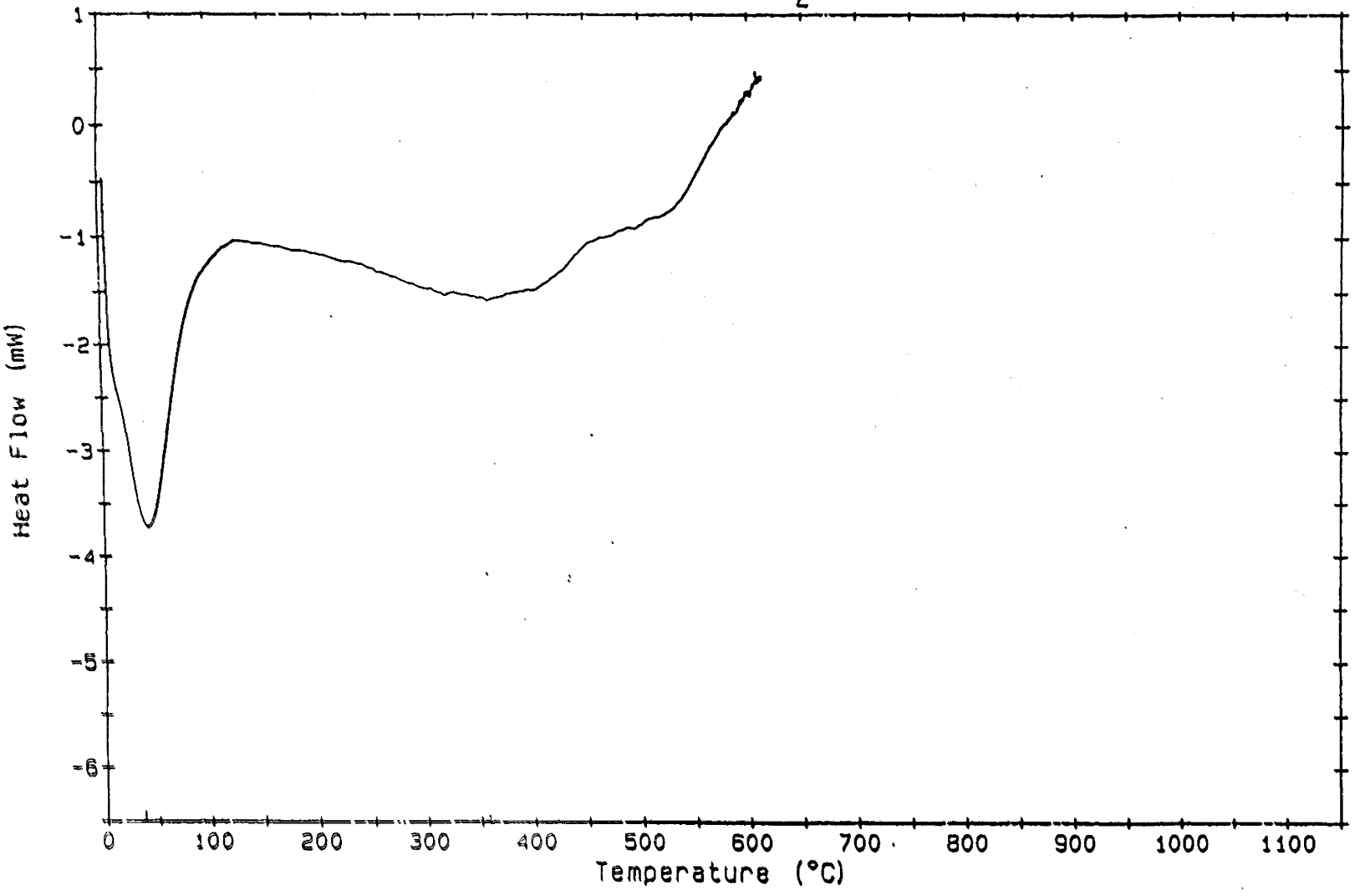

Fig. 5·25 D.S.C. Profile of $Rh/WO_3(c)$

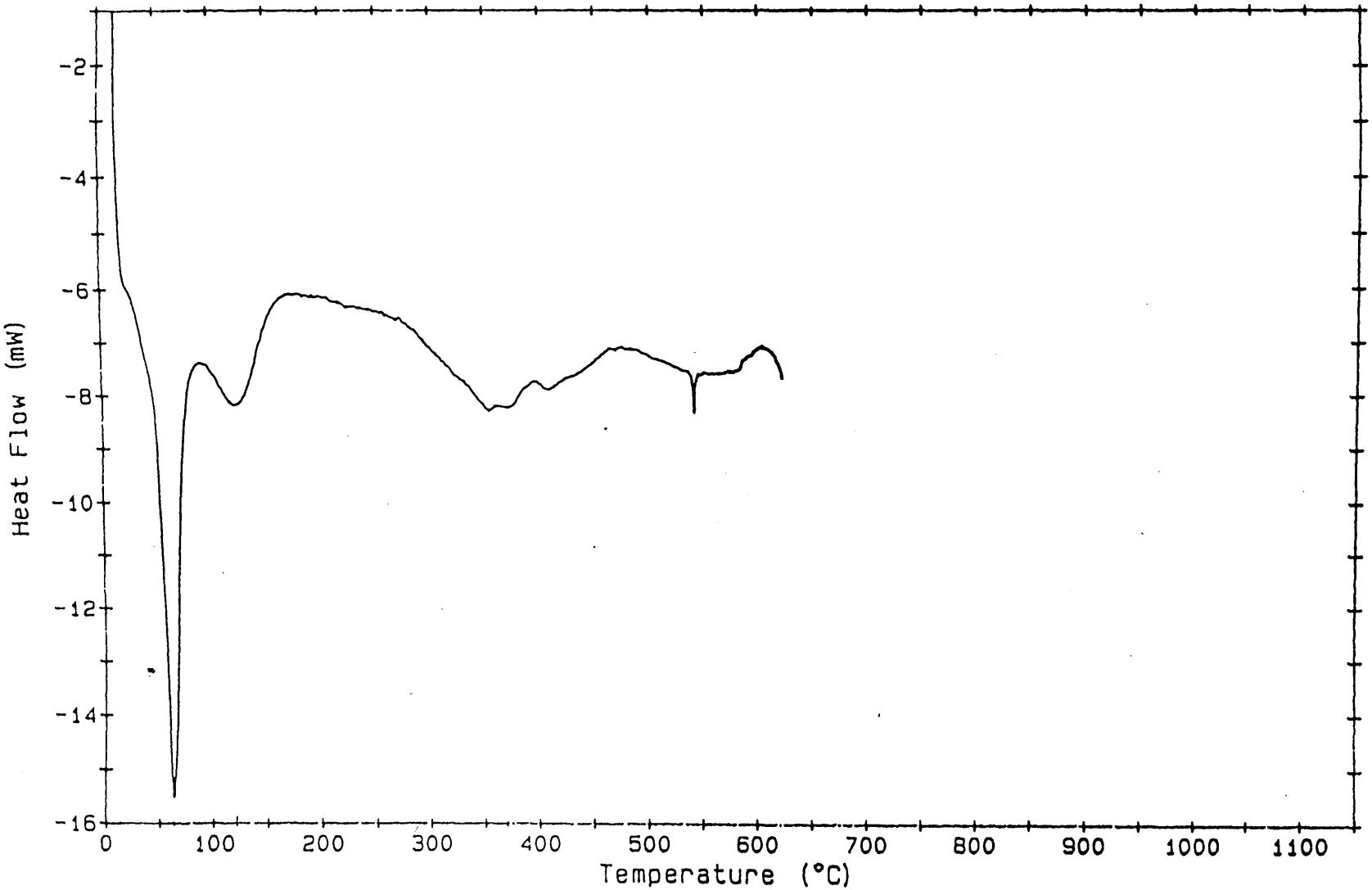

Fig. 5·26 D.S.C. Profile of $Pt/MoO_3(a)$

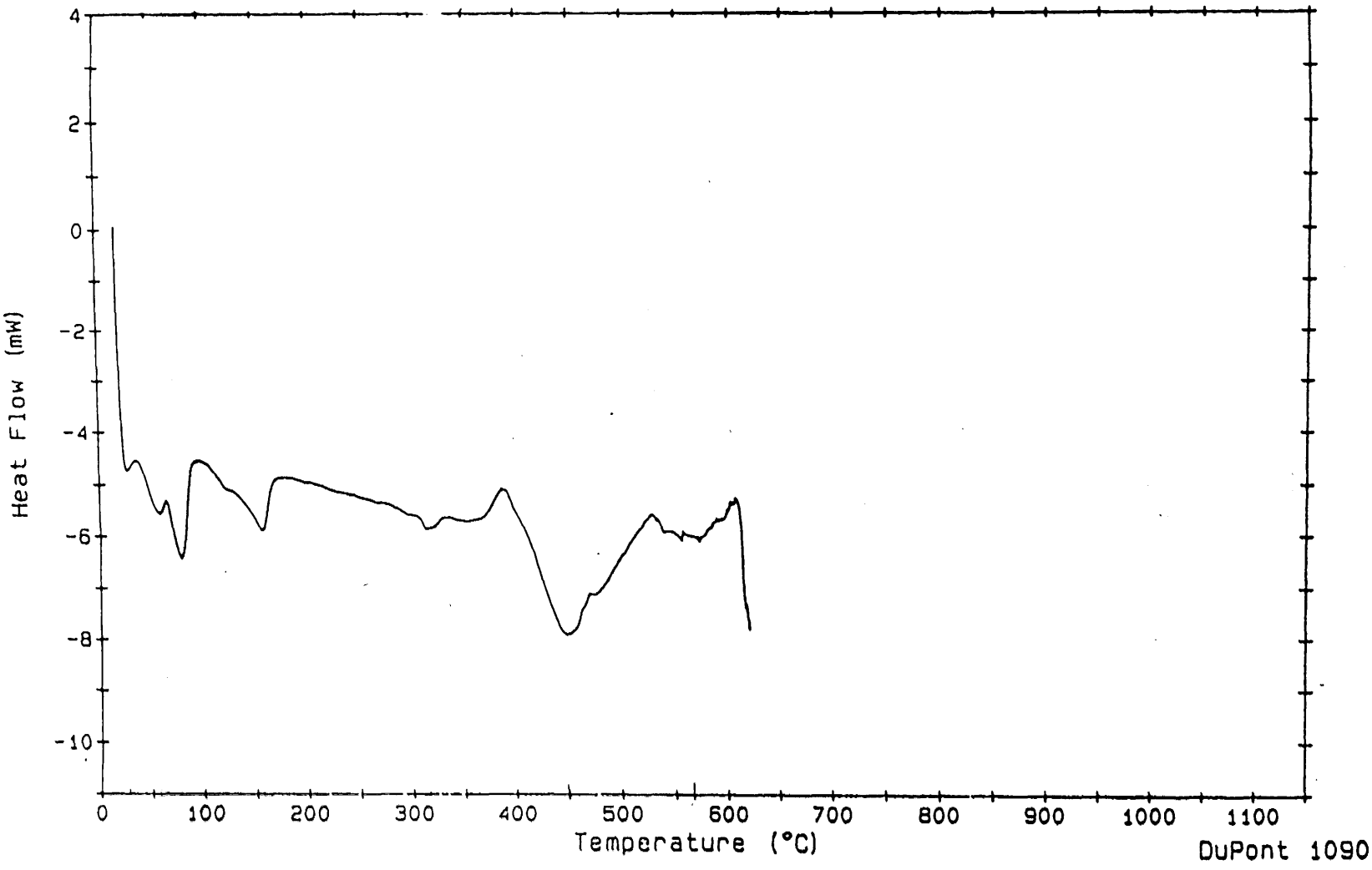

Fig. 5·27 D.S.C. Profile of $Pt/WO_3(a)$

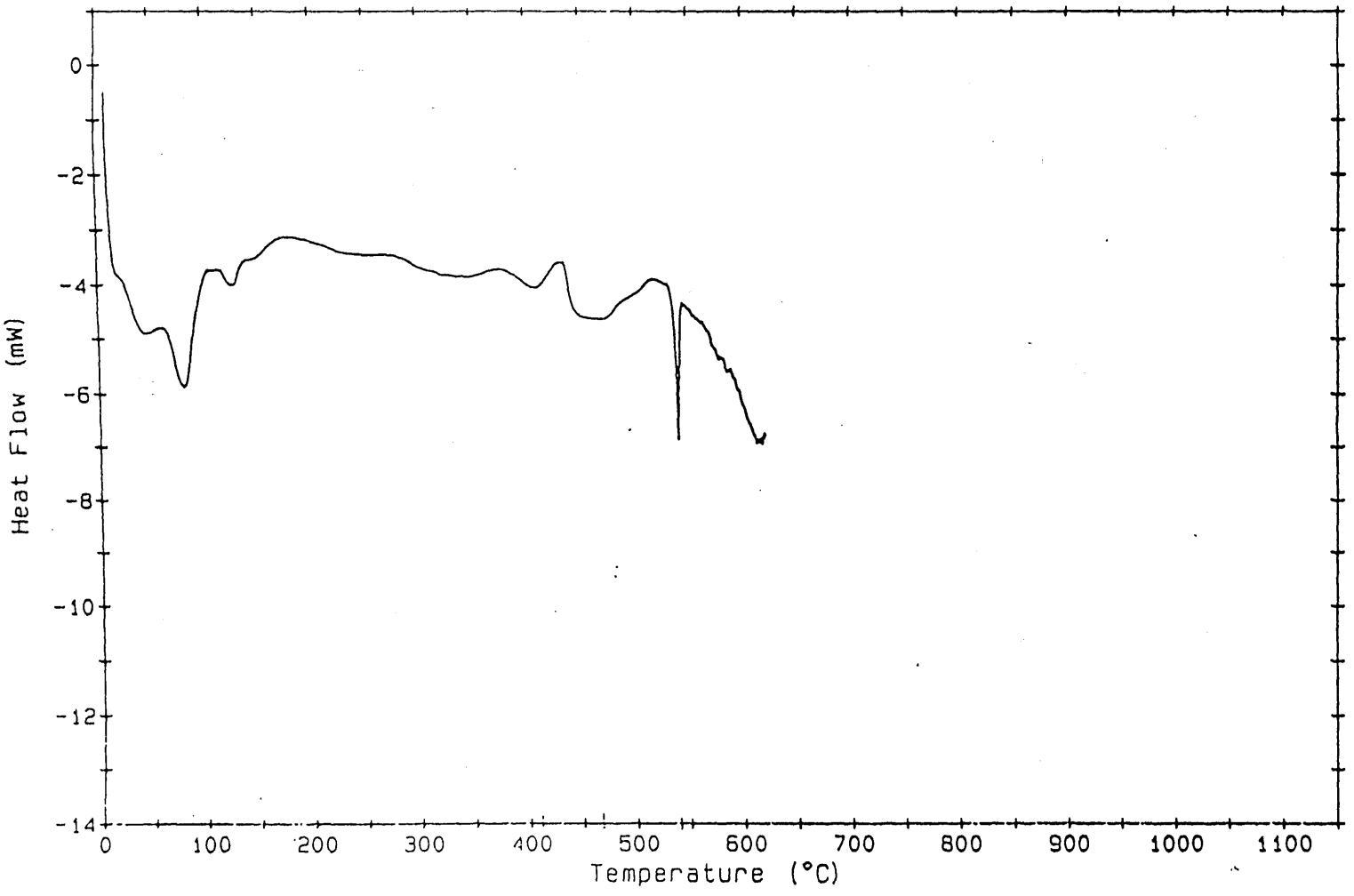

below 600°C. Above 630°C, the MoO_3 was believed to volatilise, slowly at first, but above 690°C, the rate increased as the material sublimed..

In 5.5% H_2 in N_2, no significant weight changes were observed until the start of reduction at 540°C. There is an indication that various oxides of molybdenum were formed. By 800°C, the residue contained MoO_2 and traces of molybdenum metal.

When tungsten trioxide was heated in nitrogen, a 0.5% weight loss was observed up to 250°C due to adsorbed water. Between 250°C and 500°C, a further 0.55% weight loss, which occurred in two stages, was observed, and which was attributed to further dehydration of water from the lattice. No further significant weight losses were observed between 500°C and 1150°C.

When tungsten trioxide was heated in air, a similar weight loss pattern to that found in nitrogen was observed.

X-ray diffraction studies were carried out on fresh WO_3, and WO_3 which had been heated to either 600°C in air or 1000°C in air. The same form of WO_3 was observed in all three cases, but the fresh WO_3 additionally showed signs of being hydrated, which may account for the weight losses observed to 500°C.

The tungsten trioxide was also heated in 5.5% H_2/N_2. The 0.55% weight loss observed in air or nitrogen between 250°C and 500°C was also observed in hydrogen/nitrogen. Reduction appears to commence at around 430°C. The main reduction loss begins at around 890°C, possibly due to reduction of WO_3 to metallic tungsten. The reduction to metallic tungsten was incomplete when heating was stopped at 1100°C.

T.G.A. analysis of rhodium trichloride suggested a formula close to $RhCl_3.4.34H_2O$ rather than the more commonly quoted $RhCl_3.3H_2O$. When $RhCl_3.4.34H_2O$ was heated in nitrogen, the most rapid removal of water was observed at around 65°C, slowing down between 100°C and 200°C and tailing off towards 500°C. Above about 550°C the, by now anhydrous, $RhCl_3$ started to decompose. The rate of decomposition increased with increasing temperature. The curve showed an abrupt halt in the rapid decomposition at ~810°C. Between 870°C and 1050°C there was apparently no significant weight loss. Between 1050°C to 1130°C there may be a gradual weight loss corresponding to the decomposition of Rh_2O_3.

Rh_2O_3 was believed to be formed during rhodium chloride decomposition due to the presence of a small amount of oxygen impurity in the nitrogen. The weight loss at 1130°C apparently corresponded to the formation of metallic rhodium. When rhodium trichloride is heated in air, the weight loss pattern is very similar to that found in nitrogen up to the formation of anhydrous $RhCl_3$ at ~550°C. Thereafter, the weight loss between 550°C and 810°C corresponded to the formation of Rh_2O_3. No further weight loss occurred until the decomposition of Rh_2O_3 took place between 1050 and 1125°C, resulting in the formation of rhodium metal. When rhodium trichloride was heated in 5.5% H_2/N_2 the weight loss corresponding to dehydration overlapped with the weight loss corresponding to reduction to rhodium metal. It is possible that reduction of the rhodium trichloride commenced between 85°C and 100°C, with extremely rapid reduction occurring between 120°C and 170°C. There was negligible weight loss between ~200°C and 750°C, when a

further ~ 1% weight loss took place. The total weight loss is consistent with the formation of rhodium metal, as found for heating in nitrogen.

When Pt/SiO_2(a) was heated in nitrogen, a weight loss of 7.34% occurred below 100°C, which probably corresponds to adsorbed water. In 5.5% hydrogen/nitrogen, an additional weight loss of ~ 0.5% was observed between ~ 120°C and 200°C which does not totally account for the weight loss expected on reduction of either $H_2PtCl_6 \rightarrow Pt$ or $PtO_2 \rightarrow Pt$, suggesting that reduction occurs in stages, with the initial stages of reduction occurring at the same time as the dehydration.

When Rh/SiO_2(c) was heated in 5.5% H_2/N_2, the total weight loss to 150°C was 7.57% which corresponds to weight loss due to water loss from the silica and possibly the hydrated salt, before the salt itself undergoes reduction. This may involve the formation of Rh_2O_3 from $RhCl_3$ before the reduction to Rh metal is complete.

When Pt/MoO_3(a) was heated in nitrogen only, a weight loss of only 1.78% was observed. In 5.5% H_2/N_2, a weight loss of 21.1% was observed at temperatures up to 450°C. Possibly ~ 1.2% can be attributed to reduction of H_2PtCl_6 to Pt. The remainder of the weight loss may be due to reduction of the MoO_3 to lower oxides, or even molybdenum metal.

Rh/MoO_3(c) showed a weight loss of ~3.34% up to 600°C in nitrogen. In 5.5% H_2/N_2, the weight loss was 21.28%, similar to that found for Pt/MoO_3(a) under similar conditions. This suggests that the weight loss is largely due to reduction of the support in both cases. Figure 5.28 shows a typical T.G.A. trace produced when Rh/MoO_3(c) was heated in a) N_2 and b) 5.5% H_2/N_2.

Fig. 5·28(a) T.G.A. of $Rh/MoO_3(c)$ in N_2

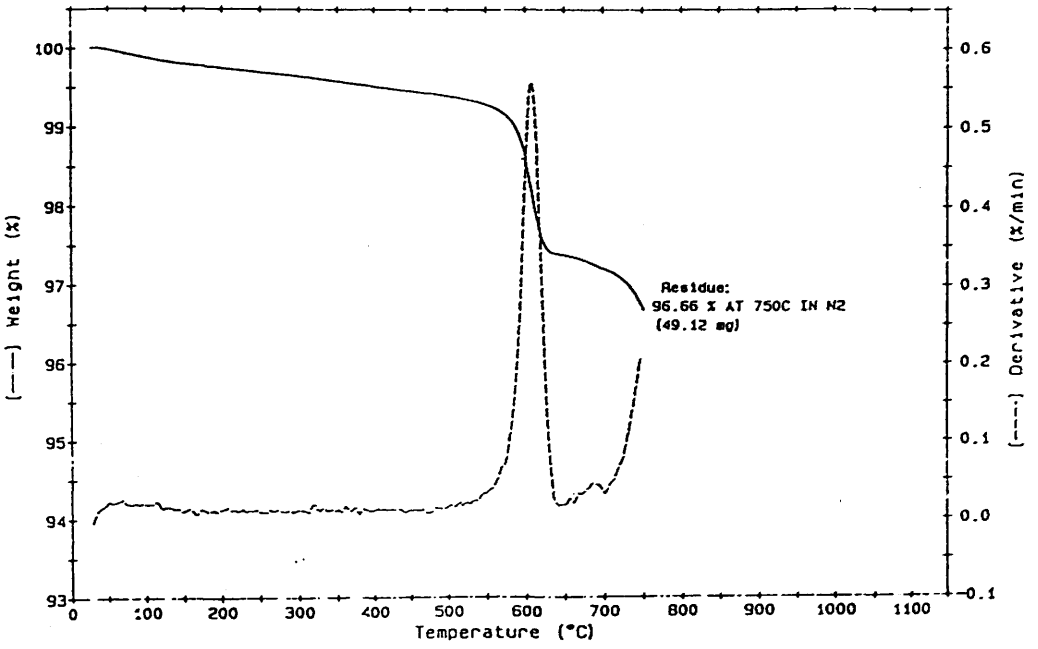

Fig. 5·28(b) T.G.A. of $Rh/MoO_3(c)$ in 5·5% H_2/N_2

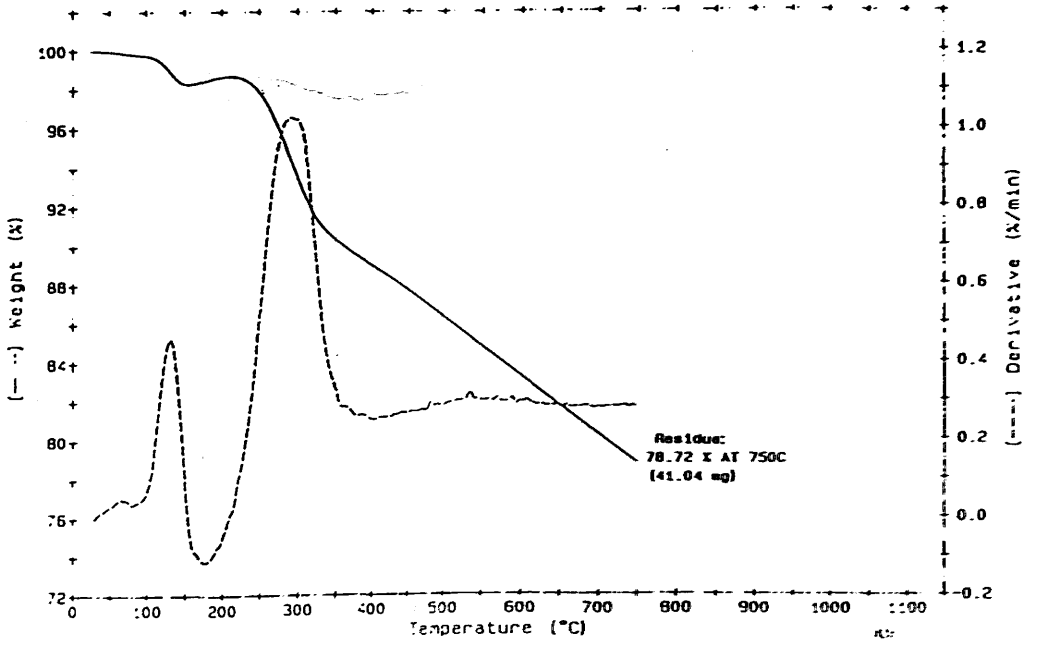

Thermal treatment of Pt/WO_3 led to a weight loss of 22.31%. Much of this must be due to reduction of the support. (A weight loss of ~20.7% can be attributed to the reduction of tungsten trioxide to tungsten metal).

When $Rh/WO_3(c)$ was heated in nitrogen, a weight loss of 3.15% due to the removal of associated water was observed. This occurred in several stages: between ambient and 200°C, at around 400°C, between 600°C and 700°C and between 800°C and 850°C, and must be attributed to loss of water from the oxide. In 5.5% H_2/N_2, the total weight loss was 22.78% up to 1000°C. This occurs in stages: ambient - 100°C, 100-150°C, 320-420°C and 580-980°C. The weight loss corresponds to reduction of the support to tungsten metal and includes the water loss found when the catalyst was heated in nitrogen alone.

5.4 Nitrogen B.E.T. Areas

Nitrogen B.E.T. areas were measured *in situ* for a selection of the catalysts, namely $Pt/SiO_2(a)$, $Pt/MoO_3(a)$, $Pt/WO_3(a)$ and $Rh/MoO_3(c)$. Measurements were made both before and after reduction of the catalyst sample. The quantity of nitrogen adsorbed and, hence the total surface area of the catalyst, was calculated as described in Chapter 4, section 4.4.

Table 5.7 shows the nitrogen B.E.T. areas calculated for a selection of catalysts both before and after reduction.

Table 5.7. N_2 B.E.T. Areas

Catalyst	Area Before Reduction ($m^2(g\ catalyst)^{-1}$)	Area After Reduction ($m^2(g\ catalyst)^{-1}$)
Pt/SiO_2	142.5	144.7
Pt/MoO_3	2.15	82.9
Pt/WO_3	*6.12	5.04
Rh/MoO_3	2.4	87.5
MoO_3	2.11	1.65

[* N_2 B.E.T. area measured after 1 T.P.R./T.P.D. cycle]

5.5 Temperature Programmed Reaction Studies

Temperature programmed reaction studies were carried out on a selection of the catalysts studied, namely $Pt/SiO_2(a)$, $Pt/MoO_3(a)$, $Pt/WO_3(a)$ and $Rh/MoO_3(c)$.

The reaction studied was the hydrogenation of carbon monoxide. This particular reaction was studied for two reasons: first, the reaction is industrially important for the removal of carbon monoxide from hydrogen feed-streams; second, it was desirable to investigate any differences which may be due to using different supports.

For $Pt/SiO_2(a)$, no reaction was observable over the temperature range studied (ambient to 400°C). However, as Figures 5.29, 5.30 and 5.31 show, reaction did take place over $Pt/MoO_3(a)$, $Pt/WO_3(a)$ and $Rh/MoO_3(c)$. These results show a decrease in carbon monoxide partial pressure with increasing temperature and a corresponding increase in methane, water and carbon dioxide partial pressures.

5.6 Buta-1,3-diene Hydrogenation Studies

Throughout this section, but-1-ene, trans-but-2-ene, cis-but-2-ene and buta-1,3-diene will be referred to as 1-B, t-2-B, c-2-B and butadiene, respectively.

5.6.1 Pressure/Time Curves

During each butadiene hydrogenation reaction carried out, the variation of the total pressure in the system with time was monitored using a pressure transducer, the output from which was plotted on a

Fig. 5·29 Temperature Programmed Reaction of 95% CO/H_2 Over Pt/MoO_3

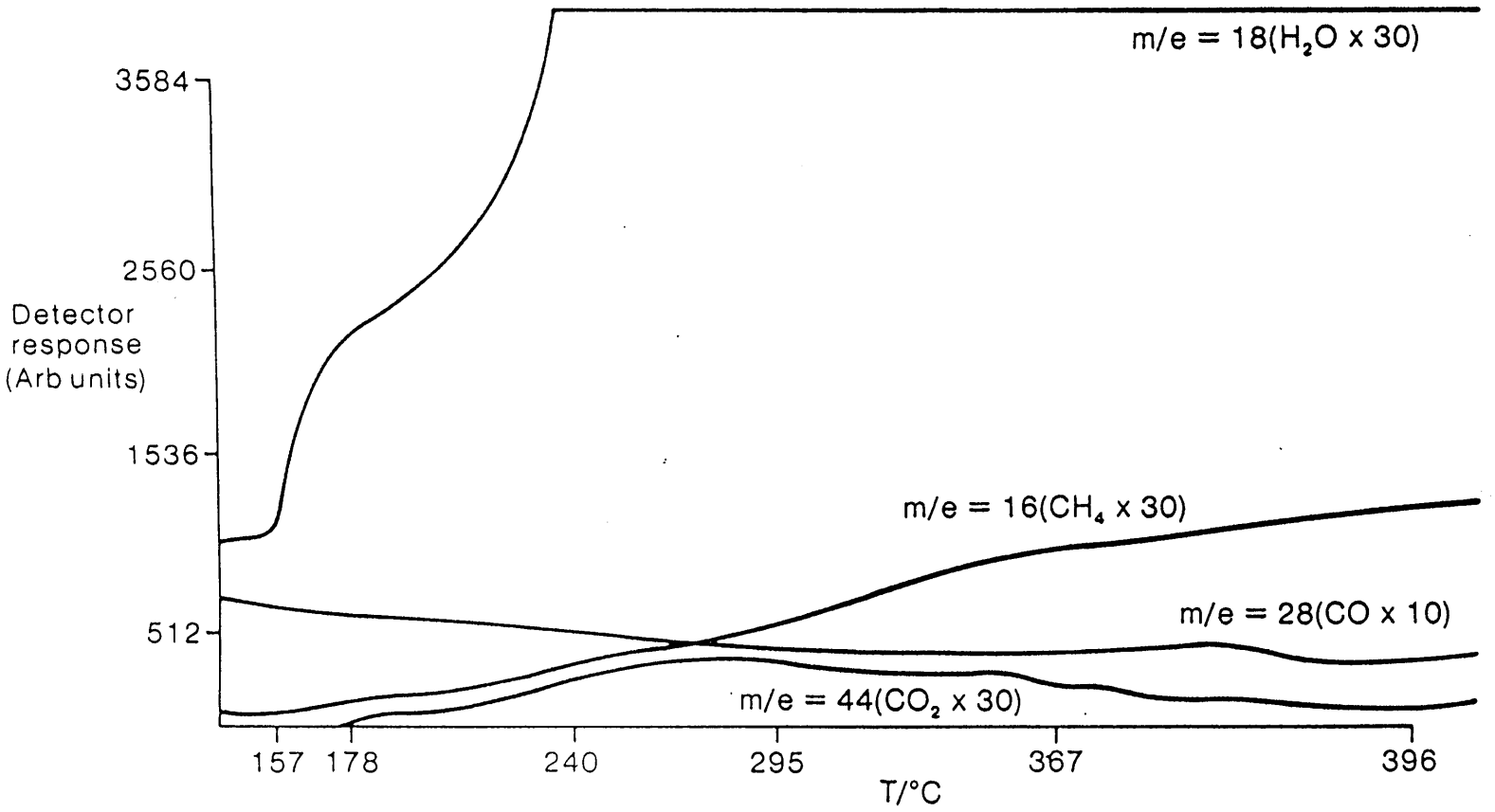

Fig. 5·30 Temperature Programmed Reaction of 8% CO/H_2 Over Pt/WO_3

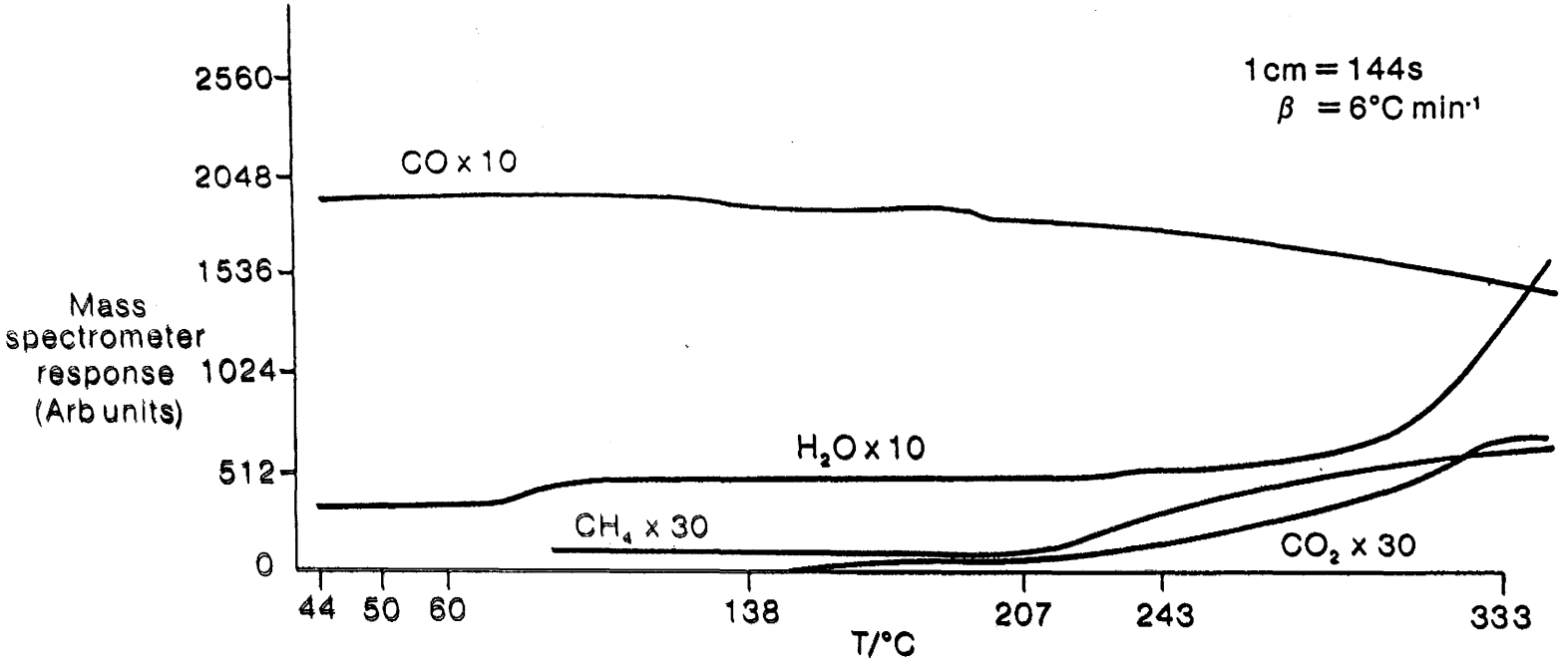

Fig. 5·31 Temperature Programmed Reaction of 9·8% CO/H_2 Over Rh/MoO_3(c)

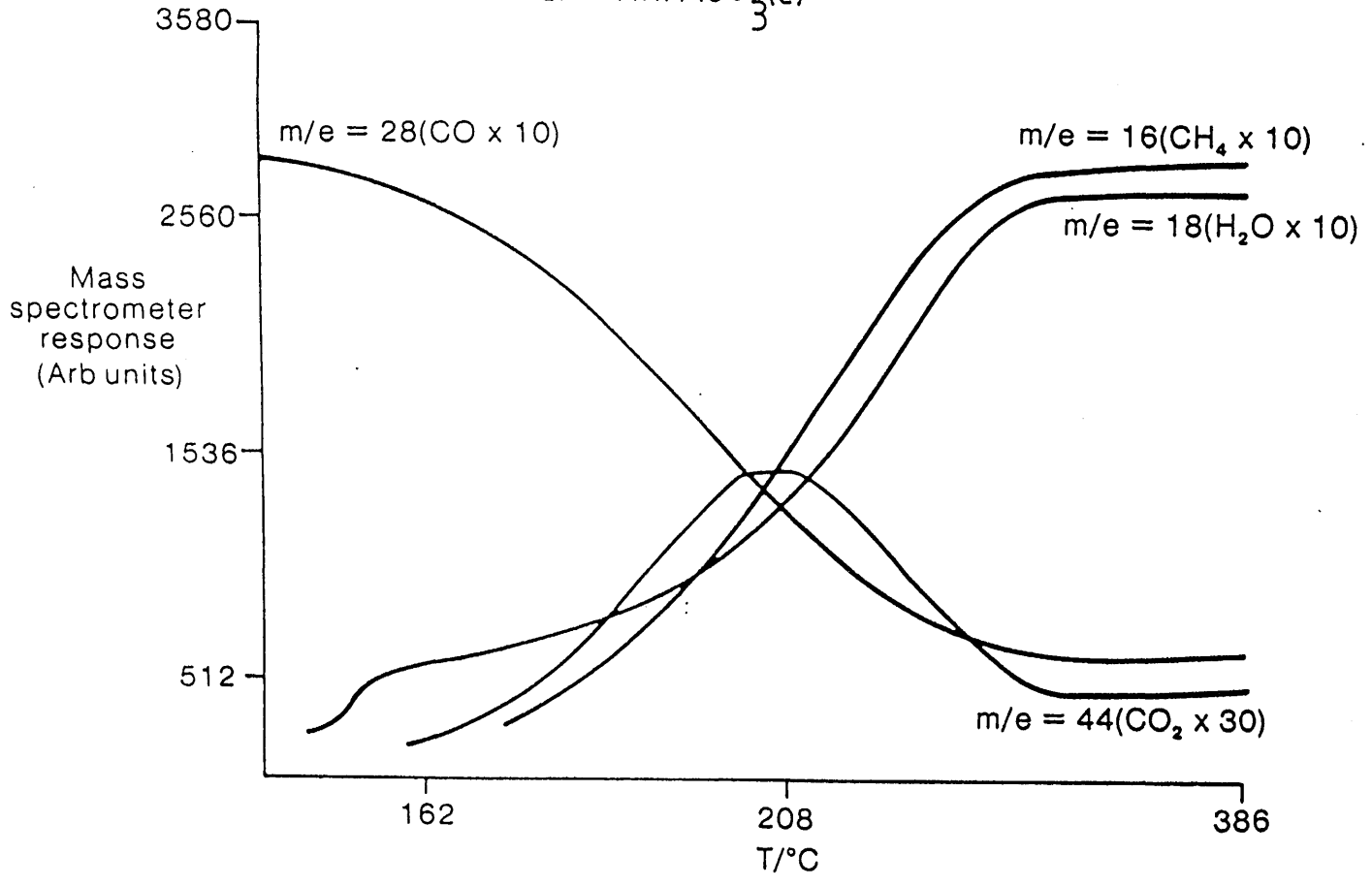

potentiometric chart recorder. In this way, pressure versus time curves were obtained.

In order to determine the overall order of reaction and to detect any acceleration points, plots of the log of the instantaneous pressure against time were made. The acceleration point is the point at which the reaction rate is observed to increase.

A plot of log P vs. t for freshly reduced Pt/SiO_2(a) indicated that rate changes were found at ΔP = 7.8 Torr, 19.3 Torr and 30.9 Torr, where the initial pressure P_o, was 104 Torr and the composition of the gas mixture was 3.1:1 $H_2:C_4H_6$. ΔP = 7.8 Torr indicates the end of an induction period. With increasing usage, the acceleration point became much less pronounced.

Pt/MoO_3(a) showed no acceleration point, either because the reactions monitored were believed to be diffusion controlled, or they were not monitored to a sufficiently high pressure fall.

Figure 5.32 shows the log P vs. t plot obtained for freshly reduced Pt/WO_3(a). The initial pressure, P_o, was 79.65 Torr and the $H_2:C_4H_6$ ratio was 3.5:1. The acceleration point was found at ΔP_{acc} = 17.55 Torr. Again, acceleration points became less noticeable with increasing catalyst usage.

The acceleration point for freshly reduced Rh/SiO_2(b) was found at ΔP_{acc} = 14.1 Torr, when P_o = 104 Torr and the $H_2:C_4H_6$ ratio was 3.0:1. Typical pressure/time curves obtained for this catalyst after further use showed a decreasing rate with increasing reaction extent.

Fig. 5·32 Log P Versus t Plot for $Pt/WO_3(a)$

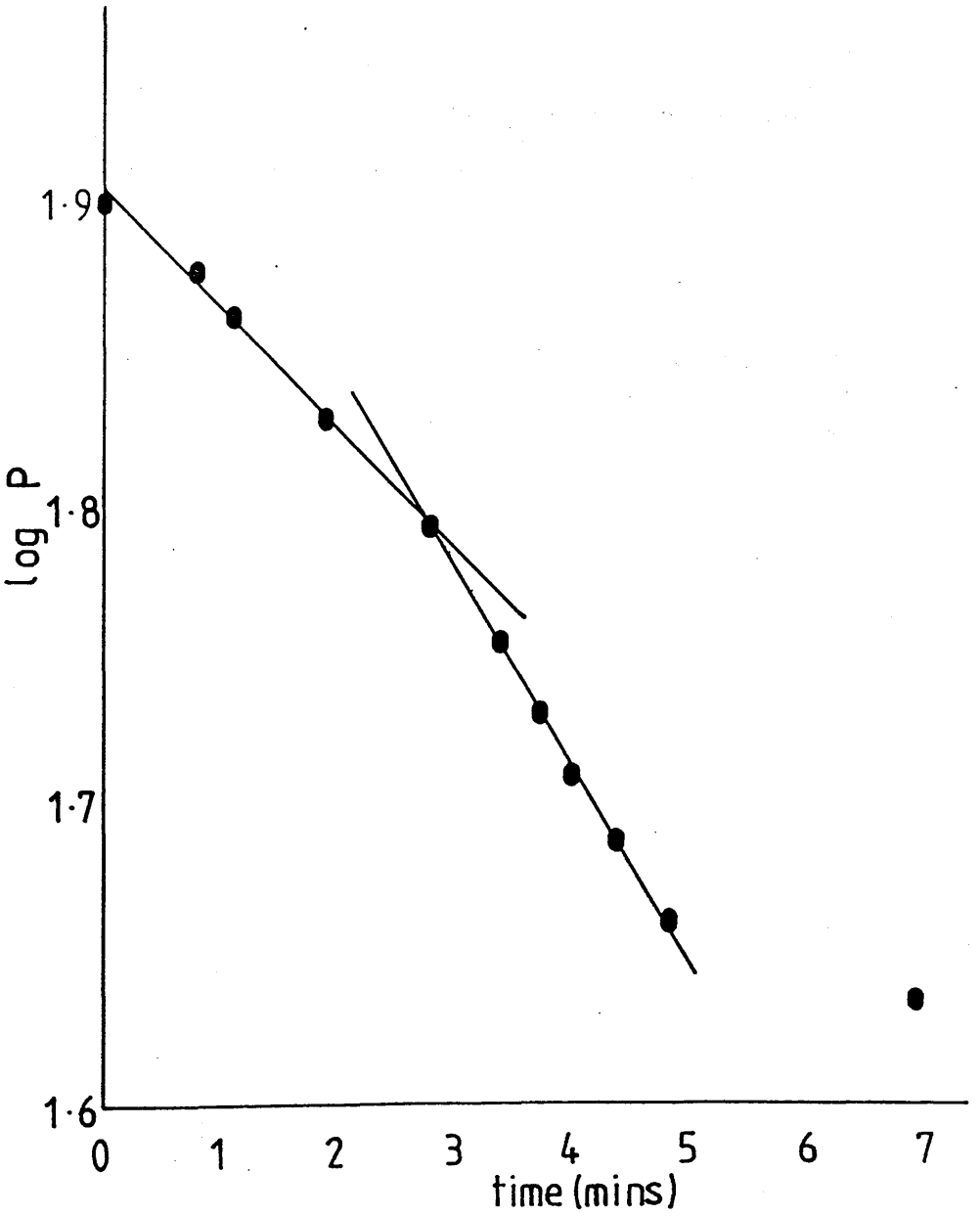

A log P versus t plot for $Rh/MoO_3(b)$ is shown in Figure 5.33. P_o was 125 Torr, and the gas mixture composition was 3:1 $H_2:C_4H_6$. The acceleration point occurred at ΔP_{acc} = 32.5 Torr. After further use, and with P_o = 80.6 Torr, ΔP_{acc} was found to be 22.0 Torr.

For $Rh/WO_3(b)$, a P_o of 83.7 Torr, and a 3:1 $H_2:C_4H_6$ gas mixture produced an acceleration point at 11.3 Torr. An induction period, which finished at ΔP = 2.4 Torr, was also observed. Figure 5.34 shows a log P versus t plot for $Rh/WO_3(b)$ after increased catalyst usage. P_o was 81 Torr, and the acceleration point was found at ΔP_{acc} = 17.6 Torr.

$Rh/SiO_2(c)$ showed no evidence of an acceleration point when the pressure fall versus time curve was monitored up to 108% reaction extent. During this time, the reaction rate decreased with increasing reaction extent.

Rate changes at ΔP = 10.7 Torr, 18.3 Torr and 23.5 Torr were observed for freshly reduced $Rh/MoO_3(c)$, when P_o was 98.8 Torr and the gas mixture was composed of 3:1 $H_2:C_4H_6$. With increasing catalyst usage, the pressure/time curves showed a decrease in rate with increasing pressure fall.

For $Rh/WO_3(c)$, the log P versus t plot indicated a slight acceleration point at ΔP_{acc} = 27.1 Torr (Fig. 5.35).

The initial pressure was 80.6 Torr, and the gas mixture was composed of 2.5:1 $H_2:C_4H_6$. With increasing catalyst usage, the rate either decreased very gently with increasing pressure fall, or was approximately constant over the pressure fall range covered.

Fig. 5·33 Log P vs. t Plot for Rh/MoO_3(b)

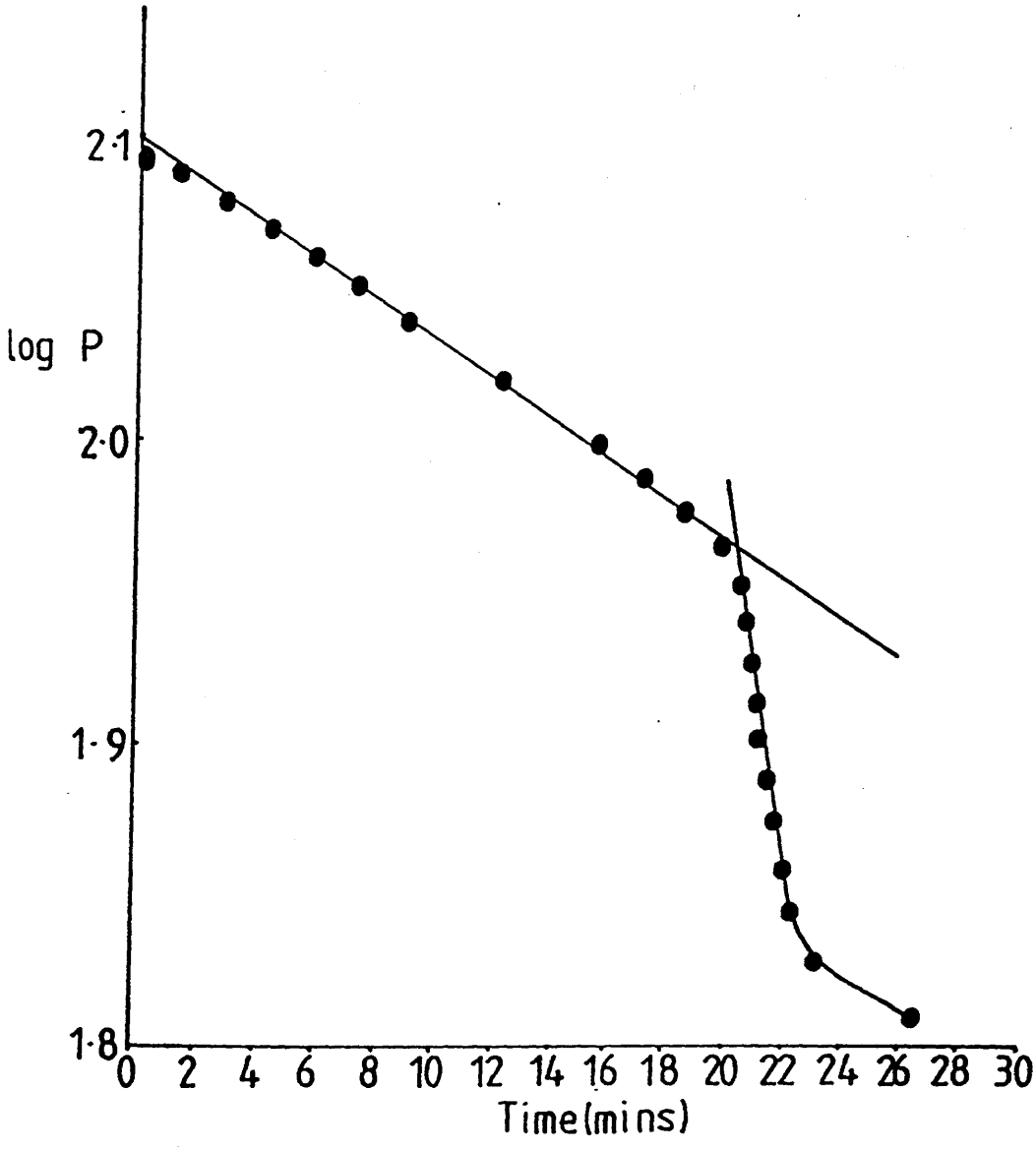

Fig. 5·34 Log P vs. t Plot for Rh/WO_3(b)

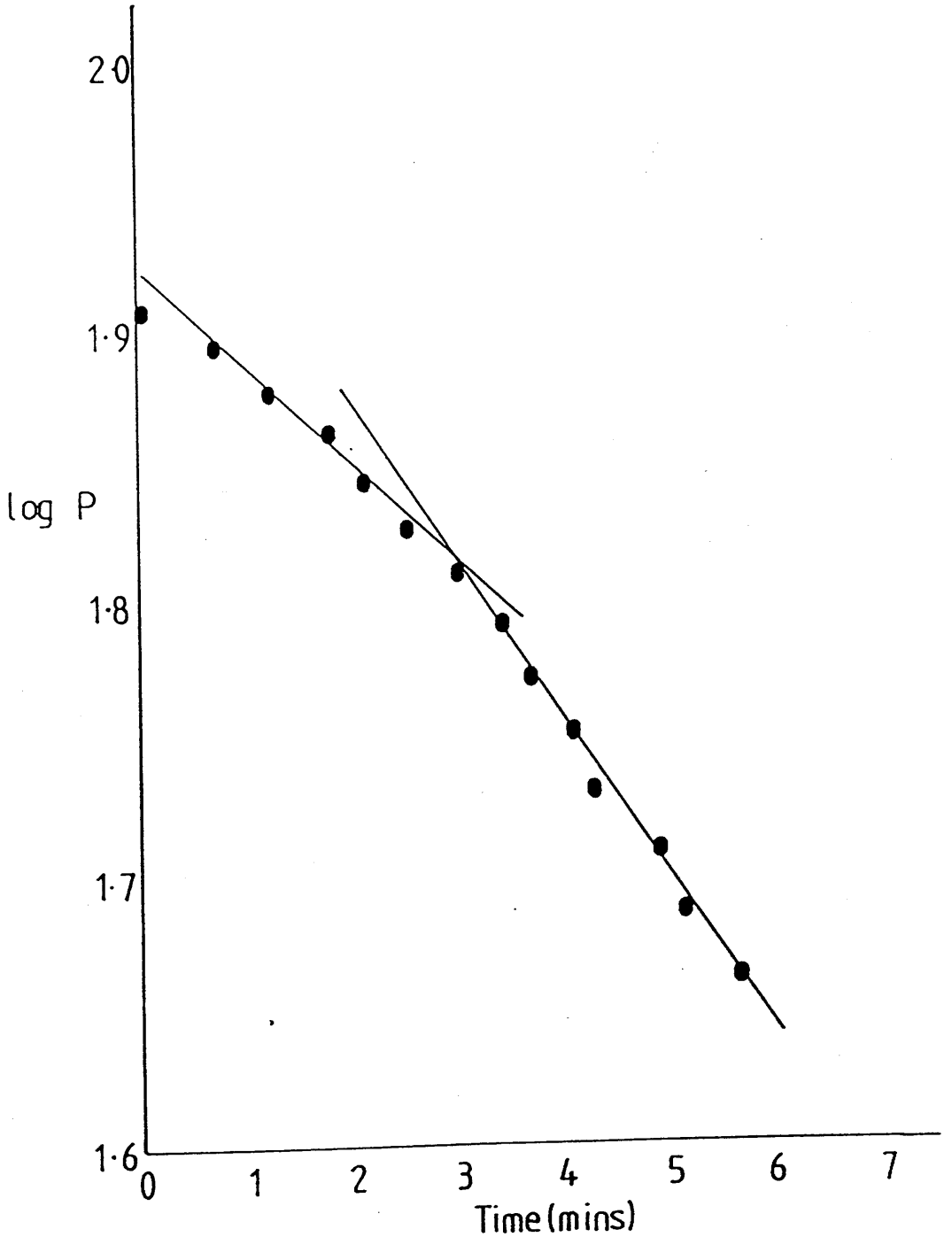

Fig. 5.35 Log P vs. t Plot for Rh/WO_3(c)

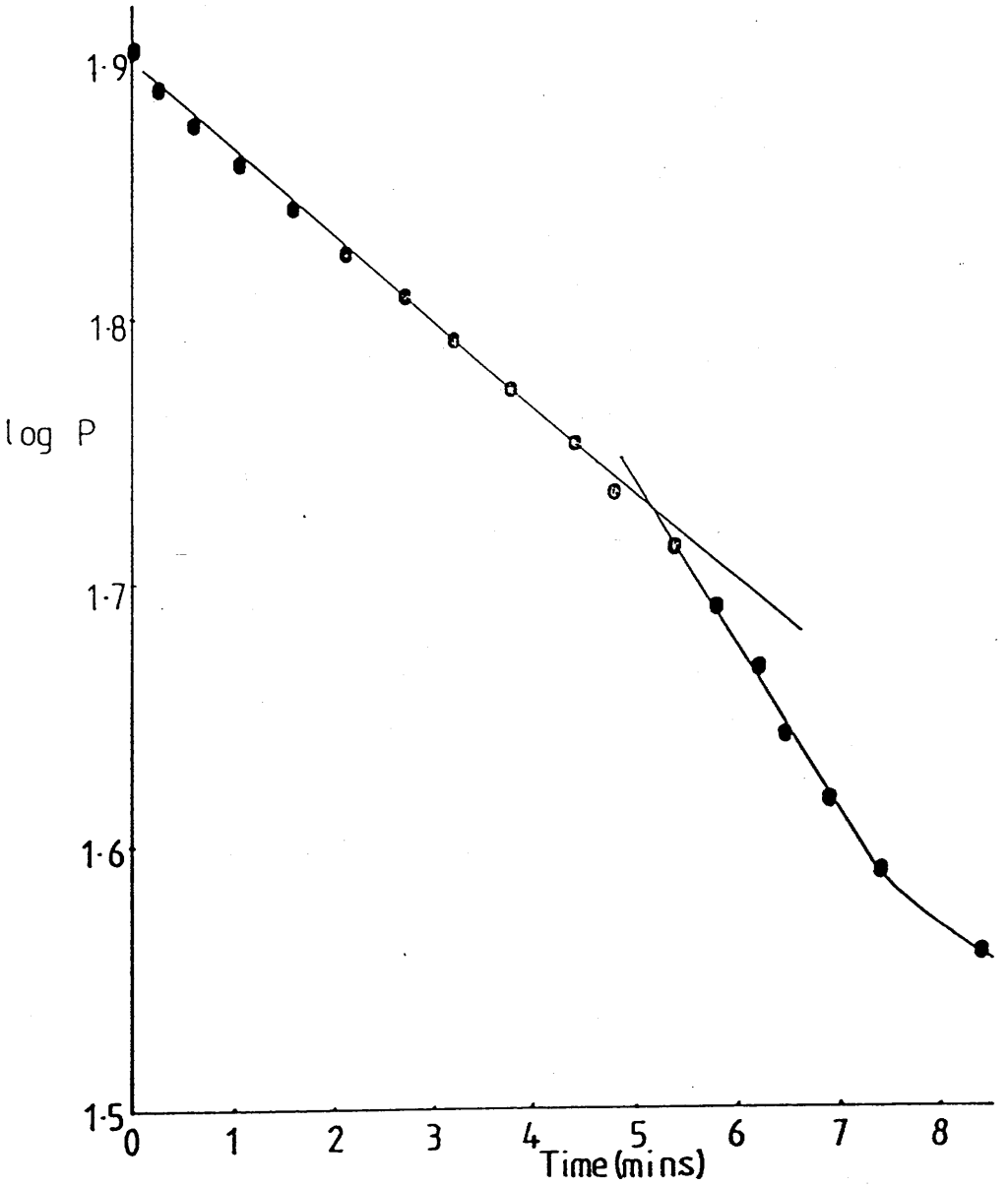

5.6.2 Variation of Selectivity and Butene Distribution with Reaction Extent

A series of butadiene hydrogenation reactions was carried out over each reduced catalyst using a 3:1 hydrogen:butadiene gas mixture. For each series, the initial pressure was constant. The reaction products were extracted at various pressure falls and the products analysed using gas chromatography. The reactions were carried out in a random order to minimise any effect on butene distribution with catalyst deactivation with increasing catalyst usage. The variation of selectivity and butene distribution with varying pressure fall is shown in Tables 5.8a to 5.8i. These results are shown diagramatically in Figures 5.36 to 5.43. There is no diagram to accompany the results for Table 5.8i.

5.6.3 Order of Reaction with Respect to a) Hydrogen and b) Butadiene

A series of experiments was carried out over each catalyst to determine the order of reaction with respect to the partial pressure of each reactant.

To determine the order of reaction with respect to hydrogen, the partial pressure of butadiene was kept constant at 26 Torr. The partial pressure of hydrogen was varied randomly from 52 to 130 Torr. The initial rate of reaction was obtained from the pressure fall versus time curves, as explained in Chapter 4, section 4.5.

Table 5.8a. Variation of Butene Distribution with Reaction Extent.

Catalyst: $Pt/SiO_2(a)$ Weight of Sample = 0.0887g

Reaction Temperature = 20°C Initial Pressure = 104 Torr

Reaction Number	Reaction Extent %	Butene Distribution 1-B %	t-2-B %	c-2-B %	trans/cis	1 - B / 2 - B	Selectivity
5	29	70.4	22.2	7.4	3.0	2.4	0.68
3	68	70.0	21.7	8.3	2.6	2.3	0.63
6	85	69.9	21.7	8.4	2.6	2.25	0.59
4	106	67.1	23.7	9.2	2.6	2.04	0.54
1	119	65.8	27.4	6.8	4.0	1.92	0.48

Fig. 5-36 Variation of Butene Distribution and Selectivity with Reaction Extent (Pt/SiO_2(a))

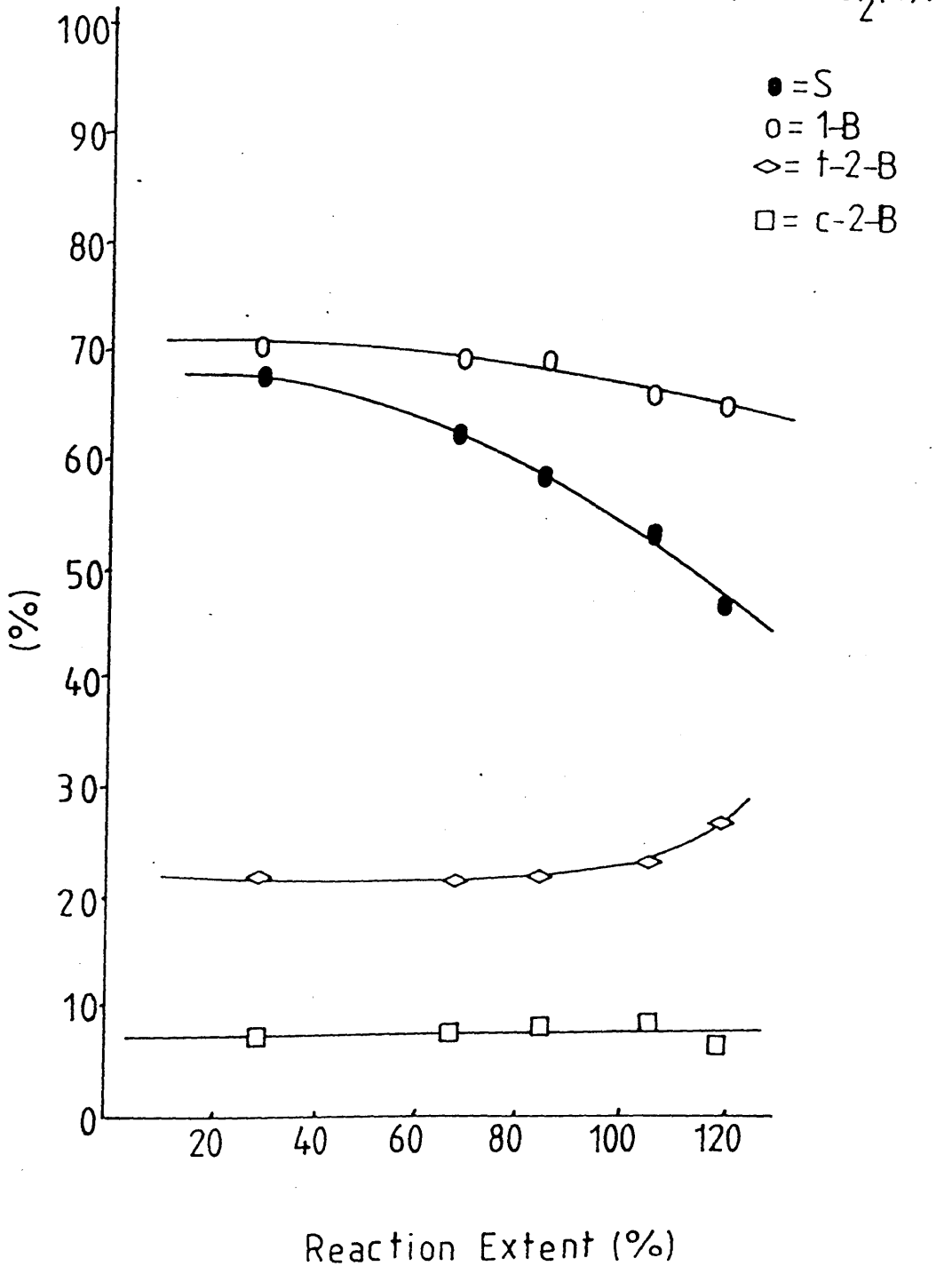

Table 5.8b. Variation of Butene Distribution with Reaction Extents.

Catalyst: $Rh/SiO_2(b)$ Weight of Sample = 0.0483g

Reaction Temperature = 20°C Initial Pressure = 104 Torr

Reaction Number	Reaction Extent %	Butene Distribution 1-B %	t-2-B %	c-2-B %	trans/cis	1 - B / 2 - B	Selectivity
4	16	58.8	29.4	11.8	2.5	1.43	0.87
2	30	59.1	27.3	13.6	2.01	1.44	0.85
6	77	50.9	33.3	15.8	2.1	1.04	0.86
7	104	49.1	36.4	14.5	2.5	0.96	0.77
5	139	29.4	52.9	17.6	3.0	0.42	n/a
3	145	34.6	46.2	19.2	2.4	0.53	n/a

Fig. 5·37 Variation of Butene Distribution and Selectivity with Reaction Extent (Rh/SiO_2(b))

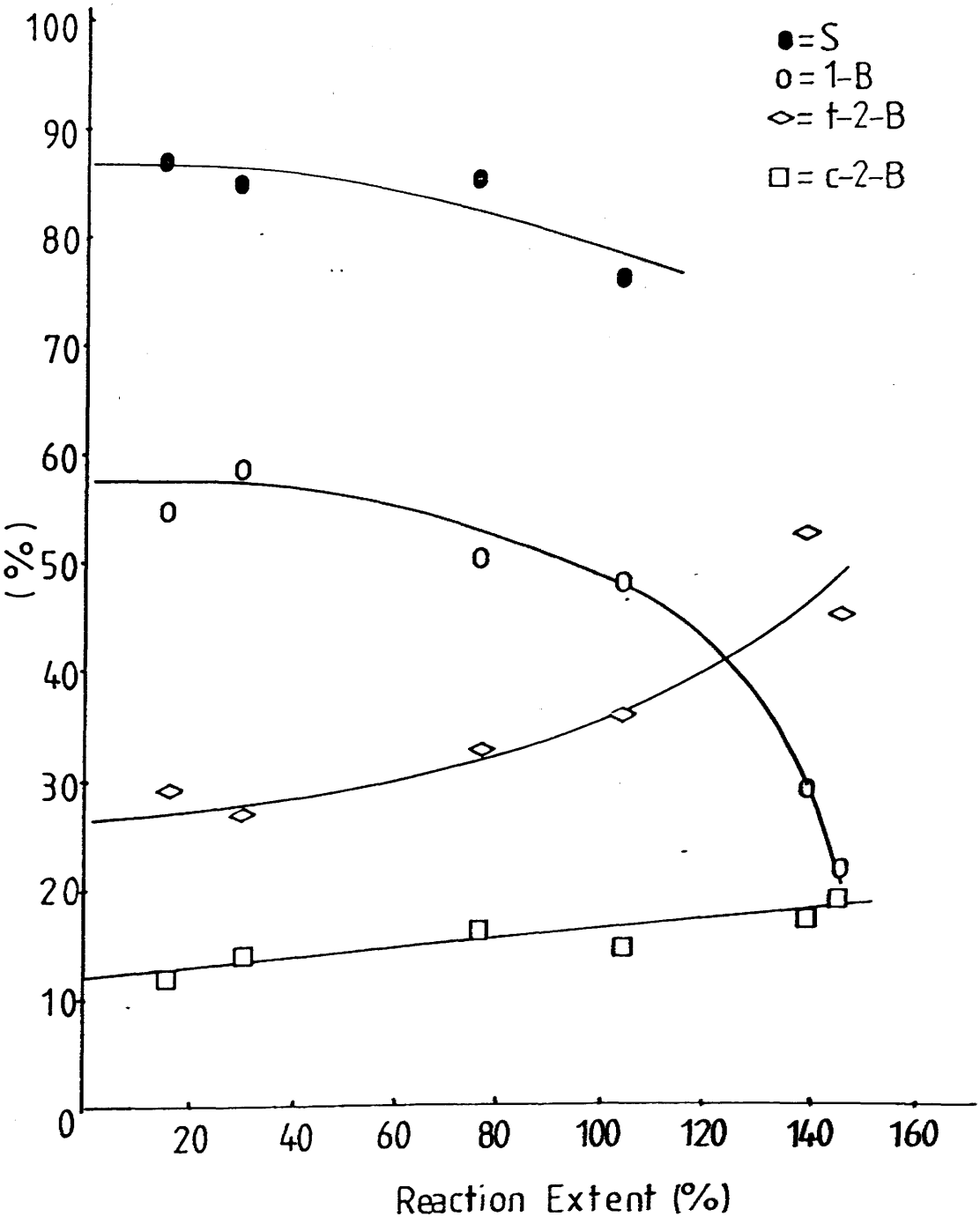

Table 5.8c. Variation of Butene Distribution with Reaction Extent.

Catalyst: $Rh/SiO_2(c)$ Weight of Sample = 0.0283g

Reaction Temperature = 45°C Initial Pressure = 125 Torr

Reaction Number	Reaction Extent %	Initial Rate Torr/min	Butene Distribution 1-B %	t-2-B %	c-2-B %	trans/cis	1 - B / 2 - B	Selectivity
2	16.4	8.3	57.7	26.4	15.9	1.66	1.36	0.76
5	33.0	24.0	54.2	28.9	16.9	1.71	1.18	0.78
3	44.7	13.3	50.7	29.9	19.4	1.54	1.03	0.73
1	67.3	22.0	46.8	34.4	18.8	1.83	0.88	0.75
4	75.1	10.0	41.0	35.8	23.2	1.54	0.69	0.72
6	107.9	8.3	22.9	48.2	28.9	1.67	0.30	0.64

Fig. 5-38 Variation of Butene Distribution and Selectivity with Reaction Extent (Rh/SiO_2(c))

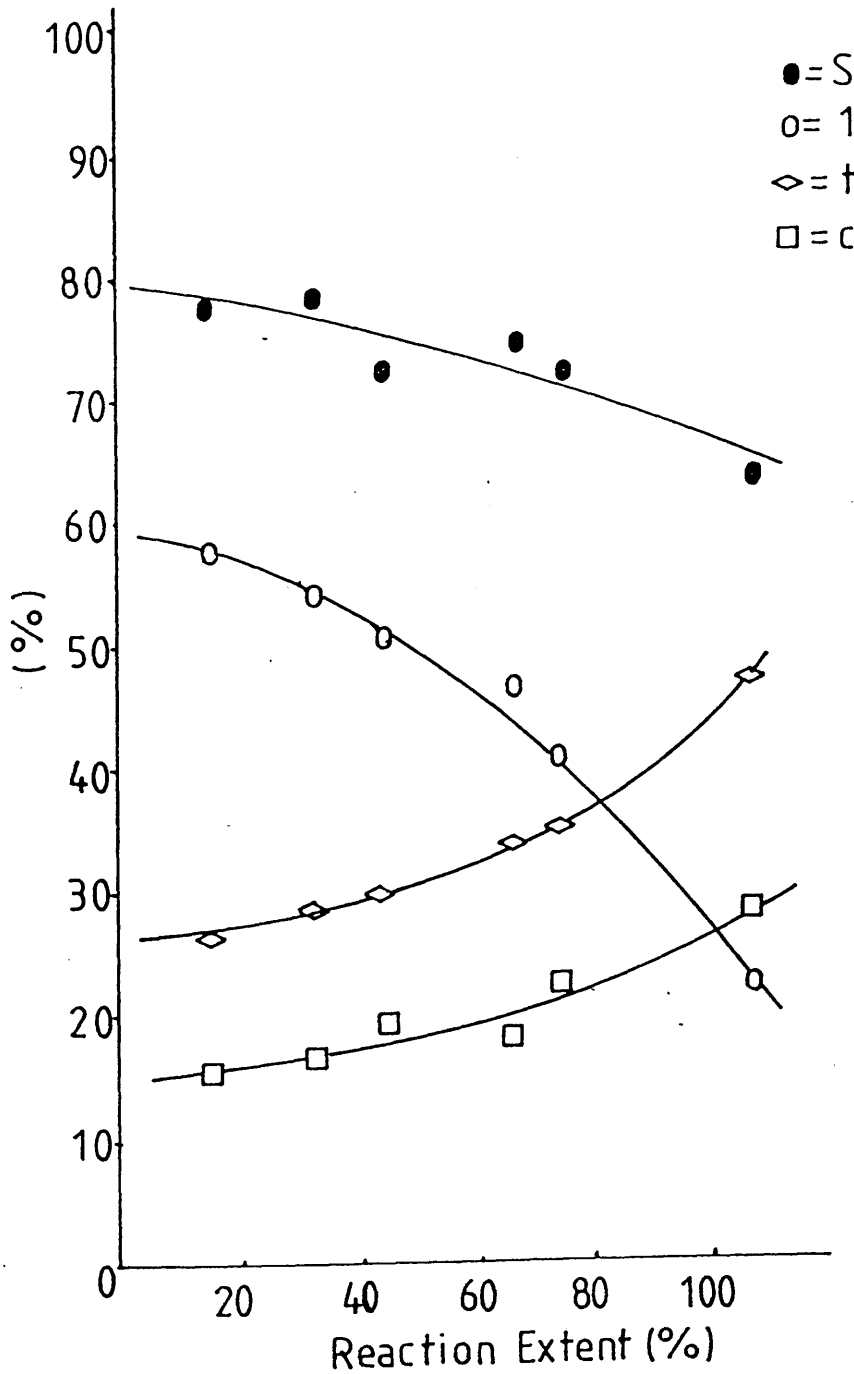

Table 5.8d. Variation of Butene Distribution with Reaction Extent.

Catalyst: $Pt/MoO_3(a)$ Weight of Sample = 0.0694g

Reaction Temperature = 20°C Initial Pressure = 104 Torr

Reaction Number	Reaction Extent %	Butene Distribution 1-B %	t-2-B %	c-2-B %	trans/cis	1-B / 2-B	Selectivity
2	34.3	53.1	28.1	18.8	1.50	1.13	0.80
4	58.2	55.1	28.6	16.3	1.75	1.23	0.73
5	88.0	46.3	33.3	20.4	1.63	0.86	0.69
3	111.0	39.024	40.244	20.732	1.94	0.64	0.54
6	124.0	24.0	50.0	26.0	1.92	0.32	0.47
1	151.6	9.1	63.6	27.3	2.33	0.10	n/a

Fig. 5-39 Variation of Butene Distribution and Selectivity with Reaction Extent ($Pt/MoO_3(a)$)

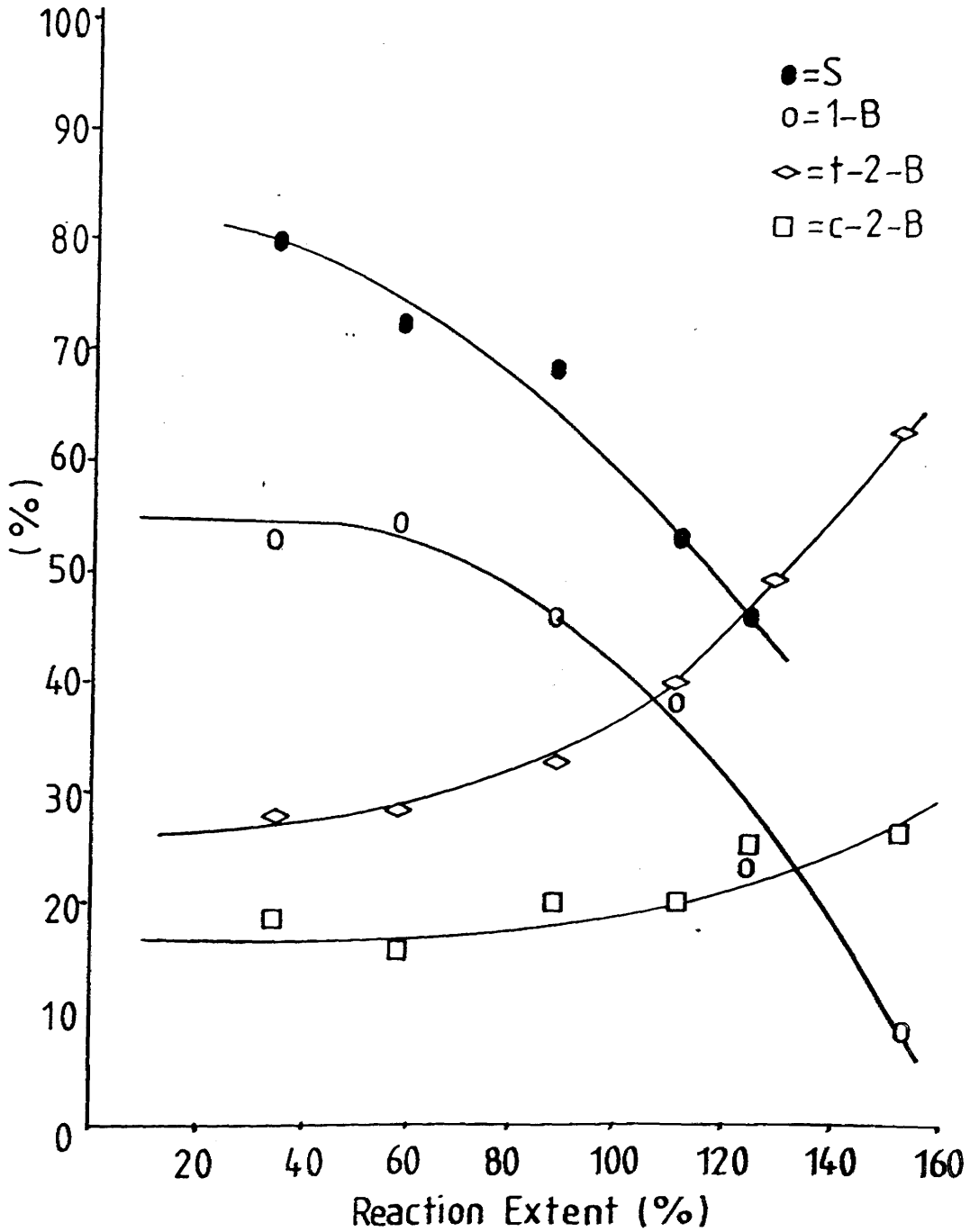

Table 5.8e. Variation of Butene Distribution with Reaction Extent.

Catalyst: $Rh/MoO_3(b)$ Weight of Sample = 0.2293g

Reaction Temperature = 20°C Initial Pressure = 78 Torr

Reaction Number	Reaction Extent %	Initial Rate Torr/min	Butene Distribution 1-B %	t-2-B %	c-2-B %	trans/cis	(1 - B)/(2 - B)	Selectivity
6	24.96	0.4	52.5	33.4	14.1	2.37	1.11	0.93
1	45.1	0.5	55.4	30.8	13.8	2.23	1.24	0.92
5	69.7	0.5	50.5	34.2	15.3	2.24	1.02	0.91
2	78.6	0.7	50.8	33.9	15.3	2.22	1.03	0.89
4	103.3	0.5	28.15	50.33	21.52	2.34	0.39	n/a
3	139.6	1.0	49.7	34.9	15.4	2.27	0.99	n/a

Fig. 5·40 Variation of Butene Distribution and Selectivity with Reaction Extent ($Rh/MoO_3(b)$)

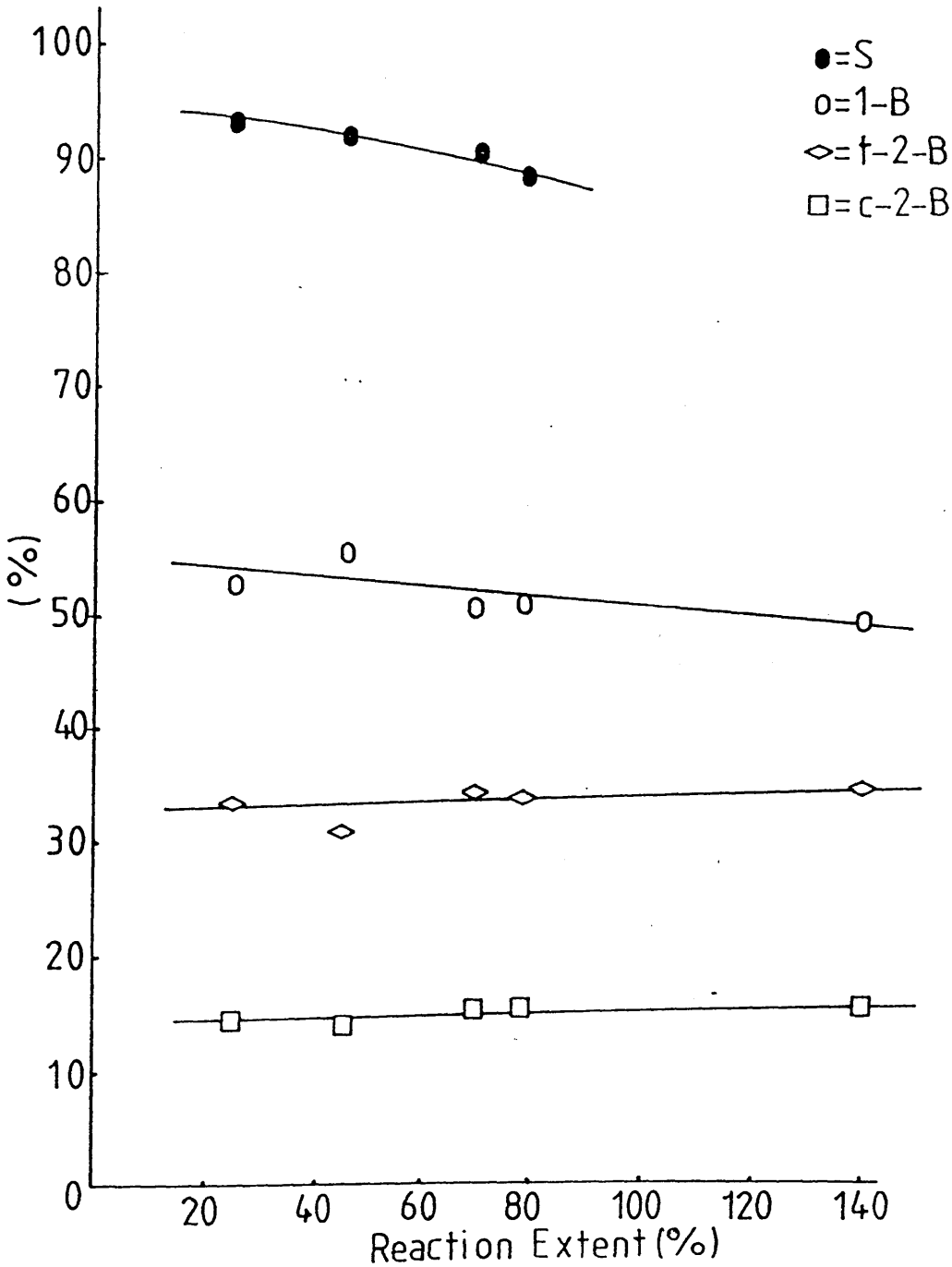

Table 5.8f. Variation of Butene Distribution with Reaction Extent.

Catalyst: $Rh/MoO_3(c)$ Weight of Sample = 0.2077g

Reaction Temperature = 20°C Initial Pressure = 78 Torr

Reaction Number	Reaction Extent %	Initial Rate Torr/min	Butene Distribution 1-B %	t-2-B %	c-2-B %	trans/cis	1 - B / 2 - B	Selectivity
4	15.9	4.2	54.0	32.0	14.0	2.29	1.17	0.71
2	32.9	7.2	52.2	34.8	13.0	2.68	1.09	0.66
6	64.2	6.7	46.6	36.2	17.2	2.10	0.87	0.65
3	98.3	5.4	40.0	41.1	18.9	2.17	0.67	0.56
1	125.0	5.7	7.7	76.9	15.4	4.99	0.08	n/a

Fig. 5·41 Variation of Butene Distribution and Selectivity with Reaction Extent ($Rh/MoO_3(c)$)

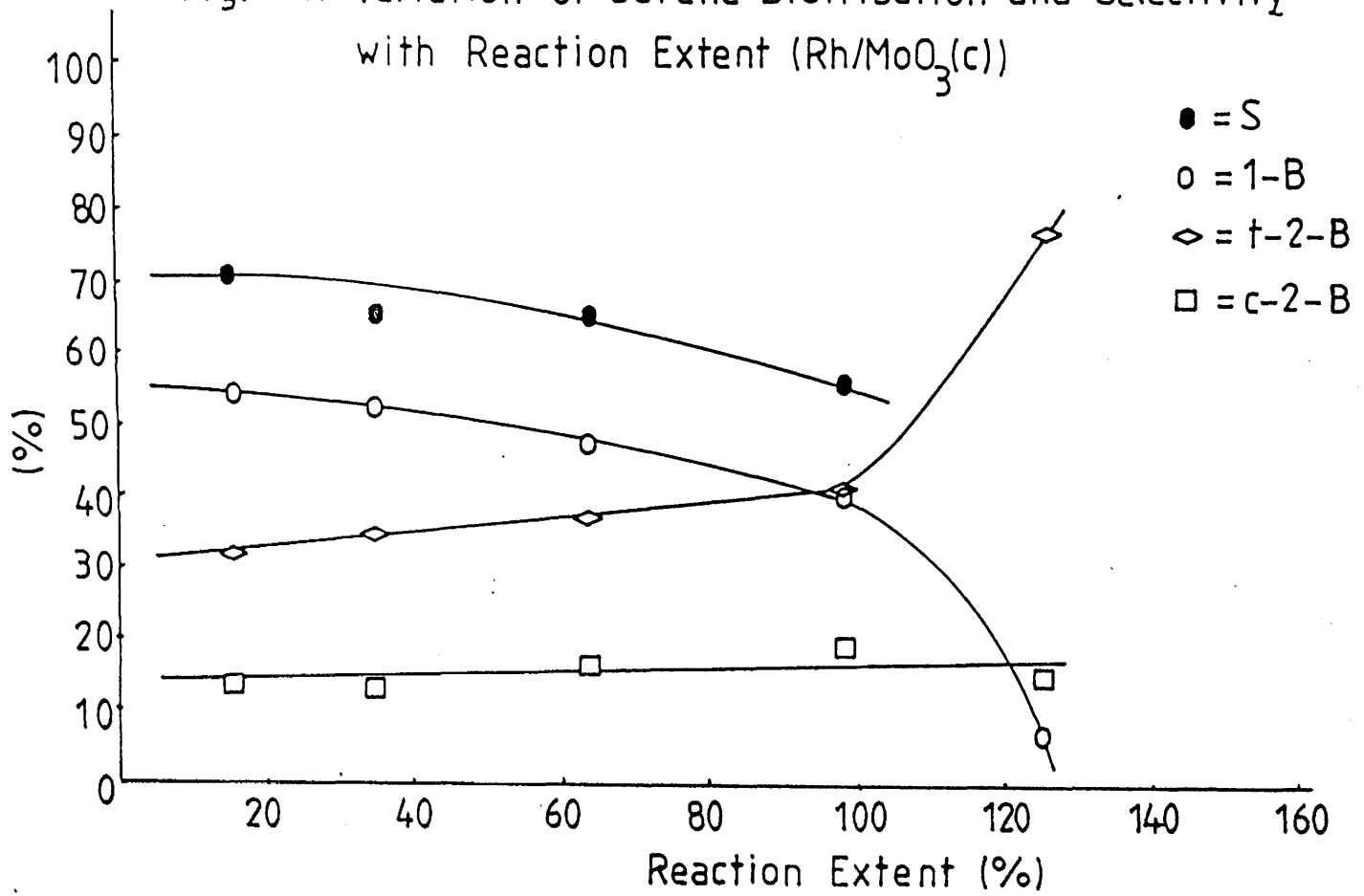

Table 5.8g. Variation of Butene Distribution with Reaction Extent

Catalyst: $Pt/WO_3(a)$ Weight of Sample = 0.0947g

Reaction Temperature = 0°C Initial Pressure = 78 Torr

Reaction Number	Reaction Extent %	Butene Distribution 1-B %	t-2-B %	c-2-B %	trans/cis	1-B / 2-B	Selectivity
3	13.3	83.3	15.1	1.7	8.9	4.96	0.60
6	49.0	77.0	17.0	6.0	2.83	3.34	0.56
4	70.0	78.6	15.7	5.7	2.75	3.67	0.55
5	119.0	71.7	20.8	7.5	2.77	2.53	0.40
1	161.0	61.0	30.0	9.0	3.33	1.56	n/a

Fig. 5·42 Variation of Butene Distribution and Selectivity with Reaction Extent ($Pt/WO_3(a)$)

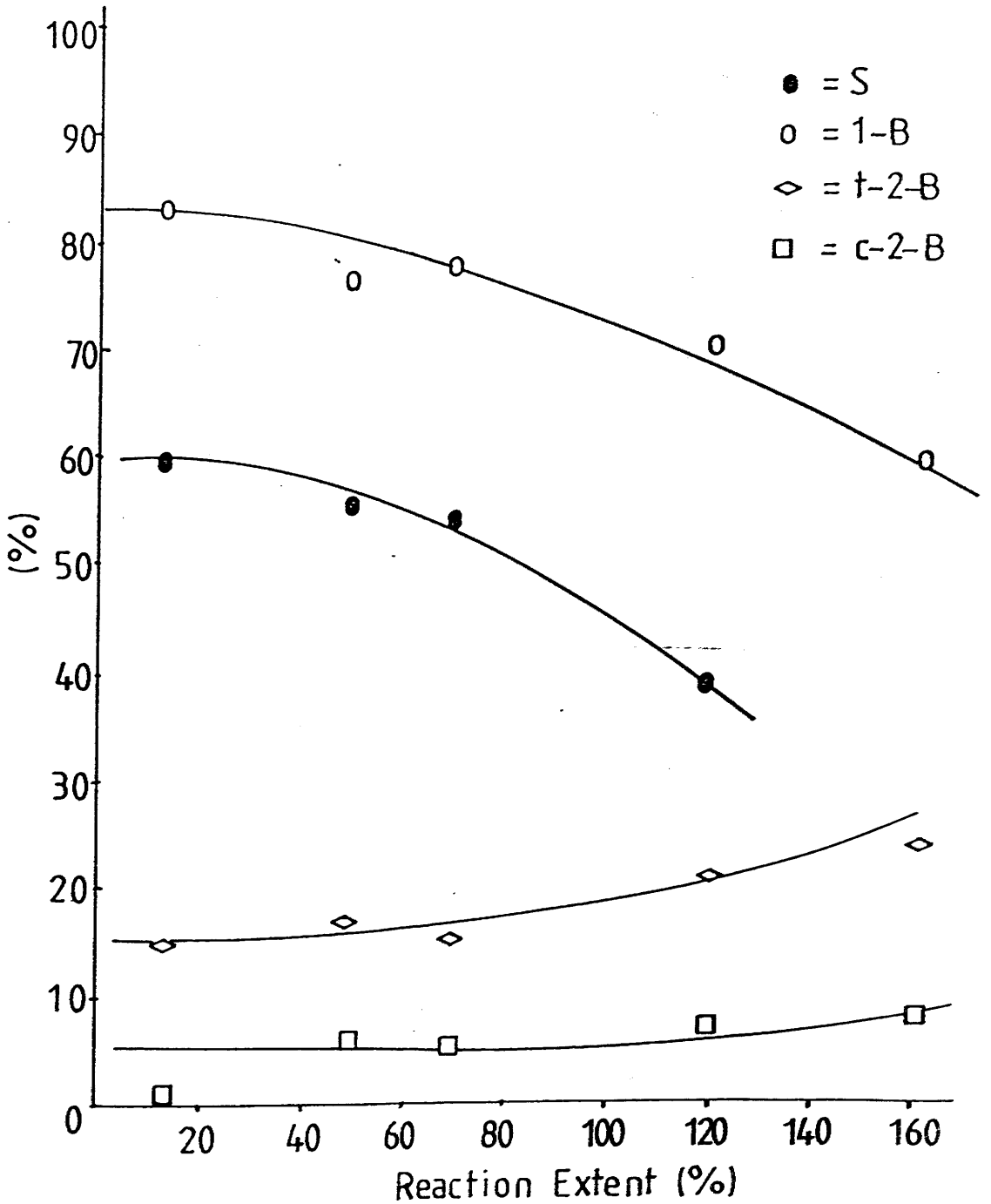

Table 5.8h. Variation of Butene Distribution with Reaction Extent.

Catalyst: $Rh/WO_3(b)$ Weight of Sample = 0.0297g

Reaction Temperature = 19°C Initial Pressure = 78 Torr

Reaction Number	Reaction Extent %	Butene Distribution 1-B %	t-2-B %	c-2-B %	trans/cis	1 - B / 2 - B	Selectivity
3	11	57.1	28.6	14.3	2.0	1.33	0.88
1	57	56.8	29.7	13.5	2.2	1.31	0.80
6	73	47.9	37.1	15.1	2.46	0.92	
4	88	46.6	35.9	17.5	2.05	0.87	0.75
2	102	38.6	43.2	18.2	2.37	0.63	0.56
5	133	31.0	51.0	18.0	2.83	0.45	n/a

Fig. 5·43 Variation of Butene Distribution and Selectivity with Reaction Extent (Rh/WO_3(b))

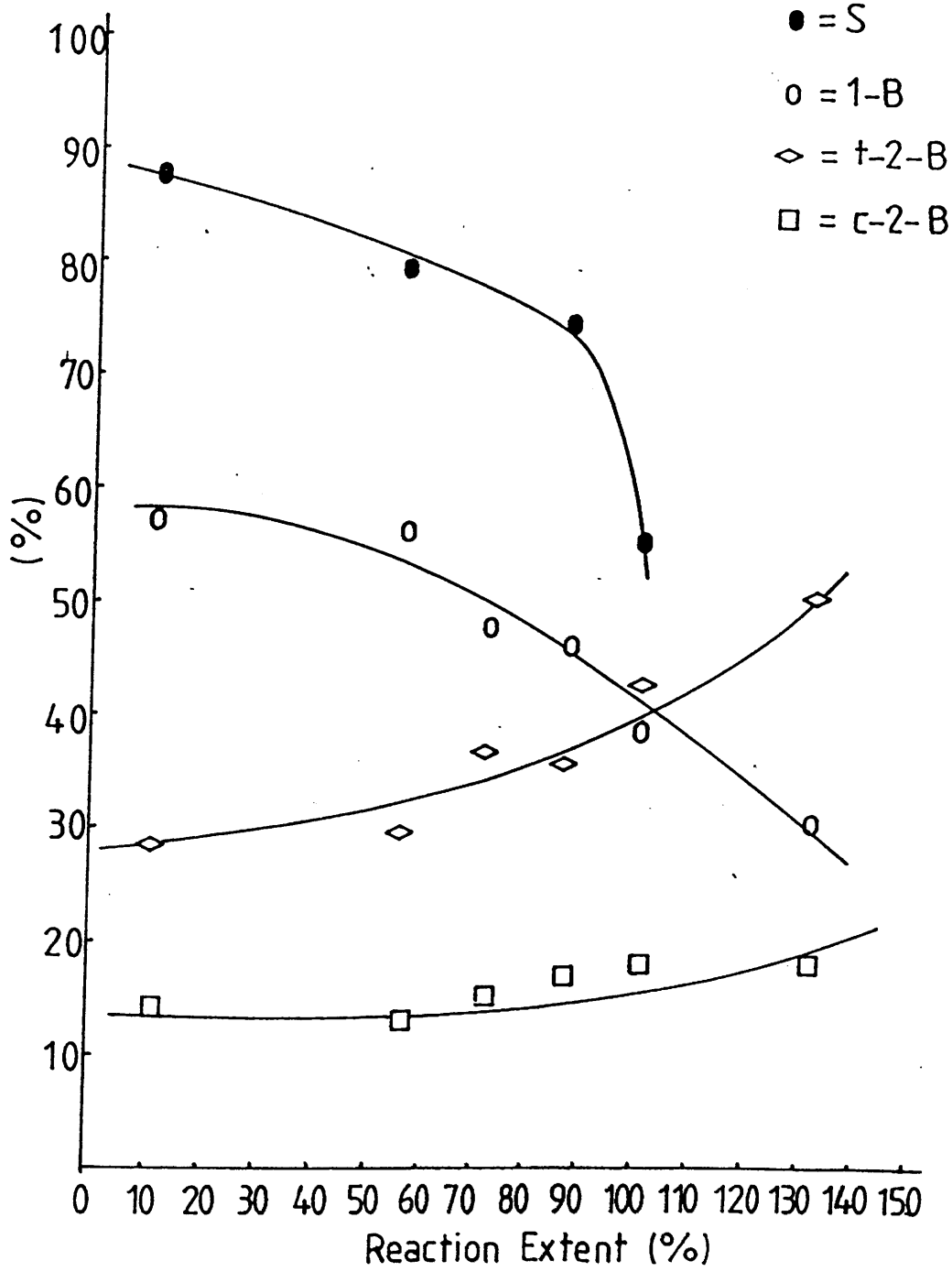

Table 5.8i. Variation of Butene Distribution with Reaction Extent.

Catalyst: $Rh/WO_3(c)$ Weight of Sample = 0.0360g

Reaction Temperature = 20°C Initial Pressure = 78 Torr

Reaction Number	Reaction Extent %	Butene Distribution 1-B %	t-2-B %	c-2-B %	trans/cis	1 - B / 2 - B	Selectivity
8	55	37.5	43.75	18.75	2.33	0.6	0.38
2	66	46.1	38.5	15.4	2.50	0.86	0.33
6	86	42.2	39.4	25.4	1.55	0.65	0.63
4	95	40.74	40.74	18.52	2.20	0.69	0.39
5	100	40.0	60.0	0.0	-	0.67	0.33
3	117	29.4	47.1	23.5	2.0	0.42	n/a
1	118	37.5	50.0	12.5	4.0	0.6	n/a
7	122	36.0	44.0	20.0	2.2	0.56	n/a

If a graph of initial rate versus hydrogen partial pressure failed to display a straight line indicating first order behaviour, a plot of $\log_{10}$ (initial rate) versus $\log_{10}$ (partial pressure of hydrogen) was made. The order of reaction with respect to hydrogen partial pressure was obtained directly from the gradient of the straight line procedure in the $\log_{10}$ (initial rate) versus $\log_{10} P_{H_2}$ plot.

In a similar manner, the order of reaction with respect to the partial pressure of butadiene was determined. This involved varying the partial pressure of butadiene from 7.8 Torr to 52 Torr while the hydrogen partial pressure was held constant at either 78 Torr or 104 Torr (constant for one series).

The results obtained from this series of reactions are presented in Table 5.9

5.6.4 Variation of Selectivity and Butene Distribution with Temperature

A series of experiments was carried out for each catalyst to examine the variation of butene distribution, selectivity and initial rate with temperature. Activation energies were calculated from the variation of initial rate with temperature.

For each series of experiments the initial pressure of 3:1 hydrogen:butadiene and the reaction extent were kept constant, while the temperature of the reaction was varied randomly to minimise variations with catalyst usage. The products were extracted at the pressure falls indicated in Tables 5.10a to 5.10i. The pressure falls,

Table 5.9. Orders of Reaction

Catalyst	Order of Reaction With Respect to P_{H_2}	Order of Reaction With Respect to $P_{C_4H_6}$
Pt/SiO_2(a)	0.7	-0.54
Pt/MoO_3(a)	2.33	-0.74
	1.2 ←corrected plots→	-1.2
Pt/WO_3(a)	0.9	-0.2
	0.7	-3.6
Rh/SiO_2(b)	0.68	-0.4
Rh/MoO_3(b)	1.0	-0.76
Rh/WO_3(b)	1.4	-0.95
	1.2	-0.6
Rh/SiO_2(c)	1.0	-0.9
Rh/MoO_3(c)	1.6	-0.4
Rh/WO_3(c)	1.0	-0.1

Fig. 5·44 Variation of Butene Distribution and Selectivity with Temperature (Pt/SiO_2(a))

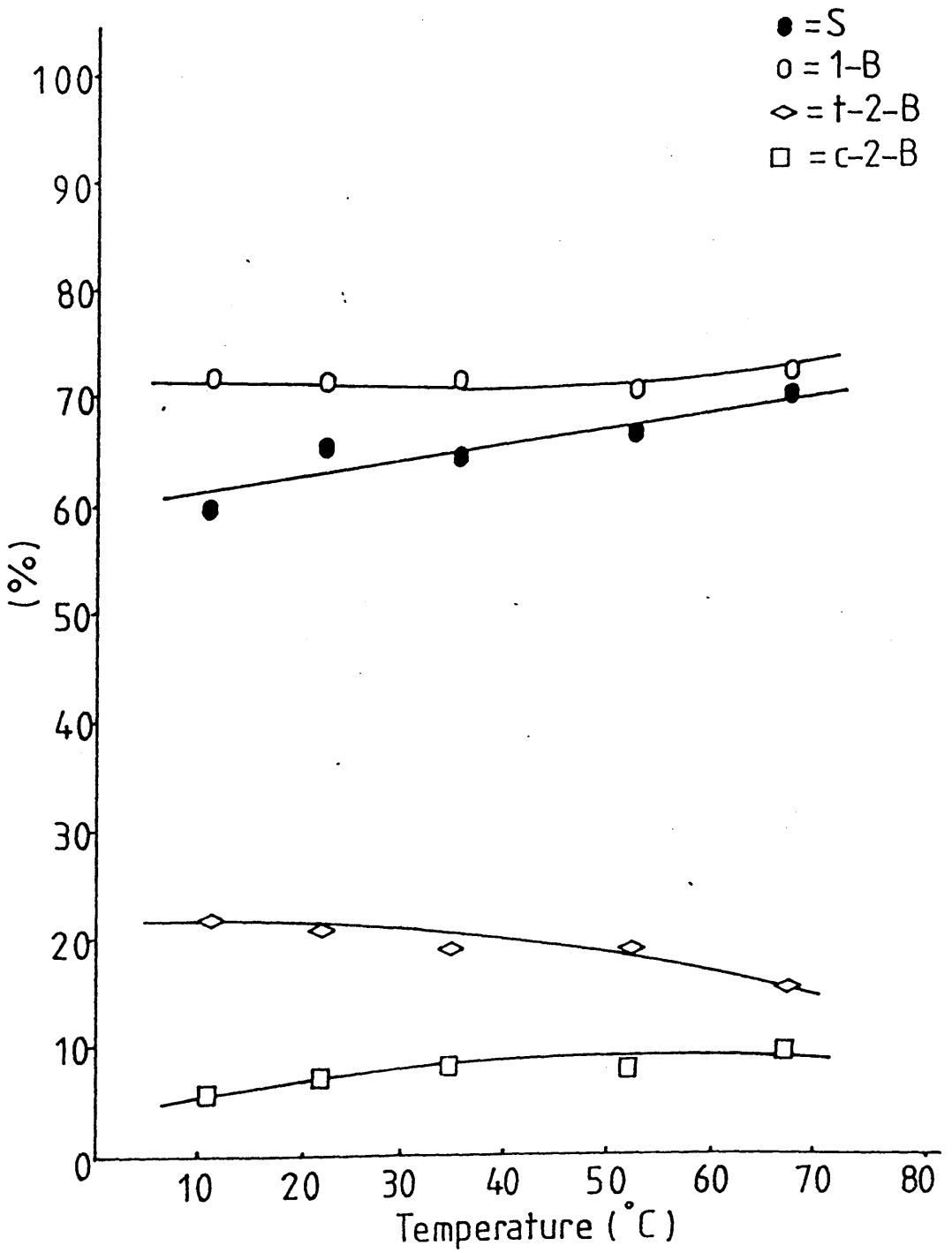

Table 5.10a. Variation of Butene Distribution with Temperature

Catalyst: $Pt/SiO_2(a)$ Weight of Sample = 0.0887g Initial Fressure = 104 Torr

Reaction Number	Reaction Extent %	Initial Rate Torr/min	Temperature °C	Butene Distribution 1-B %	t-2-B %	c-2-B %	trans/cis	1 - B / 2 - B	Selectivity
4	51	0.28	11	72.2	22.2	5.6	3.96	2.60	0.60
1	43	2.17	22	72.1	20.9	7.0	2.99	2.58	0.66
2	54	6.5	35	72.22	19.44	8.33	2.33	2.60	0.65
3	45	7.9	52	72.22	19.44	8.33	2.33	2.60	0.68
6	45	10.4	67	73.7	15.8	10.5	1.5	2.80	0.72
*5	42	18.6	80	80.25	18.52	1.23	15.1	4.1	0.64
	48 ± 6%								

Table 5.10b. Variation of Butene Distribution with Temperature

Catalyst: $Rh/SiO_2(b)$ Weight of Sample = 0.0483g Initial Pressure = 107 Torr

Reaction Number	Reaction Extent %	Initial Rate Torr/min	Temperature °C	Butene Distribution 1-B %	t-2-B %	c-2-B %	trans/cis	1 - B / 2 - B	Selectivity
3	56	0.7	0	55.9	29.7	14.4	2.06	1.27	0.82
1	55	3.5	16	65.7	25.7	8.6	2.99	1.92	0.88
2	49	6.5	30	53.9	32.6	13.5	2.40	1.17	0.87
5	61	3.3	33	56.1	31.6	12.3	2.57	1.28	0.88
*6	51	13.9	43	52.1	33.3	14.6	2.28	1.09	0.66
*4	71	35.75	54	42.9	40.0	17.1	2.34	0.75	0.44
	55 ± 6% except reaction 4								

Fig. 5·45 Variation of Butene Distribution and Selectivity with Temperature (Rh/SiO_2(b)

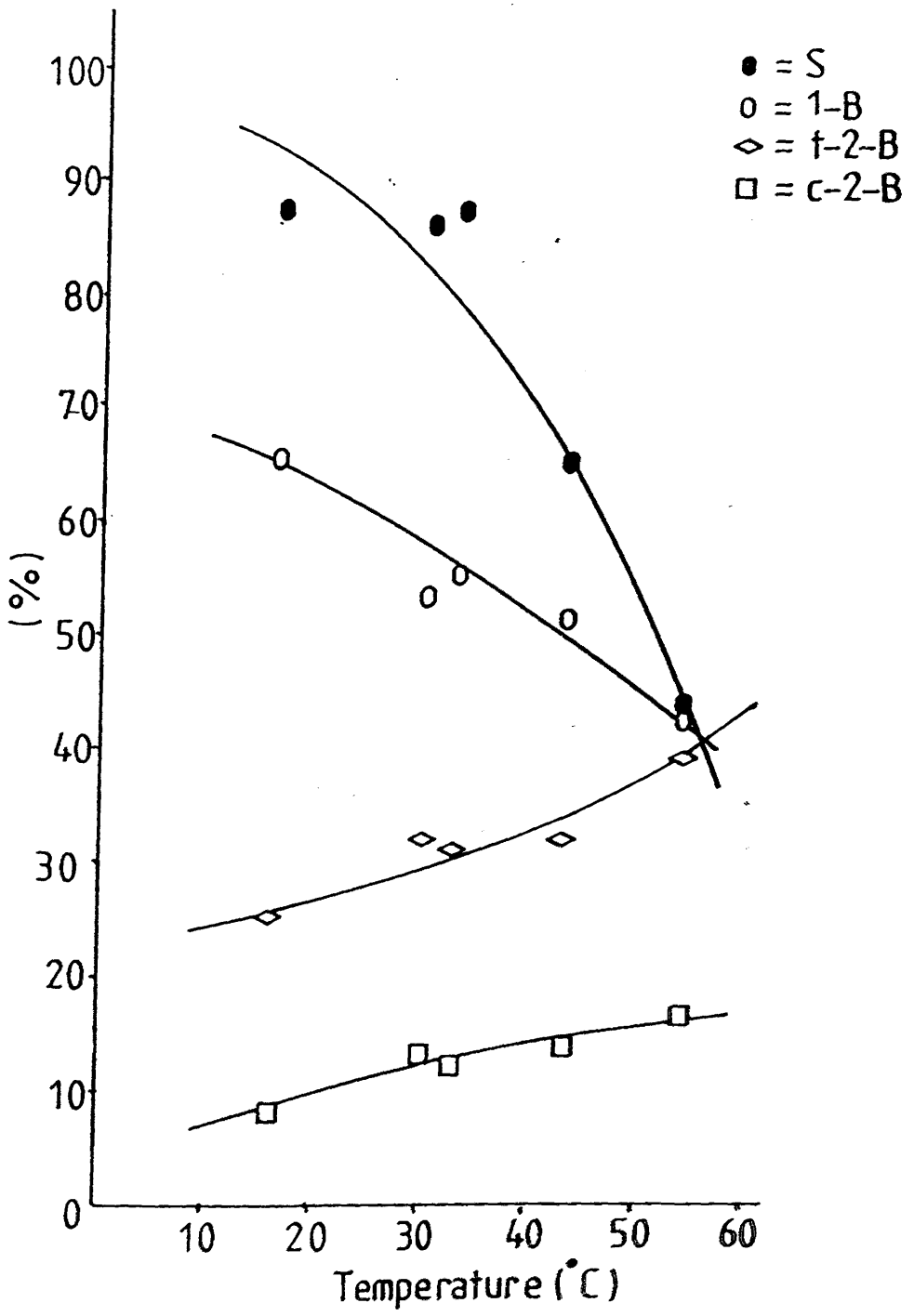

Table 5.10c. Variation of Butene Distribution with Temperature

Catalyst: $Rh/SiO_2(c)$ Weight of Sample = 0.0246g Initial Pressure = 161 Torr

Reaction Number	Reaction Extent %	Initial Rate Torr/min	Temperature °C	Butene Distribution 1-B %	t-2-B %	c-2-B %	trans/cis	1-B / 2-B	Selectivity
1	50	2.3	49	50.92	35.04	14.04	2.5	1.04	0.89
*6	59	17.3	73	23.2	22.6	54.2	0.42	0.30	0.87
*5	54	13.0	77	36.2	43.1	20.7	2.08	0.57	0.82
*3	45	52.0	100	35.74	45.82	18.44	2.48	0.56	0.67
*4	54	65.0	118	39.2	41.8	19.0	2.2	0.64	0.62
*2	60	130.0	148	35.74	45.82	18.44	2.48	0.56	0.60
	52 ± 8%								

Fig. 5·46 Variation of Butene Distribution and Selectivity with Temperature ($Rh/SiO_2(c)$)

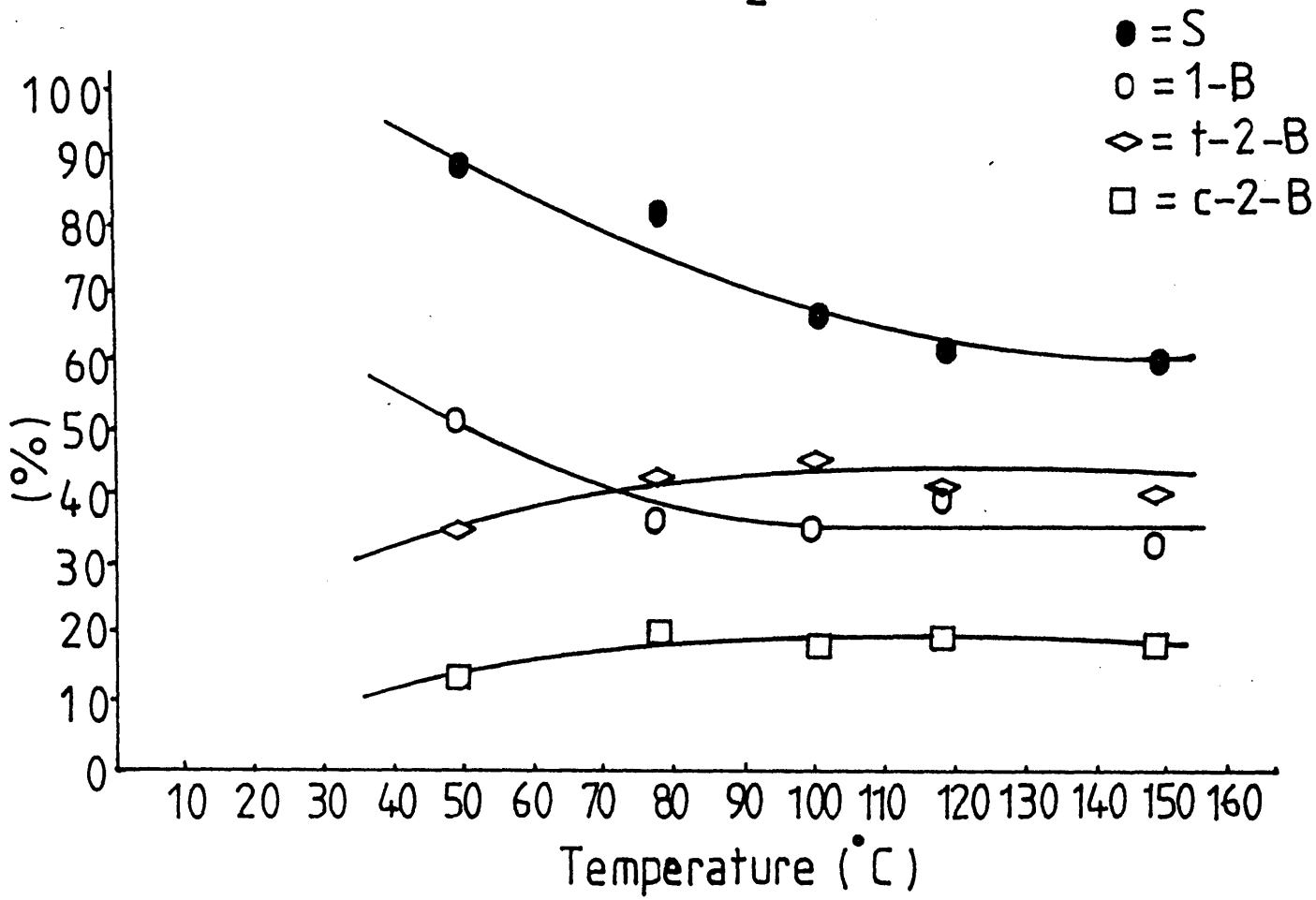

Table 5.10d. Variation of Butene Distribution with Temperature

Catalyst: $Pt/MoO_3(a)$ Weight of Sample = 0.0694g Initial Pressure = 78 Torr

Reaction Number	Reaction Extent %	Initial Rate Torr/min	Temperature °C	Butene Distribution 1-B %	t-2-B %	c-2-B %	trans/cis	1 - B / 2 - B	Selectivity
1	42	1.08	18	50	29	21	1.38	1.0	0.82
4	68	0.25	36	47	29	24	1.21	0.89	0.89
2	42	4.8	80	51	27	22	1.23	1.04	0.93
*3	47	12.3	120	53	28	19	1.47	1.13	0.94
*5	47	19.6	150	48	31	21	1.48	0.92	0.95
	45 ± 3% except reaction 4								

Fig. 5·47 Variation of Butene Distribution and Selectivity with Temperature ($Pt/MoO_3(a)$)

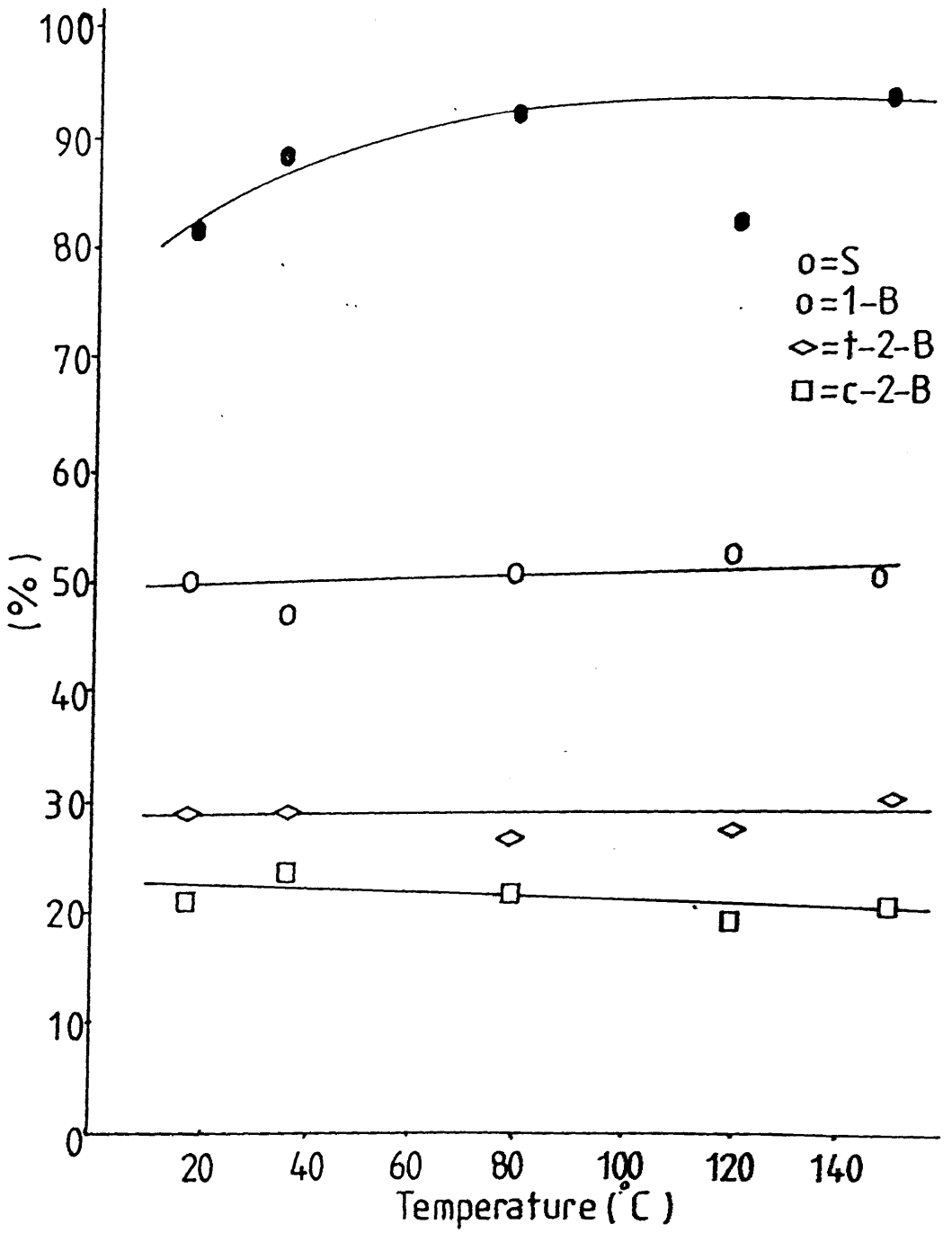

Table 5.10e. Variation of Butene Distribution with Temperature

Catalyst: $Rh/MoO_3(b)$ Weight of Sample = 0.2293g Initial Pressure = 78 Torr

Reaction Number	Reaction Extent %	Initial Rate Torr/min	Temperature °C	Butene Distribution 1-B %	t-2-B %	c-2-B %	trans/cis	1 - B / 2 - B	Selectivity
6	28.1	0.1	0	57.3	29.5	13.2	2.23	1.34	0.82
5	19.2	0.22	16	55.4	30.7	13.9	2.21	1.24	0.85
4	17.8	0.4	20	53.2	32.1	14.8	2.17	1.13	0.87
1	26.3	0.6	38	53.9	31.5	14.6	2.16	1.17	0.93
2	30.0	1.04	62	53.0	32.9	14.1	2.33	1.13	0.92
3	19.3	1.7	78	53.6	32.1	14.3	2.24	1.16	0.80
	23 ± 7%								

Fig. 5·48 Variation of Butene Distribution and Selectivity with Temperature ($Rh/MoO_3(b)$)

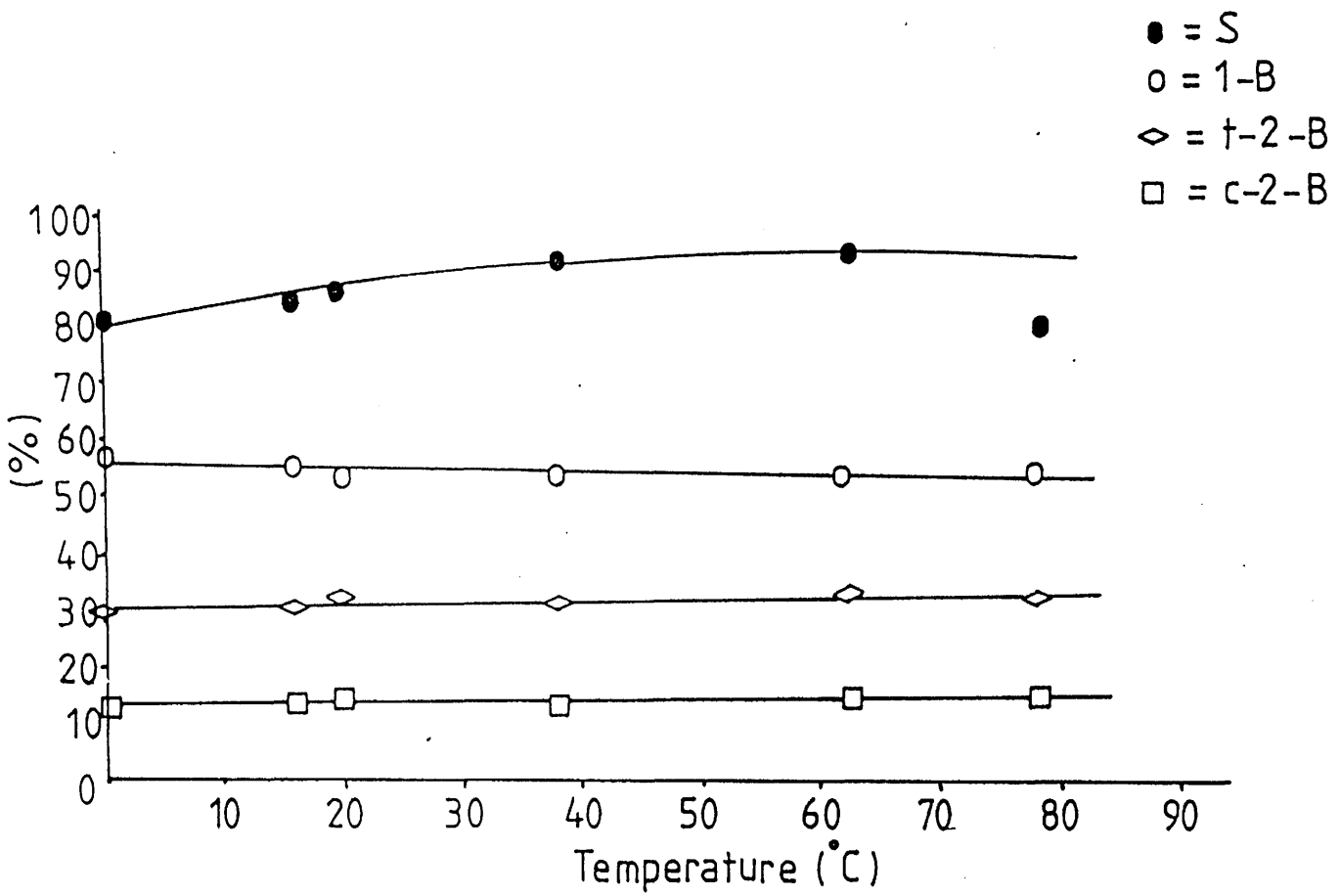

Table 5.10f. Variation of Butene Distribution with Temperature

Catalyst: $Rh/MoO_3(c)$ Weight of Sample = 0.2077g Initial Pressure = 78 Torr

Reaction Number	Reaction Extent %	Initial Rate Torr/min	Temperature °C	Butene Distribution 1-B %	t-2-B %	c-2-B %	trans/cis	1-B / 2-B	Selectivity
3	34.8	5.6	0	56.9	28.4	14.7	1.93	1.32	0.55
4	-	4.2	2	-	-	-	-	-	-
7	28	4.2	6	56.25	25.0	18.75	1.33	1.29	0.62
*5	30	11.6	12	63.2	26.3	10.5	2.50	1.72	0.59
*2	34.2	43.3	21	47.1	35.3	17.6	2.01	0.89	0.43
*1	32.2	63.6	29	57.1	28.6	14.3	2.0	1.33	0.17
*6	32.8	39	49	44.01	35.55	20.44	1.74	0.79	0.65
	31 ± 4%								

Fig. 5·49 Variation of Butene Distribution and Selectivity with Temperature ($Rh/MoO_3(c)$)

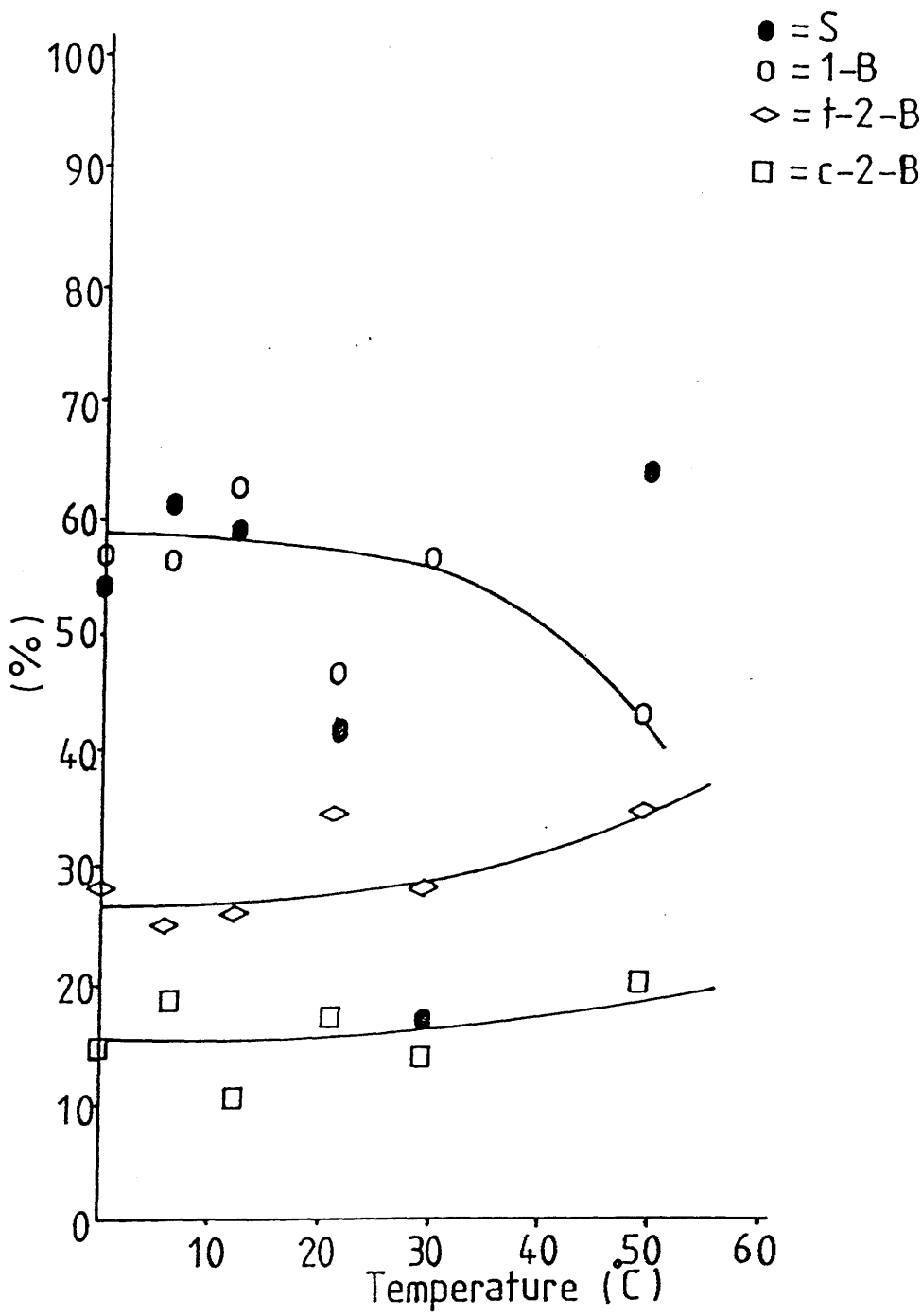

Table 5.10g. Variation of Butene Distribution with Temperature

Catalyst: $Pt/WO_3(a)$ Weight of Sample = 0.0947g Initial Pressure = 78 Torr

Reaction Number	Reaction Extent %	Initial Rate Torr/min	Temperature °C	Butene Distribution 1-B % t-2-B % c-2-B %	trans/cis	1 - B / 2 - B	Selectivity
5	57	0.8	-4	82.1 14.3 3.6	3.97	4.6	0.55
3	50.3	1.7	0	79.31 17.24 3.45	5.0	3.83	0.57
2	56	4.4	12	77.0 17.0 6.0	2.83	3.35	0.56
1	61	6.4	18	80.0 16.0 4.0	4.0	4.0	0.55
*4	53	11.6	28	73.3 20.0 6.7	2.99	2.75	0.44
*6	71	22.8	44	72.7 18.2 9.1	2.0	2.66	0.27
	61 ± 10%						

Fig. 5·50 Variation of Butene Distribution and Selectivity with Temperature(Pt/WO_3(a))

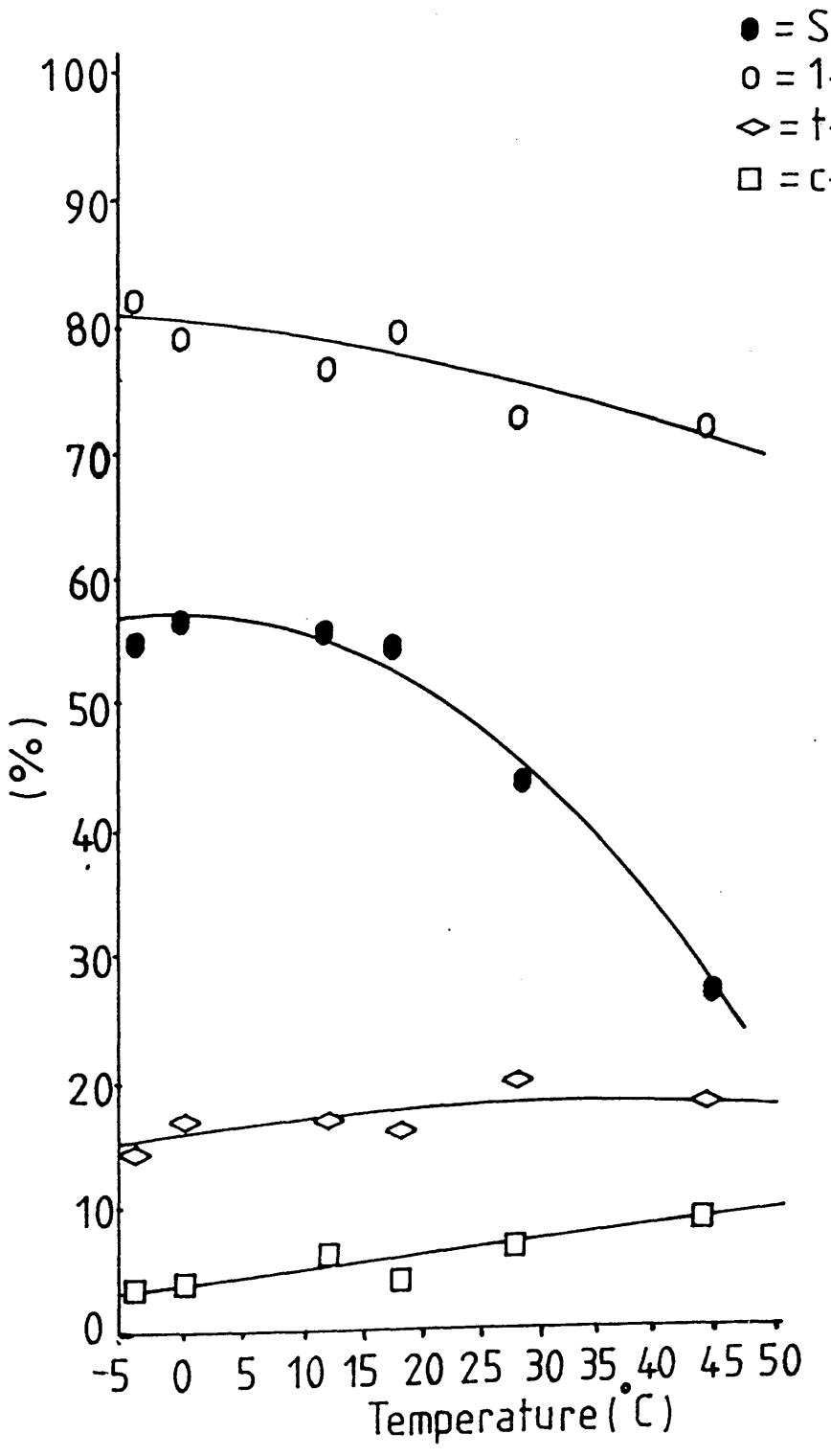

Table 5.10h. Variation of Butene Distribution with Temperature

Catalyst: $Rh/WO_3(b)$ Weight of Sample = 0.0297g Initial Pressure = 78 Torr

Reaction Number	Reaction Extent %	Initial Rate Torr/min	Temperature °C	Butene Distribution 1-B %	t-2-B %	c-2-B %	trans/cis	1 - B / 2 - B	Selectivity
4	68	0.76	0	52.9	32.4	14.7	2.20	1.12	0.77
5	65	0.9	9	51.9	33.3	14.8	2.25	1.08	0.79
1	62	5.7	20	60.5	27.9	11.6	2.41	1.53	0.80
2	71	2.6	38	51.9	32.7	15.4	2.12	1.08	0.78
*3	67	30.9	82	60.0	28.0	12.0	2.33	1.5	0.41
	67 ± 5%								

Fig. 5·51 Variation of Butene Distribution and Selectivity with Temperature ($Rh/WO_3(b)$)

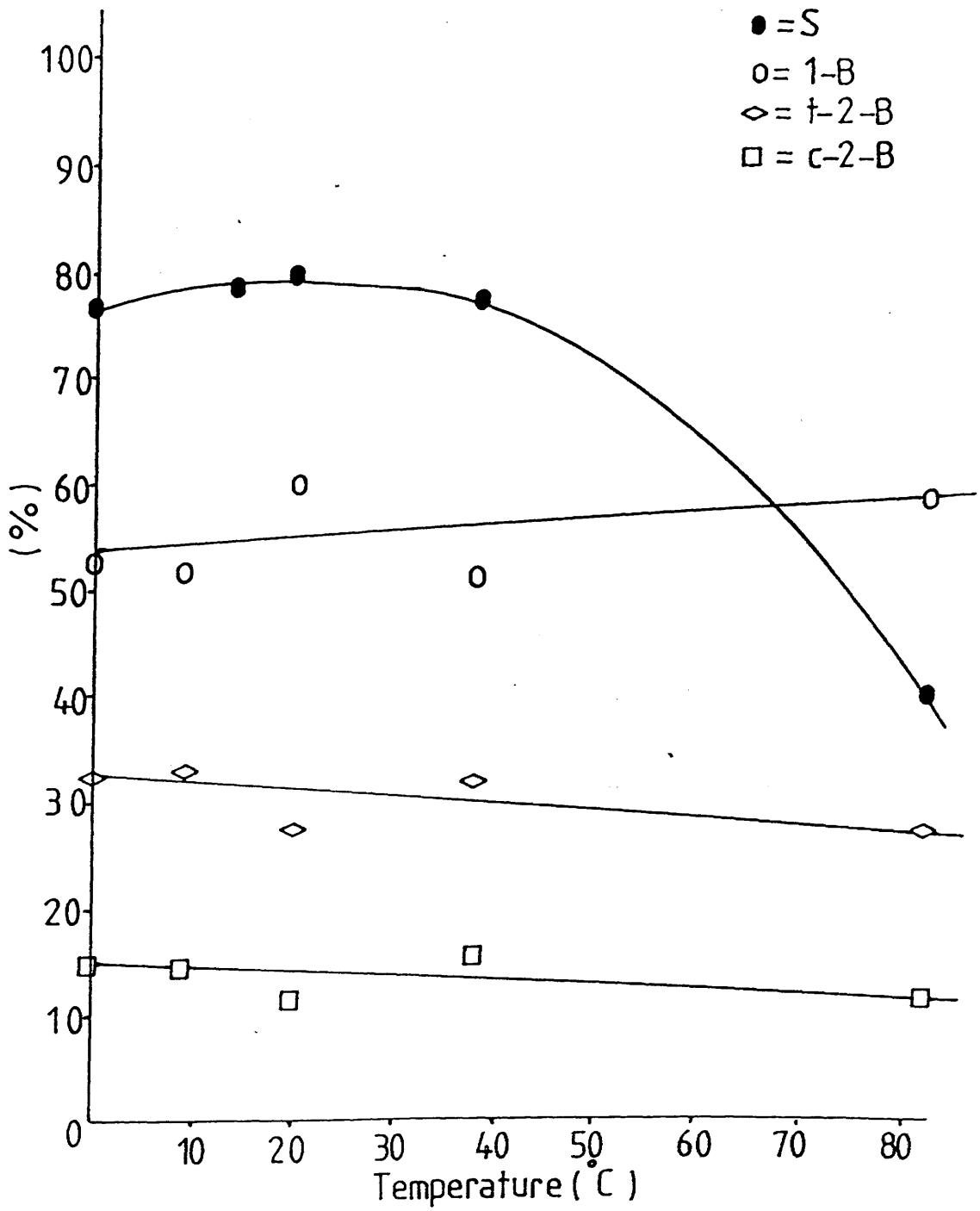

Table 5.10i. Variation of Butene Distribution with Temperature

Catalyst: $Rh/WO_3(c)$ Weight of Sample = 0.0360g Initial Pressure = 78 Torr

Reaction Number	Reaction Extent %	Initial Rate Torr/min	Temperature °C	Butene Distribution 1-B %	t-2-B %	c-2-B %	trans/cis	1-B / 2-B	Selectivity
4	90	1.4	-4	48.5	36.4	15.1	2.4	0.94	0.45
2	78	2.7	4	50.0	33.3	16.7	1.99	1.0	0.48
1	84	3.7	18	52.9	35.3	11.8	2.99	1.12	0.43
*3	88	11.6	31	41.2	41.2	17.6	2.34	0.70	0.41
*6	86	20.8	44	46.1	38.5	15.4	2.50	0.86	0.33
*5	85	28.6	64	44.44	33.33	22.22	1.50	0.80	0.38
	84 ± 6%								

Fig. 5·52 Variation of Butene Distribution and Selectivity with Temperature ($Rh/WO_3(c)$)

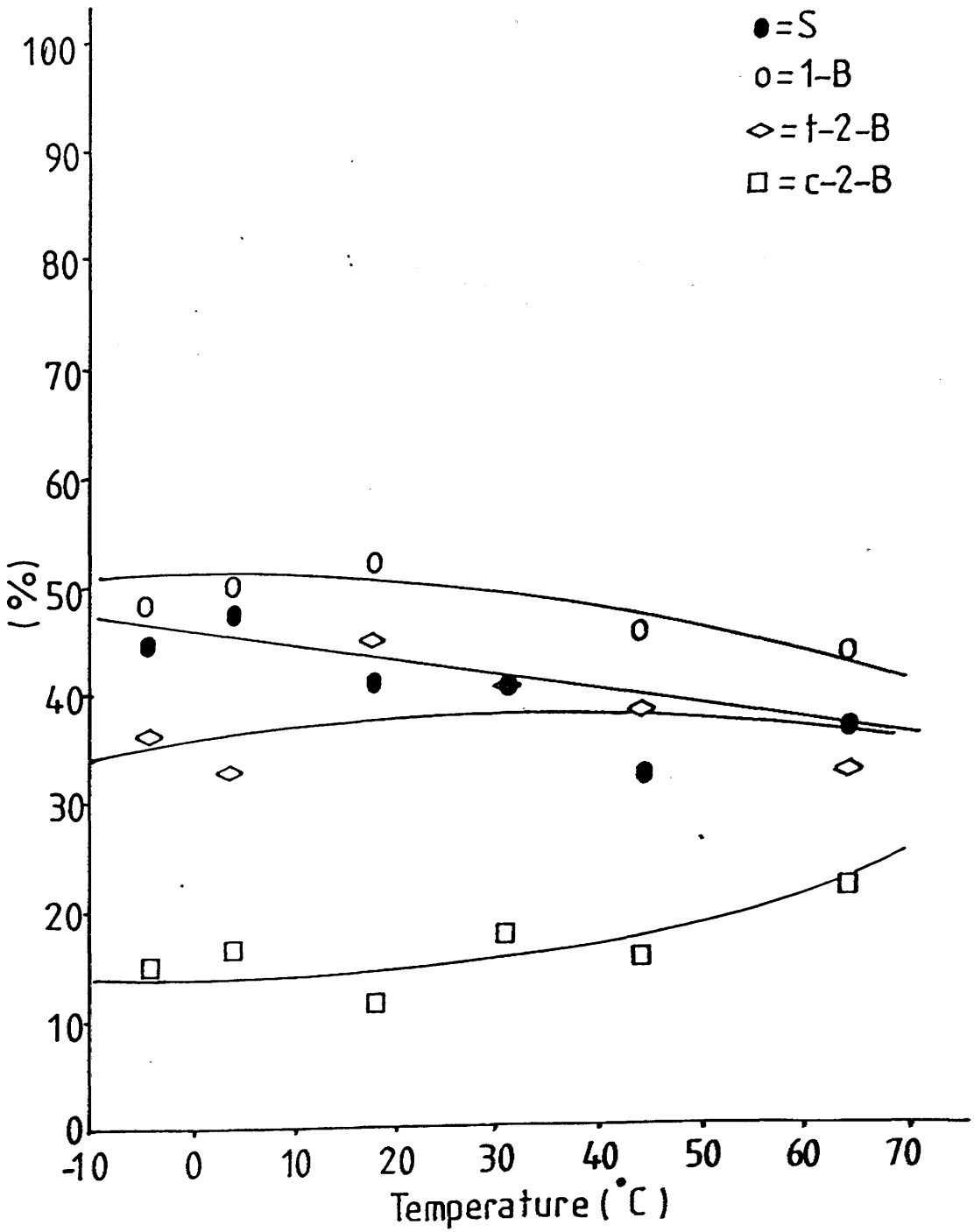

quoted as reaction extents, were approximately constant for one catalyst, but varied from one catalyst to another. Tables 5.10a to 5.10i show the results obtained from these experiments. These results are shown diagramatically in Figures 5.44 to 5.52. The initial rate of reaction was determined for each reaction in the series using the method described in Chapter 4, section 4.5 For each series of reactions, an Arrhenius type plot of ℓn (initial rate) versus (temperature in Kelvin)$^{-1}$ allowed calculation of the activation energy. The activation energy values calculated for each catalyst are presented in Table 5.13. Figures 5.53 to 5.55 show the Arrhenius type plots obtained for each catalyst.

If the initial rate exceeds ca. 10 Torr/min, it is expected that the reaction is diffusion controlled. Such reactions will be marked with an asterisk (*).

Table 5.11 contains the activation energies for each catalyst. Figure 5.53 to 5.55 are the Arrhenius plots (ℓn (initial rate) vs. $\frac{1}{T}$) which were made to obtain the activation energies for each catalyst. Figure 5.53 shows the activation energy plots for the supported platinum catalysts, Figure 5.54 for the catalysts prepared from rhodium(III)nitrate and Figure 5.55 shows the activation energy plots for catalysts prepared from rhodium(III)chloride.

In Table 5.11, the E_a values quoted for Rh/MoO_3(b) were both obtained from fresh samples. No E_a value was obtained for used Rh/MoO_3(b). The E_a value quoted for Rh/SiO_2(c) corresponds to diffusion controlled reactions.

Table 5.11. Activation Energies

Catalyst	Activation Energy (kJ mol^{-1})	
	Fresh Catalyst	Used Catalyst
Pt/SiO_2(a)	28	34
Pt/MoO_3(a)	72	22
Pt/WO_3(a)	55	
Rh/SiO_2(b)	56	42
Rh/MoO_3(b)	* { 31 / 39 }	
Rh/WO_3(b)	30	45
Rh/SiO_2(c)	72	
Rh/MoO_3(c)	120	68
Rh/WO_3(c)	44	39

Fig. 5·53 Activation Energy Plots for Supported Platinum Catalysts

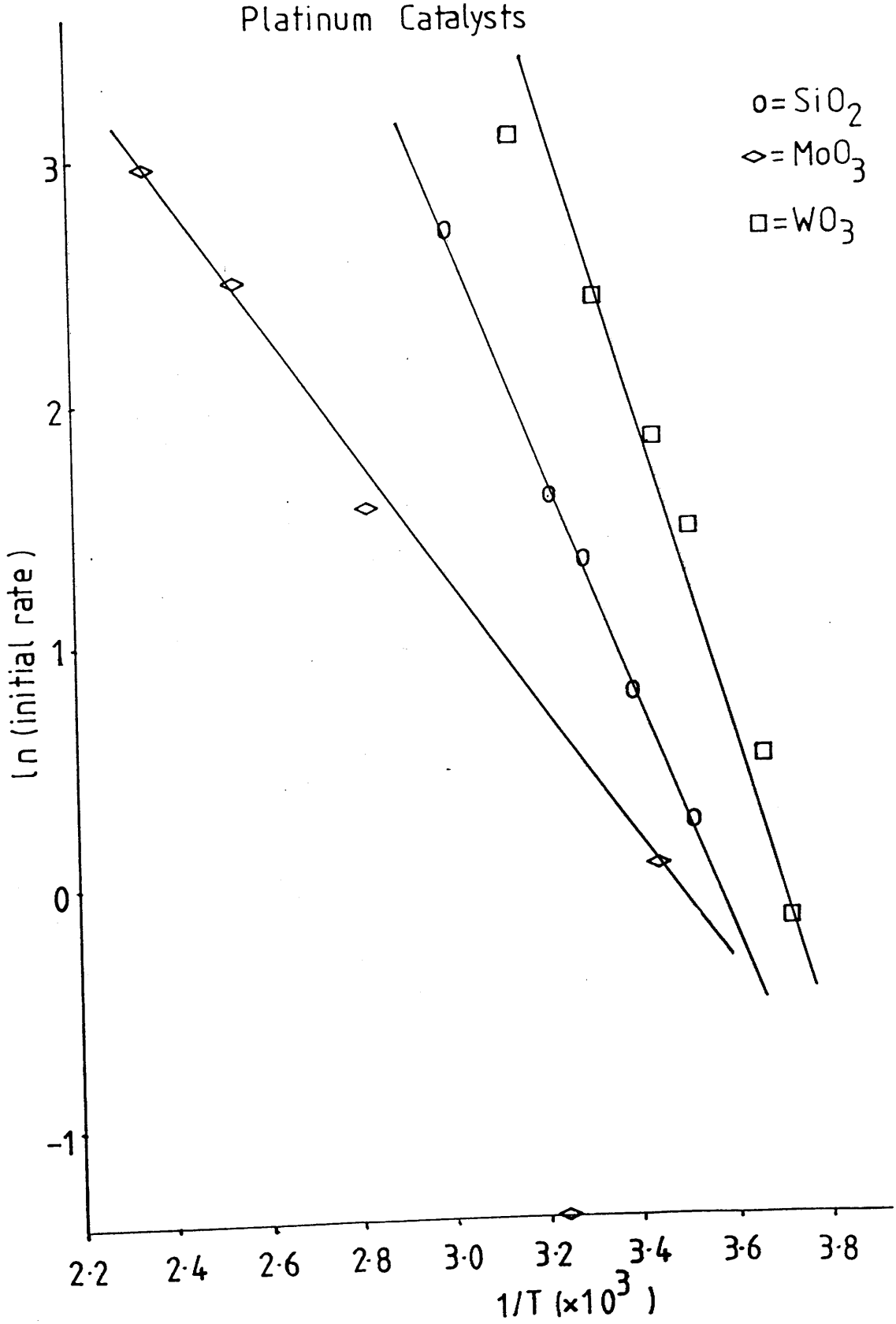

Fig. 5·54 Activation Energy Plot For Supported Rhodium Catalysts Prepared From $Rh(NO_3)_3$

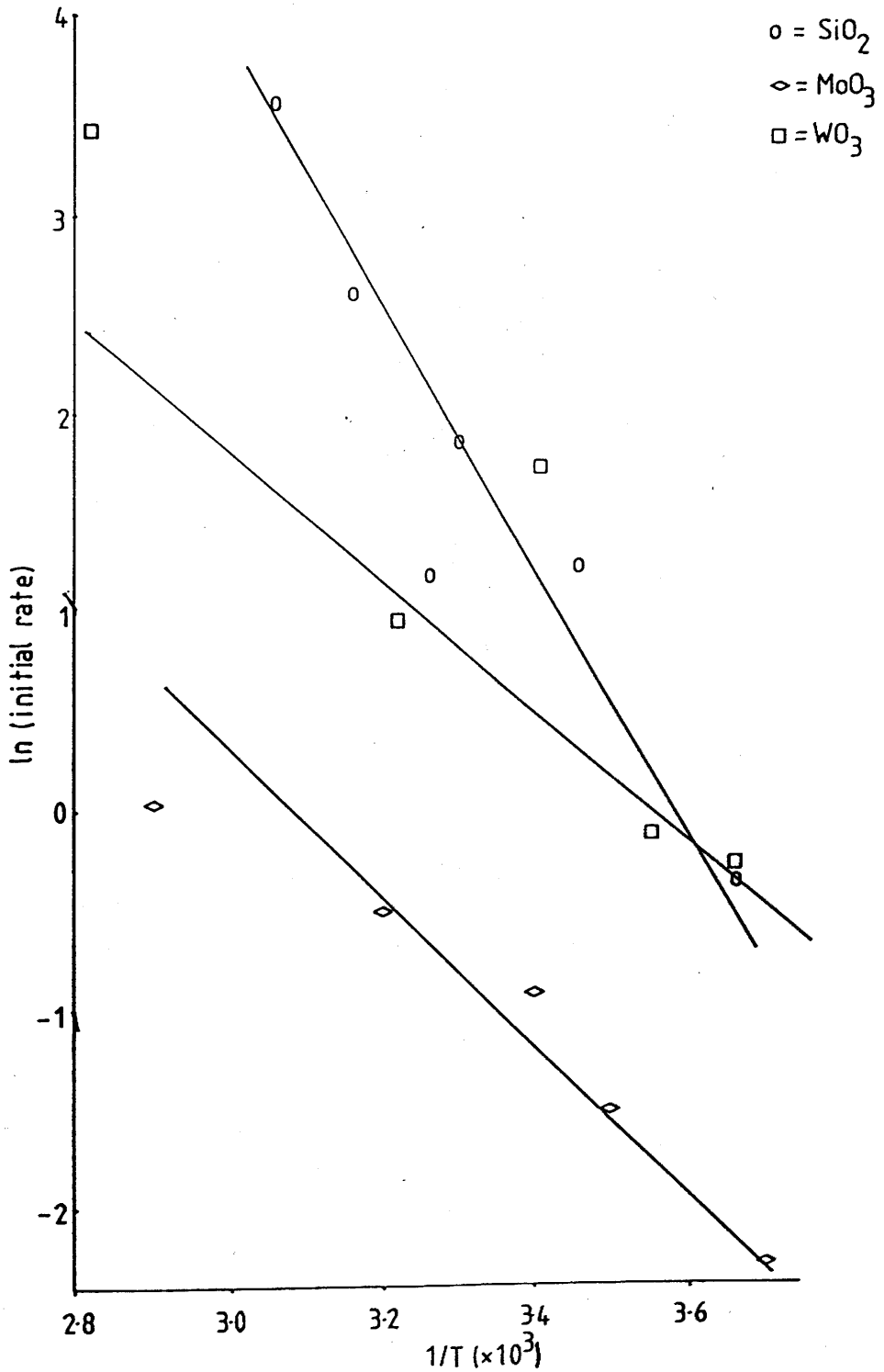

Fig. 5·55 Activation Energy Plots for Supported $RhCl_3$ Derived Catalysts

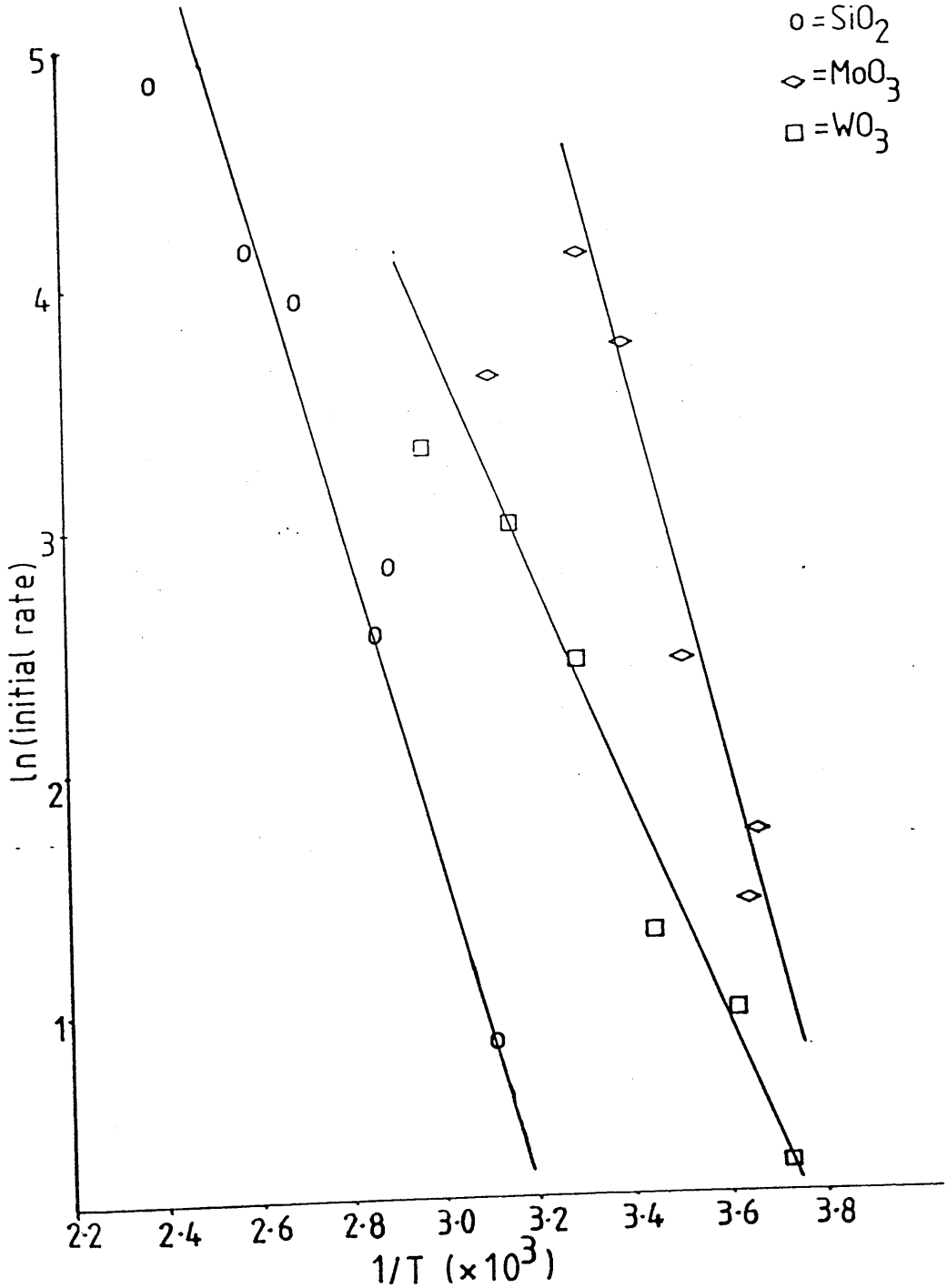

CHAPTER SIX

CHAPTER 6

DISCUSSION

6.1 Temperature Programmed Reduction and Thermal Analysis

The results obtained by carrying out temperature programmed reduction, differential scanning calorimetry and thermogravimetric analysis on the various supported platinum and rhodium catalysts show that there is evidence for reduction of both the metal salt and the support, when the latter is molybdenum trioxide or tungsten trioxide.

Considering first the T.G.A. and D.S.C. results, the T.G.A.'s provide direct evidence for hydrogen molybdenum bronze formation, while the quantity of hydrogen consumed during the reduction of many of the salts gives a strong indication that hydrogen spillover on to the support has taken place. In the case of molybdenum trioxide and tungsten trioxide as supports, it is believed that the spillover hydrogen has led to hydrogen metal bronze formation, and to reduction of the support at elevated temperatures.

Thermo-gravimetric analysis of rhodium chloride ($RhCl_3.xH_2O$) in air strongly suggests that during its decomposition, some rhodium chloride may react to form rhodium oxide, Rh_2O_3. This is consistent with the weight loss found between ca. 550°C and ca. 810°C. Rhodium oxide itself decomposes in air to rhodium metal between ca. 1050°C and 1125°C. In 5.5% H_2/N_2, there is an overlap between the reduction of the rhodium chloride with water loss from the catalyst. However, the results show that reduction begins between 85°C and 100°C, with the

most rapid reduction occurring between 120°C and 170°C. $RhCl_3.xH_2O$ decomposes at 100°C (124) and it is, therefore, possible that, during catalyst preparation, the decomposing $RhCl_3.xH_2O$ has reacted with water during the dehydration process. This may have resulted in some of the rhodium being present as rhodium oxide, Rh_2O_3, in the unreduced state, the remainder being present as $RhCl_3.xH_2O$.

Jackson (117) suggested that when rhodium trichloride was supported on silica, the support hydrolysed the rhodium trichloride resulting in the formation of oxy-chloride species, which are difficult to reduce, and a chlorinated support.

Differential scanning calorimetry carried out on $RhCl_3/SiO_2$ shows only one major decomposition peak with a peak maximum at 35°C (Fig. 5.24). The D.S.C. profile obtained for $RhCl_3/WO_3$ (Fig. 5.25), however, shows that the first decomposition peak occurs with T_{max} = 65°C, with a shoulder at 135°C. It is possible in both cases that these peaks are attributable to rhodium chloride decomposition. In addition, for $RhCl_3/WO_3$, a further decomposition peak can be observed with T_{max} = 370°C, which may be due either to dehydration or decomposition of the support.

T.G.A. of Rh/SiO_2(c) in 5.5% H_2/N_2 shows that reduction is complete by 150°C, but the reduction is not distinct from the dehydration of the supported salt. Formation of rhodium oxide, Rh_2O_3, from rhodium chloride may take place before reduction to rhodium metal.

T.G.A. of Rh/WO_3(c) in 5.5% H_2/N_2 occurs in stages. The weight loss up to 150°C occurs in two stages: ambient to 100°C and 100°C to 150°C. The total weight loss up to 150°C corresponds to dehydration of the metal salt together with reduction of the salt to rhodium metal.

Although these processes overlap, it is likely that the salt dehydration, together with the formation of rhodium oxide from rhodium chloride takes place below 100°C. However, these processes overlap with the weight loss between 100°C and 150°C which are attributed to reduction of rhodium oxide to rhodium metal. Further, more extensive weight loss occurs between 320°C and 420°C, and between 580°C and 980°C. This weight loss is consistent with support reduction.

The T.G.A. of Pt/WO_3(a) showed a similar weight loss pattern to that observed for Rh/WO_3(c). The initial reduction period up to 150°C would seem to correspond to reduction of the platinum salt, whereas between 350°C and 450°C, 620-750°C and 750-1020°C, the weight losses must be due to support reduction. The D.S.C. profile obtained for Pt/WO_3(a) (Fig. 5.27) shows peak maxima at 40°C, 80°C and 130°C, which are most probably due to decomposition of the platinum salt, and which are similar to those found by T.G.A.. The peak maxima at 410°C, 465°C and 540°C correlate closely with the T.G.A. peaks attributed to reduction of the support.

The D.S.C. profile obtained for Pt/MoO_3(a) (Fig. 5.26) shows major peak maxima at 75°C and 155°C, which can be attributed to decomposition of the platinum salt. This can be related to the T.G.A. profile which shows that platinum salt reduction is apparently complete by ca. 120°C. Further, more extensive weight loss, corresponding to support reduction is observed by T.G.A. between ca. 300°C and 750°C. Similarly, the D.S.C. profile shows evidence of support decomposition, with peak maxima at 315°C, 450°C and 565°C. In addition, the T.G.A. profile of Pt/MoO_3(a) in 5.5% H_2/N_2 shows a weight <u>increase</u> which

immediately follows the weight loss corresponding to platinum salt reduction. It is proposed that this weight increase is due to hydrogen molybdenum bronze, H_xMoO_3, formation. The weight increase corresponds to a value of x of 0.9.

The T.G.A. profile of $Rh/MoO_3(c)$ shows that, in addition to the weight loss found for $Rh/SiO_2(c)$ up to 150°C, attributable to reduction of the rhodium salt, a weight gain, similar to that found for $Pt/MoO_3(a)$ is observed. This weight gain may be due to hydrogen molybdenum bronze formation. In this case, x is found to be 0.7, and the bronze, therefore, has the composition $H_{0.7}MoO_3$. Hydrogen metal bronze formation occurs when the dissociative adsorption of molecular hydrogen takes place on the supported metal. The atomic hydrogen so-formed can then spill over on to the support, in this case molybdenum trioxide. Subsequent migration of the hydrogen in to the support results in the formation of the hydrogen molybdenum bronze. However, as the temperature is further increased, for example during T.G.A., the hydrogen molybdenum bronze will undergo both dehydrogenation and dehydration, leading to support reduction (80), as can be seen from the T.G.A. profiles. The T.G.A. profile obtained for $Rh/MoO_3(c)$ shows that weight loss occurs between 200 and 350°C and between ca. 450 and 700°C. This must correspond to bronze dehydrogenation-dehydration and support reduction.

The T.P.R. results will now be considered in the light of the T.G.A. and D.S.C. results discussed above. The temperature programmed reduction profiles obtained using Flow System II, presented in Chapter 5, section 5.1.2, show that the reduction is signified by

water formation. This is significant since the T.P.R. profiles shown in Figures 5.10 to 5.13 follow the reduction of fresh samples of supported salts. For these particular samples, it would be expected that reduction would be accompanied by the formation of HCl. However, only tiny quantities of HCl were detected, with water being the species present in highest abundance. This suggests that during catalyst preparation the metal salts have reacted to form oxides. Figure 5.10 shows the reduction profile obtained for $Pt/MoO_3(a)$. The first reduction peak occurs at ca. 80°C. By comparison with the T.G.A. results, this can be attributed to platinum salt (or oxide) reduction. The T.G.A. profile indicates that reduction of the support takes place above 300°C. This suggests that the reduction peak maxima observable at 176°C and 250°C could still be due to platinum salt reduction, although since the hydrogen molybdenum bronze formation occurs at approximately 150°C, as shown by T.G.A., the 176°C peak maximum may be due to bronze formation during T.P.R., with the peak at 250°C being either further hydrogen spillover in to the molybdenum trioxide, or the early stages of support reduction.

Figure 5.11 shows the T.P.R. profile of $Pt/WO_3(a)$. By comparison with the T.G.A. results, it appears that the T.P.R. profile is mainly showing evidence of platinum oxide reduction. Although the T.G.A. provided no evidence of hydrogen tungsten bronze formation, it is possible that such a bronze is formed during T.P.R..

The T.P.R. profile of $Pt/SiO_2(a)$ is shown in Figure 5.12. The peak maximum of ca. 100°C, with a shoulder at ca. 170°C agrees with the temperature of platinum oxide reduction obtained for $Pt/MoO_3(a)$

and $Pt/WO_3(a)$. The T.P.R. profile of $Rh/MoO_3(c)$ shown in Figure 5.13 provides evidence of rhodium oxide reduction starting at ca. 50°C, with T_{max} = 85°C. This agrees with the T.G.A. profile, which provides evidence for rhodium chloride, or oxide, reduction up to ca. 150°C. The T.P.R. profile also provides evidence of support reduction, or bronze decomposition, above 300°C, which again agrees with the T.G.A. results.

The temperature programmed reduction results presented in Chapter 5, section 5.1.1 were obtained using Flow System I. The T.P.R. profiles shown in Figures 5.1 to 5.9 are characteristic "finger-prints" of the catalysts involved. Figure 5.1 shows the T.P.R. profile for $Pt/SiO_2(a)$. Only one reduction peak is observable, with T_{max} = 162°C. This agrees with the T.P.R. profile for $Pt/SiO_2(a)$ shown in Figure 5.12, which has a shoulder at ca. 170°C. The hydrogen consumption was calculated to be 2.12×10^{19} molecules of hydrogen per gram of catalyst. This is less than one third of the theoretical quantity of 6.8×10^{19} H_2 molecules required to reduce Pt^{IV} to $Pt^{\bar{0}}$. Since chloroplatinic acid, the platinum salt used to prepare the supported platinum catalysts in this study, melts at 60°C (124), it is possible that the decomposing platinum salt has reacted with water during catalyst preparation to form platinum oxide, PtO_2. However, this does not explain the lower than expected hydrogen consumption which could be due to incomplete reduction of the platinum salt or oxide. However, both $Pt/MoO_3(a)$ and $Pt/WO_3(a)$ consumed more hydrogen during reduction than was theoretically predicted. For $Pt/MoO_3(a)$, the reduction peaks at 29°C and 106°C are attributed to platinum salt, or oxide reduction while those with T_{max} = 257°C and 500°C

are attributed to bronze decomposition and support reduction. The hydrogen consumption is 9.7 times the theoretically calculated amount. If we assume that the supported platinum salt or oxide is reduced from Pt^{IV} to Pt^{o}, which requires 6.8×10^{19} molecules per gram of catalyst, the difference between the theoretically calculated quantity, and the actual hydrogen consumption can be accounted for in terms of hydrogen molybdenum bronze formation. In the case of $Pt/MoO_3(a)$, the excess hydrogen corresponds to the formation of $H_{0.3}MoO_3$. This is based on the assumption that all hydrogen consumption above that required for complete reduction of the salt is used in hydrogen metal bronze formation. It is also assumed that little chemisorption of hydrogen by the supported metal has taken place under the conditions of the experiment. The composition of the bronze calculated in this way is lower than the bronze composition of $H_{0.9}MoO_3$ calculated by T.G.A. .

The reduction profile obtained for $Pt/WO_3(a)$ (Figure 5.3) shows two major reduction peaks. The peak with T_{max} = 118°C can be attributed to platinum salt or oxide reduction, while the peak with T_{max} = 385°C can be attributed to spillover leading to bronze formation and subsequent decomposition, and further reduction of the support. The hydrogen consumption is 6.8 times higher than the theoretically predicted hydrogen consumption. Assuming that this excess hydrogen is due to hydrogen tungsten bronze formation, the bronze has the composition $H_{0.3}WO_3$.

Sermon and Bond (57) found that for H_xWO_3 formed by hydrogen spillover, x had a maximum value of 0.46. These authors also found that for H_xMoO_3 formed by hydrogen spillover, x had a maximum value of 1.63. These values are higher than the values calculated from the present study.

This may be because bronze formation is incomplete in this study due to the method of reduction. During the T.P.R. procedure, the temperature is increased linearly at 5°C min^{-1}. It is, therefore, possible that during the reduction process, the hydrogen has spilled over to form a bronze with the oxide support in closest proximity to the metal. As the temperature is further increased, dehydrogenation and dehydration of the bronze may take place. Thus, not all of the oxide present can undergo bronze formation in a single reduction cycle. Indeed, there is evidence from the sub-ambient carbon monoxide chemisorption results, presented in Chapter 5, section 5.3.4, which suggests that at least for the MoO_3-supported catalysts, further reduction of the support may take place with every temperature programmed reduction/temperature programmed desorption cycle. There is also evidence to suggest that for Pt/WO_3, movement of hydrogen through WO_3 remote from Pt was slow (52).

The T.P.R. results obtained for the supported rhodium catalysts show that the catalysts prepared from rhodium chloride undergo reduction at lower temperatures than those prepared from rhodium(III) nitrate. This is contrary to the reports of Jackson (117) and Worley *et al.* (119), who suggested that catalysts prepared from rhodium nitrate were reduced more easily than those prepared from rhodium chloride.

The results presented in Table 5.1 show that the supported metal catalysts prepared from rhodium(III) nitrate all consume more hydrogen than the theoretically predicted quantity required to reduce Rh^{III} to Rh metal (1.32×10^{20} H_2 molecules per gram of catalyst). The silica supported catalyst consumed 5.2 times as much hydrogen as the theoretically calculated value. Two reduction peaks with T_{max} = 167°C

The volume of hydrogen consumed during temperature programmed reduction of $Rh/SiO_2(c)$ is approximately 1.3 times the theoretically calculated value. The T_{max} value of the single reduction peak is 120°C, which is nearly 50°C lower than the reduction peak maximum for the analogous $Rh/SiO_2(b)$. This must be a consequence of using the different metal salt precursor.

The difference in reduction temperature found for the silica-supported rhodium catalysts is also shown by the molybdenum trioxide supported catalysts, although in this case the difference in reduction peak maxima is 25°C. By comparison with the T.G.A. results, it appears that the reduction peaks with T_{max} = 106°C and 140°C for $Rh/MoO_3(c)$ can be attributed to the reduction of the rhodium salt, or oxide, whereas the peaks with T_{max} = 262°C and 500°C are probably due to bronze decomposition and support reduction. The total hydrogen consumption was 11.3 times the theoretically calculated value. Again assuming the hydrogen consumption in excess of the theoretical quantity was due to hydrogen molybdenum bronze formation, the calculated composition of the bronze is $H_{0.7}MoO_3$, which is the same as the bronze composition calculated by T.G.A..

The reduction of $Rh/WO_3(c)$ also takes place at a lower temperature than $Rh/WO_3(b)$; the temperature difference is over 50°C. The reduction peak with T_{max} = 111°C can be ascribed to reduction of the rhodium salt, or oxide, whereas the peaks with T_{max} = 385°C and 500°C are ascribed to support reduction and bronze decomposition. The hydrogen consumption during reduction is 4.5 times the theoretically

and 250°C can be observed. These must be attributed to the reduction of rhodium(III) (either nitrate or oxide) to rhodium metal. The higher than expected value of hydrogen consumption may be due to some dehydration of the silica support as the temperature is increased. Alternatively, hydrogen may have spilled over on to the silica support. This is supported by the findings of Altham and Webb (66), who found that there was significant hydrogen migration between the metal and the silica support.

The results obtained for $Rh/MoO_3(b)$ show that the hydrogen consumption is approximately 5.1 times the theoretically calculated figure. The peaks with T_{max} = 24°C and 164°C can be attributed to Rh^{3+} reduction to rhodium metal. The higher temperature reduction peaks, with T_{max} = 269°C and 584°C may be due to bronze decomposition and support reduction. It can be calculated that, assuming the excess hydrogen consumption above that required for metal salt, or oxide, reduction, is attributable to hydrogen molybdenum bronze formation, the bronze has the composition $H_{0.3}MoO_3$.

For $Rh/WO_3(b)$, the reduction peak with T_{max} = 158°C must be attributable to metal salt, or oxide reduction, whereas, by comparison with T.G.A. results, the peak with T_{max} = 406°C may be due to support reduction. Again, the hydrogen consumption during T.P.R. exceeds the theoretically predicted quantity. The actual hydrogen consumption is 8.3 times the theoretically predicted quantity. A hydrogen tungsten bronze composition of $H_{0.7}WO_3$ is calculated, which is higher than the highest value predicted by Sermon and Bond (57), which was 0.46.

predicted value. This leads to a calculated hydrogen tungsten bronze composition of $H_{0.36}WO_3$.

The differences in reduction temperature between rhodium chloride and rhodium nitrate derived catalysts are most likely due to differences in the salts themselves. Thermo-gravimetric analysis has shown that rhodium chloride reacts to form rhodium oxide, Rh_2O_3, before being reduced to rhodium metal. As noted earlier, Jackson (117) also claimed that rhodium chloride reacted with supports such as silica to form oxy-chlorides, which were found to be difficult to reduce, and often the rhodium retained a positive charge even after reduction up to 773K. However, Jackson (117) found that if the supported salt was calcined, resulting in the formation of rhodium oxide, reduction led to the formation of rhodium metal.

It is possible that the rhodium chloride reacts to form supported rhodium oxide during catalyst preparation, which could lead to a lowering of the reduction temperature compared with the reduction temperature of rhodium chloride itself, or rhodium nitrate. If the supported rhodium chloride reacted more easily than the supported rhodium nitrate to form rhodium oxide, this could explain why the rhodium chloride derived catalysts undergo reduction at lower temperatures than the rhodium nitrate derived catalysts.

6.2 Carbon Monoxide Chemisorption

The carbon monoxide chemisorption results presented in Table 5.3 were obtained using pulsed flow carbon monoxide chemisorption. Consequently, the quantity of carbon monoxide calculated to be adsorbed on each catalyst represents only irreversibly bound carbon monoxide, since the reversibly bound fraction of carbon monoxide would be removed by the helium carrier gas, which has the same effect as evacuation. [^{14}C] radiotracer studies show that evacuation removed up to ca. 33% of the carbon monoxide from supported platinum catalysts (125) and ca. 25% of the carbon monoxide from supported rhodium catalysts (126). The dispersion results presented in Table 6.1 have, therefore, been calculated by assuming that the monolayer coverage of carbon monoxide is given by:

$$(n_{CO})_{TOTAL} = (n_{CO})_{IRREV} + (n_{CO})_{REV}$$

(where $(n_{CO})_{REV} = x(n_{CO})_{TOTAL}$, with x = 0.33 (Pt) and 0.25 (Rh)). It is also assumed that the $CO_{ads}:M_{surface}$ ratio is one in each case, although this may not be absolutely valid, particularly for rhodium (119).

The dispersion figures show that for the supported platinum catalysts, the molybdenum trioxide-supported catalyst has the poorest dispersion, whereas the dispersions for the tungsten trioxide- and silica-supported catalysts are much higher, and comparable at ca. 40%. The molybdenum trioxide-supported rhodium catalysts are also poorly dispersed which must be a reflection of the low surface area of the molybdenum trioxide (ca. 5 $m^2 g^{-1}$). However, a similar reason cannot be advanced

Table 6.1. Catalyst Dispersion Figures Calculated from Reversibly and Irreversibly Bound Carbon Monoxide

Catalyst	$(n_{CO})_{IRREV}$ (molecules(g.catalyst)$^{-1}$)	$(n_{CO})_{TOTAL}$ (molecules(g.catalyst)$^{-1}$	Dispersion Based on $(n_{CO})_{TOTAL}$ (%)
Pt/SiO_2(a)	8.69×10^{18}	1.30×10^{19}	38.2
Pt/MoO_3(a)	2.50×10^{17}	3.75×10^{17}	1.1
Pt/WO_3(a)	9.23×10^{18}	1.38×10^{19}	40.6
Rh/SiO_2(b)	1.40×10^{19}	1.87×10^{19}	21.3
Rh/MoO_3(b)	-	-	-
Rh/WO_3(b)	6.61×10^{18}	8.81×10^{18}	10.0
Rh/SiO_2(c)	4.17×10^{18}	5.56×10^{18}	6.3
Rh/MoO_3(c)	2.14×10^{18}	2.85×10^{18}	3.2
Rh/WO_3(c)	2.76×10^{19}	3.68×10^{19}	41.9

to explain why $Rh/SiO_2(c)$ has only a 6.3% dispersion. One possibility is that excess chloride present reacts with the support to form $SiCl_4$, which can then migrate and decompose to form SiO_2 on the metal, leading to encapsulation of the metal (127). This would lead to a reduction in the available metal surface for CO chemisorption. By comparison, $Rh/SiO_2(b)$ has a dispersion of 21.3%, which highlights the detrimental effect on dispersion observed in the case of $Rh/SiO_2(c)$ which occurs when a chloride-containing metal salt is used during catalyst preparation.

$Rh/WO_3(c)$ has a dispersion of 41.9%, which shows that the dispersion is a reflection not only of the metal salt precursor but of the support itself. It has been postulated above that the presence of Cl^- has an adverse effect on the dispersion of silica-supported rhodium prepared from rhodium(III) chloride. However, in the case of $Rh/WO_3(c)$, if anything, an enhanced dispersion has been observed, since if the dispersion only depended on the surface area of the support, it would be expected that the molybdenum trioxide- and tungsten trioxide-supported catalysts would have comparable, relatively low dispersions, reflecting their low surface areas of ca. 5 $m^2\ g^{-1}$, compared with the high surface area silica (250 $m^2\ g^{-1}$) which should enable highly dispersed catalysts to be prepared. The enhanced dispersion observed for $Rh/WO_3(c)$ may be the result of an interaction between the metal salt and the support. It is possible that the tungsten trioxide support may be able to stabilise any excess chloride ions which remain after reduction. This may also lead to a stabilisation of the metal particles in a highly dispersed manner. The dispersion of $Rh/WO_3(c)$ is just over four times the dispersion calculated for $Rh/WO_3(b)$. This again suggests that Cl^- interacts

with the WO_3 support in the case of $Rh/WO_3(c)$, leading to enhanced dispersion. The lower dispersion of $Rh/WO_3(b)$ may simply be a reflection of the low surface area of the tungsten trioxide support. Although the dispersion calculated for $Rh/SiO_2(b)$ is fairly low at 21.3%, it is higher than the 10.0% dispersion obtained for $Rh/WO_3(b)$, reflecting the higher surface area of silica compared with tungsten trioxide.

No carbon monoxide chemisorption could be observed for $Rh/MoO_3(b)$, indicating that it was either incompletely reduced, very poorly dispersed, or perhaps the reduced molybdenum oxide had migrated to cover the rhodium metal. If the rhodium retains a net positive charge on reduction, there is evidence to suggest that when carbon monoxide chemisorption is carried out, the resultant M^{n+}-CO bond strength is weaker than that found between completely reduced metal and CO (117). However, it may be that in this case only reversibly bound CO is formed, and therefore, it would not be seen in the flow measurements made in the present study.

During hydrogen molybdenum bronze formation there is a tendency for the MoO_3 to be cleaved along its c crystallographic axis (79). This leads to an increase in surface area, and a decrease in contact between the supported metal particles and the support. These authors (79) also observed that the platinum particles tended to form large clusters as a result of the structural changes taking place. The increase in particle size and the decrease in contact between the metal and the support leads to a decrease in dispersion. This could explain why $Pt/MoO_3(a)$ and $Rh/MoO_3(c)$ have such poor dispersions.

The particle sizes obtained by transmission electron microscopy show that, as discussed below, the metal particle sizes are actually much smaller than the CO chemisorption results suggest. Figures 6.1 to 6.3 show the particle size distributions for the catalysts prepared from chloroplatinic acid, rhodium(III) nitrate and rhodium(III) chloride respectively. For each catalyst, the distribution is quite broad, with the narrowest distribution and smallest particles being found for the silica supported catalysts. Larger particles were found with the molybdenum trioxide and tungsten trioxide supports.

Table 6.2 shows a comparison of the average particle sizes calculated from carbon monoxide chemisorption (irreversibly bound CO only) with the particle sizes corrected to include the reversibly as well as the irreversibly bound CO, and with the particle sizes obtained by transmission electron microscopy. The calculation of the particle sizes from CO chemisorption figures is described in Chapter 5, section 5.3.1.

The particle sizes calculated from carbon monoxide chemisorption are, by comparison with the electron microscopic values, rather high, indicating that carbon monoxide chemisorption is a poor predictor of particle sizes. Possible reasons for this include site-blocking of the supported metal which occurs as a result of support migration. It is also possible that Cl^- not removed during metal salt reduction could poison the surface for CO chemisorption, as could support O^{2-}. Another possible reason for the inaccuracy of the figures is the assumption that the metal to CO ratio is one to one. There is evidence to show that carbon monoxide can bond to rhodium as linear, bridging or digeminal species (119):

Fig. 6·1 Particle Size Distribution: Supported Platinum Catalysts

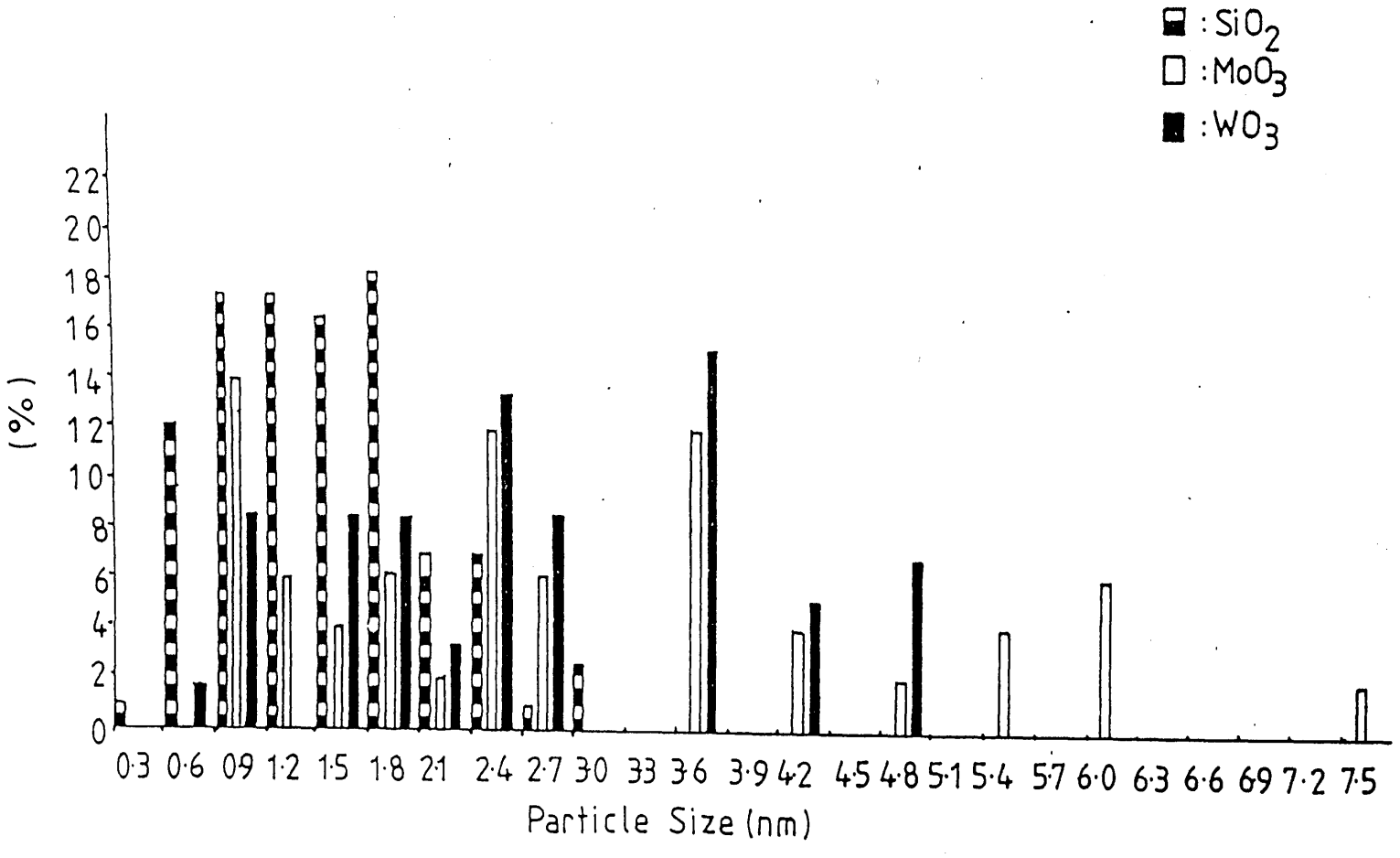

Fig. 6·2 Particle Size Distribution: Supported Rhodium Catalysts Prepared From $Rh(NO_3)_3$

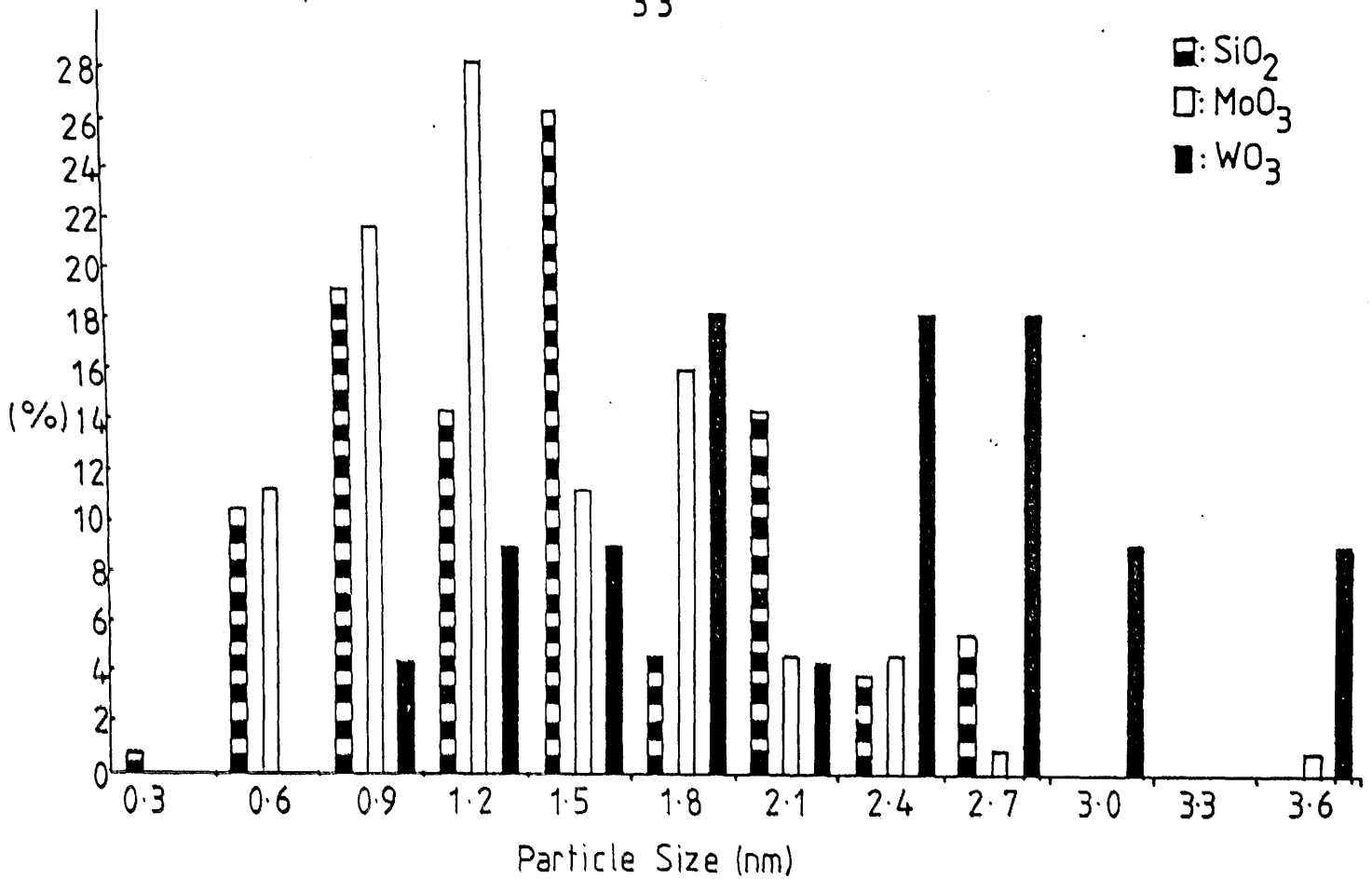

Fig. 6·3 Particle Size Distribution : Supported Rhodium Catalysts Prepared From $RhCl_3$

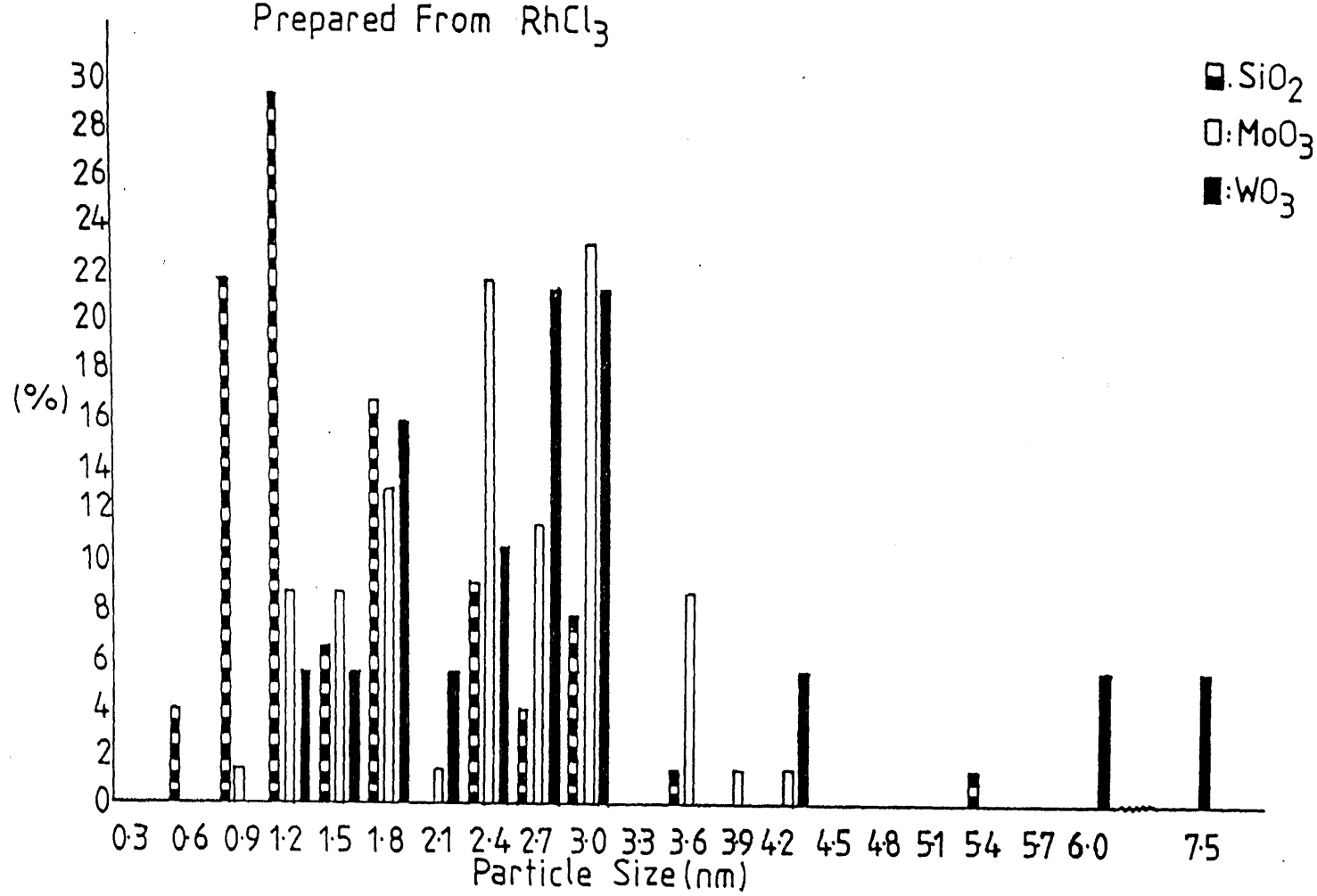

Table 6.2. Comparison of Particle Sizes

Catalyst	Particle Sizes Calculated from $(n_{CO})_{IRREV}$ (nm)	Particle Sizes Calculated from $(n_{CO})_{TOTAL}$ (nm)	Average Particle Sizes Obtained by T.E.M. (nm)
Pt/SiO_2(a)	210	141	1.4
Pt/MoO_3(a)	7400	4890	2.7
Pt/WO_3(a)	198	133	2.7
Rh/SiO_2(b)	310	231	1.7
Rh/MoO_3(b)	-	-	-
Rh/WO_3(b)	650	490	2.2
Rh/SiO_2(c)	1000	776	1.6
Rh/MoO_3(c)	2000	1516	2.4
Rh/WO_3(c)	160	117	2.9

Linear

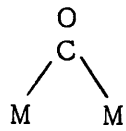

Bridging

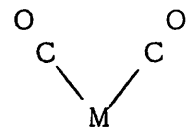

Digeminal

The bonding of carbon monoxide to platinum is mainly linear, with some digeminal and a small amount of bridging species (128). It would, therefore, be expected that better agreement should be obtained between the particle sizes calculated by CO chemisorption and those obtained by transmission electron microscopy for platinum than for rhodium. However, the results presented in Table 6.2 show that the particle sizes calculated from CO chemisorption are no more accurate for the supported platinum catalysts than they are for the supported rhodium catalysts.

When temperature programmed desorption experiments were carried out immediately after carbon monoxide chemisorption, various species, namely carbon monoxide, carbon dioxide, hydrogen and water, were observed to desorb, depending on the catalyst. Table 6.3 summarises the species which were observed to desorb, and the temperatures at the peak maxima at which they desorbed.

The desorption of hydrogen from $Pt/SiO_2(a)$ may indicate that dehydration or dehydroxylation of the silica is taking place. The absence of carbon monoxide in the gas phase may be an indication that the carbon monoxide was bonded fairly weakly to the platinum, and may have been desorbed during the initial sweep out of the catalyst reaction system with the helium carrier gas at room temperature. This is supported by the observation that T.P.D. following sub-ambient carbon monoxide chemisorption shows evidence for desorption maxima below 0°C.

Table 6.3. T.P.D. Following CO Chemisorption

Catalyst	Desorbing Species	$T_{max(des)}$ (°C)
$Pt/SiO_2(a)$	H_2	358
$Pt/MoO_3(a)$	CO	251
	CO_2	426
$Pt/WO_3(a)$	CO	140
	CO_2	303
$Rh/SiO_2(b)$	CO	90
	CO_2	350
$Rh/MoO_3(b)$	H_2	471
$Rh/WO_3(b)$	none	-
$Rh/SiO_2(c)$	CO_2	114
	CO_2	361
$Rh/MoO_3(c)$	H_2	250
	H_2O	500
$Rh/WO_3(c)$	CO	295
	CO_2	295

Carbon monoxide desorbed from $Pt/MoO_3(a)$ at 251°C, followed by carbon dioxide desorption at 426°C. The formation of carbon dioxide could have arisen from:

(a) The Boudouard reaction:

$$2CO \longrightarrow C + CO_2 \quad ,$$

(b) by reaction of carbon monoxide with any oxygen present as a contaminant, for example in the carrier gas, or

(c) the water-gas shift reaction:

$$CO + H_2O \rightleftharpoons CO_2 + H_2$$

which involves water from the support. It is notable in this context that water is produced during hydrogen molybdenum bronze decomposition.

Carbon monoxide desorption from $Pt/WO_3(a)$ at 140°C is followed by carbon dioxide desorption at 303°C. The carbon dioxide is formed by one of the routes suggested above.

Similar results were obtained for $Rh/SiO_2(b)$ and $Rh/SiO_2(c)$ with respect to the temperatures at which desorption peaks were observed. However, whereas carbon monoxide was desorbed from $Rh/SiO_2(b)$ at 90°C, carbon dioxide was the product of desorption at 114°C from $Rh/SiO_2(c)$. Carbon dioxide desorption peaks were also observed with $Rh/SiO_2(b)$ and Rh/SiO_2 (c) at 350°C and 361°C, respectively. The results obtained with $Rh/SiO_2(c)$ imply that either this catalyst was incompletely reduced, that is the surface was contaminated with surface oxygen, or that the presence of surface chlorine following reduction

effectively promotes the Boudouard reaction at low temperature. However, from the present study it is not possible to distinguish between these possibilities.

Hydrogen was observed to desorb from $Rh/MoO_3(b)$ at 471°C. This can be compared with the desorption of hydrogen at 250°C and water at 500°C from $Rh/MoO_3(c)$. Desorption of hydrogen and water from these catalysts can be considered as being due to decomposition of the hydrogen molybdenum bronze. The absence of carbon monoxide, or even carbon dioxide, may be a consequence of the low carbon monoxide coverage obtained during chemisorption.

Carbon monoxide desorption from $Rh/WO_3(c)$ was observed at 130°C, with carbon dioxide desorption occurring at ca. 295°C. These temperatures are close to the desorption temperatures found for both $Rh/SiO_2(b)$ and $Rh/SiO_2(c)$, although it must be noted that carbon dioxide desorbed from $Rh/SiO_2(c)$ at the lower desorption temperature, whereas carbon monoxide desorbed from both $Rh/SiO_2(b)$ and $Rh/WO_3(c)$ at similar temperatures. The similarity in desorption temperatures for $Rh/SiO_2(b)$, $Rh/SiO_2(c)$ and $Rh/WO_3(c)$ indicates that the strength of adsorption of carbon monoxide on rhodium is not significantly affected by the use of a different support, or a different metal salt precursor, in these particular cases.

In a recent study (129) it has been found that the heat of adsorption of carbon monoxide was approximately constant for a variety of different supported rhodium catalysts. The heat of adsorption of carbon monoxide on Rh/SiO_2 was -92.49 kJ mol^{-1}. On Rh/MoO_3, it was -99.77 kJ mol^{-1}. Both catalysts were prepared from rhodium chloride.

Table 6.4 shows the activation energy of desorption calculated for the desorption temperatures for the supported platinum and rhodium catalysts in this study. The Redhead equation (130):

$$\frac{E}{RT_{max}^2} = \frac{A}{\beta} e^{-E/RT_{max}}$$

where E is the activation energy of desorption, β is the heating rate and T_{max} is the temperature at the desorption peak maximum, can be used to calculate the activation energy of desorption.

A useful crude approximation to the desorption activation energy is:

$$E = T_{max} \times 0.294 \quad (131)$$

where T_{max} is the temperature in Kelvin, and E is in kJ mol^{-1}. Using this approximation, the activation energy of desorption values presented in Table 6.4 were calculated.

It can be seen that the activation energy of desorption figures calculated for the lower of the two desorption peak maxima temperatures for Rh/SiO_2(b), Rh/SiO_2(c) and Rh/WO_3(c) are similar in value to the ΔH_{ads} figures obtained by Green and Webb (129).

By carrying out temperature programmed desorption experiments immediately after temperature programmed reduction using the molybdenum trioxide-supported catalysts, it was confirmed that the appearance of hydrogen and water in the gas phase during T.P.D. after carbon monoxide chemisorption was due to the desorption of

Table 6.4. Heats of Desorption

Catalyst	Desorbing Species	Temperature (K)	Activation Energy of Desorption (kJ mol^{-1})
Pt/MoO_3(a)	CO	524	154
	CO_2	699	206
Pt/WO_3(a)	CO	413	121
	CO_2	576	169
Rh/SiO_2(b)	CO	363	107
	CO_2	623	183
Rh/SiO_2(c)	CO_2	387	114
	CO_2	634	186
Rh/WO_3(c)	CO	403	118
	CO_2	568	167

hydrogen and water produced during the dehydrogenation and dehydration of the hydrogen metal bronzes. For example, hydrogen desorbed from freshly reduced $Pt/MoO_3(a)$ at 305°C, compared with 250°C from $Pt/MoO_3(a)$ on which carbon monoxide chemisorption had been carried out. Hydrogen desorbed at 239°C from freshly reduced $Rh/MoO_3(b)$, compared with 471°C from $Rh/MoO_3(b)$ on which carbon monoxide chemisorption had been carried out. The temperature difference of approximately 200°C could be due to the presence of carbon monoxide on the rhodium surface. Jackson (132) has shown that deuterium exchange with the bronze hydrogen will not take place if carbon monoxide has been chemisorbed on to the supported metal, whereas deuterium exchange will take place in the absence of carbon monoxide. The 200°C difference in desorption temperature for hydrogen from $Rh/MoO_3(b)$ is consistent with a site-blocking effect in which the metal sites are blocked, preventing reverse spillover from the hydrogen molybdenum bronze. It is not known whether the sites are blocked by carbon monoxide or by reduced support species which have migrated to partially cover the rhodium particles.

Because of the relatively low quantity of carbon monoxide adsorbed at ambient temperature, it was decided to carry out carbon monoxide chemisorption experiments at temperatures between -78°C and -196°C. These results are presented in Table 5.6 in Chapter 5.

Carbon monoxide chemisorption carried out on $Pt/SiO_2(a)$ gave an area of 2.22 m^2 $(g.catalyst)^{-1}$. The number of CO molecules adsorbed was 1.32×10^{19}, which corresponds to approximately 39% of the platinum atoms present, assuming a 1:1 Pt:CO ratio. At -196°C,

1.14×10^{21} molecules of CO were adsorbed by the catalyst, corresponding to an area of 191.52 m^2 $(g.catalyst)^{-1}$. The number of CO molecules is greater than the total number of platinum atoms present in the sample, indicating that some carbon monoxide has been adsorbed by the support.

With $Pt/MoO_3(a)$ at -78°C, the amount of CO adsorbed corresponds to a ratio of CO:Pt of greater than unity, indicating that some carbon monoxide was adsorbed on the support. A proportion of the carbon monoxide may have been adsorbed on sites formed by the partial reduction of the molybdenum oxide during catalyst reduction/activation. As the temperature is further decreased towards -196°C, the proportion of carbon monoxide which is adsorbed on the support increases.

Since the proportion of carbon monoxide in helium was less than 10% during each experiment, it is highly unlikely that physical adsorption of carbon monoxide on the catalyst has taken place.

On $Pt/WO_3(a)$, the ratio of CO:Pt is approximately 1:10 at -78°C. This increases to 0.98:1 CO:Pt at -196°C. In this case, the increase may be attributed to greater coverage of the platinum by carbon monoxide at lower temperatures. However, the possibility that some of the carbon monoxide may have been adsorbed by the tungsten trioxide support cannot be discounted.

With $Rh/MoO_3(c)$, the extent of carbon monoxide adsorption is consistent with almost 93% of the available rhodium chemisorbing one carbon monoxide molecule. However, as with $Pt/MoO_3(a)$, it is likely that some of the carbon monoxide has been adsorbed on to the support at this low temperature. At -70°C, it appears that the amount of carbon

monoxide chemisorbed corresponds to a CO:Rh ratio of 1.1:1, which is higher than the ratio found at -196°C. However, since the chemisorption study at -196°C was carried out first, followed by a T.P.R./T.P.D. cycle before carrying out the chemisorption study at -70°C, it is likely that a greater proportion of the molybdenum trioxide support had undergone reduction by the time the latter experiment had been carried out, and, therefore, adsorption on the support is considered to account for the increase in the amount of carbon monoxide adsorbed.

From the results obtained for low temperature adsorption of carbon monoxide on both platinum and rhodium catalysts, it would appear that the carbon monoxide has chemisorbed on to a higher proportion of the total number of supported metal atoms than at ambient temperature. However, as noted above, it is likely that the sub-ambient chemisorption is complicated by the carbon monoxide chemisorbing on the partially reduced support. As yet, we have no means of distinguishing between carbon monoxide adsorbed on the metal and carbon monoxide adsorbed on the support at such low temperatures.

6.3 Nitrogen N.E.T. Areas

The nitrogen B.E.T. areas of four catalysts, $Pt/SiO_2(a)$, $Pt/MoO_3(a)$, $Pt/WO_3(a)$ and $Rh/MoO_3(c)$ were measured both before and after the catalyst had been reduced. With $Pt/SiO_2(a)$ and $Pt/WO_3(a)$, there is little difference in the total surface areas found before or after reduction. $Pt/SiO_2(a)$ shows a slight increase in area after reduction and $Pt/WO_3(a)$ shows a slight decrease in area after reduction. However,

the results obtained for $Pt/MoO_3(a)$ indicate that the surface area has increased from 2.15 $m^2 g^{-1}$ to 82.9 $m^2 g^{-1}$. Similarly, for $Rh/MoO_3(c)$, the pre-reduction surface area of 2.4 $m^2 g^{-1}$ increases to 87.5 $m^2 g^{-1}$ after reduction. In both cases this must be a result of the partial reduction of the molybdenum trioxide support. Reduction of molybdenum trioxide to molybdenum dioxide, for example, results in a change in structure from distorted ReO_3 (72) to rutile (133), which has a more open structure.

During the formation of hydrogen metal bronzes by hydrogen spillover, the surface area of the molybdenum trioxide can increase by a factor of two or three (68). Decomposition of hydrogen metal bronzes by either thermal or vacuum treatment leads to reduction of the molybdenum trioxide to a lower oxide (79) and this reduction is accompanied by some structural modifications which must be responsible for the large increase in total surface area, found for both $Pt/MoO_3(a)$ and $Rh/MoO_3(c)$.

6.4 Temperature Programmed Reaction Studies

Carbon monoxide hydrogenation was carried out as a temperature programmed reaction over $Pt/SiO_2(a)$, $Pt/MoO_3(a)$, $Pt/WO_3(a)$ and $Rh/MoO_3(c)$. The eluant gas was monitored for the presence of methane, carbon dioxide and water.

Over the temperature range ambient to 400°C, no reaction was observed over $Pt/SiO_2(a)$. However, over $Pt/MoO_3(a)$, $Pt/WO_3(a)$ and $Rh/MoO_3(c)$, reaction did take place, as shown by the temperature programmed reaction profiles reproduced in Figures 5.29, 5.30 and 5.31, respectively.

These show that the increasing order of activity for these catalysts is:

$$Pt/SiO_2(a) \ll Pt/WO_3(a) < Pt/MoO_3(a) < Rh/MoO_3(c)$$

The reaction products which are observed to form over $Pt/MoO_3(a)$, $Pt/WO_3(a)$ and $Rh/MoO_3(c)$ are consistent with a model in which methane production occurs by the reaction:

$$CO + 3H_2 \longrightarrow CH_4 + H_2O \quad ,$$

which is accompanied by the water-gas shift reaction:

$$CO + H_2O \rightleftharpoons CO_2 + H_2 \quad ,$$

An alternative proposal which involves

$$CO + H_2O \rightleftharpoons CO_2 + H_2$$

followed by

$$CO_2 + 4H_2 \longrightarrow CH_4 + 2H_2O$$

can be ruled out because carbon dioxide will not undergo hydrogenation in the presence of carbon monoxide (100).

The reaction profile obtained for the reaction of carbon monoxide with hydrogen over $Rh/MoO_3(c)$ (Figure 5.31) shows a maximum in

carbon dioxide at 208°C. The rate of carbon dioxide formation then decreases with increasing temperature as the water-gas shift reaction:

$$CO + H_2O \longrightarrow CO_2 + H_2$$

becomes less feasible.

The results obtained for the hydrogenation of carbon monoxide over these four catalysts support the work of Jackson et al. (84), who investigated the hydrogenation of carbon monoxide over iron, nickel, ruthenium, rhodium and palladium supported on molybdenum trioxide and tungsten trioxide. With the exception of iron, the activity of these metals was enhanced by up to two orders of magnitude when molybdenum trioxide or tungsten trioxide was used as a support, rather than silica. The activity enhancement was attributed to the fast spillover/reverse spillover of hydrogen which can occur between molybdenum trioxide and tungsten trioxide and the supported metal. This increases the concentration of adsorbed hydrogen which can react with the adsorbed carbon monoxide, facilitating the carbon monoxide hydrogenation reaction (84).

The temperature programmed reaction results presented in Chapter 5 would seem to indicate that fast hydrogen spillover/reverse spillover occurs most easily between rhodium and molybdenum trioxide. The rate and extent of hydrogen spillover/reverse spillover seems to be faster between platinum and molybdenum trioxide than between platinum and tungsten trioxide. The higher activity of $Rh/MoO_3(c)$ compared with $Pt/MoO_3(a)$ results from the fact that rhodium is a more active catalyst for carbon monoxide hydrogenation than platinum (103, 104).

Indeed, since platinum is a notoriously poor catalyst for the methanation reaction (100) it was somewhat surprising to observe any reaction at all over $Pt/MoO_3(a)$ and $Pt/WO_3(a)$. The fact that no reaction was observed over $Pt/SiO_2(a)$ strongly supports the view that, with molybdenum trioxide and tungsten trioxide as catalyst supports, there is an interaction between the metal and the support which results in the platinum and the rhodium possessing a significantly enhanced activity for methanation, not present when more conventional support oxides are used.

6.5 Buta-1,3-diene Hydrogenation Studies

Buta-1,3-diene hydrogenation studies were carried out using the various supported platinum and rhodium catalysts to examine the effects, if any, of changing either the support, or in the case of the supported rhodium catalysts, the metal salt precursor. The results of these studies are presented in Chapter 5, section 5.6.

Table 6.5 summarises the initial butene distributions and selectivities obtained by extrapolating the graphs showing the variation of butene distribution and selectivity with reaction extent to 0% conversion. It can be seen that the highest selectivity obtained for any of the catalysts was found for $Rh/MoO_3(b)$ which showed an initial selectivity of 0.945 for butene formation at 0% conversion.

Previous work using radio-tracers to follow the hydrogenation of acetylene to ethylene and ethane has shown that the selectivity is determined by the relative amounts of the competitive reactions:

Table 6.5. Summary Table of Buta-1,3-diene Hydrogenation: Variation of Product Distribution and Selectivity with Reaction Extent, Extrapolated to 0% Conversion.

	Initial Butene Distribution (%)			
Catalyst	1-B	t-2-B	C-2-B	S
Pt/SiO_2(a)	71.0	22.0	7.0	0.705
Pt/MoO_3(a)	55.5	27.5	17.0	0.85
Pt/WO_3(a)	84.5	14.5	1.0	0.61
Rh/SiO_2(b)	61.5	22.0	11.5	0.895
Rh/MoO_3(b)	54.0	33.0	13.0	0.945
Rh/WO_3(b)	60.0	28.5	11.5	0.89
Rh/SiO_2(c)	60.5	24.0	15.5	0.78
Rh/MoO_3(c)	58.3	29.2	12.5	0.746

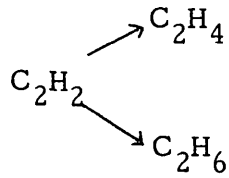

With $^{12}C_2H_2$ as the initial reactant and $^{14}C_2H_4$ introduced as an intermediate, it was found that very little $^{14}C_2H_6$ was formed. This was the case regardless of the metal used and hence of the actual value of the selectivity. Similarly, ^{13}C-isotope labelling experiments have also shown that with platinum and palladium catalysts, the reactions to form the n-butenes or n-butane from buta-1,3-diene are also competitive. However, these experiments also showed that during the first stage of the reaction on platinum, but-1-ene could isomerise to but-2-ene (cis or trans) or could be hydrogenated to n-butane (135).

In the reactions studied in the present work, n-butane was always present as an initial product, even at the very earliest stages of the reaction between buta-1,3-diene and hydrogen. These results are, therefore, consistent with the ^{13}C- and ^{14}C-isotopic labelling studies discussed above. The results presented in this study are consistent with the formation of n-butane directly by hydrogenation of buta-1,3-diene as well as by the subsequent hydrogenation of but-1-ene or but-2-ene, which are formed as intermediate products. But-2-ene can be formed by either isomerisation of but-1-ene or directly by 1,4-addition of hydrogen to adsorbed buta-1,3-diene. The decreasing 1-B:2-B ratio with increasing reaction extent is consistent with the 1-B to 2-B isomerisation mechanism, although some but-2-ene is formed directly by hydrogenation of buta-1,3-diene. The overall reaction scheme can thus

be represented as:

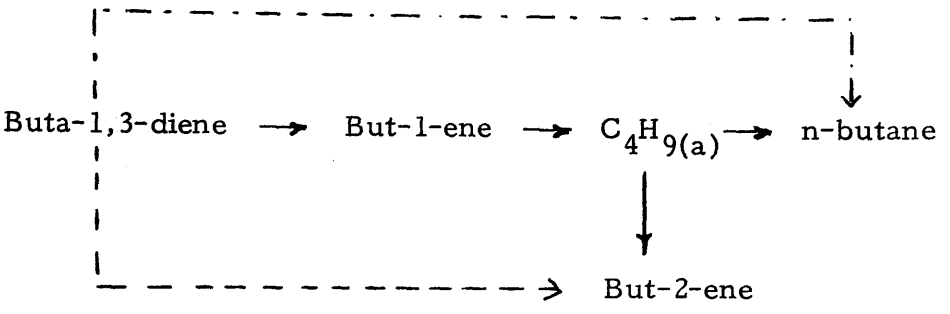

For the supported platinum catalysts, selectivity decreases in the order:

$$Pt/MoO_3(a) > Pt/SiO_2(a) > Pt/WO_3(a).$$

The low trans to cis ratios determined for the supported platinum catalysts suggest that Mechanism A, as proposed by Wells et al. (95) is operative.

For the supported rhodium catalysts prepared from rhodium(III) nitrate, the selectivity is found to decrease in the order:

$$Rh/MoO_3(b) > Rh/SiO_2(b) > Rh/WO_3(b)$$

This was the same order as was found for the supported platinum catalysts which suggests that the support can influence the selectivity of the metal. The results obtained, which show a low trans to cis ratio, are again consistent with Mechanism A (95) being followed. However, since Mechanism A does not allow for the formation of n-butane as an initial product, an additional mechanism for n-butane formation directly from

adsorbed buta-1,3-diene must also be considered. The following sequence of reactions are proposed:

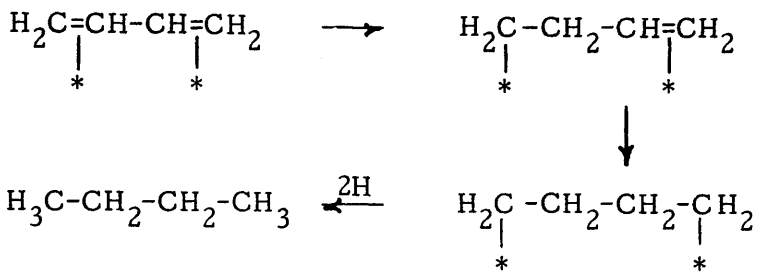

The results obtained for the supported rhodium catalysts prepared from rhodium(III) chloride show a different order of decreasing selectivity than that obtained for the rhodium(III) nitrate derived catalysts, namely:

$$Rh/SiO_2(c) \; > \; Rh/MoO_3(c) \; > \; Rh/WO_3(c).$$

The difference in the order of selectivity must be a reflection of the change in the metal salt precursor.

The differences observed in selectivity by changing the support may be related to the differences in dispersion as determined by carbon monoxide chemisorption. For the supported platinum catalysts, the decreasing order of dispersion is:

$$Pt/WO_3(a) \; > \; Pt/SiO_2(a) \; > \; Pt/MoO_3(a).$$

which would suggest that the most highly selective catalyst has the lowest dispersion. However, the same argument does not hold for the supported

rhodium catalysts derived from rhodium nitrate, which show that $Rh/SiO_2(b)$ has a higher dispersion than $Rh/WO_3(b)$. The supported rhodium catalysts prepared from rhodium chloride show a decreasing order of dispersion of:

$$Rh/WO_3(c) > Rh/SiO_2(c) > Rh/MoO_3(c)$$

Overall, the results obtained in the present work strongly suggest that selectivity is dependent upon the support, the metal and, for a given metal, the precursor salt.

There is considerable evidence that spillover hydrogen present in hydrogen metal bronzes can undergo a reverse spillover process, where it can then react with a hydrogen acceptor such as ethylene (79, 80, 83). It is generally accepted that as the surface concentration of hydrogen increases, selectivity decreases. Since the molybdenum trioxide-supported catalysts are the most highly selective, it would appear that bronze hydrogen is not involved in the hydrogenation of buta-1,3-diene. If bronze hydrogen were involved, the increase in the available hydrogen concentration would lead to a decrease in selectivity. Following the findings of Fripiat et al. (79), and in agreement with the present results, bronze hydrogen is not expected to be consumed until all the gas phase hydrogen has been consumed. In the present study, excess gaseous hydrogen was present at all times and thus any effect of bronze hydrogen would be difficult to observe.

It has been proposed that the rate of hydrogenation of ethylene and other hydrogen acceptors is a measure of the rate of reverse spill-

over (55). The rate depends on the hydrogen spillover concentration, its stability and the degree of contact between the metal and the support. The present results have shown that the molybdenum trioxide-supported catalysts are poorly dispersed, with large metal particles and consequent poor contact between the metal and the support which, therefore, leads to poor reverse spillover. However, the situation may be different with the tungsten trioxide-supported catalysts which are the least selective of the catalysts studied. It is, therefore, proposed that with the tungsten trioxide-supported catalysts, reverse spillover of hydrogen from the hydrogen tungsten bronze takes place and that the spillover hydrogen can react with buta-1,3-diene. This is in keeping with the observations of Sermon and Bond (57), who found that the reactivities of hydrogen molybdenum bronze, $H_{1.6}MoO_3$, and hydrogen tungsten bronze, $H_{0.5}WO_3$, were different in that it was more difficult to remove hydrogen from $Pt/H_{1.6}MoO_3$ than from $Pt/H_{0.5}WO_3$ by reverse spillover using oxygen or other hydrogen acceptors.

The initial butene distributions presented in Table 6.5 show that the yield of but-1-ene is greater than the yield of the but-2-enes. The results presented in Tables 5.8a to 5.8i show that as the reaction extent increases, the 1-B/2-B ratio decreases, although the t-2-B to c-2-B ratio remains approximately constant, indicating that the but-1-ene is isomerised to but-2-ene.

Kinetic studies were carried out to determine the order of reaction with respect to the reactants. However, the order of reaction with respect to both hydrogen and buta-1,3-diene was found to vary considerably with catalyst usage and, in consequence, accurate

values proved difficult to obtain. However, overall, positive reaction orders were obtained for hydrogen and negative orders were found for buta-1,3-diene for each of the nine catalysts. This indicates that, as expected, buta-1,3-diene is the more strongly adsorbed reactant.

A comparison between the activation energy values obtained on freshly reduced and used catalysts, as shown in Table 5.11, indicates that both Pt/MoO_3(a) and Rh/MoO_3(c), when freshly reduced, give a very high activation energy value. However, these values decreased by about 50 kJ mol^{-1} when the activation energy was determined over a well-used catalyst. This suggests that during the initial reactions carried out on the catalyst, a change in the catalyst is taking place. There is evidence (136) to suggest that such changes may involve the build-up of carbonaceous overlayers. Although, in general, this process is simply a deactivating process, it appears that, in the case of the molybdenum trioxide-supported catalysts, other changes may also occur. The decrease in activation energy to the more typical levels shown by the other catalysts may indicate a change in the rate determining step for the molybdenum trioxide-supported catalysts during the initial running in phase.

The variation of the butene distribution and selectivity with temperature was examined over each catalyst. Because of the difficulties involved in obtaining measurable reaction rates, it was not possible to obtain overlap in terms of temperature or reaction extent which would have enabled better comparisons to be made. However, certain trends are evident in the results presented in Tables 5.10a to 5.10i. In general, it can be concluded that, as the temperature is

increased, the but-1-ene yield decreases and both the trans- and cis-but-2-ene yields increase. The selectivity increased as the temperature is increased, in agreement with previous studies (137), provided the reaction did not become diffusion controlled, in which case the selectivity fell drastically to very low levels. The results obtained suggest that, with increasing temperature, the reaction pathway to butene formation becomes more favourable than that to butane or, alternatively, that the concentration of adsorbed hydrogen decreases as the temperature is increased.

Pressure fall versus time curves have been examined for each of the nine catalysts studied. For all catalysts studied except $Pt/MoO_3(a)$ and $Rh/SiO_2(c)$, acceleration points could be found, at least during the initial reactions carried out over freshly reduced catalyst samples. The data obtained from the pressure fall versus time curves is summarised in Table 6.6. Induction periods were observed for freshly reduced samples of $Rh/WO_3(b)$, $Rh/MoO_3(c)$ and $Pt/SiO_2(a)$. These induction periods are suggested as corresponding to the build-up of hydrocarbonaceous material on the catalyst which is considered to take place before the catalyst reaches its steady state. This would explain why the induction periods were not observed on well-used catalysts. The pressure fall versus time curves for all catalysts show a decrease in initial rate with increasing catalyst usage, which is again consistent with the suggestion that a carbonaceous overlayer is built-up and that, in general, this causes catalyst deactivation.

In general, the rate of buta-1,3-diene hydrogenation has been found to be less than the rate of butene hydrogenation (98) and

Table 6.6. Summary of Acceleration Point Data

Catalyst	P_o (Torr)	ΔP_{acc} (Torr)	Catalyst State	$H_2:C_4H_6$
Pt/SiO_2(a)	104	7.8 19.3 30.9	fresh	3:1
		acc. points less pronounced	used	
Pt/WO_3(a)	79.65	17.55	fresh	3.5:1
Rh/SiO_2(b)	104	14.1	fresh	3.5:1
		Decreasing rate with increasing usage	used	
Rh/MoO_3(b)	125	32.5	fresh	3:1
	80.6	22.0	used	3:1
Rh/WO_3(b)	83.7	2.4 11.3	fresh	3:1
	81	17.6	used	3:1
Rh/MoO_3(c)	98.8	10.7 18.3 23.5	fresh	3:1
		Decreasing rate with increasing usage	used	
Rh/WO_3(c)	80.6	27.1	fresh	2.5:1
		Gently decreasing on constant rate with increasing usage		

this is consistent with the observation of acceleration points in the present study. Whilst it is generally accepted that buta-1,3-diene is more strongly adsorbed than the butenes (88), the surface concentration of the mono-olefin may be unaffected by the presence of the diunsaturated hydrocarbon (134). The occurrence of an acceleration point, nevertheless, shows that buta-1,3-diene is hydrogenated in preference to the butenes, either due to site-blocking by buta-1,3-diene for the re-adsorption of butene or because of a lack of availability of surface hydrogen for the butene hydrogenation reaction when buta-1,3-diene is present in the system.

With increased catalyst usage, the acceleration points become less pronounced, and the rate either decreases gently or remains approximately constant with increasing pressure fall. This suggests that the catalyst deactivation which occurs with increasing catalyst usage has a greater effect on the rate of butene hydrogenation than on the rate of buta-1,3-diene hydrogenation.

A comparison of the turnover frequencies calculated for each catalyst at the nearest temperature to 293K is presented in Table 6.7.

For the supported platinum catalysts, the decreasing order of turnover frequency is:

$$Pt/MoO_3(a) > Pt/WO_3(a) > Pt/SiO_2(a).$$

$Rh/WO_3(b)$ has a higher turnover frequency than $Rh/SiO_2(b)$. No value could be obtained for $Rh/MoO_3(b)$ since, as noted earlier, it was not possible to calculate the metal area by carbon monoxide chemisorption.

Table 6.7. Initial rate at as close to 293K as possible - rate data from variation with temperature results. All results from used catalysts.

Catalyst	Temperature (K)	Initial Rate (Torr/min)	Weight (g)	No. of surface metal atoms	Turnover Frequency Torr/min/surface metal atom
Pt/SiO_2(a)	295	2.2	0.0087	7.7×10^{17}	2.9×10^{-18}
Pt/MoO_3(a)	291	1.1	0.0694	1.7×10^{16}	6.5×10^{-17}
Pt/WO_3(a)	291	6.4	0.0947	8.7×10^{17}	7.4×10^{-18}
Rh/SiO_2(b)	289	3.5	0.0483	6.8×10^{17}	5.1×10^{-18}
Rh/MoO_3(b)	294	0.4	0.2293	-	-
Rh/WO_3(b)	293	5.7	0.0297	2.0×10^{17}	2.9×10^{-17}
Rh/SiO_2(c)	323	2.4	0.0246	1.0×10^{17}	2.4×10^{-17}
Rh/MoO_3(c)	294	43.3	0.2077	4.4×10^{17}	9.8×10^{-17}
Rh/WO_3(c)	291	3.7	0.0360	9.9×10^{17}	3.7×10^{-18}

The decreasing order of turnover frequency found for the supported rhodium catalysts prepared from rhodium chloride is:

$$Rh/MoO_3(c) \; > \; Rh/SiO_2(c) \; > \; Rh/WO_3(c).$$

Therefore, in terms of their turnover frequencies, the most active catalysts are those supported on molybdenum trioxide. This suggests that a metal-support interaction may take place between the supported metal and the reduced molybdenum species present following reduction. The results presented in this section clearly indicate that the support exerts a direct influence on the metal. This influence is greater when molybdenum trioxide is the support. It is also notable that molybdenum trioxide undergoes extensive reduction under the conditions used to reduce the supported metal salt. Interaction between the supported metal and the reduced metal ions of the support may result in a greater modification of physical and catalytic characteristics of molybdenum trioxide-supported catalysts than occurs with the other oxide supported catalysts.

CHAPTER SEVEN

CHAPTER 7

GENERAL CONCLUSIONS

The results presented in this thesis provide evidence for effects of changes in the metal salt precursor and the support, which give rise to variations in reduction temperatures, the quantities of carbon monoxide chemisorbed, dispersions, and activities and selectivities in buta-1,3-diene hydrogenation with the various supported platinum and rhodium catalysts.

As well as providing direct evidence for hydrogen molybdenum bronze formation, thermo-gravimetric analysis provided evidence which was consistent with rhodium(III) chloride reacting to form rhodium oxide, Rh_2O_3, before being reduced to rhodium metal. The formation of rhodium oxide as an intermediate may explain why supported rhodium catalysts prepared from rhodium(III) chloride can be reduced at lower temperatures than those prepared from rhodium(III) nitrate.

Examination of the results obtained by T.P.R., in the light of the T.G.A. results, leads to the conclusion that in the cases of molybdenum trioxide and tungsten trioxide, reduction of the supports had taken place.

By examining the carbon monoxide chemisorption and dispersion figures obtained, it can be concluded that the molybdenum trioxide and tungsten trioxide supported catalysts exhibit the poorest dispersion. However, the tungsten trioxide-supported rhodium catalyst prepared from rhodium(III) chloride appears to show enhanced dispersion compared with

the rhodium on tungsten trioxide prepared from rhodium nitrate or even the rhodium on silica prepared from rhodium chloride, which shows a poorer than expected dispersion. The variations in dispersion from the expected values for both $Rh/SiO_2(c)$ and $Rh/WO_3(c)$ suggests the existence of a metal support interaction. The dispersions of the supported rhodium catalysts prepared from rhodium nitrate, on the other hand, follow the order expected if the dispersion depended only on the surface area of the support. From this it can be concluded that dispersion depends on both the support and the metal salt precursor.

Comparison of the average particle sizes obtained by carbon monoxide chemisorption with those obtained by transmission electron microscopy, shows that carbon monoxide chemisorption is a poor predictor of particle size. In addition, the low carbon monoxide chemisorption figures obtained for the supported rhodium catalysts prepared from rhodium(III) chloride suggests that chloride present after reduction may act as a poison, preventing carbon monoxide from being chemisorbed.

By temperature programmed desorption it has been found that desorption of hydrogen after carbon monoxide chemisorption on $Rh/MoO_3(b)$ occurs at a temperature 200°C higher than from a freshly reduced catalyst. This is believed to be due to site-blocking by either reduced support species which have migrated to partially encapsulate the rhodium, or to the continued presence of carbon monoxide on the rhodium even at elevated temperatures, in both cases preventing the reverse spillover of hydrogen.

By examination of the sub-ambient carbon monoxide chemisorption results, it can be concluded that although the quantity of carbon monoxide chemisorbed increases with decreasing temperature, there was no way to determine how much carbon monoxide had been chemisorbed by the supported metal, and how much by the support.

The large increase in total surface area of molybdenum trioxide-supported platinum and rhodium catalysts following reduction provides evidence for the occurrence of structural changes within the molybdenum trioxide during reduction.

The use of molybdenum trioxide and tungsten trioxide as supports has been shown to facilitate the hydrogenation of carbon monoxide over supported platinum catalysts, compared with the use of silica as a support. This is believed to be the result of a metal-support interaction and the involvement of spillover hydrogen in the reaction.

Several conclusions can be drawn from the buta-1,3-diene hydrogenation studies. The support is seen to influence selectivity, as shown by the decreasing order of selectivity:

$$Pt/MoO_3(a) > Pt/SiO_2(a) > Pt/WO_3(a)$$

and

$$Rh/MoO_3(b) > Rh/SiO_2(b) > Rh/WO_3(b)$$

However, in the case of rhodium, the metal salt precursor also influences the selectivity, as shown by the decreasing order of selectivity obtained for supported rhodium catalysts prepared from rhodium chloride:

$$Rh/SiO_2(c) > Rh/MoO_3(c) > Rh/WO_3(c)$$

It is concluded, therefore, that for a given metal, selectivity is dependent upon both the support and the metal salt precursor.

The molybdenum trioxide-supported catalysts exhibit the highest selectivity, which suggests that bronze hydrogen is not involved in the hydrogenation of buta-1,3-diene over these catalysts. However, in the case of the tungsten trioxide-supported catalysts, it is likely that bronze hydrogen is involved since these catalysts exhibit a poorer selectivity.

Whilst the results obtained for variation of product distributions and selectivities with increasing conversion can be interpreted in terms of a mechanism by which (i) but-2-ene formation occurs by both 1,4-addition of hydrogen to adsorbed buta-1,3-diene and by the subsequent isomerisation of but-1-ene formed by 1,2-addition of hydrogen and (ii) a direct route for the formation of n-butane from adsorbed buta-1,3-diene, not involving the intermediate formation of butenes, is extant.

The pressure fall versus time curves show that with freshly reduced catalysts, induction periods are often observed, although these are not evident with well-used catalysts. These induction periods are believed to correspond to an initial build-up of carbonaceous overlayers on the surface to produce the active catalyst. The observed decrease in rate with increasing catalyst usage is also consistent with the build-up of surface carbonaceous overlayers which give rise to deactivation. Although the latter is true in the majority of cases, this process appears to cause a change in the overall mechanism of the reaction over

$Rh/MoO_3(c)$ and $Pt/MoO_3(a)$, since these catalysts exhibit a marked decrease in activation energy of ca. 50 kJ mol^{-1} after they have been well used relative to when they are freshly reduced. This decrease in activation energy to a more expected value may be consistent with the suggestion that the rate determining step becomes the same for a given metal for all of the catalysts used in the present study following the build-up of hydrocarbonaceous overlayers. The absence of acceleration points on well-used catalysts is consistent with the catalyst deactivation having a greater effect on the butene hydrogenation than on the buta-1,3-diene hydrogenation.

Comparison of the turnover frequencies show that the support has an influence. This influence is greatest in the case of molybdenum trioxide. This may be due to an interaction between the reduced molybdenum species known to be present following catalyst reduction, and the supported metal particles.

Overall, it can be concluded that the physical characteristics and the catalytic properties of the supported platinum and rhodium catalysts are influenced by a combination of the support, the metal, and the metal salt precursor.

References

1. Appendix based on "A History of Platinum and its Allied Metals", by Donald McDonald and Leslie B. Hunt, Johnson Matthey, 1982.
2. Henry M. Leicester, "The Historical Background of Chemistry", Dover Publications Inc., New York, 1971.
3. C.B. Désormes and N. Clément, Ann. Chim. Phys., 59, 329-339 (1806).
4. J.W. Döbereiner, Scweigers, J. Chem. Phys., 38, 321-325 (1823).
5. W. Ostwald, Z. Physik. Chem., 15, 705-706 (1894).
6. S.J. Thomson and G. Webb, "Heterogeneous Catalysis", Oliver and Boyd, 1967.
7. G.C. Bond, "Catalysis by Metals", Academic Press, London, 1962.
8. G.C. Bond and R. Burch, Catalysis, ed. G.C. Bond and G. Webb, (Specialist Periodical Reports), The Royal Society of Chemistry, London, 1983, Vol. 6, 27-60.
9. S.J. Tauster, S.C. Fung and R.L. Garten, J. Amer. Chem. Soc., 100, 170 (1978).
10. S.J. Tauster and S.C. Fung, J. Catal., 55, 29-35 (1978).
11. J.A. Horsley, J. Amer. Chem. Soc., 101, 2870-2874 (1979).
12. S.J. Tauster in "Strong Metal-Support Interactions", Ed. R.T.K. Baker, S.J. Tauster and J.A. Dumesic, A.C.S. Symposium Series 298 (1986), 1-9 .
13. G.M. Schwab, Adv. Catal., 27, 1-22 (1978).
14. F. Solymosi, Catal. Rev., 1, 233-255 (1967).
15. S.C. Fung, J. Catal., 76, 225-230 (1982).

16. J.M. Herrmann, J. Catal., 89, 404-412 (1984).

17. B.-H. Chen and J.M. White, J. Phys. Chem., 86, 3534-3541 (1982).

18. H.R. Sadeghi and V.E. Henrich, J. Catal., 109, 1-11 (1988).

19. S.D. Jackson, P.B. Wells, R. Whyman and P. Worthington, in Catalysis, ed. C. Kemball and D.A. Dowden (Specialist Periodical Report), The Royal Society of Chemistry, London, 1981, Vol. 4, p.75.

20. R.T.K. Baker, E.B. Prestridge and R.L. Garten, J. Catal., 59, 293-302 (1979).

21. R.T.K. Baker, E.B. Prestridge and R.L. Garten, J. Catal., 56, 390-406 (1979).

22. M.S. Spencer, J. Catal., 93, 216-223 (1985).

23. J.A. Cairns, J.E.E. Baglin, G.J. Clarke and J.F. Ziegler, J. Catal., 83, 301 (1983).

24. R.R. Powell and S.E. Whittington, J. Catal., 81, 382-393 (1983).

25. D.N. Belton, Y.-M. Sun and J.M. White, J. Phys. Chem., 88, 5172-5176 (1984).

26. B.J. Tatarchuk and J.A. Demesic, J. Catal., 70, 323-334 (1981).

27. H.R. Sadeghi and V.E. Henrich, J. Catal., 87, 279-282 (1984).

28. H. Miessener, S. Naito and K. Tamaru, J. Catal., 94, 300-302 (1985).

29. D.N. Belton, Y.-M. Sun and J.M. White, J. Amer. Chem. Soc., 106, 3059-3060 (1984).

30. D.N. Belton, Y.-M. Sun and J.M. White, J. Catal., 102, 338-347 (1986).

31. R.T.K. Baker, J.J. Chlidzinski and J.A. Dumesic, J. Catal., 93, 312-320 (1985).

32. M.C. Sanchez and J.L. Gazquez, J. Catal., 104, 120-135 (1987).

33. S. Sakellson, M. McMillan and G.L. Haller, J. Phys. Chem., 90, 1733-1736 (1986).

34. T. Huizinga, J.C. Vis, H.F.J. van't Blik and R. Prins, Recl. Trav. Chim. Pays-Bas, 102, 496-497 (1983).

35. M.A. Vannice and R.L. Garten, J. Catal., 56, 236-248 (1979).

36. S.-Y. Wang, S.H. Moon and M.A. Vannice, J. Catal., 71, 167-174 (1981).

37. M.A. Vannice, J. Catal., 74, 199-202 (1982).

38. R. Burch and A.R. Flambard, J. Catal., 78, 389-405 (1982).

39. D.E. Resasco and G.L. Haller, J. Catal., 82, 279-288 (1983).

40. B. Boumarafi, M.Sc. Thesis, University of Glasgow, 1986.

41. P.A. Sermon and G.C. Bond, Catal. Rev., 8, 211-239 (1973).

42. P.A. Sermon and G.C. Bond, J. Chem. Soc. Faraday Trans. I, 76, 889-900 (1980).

43. J.C. Kuriacose, Ind. J. Chem., 5, 646-647 (1967).

44. E.H. Taylor, 2nd Int. Congr. Catal., 1961, 159-166, Vol. I.

45. S. Khoobiar, J. Phys. Chem., 68, 411-412 (1964).

46. M. Boudart, M.A. Vannice and J.E. Benson, Z. Phys. Chem. (N.F.), 64, 171-177 (1969).

47. A.J. Robell, E.V. Ballou and M. Boudart, J. Phys. Chem., 68, 2748-2753 (1964).

48. M. Boudart, A.W. Aldag and M.A. Vannice, J. Catal., 18, 46-51 (1970).

49. W.C. Conner, G.M. Pajonk and S.J. Teichner, Adv. Catal., 34, 1-79 (1986).

50. K.M. Sancier, J. Catal., 23, 298-300 (1971).

51. E.J. Nowak, J. Phys. Chem., 73, 3790-3794 (1969).

52. R.B. Levy and M. Boudart, J. Catal., 32, 304-314 (1974).

53. W.J. Ambs and M.M. Mitchell, J. Catal., 82, 226-229 (1983).

54. J.E. Benson, H.W. Kohn and M. Boudart, J. Catal., 5, 307-313 (1966).

55. G.C. Bond, in "Spillover of Adsorbed Species", Ed. G.M. Pajonk, S.J. Teichner and J.E. Germain, Elsevier, Amsterdam, 1983.

56. J.L. Carter, P.J. Lucchesi, P. Corneil, D.J.C. Yates and J.H. Sinfelt, J. Phys. Chem., 69, 3070-3074 (1965).

57. P.A. Sermon and G.C. Bond, J. Chem. Soc. Faraday Trans. I, 72, 730-744 (1976).

58. T. Huizinga and R. Prins, J. Phys. Chem., 85, 2156 (1981).

59. D.D. Beck and J.M. White, J. Phys. Chem., 88, 174-175 (1984).

60. G.C. Bond and J.B. Tripathi, J. Chem. Soc. Faraday Trans. I, 72, 933-941 (1976).

61. P.A. Sermon and G.C. Bond, J. Chem. Soc. Faraday Trans. I, 72, 745-754 (1976).

62. D. Bianchi, G.E.E. Gardes, G.M. Pajonk and S.J. Teichner, J. Catal., 38, 135-146 (1975).

63. D.H. Lenz and W.C. Conner, J. Catal., 104, 288-298 (1987).

64. M. Lacroix, G.M. Pajonk and S.J. Teichner, Bull. Soc. Chim. France, 1981, I - 87-93 and I - 94-100.

65. M.A. Henderson and S.D. Worley, J. Phys. Chem., 89, 392-394 (1985).

66. J.A. Altham and G. Webb, J. Catal., 18, 133-141 (1970).

67. E. Baumgarten, R. Wagner and C. Lentes-Wagner, J. Catal., 104, 307-311 (1987).

68. J.J. Fripiat, NATO ASI SER., SER. C, 105, 477-491 (1983).

69. F. Wohler, Philos. Mag., 66, 263 (1825).

70. P.G. Dickens, D.J. Murphy and T.K. Halstead, J. Solid State Chem., 6, 370-373 (1973).

71. M. Greenblatt, Chem. Rev., 88, 31-53 (1988).

72. A.F. Wells, Structural Inorganic Chemistry, 5th Edition, Clarendon Press, Oxford, 1984.

73. P.G. Dickens, J.J. Birtill and C.J. Wright, J. Solid State Chem., 28, 185-193 (1979).

74. R.C.T. Slade, T.K. Halstead and P.G. Dickens, J. Solid State Chem., 34, 183-192 (1980).

75. Cl. Ritter, W. Müller-Warmuth and R. Schöllhorn, J. Chem. Phys., 83, 6130-6138 (1985).

76. A.C. Cirillo, L. Ryan, B.C. Gerstein and J.J. Fripiat, J. Chem. Phys., 73, 3060-3068 (1980).

77. M.J. Sienko and H. Oesterreicher, J. Amer. Chem. Soc., 90, 6568-6570 (1968).

78. C.J. Wright, J. Solid State Chem., 20, 89-92 (1977).

79. J.P. Marcq, X. Wispenninckx, G. Poncelet, D. Keravis and J.J. Fripiat, J. Catal., 73, 309-328 (1982).

80. P.G. Dickens, J.H. Moore and D.J. Nield, J. Solid State Chem., 7, 241-244 (1973).

81. R.E. Taylor, L.M. Ryan, P. Tindall and B.C. Gerstein, J. Chem. Phys., 73, 5500-5507 (1980).

82. H.W. Kohn and M. Boudart, Science, 145, 149 (1964).

83. R. Benali, C. Hoang-Van and P. Vergnon, Bull. Soc. Chim. France, 1985, 417.

84. S.D. Jackson, B.J. Brandreth and D. Winstanley, Appl. Catal., 27, 325-333 (1986).

85. W.M.H. Sachtler, Proceedings, 8th Int. Congr. Catal., 1, 151 (1984).

86. J. Massardier and J.C. Bertolini, J. Catal., 90, 358-361 (1984).

87. J. Oudar, S. Pinol and Y. Berthier, J. Catal., 107, 434-444 (1987).

88. G.C. Bond, G. Webb, P.B. Wells and J.M. Winterbottom, J. Chem. Soc., 1965, 3218-3227.

89. G.C. Bond and P.B. Wells, Adv. Catal., 15, 91-226 (1964).

90. G.C. Bond, J.J. Phillipson, P.B. Wells and J.M. Winterbottom, Trans. Faraday Soc., 60, 1847 (1964).

91. G.C. Bond,and J. Turkevitch, Trans. Faraday Soc., 49, 281 (1953).

92. G.C. Bond, Trans. Faraday Soc., 52, 1235 (1956).

93. J. Addy and G.C. Bond, Trans. Faraday Soc., 53, 377 (1957).

94. L.B. Smith and J.L. Massingil, J. Amer. Chem. Soc., 83, 4301 (1961).

95. J.J. Phillipson, P.B. Wells and G.R. Wilson, J. Chem. Soc. A, 1351-1363 (1969).

96. A.J. Bates, Z.K. Leszczyński, J.J. Phillipson, P.B. Wells and G.R. Wilson, J. Chem. Soc. A, 2435-2441 (1970).

97. C.-M. Pradier, E. Margot, Y. Berthier and J. Oudar, Appl. Catal., 31, 243-257 (1987).

98. J.P. Boitiaux, J. Cosyns and E. Robert, Appl. Catal., 32, 145-168 (1987).

99. J.P. Boitiaux, J. Cosyns and E. Robert, Appl. Catal., 32, 169-183 (1987).

100. G.A. Mills and F.W. Steffgen, Catal. Rev., 8, 159-210 (1973).

101. P. Sabatier and J.B. Senderens, C.R. Acad. Sci., 134, 514 (1902).

102. P. Sabatier and J.B. Senderens, Ann. Chim. Phys., 4, 319-432 and 433-488 (1905).

103. F. Fischer, H. Tropsch and P. Dilthey, Brennst. Chem., 6, 265 (1925).

104. M.A. Vannice, J. Catal., 37, 449-461 (1975).

105. M.A. Vannice, J. Catal., 37, 462-473 (1975).

106. M.A. Vannice, J. Catal., 40, 129-134 (1975).

107. J. Freel, J. Catal., 25, 139-148 and 149-160 (1972).

108. F. Solymosi, I. Tombacz and M. Kocsis, J. Catal., 75, 78-93 (1982).

109. M.A. Vannice, J. Catal., 44, 152-162 (1976).

110. M.A. Vannice, Catal. Rev. Sci. Eng., 14, 153-191 (1976).

111. K. Gilhooley, S.D. Jackson and S. Rigby, J. Chem. Soc. Faraday Trans. I, 82, 431-438 (1986).

112. S.D. Jackson, B.J. Brandreth and D. Winstanley, J. Catal., 106, 464-470 (1987).

113. M. Araki and V. Ponec, J. Catal., 44, 439-448 (1976).

114. V. Ponec, Catal. Rev. Sci. Eng., 18, 151-171 (1978).

115. T. Iizuka, Y. Tanaka and K. Tanabe, J. Catal., 76, 1-8 (1982).

116. H.D. Vandervell and M. Bowker, Appl. Catal., 30, 151-158 (1987).

117. S.D. Jackson, J. Chem. Soc. Faraday Trans. I, 81, 2225-2233 (1985).

118. C.A. Rice, S.D. Worley, C.W. Curtis, J.A. Guin and A.R. Tarrer, J. Chem. Phys., 74, 6487-6497 (1981).

119. S.D. Worley, C.A. Rice, C.W. Curtis. J.A. Guin and A. Tarrer, J. Chem. Phys., 76, 20-25 (1982).

120. E.A. Hyde, R. Rudham and C.H. Rochester, J. Chem. Soc. Faraday Trans. I, 79, 2405-2423 (1983).

121. S.D. Jackson, B.J. Brandreth and D. Winstanley, J. Chem. Soc. Faraday Trans. I, 84, 1741-1749 (1988).

122. S. Brunauer, P.H. Emmett and E. Teller, J. Amer. Chem. Soc., 60, 309 (1938).

123. G.C. Chinchen, C.M. Hay, H.D. Vandervell and K.C. Waugh, J. Catal., 103, 79-86 (1987).

124. CRC Handbook of Chemistry and Physics, Ed. R.C. Weast, 68th Edition, 1987.

125. G.D. McLellan and E.A. Arafa, unpublished results.

126. J.U. Reid, Ph.D. Thesis, University of Glasgow, 1971.

127. F.J. Schepers, J.G. van Senden, E.H. van Broekhoeven and V. Ponec, J. Catal., 94, 400-407 (1985).

128. G.D. McLellan, unpublished results.

129. K. Green and G. Webb, unpublished results.

130. P.A. Redhead, Trans. Faraday Soc., 57, 641 (1961).

131. K.C. Waugh, private communication.

132. S.D. Jackson, private communication.

133. A. Magneti and G. Andersson, Acta Chem. Scand., 9, 1378-1381 (1955).

134. A.S. Al-Ammar and G. Webb, J. Chem. Soc. Faraday Trans. I, 75, 1900-1911 (1979).

135. A. Simpson and G. Webb, unpublished results.

136. A.S. Al-Ammar and G. Webb, J. Chem. Soc. Faraday Trans. I, 74, 195-205 (1978).

137. G. Webb in "Comprehensive Chemical Kinetics", ed. C.H. Bamford and C.F.H. Tipper, Vol. 20, 1-121 (1978).